nature

THE INTERNATIONAL WEEKLY JOURNAL OF SCIENCE

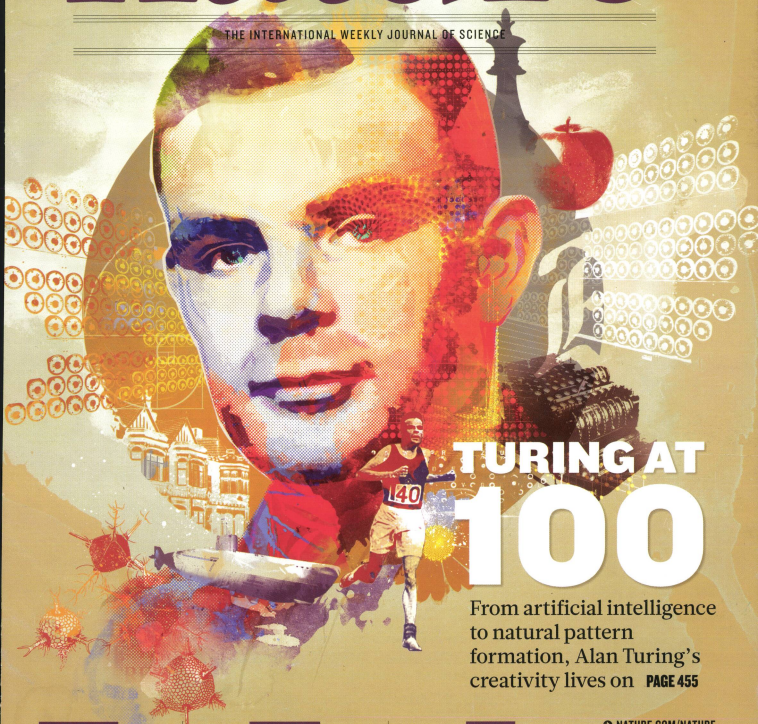

TURING AT 100

From artificial intelligence to natural pattern formation, Alan Turing's creativity lives on PAGE 455

NEUROSCIENCE

STAGE CRAFT

How actors stir the emotions

PAGE 466

OPEN ACCESS

GET WITH THE PROGRAMS

Computer codes and the publication process

PAGE 485

CAREERS

INDUSTRIAL RELATIONS

European PhD programme breaks new ground

PAGE 557

NATURE.COM/NATURE

23 February 2012 £10

Vol. 482, No. 7386

08

9 770028 083095

immunoLOGICAL

Infiltration of tumors by regulatory T (Treg) cells suppresses anti-tumor immune responses and promotes tumor growth. As a result, mechanisms to inhibit Treg cell differentiation, expansion, recruitment, and function are being widely explored. With over 25 years of experience developing and manufacturing immunology-related research reagents, R&D Systems is the logical choice for products you can trust.

- More than **200** different antibodies for Treg cell research
- Treg Cell Selection & Multi-color Flow Cytometry Kits
- Bioactive proteins for Treg cell differentiation & functional studies

Inhibition of T Cell Proliferation by LRRC32

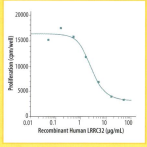

LAP Suppresses TGF-β-induced Inhibition of Mouse T helper Cells

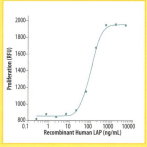

CTLA-4 Inhibition of B7-1/CD80-induced IL-2 Secretion

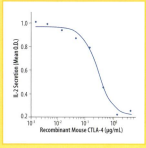

Visit our website at www.RnDSystems.com/Treg

R&D Systems, Inc. www.RnDSystems.com
R&D Systems Europe, Ltd. www.RnDSystems.co.uk
R&D Systems China Co., Ltd. www.RnDSystemsChina.com.cn

For research use only. Not for use in diagnostic procedures.

R&D SYSTEMS®

Instruments that are music to your hands.

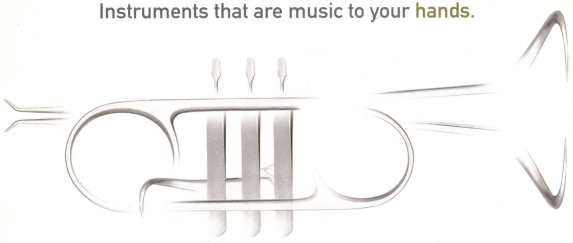

FINE SURGICAL INSTRUMENTS FOR RESEARCH™

SHIPPING GLOBALLY SINCE 1974

Request a catalog at finescience.com or call 1-800-521-2109.

F · S · T®

FINE SCIENCE TOOLS

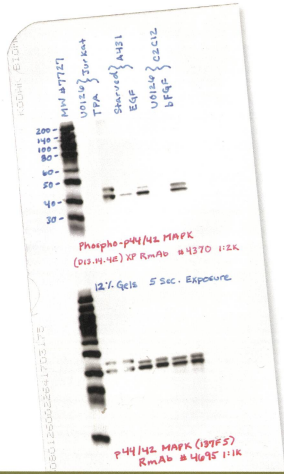

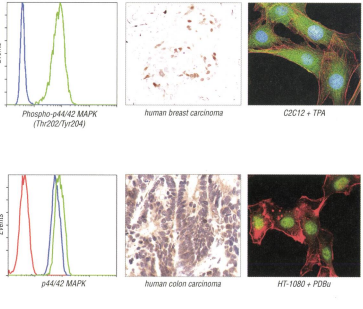

Phospho-p44/42 MAPK (Erk1/2) (Thr202/Tyr204) (D13.14.4E) XP® Rabbit mAb #4370 *(top) and* ***p44/42 MAPK (Erk1/2) (137F5) Rabbit mAb #4695*** *(bottom).*

For full validation details see www.cellsignal.com

The Highest Quality MAPK Antibodies

are from Cell Signaling Technology

Unparalleled product quality, validation, and technical support

Over 30 thoroughly validated MAPK Antibodies available

Cell Signaling Technology (CST™) offers the widest range of phospho and total protein MAPK antibodies. These reagents are the most thoroughly validated, widely used, and highly cited MAPK antibodies available.

- CST™ phospho and total protein MAPK antibodies offer **unsurpassed specificity, sensitivity, and performance**.
- **Extensive in-house validation** in a wide range of applications means that optimization is not left up to you, the user.
- **Technical support is provided by scientists** who produce the products and know them best.

WINNER! Life Science Industry Awards®
Best Antibodies :: Best Breakthrough Products for Cancer Research

for quality products you can trust...

www.cellsignal.com

Cell Signaling TECHNOLOGY®

Orders (toll-free) 1-877-616-CELL (2355) orders@cellsignal.com | **Fax ordering** 1-978-867-2488 | **Technical support** (toll-free) 1-877-678-TECH (8324) support@cellsignal.com | **Inquiries** info@cellsignal.com

Cell Signaling Technology, CST, and XP® are trademarks of Cell Signaling Technology, Inc. Limited label, noncommercial distribution permitted under license. Upon first use, cyanine reagents may be subject to one or more third-party patents, including U.S. Patent No. 6,573,363 and 7,429,487 from Epitomics, Inc.

CONTENTS

23 February 2012 / Vol 482 / Issue No 7386

TURING AT 100

EDITORIAL

440 Turing at 100
A chance to meet a unique mind

WORLD VIEW

441 The man behind the machine
Andrew Hodges
What happened to Turing's reputation

FEATURES

455 Legacy of a universal mind
Nature tours Turing's many facets

456 Brain in a box
On a quest to model the human brain

COMMENT

459 The dawn of computing
George Dyson
Turing paved the way to computers

Andy Potts/Turing family/NPL/King's College

461 Life's code script
Sydney Brenner
A 'Turing machine' in every cell

462 Is the brain a good model for machine intelligence?
Rodney Brooks, Demis Hassabis, Dennis Bray & Amnon Shashua
Should computers mimic neurons?

464 Pattern formation
John Reinitz
'Turing instabilities' pervade nature

465 The incomputable reality
Barry Cooper
The Universe beyond the limits of computation

TURING AT 100
A legacy that spans science:
nature.com/turing

THIS WEEK

EDITORIALS

439 PUBLICATION
Flu papers warrant full publication
Summit declares benefits exceed risks

440 CLIMATE
Over the line
Dishonesty is not suited to scientists

RESEARCH HIGHLIGHTS

442 SELECTIONS FROM THE SCIENTIFIC LITERATURE
Immunity beats time / Stem-cell heart therapy / A lizard meets its match / New route to fluorine compounds

SEVEN DAYS

444 THE NEWS IN BRIEF
Animals spared from testing / Fracking doesn't contaminate groundwater / Greek artefacts stolen / Nanotech firm presents first data / Nobel virologist dies

NEWS IN FOCUS

447 BIOSECURITY
WHO favours full publication of flu work

448 EPIDEMIOLOGY
Children's study copes with cutbacks

449 BIOETHICS
Editor's career move sparks backlash

450 FUNDING
The top seven NIH grant recipients

453 HIGH-ENERGY PHYSICS
Tevatron plundered for parts

453 PALAEOBOTANY
Viable plant created from Ice-Age seeds

CAREERS

557 EDUCATION
Outside the box
Industrial PhDs make sense

559 TURNING POINT
Christopher Wilson on California biotech

NATUREJOBS ADVERTISING FEATURE
Spotlight on post-grad opportunities

COMMENT

BOOKS & ARTS

466 NEUROSCIENCE
Powerful acts
Giovanni Frazzetto

467 BOOKS IN BRIEF

468 INFECTIOUS DISEASE
Chronicles of a killer virus
Robin Weiss

469 Q&A
The eternal optimist
The down-to-Earth ambitions of space-flight entrepreneur Peter Diamandis

CORRESPONDENCE

470 Prepare for next flu pandemic / Biosecurity priorities / Questionable use of chimps in research / The case against sugar / Managing the Australian bush

FUTURES

562 **Ghost in the machine**
Grace Tang

MERCK MILLIPORE

Break free from routine sample prep. Go from boring to bold.

The Samplicity™ Filtration System takes sample prep in a flexible, new direction. This vacuum-powered system filters one sample or eight, of virtually any viscosity or composition, into HPLC vials in seconds—with minimal manual effort.

With the Samplicity filtration system and Millex Samplicity™ filters, Merck Millipore has transformed multi-sample filtration forever.

Samplicity makes it simple.

Discover how at www.millipore.com/GoBold

Merck Millipore is a division of MERCK

Merck Millipore, the M mark, Samplicity and Millex Samplicity are trademarks of Merck KGaA, Darmstadt, Germany.
© 2012 EMD Millipore Corporation, Billerica MA USA. All rights reserved.

CONTENTS

23 February 2012 / Vol 482 / Issue No 7386

RESEARCH

NEW ONLINE

473 Papers published this week at nature.com

NEWS & VIEWS

474 CELL BIOLOGY
Collagen secretion explained
Ubiquitination of vesicle coats allows packaging of large proteins
David J Stephens SEE ARTICLE P.495

475 ASTROPHYSICS
First results from Planck observatory
Studying dust in distant galaxies and gas in galaxy clusters
Uroš Seljak

476 FLUID MECHANICS
Mist opportunities
The rules of fibre wetting
Rosamund Daw SEE LETTER P.510

477 MATERIALS SCIENCE
Cell environments programmed with light
Controlled attachment of cells to hydrogels
Matthias P Lutolf

478 QUANTUM COMPUTING
A topological route to error correction
Reducing the sensitivity of quantum computing to errors
James D Franson SEE ARTICLE P.489

480 STRUCTURAL BIOLOGY
Muscarinic receptors become crystal clear
Structures of two muscarinic acetylcholine receptors
Rebecca L Kow & Neil M Nathanson SEE LETTERS P.547 & P.552

481 CANCER GENETICS
Evolution after tumour spread
Primary and metastatic medulloblastoma features divergent mutations
Steven C Clifford SEE LETTER P.529

482 CLIMATE CHANGE
Shrinking glaciers under scrutiny
Measuring the mass-loss rate of glaciers using satellite gravity data
Jonathan Bamber SEE LETTER P.514

PERSPECTIVE

485 COMPUTING SCIENCE **The case for open computer programs**
D C Ince, L Hatton & J Graham-Cumming

ARTICLES

489 PHYSICS **Experimental demonstration of topological error correction**
X-C Yao et al. SEE N&V P.478

495 CELL BIOLOGY **Ubiquitin-dependent regulation of COPII coat size and function**
L Jin et al. SEE N&V P.474

501 STRUCTURAL BIOLOGY **Structural basis of highly conserved ribosome recycling in eukaryotes and archaea**
T Becker et al.

LETTERS

507 ASTRONOMY **Abrupt acceleration of a 'cold' ultrarelativistic wind from the Crab pulsar**
F A Aharonian, S V Bogovalov & D Khangulyan

510 FLUID MECHANICS **Wetting of flexible fibre arrays**
C Duprat, S Protière, A Y Beebe & H A Stone SEE N&V P.476

514 CLIMATE SCIENCE **Recent contributions of glaciers and ice caps to sea level rise**
T Jacob, J Wahr, W T Pfeffer & S Swenson SEE N&V P.482

519 NEURODEGENERATION **The microRNA miR-34 modulates ageing and neurodegeneration in *Drosophila***
N Liu et al.

524 STEM CELLS **Maintenance of muscle stem-cell quiescence by microRNA-489**
T H Cheung et al.

529 CANCER **Clonal selection drives genetic divergence of metastatic medulloblastoma**
X Wu et al. SEE N&V P.481

534 CANCER **DCC constrains tumour progression via its dependence receptor activity**
M Castets et al.

538 CANCER **Deleted in colorectal carcinoma suppresses metastasis in p53-deficient mammary tumours**
P Krimpenfort, J-Y Song, N Proost, J Zevenhoven, J Jonkers & A Berns

542 STRUCTURAL BIOLOGY **The same pocket in menin binds both MLL and JUND but has opposite effects on transcription**
J Huang et al.

547 STRUCTURAL BIOLOGY **Structure of the human M2 muscarinic acetylcholine receptor bound to an antagonist**
K Haga et al. SEE N&V P.480

552 STRUCTURAL BIOLOGY **Structure and dynamics of the M3 muscarinic acetylcholine receptor**
A C Kruse et al. SEE N&V P.480

PHYSICS

Fault lines

Topological error correction in quantum computing. PAGE 489

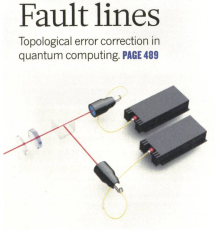

CLIMATE

GRACE notes

Gravity data from the GRACE satellite used to map sea-level trends. PAGE 514

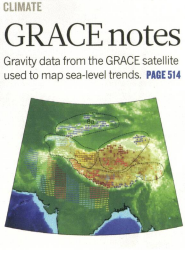

nature

23 February 2012 / Vol 482 / Issue No. 7386

EDITORIAL

LONDON, MUNICH, WASHINGTON DC, NEW YORK, BOSTON, PARIS, SAN FRANCISCO, TOKYO nature@nature.com

EDITOR-IN-CHIEF: Philip Campbell
EXECUTIVE EDITOR: Nick Campbell
PUBLISHING EXECUTIVE EDITOR: Maxine Clarke **EXECUTIVE EDITOR:** Véronique Kiermer
CHIEF MAGAZINE EDITOR: Tim Appenzeller
THIS WEEK/NEWS/FEATURES: Alison Abbott, David Adam, Ananyo Bhattacharya, Geoff Brumfiel, Declan Butler, Ewen Callaway, Erika Check Hayden, Daniel Cressey, David Cyranoski, Natasha Gilbert, Eric Hand, Heidi Ledford, Corrie Lok, Brendan Maher, Emma Marris, Richard Monastersky, Brian Owens, Helen Pearson, Mark Peplow, Eugenie Samuel Reich, Ivan Semeniuk, Quirin Schiermeier, Jeff Tollefson, Richard Van Noorden, Meredith Wadman, M Mitchell Waldrop **COMMENT:** Sara Abdulla, Joanne Baker, Rosalind Cotter, Barbara Kiser, Alison McCook, Lucy Odling-Smee, Sarah Tomlin **NATURE PODCAST/VIDEO:** Adam Rutherford, Eric Olson, Kerri Smith, Charlotte Stoddart **NEWS AND VIEWS:** Sadaf Shadan, Ana Lopes, Andrew Mitchinson, Cesar Sanchez, Marian Turner **RESEARCH:** Ritu Dhand, Karl Ziemelis, Francesca Cesari, I-han Chou, Tanguy Chouard, Rosamund Daw, Alex Eccleston, Angela Eggleston, Joshua Finkelstein, Henry Gee, Patrick Goymer, Noah Gray, Marie-Thérèse Heemels, Magdalena Helmer, Karen Howell, Claudia Lupp, Barbara Marte, Andrew Mitchinson, Juliane Mössinger, Deepa Nath, Leslie Sage, Magdalena Skipper, Clare Thomas, John VanDecar, Liesbeth Venema, Ursula Weiss, Michael White **INSIGHTS/REVIEWS/PERSPECTIVES:** Ursula Weiss **CAREERS:** Gene Russo, Karen Kaplan **TECHNOLOGY FEATURES:** Moriya Baker **FUTURES:** Henry Gee **SUPPLEMENENTS:** Herb Brody, Michelle Grayson, Tony Scully **SUBEDITORS:** Colin Sullivan, Sarah Archibald, Nicola Bailey, Anne Blewett, Nicolas Fanget, Isobel Flanagan, Paul Fletcher, Afsaneh Gray, Dinah Loon, Anna Novitzky, Yukie Ozawa, Katherine Perry, David Price, Jenny Rooke, David Winters, Anna York **PRODUCTION:** Jenny Henderson, Leonora Dawson-Bowling, Dan Foley, Stewart Fraser, Susan Gray, Simon Gribbin, Rachel Mayhew, James McQuat, Emilia Orviss, Yvonne Strong, Robert Sullivan, Roberta Tarran, Charles Wenz **ART AND DESIGN:** Kelly Buckheit Krause, Wesley Fernandes, Madeline Hutchinson, Barbara Izdebska, Paul Jackman, Jasiek Krzyszkofiak, Annthea Lewis, Nik Spencer, Claire Welsh, Mark Wood **JAPAN EDITOR:** Eiji Matsuda, Mitsuyo Utsugi, Sayaka Ayame **PRESS OFFICE:** Ruth Francis, Neda Afsarmanesh, Lisa Boucher, Rachel Twinn, Rebecca Walton **ADMINISTRATION:** Paul Sng, Liz Bankes, Roseann Campbell, Fhion Cleverley, Faye Fornasier, Ashlee Gagui, Amy Invernizzi, Diane Kempinski, Katie McGoldrick, Jenny Meyer, Rina Nozawa, Anastasia Panoutsou, Kenneth Simpson, Claire Smith

PUBLISHING

LONDON feedback@nature.com
MANAGING DIRECTOR & PUBLISHER: Steven Inchcoombe
ASSOCIATE PUBLISHER: Arash Hejazi
PUBLISHING PROJECT MANAGER: Christian Manco

TOKYO feedback@natureasia.com
DIRECTOR — ASIA-PACIFIC: David Swinbanks
REGIONAL MANAGING DIRECTOR — ASIA-PACIFIC: Antoine E Bocquet
OPERATIONS DIRECTOR — ASIA-PACIFIC: Hiroshi Minemura

DISPLAY ADVERTISING, SPONSORSHIP & NATUREJOBS

GLOBAL HEAD: Andrew Douglas a.douglas@nature.com

DISPLAY ADVERTISING AND SPONSORSHIP
GLOBAL HEAD: Gerard Preston g.preston@nature.com
ASSISTANT SPONSORSHIP MANAGER: Reya Silao Tel: +44 (0)20 7843 4977 (rsilao@nature.com)

EUROPE/REST OF WORLD display@nature.com Tel: +44 (0)20 7843 4960
GERMANY/SWITZERLAND/AUSTRIA: Sabine Hugi-Fürst Tel: +41 52761 3386
UK/IRELAND/SCANDINAVIA/SPAIN/PORTUGAL: Evelina Rubio Hakansson Tel: +44 (0)20 7843 4079
FRANCE/BELGIUM/THE NETHERLANDS/LUXEMBOURG/ITALY/OTHER EUROPE: Nicola Wright Tel: +44 (0)20 7843 4959

NORTH AMERICA display@naturenyc.com
NEW ENGLAND/ EASTERN CANADA: Sheila Reardon Tel: +1 617 494 4900
NEW YORK/MID-ATLANTIC/SOUTHEAST: Jim Breault Tel: +1 212 726 9334
MIDWEST: Mike Rossi Tel: +1 212 726 9255
WEST COAST/ WESTERN CANADA: George Lui Tel: +1 415 781 3804
WEST COAST NORTH: Kayla McCutchan Tel: +1 415 403 9038

ASIA-PACIFIC display@natureasia.com
ASIA-PACIFIC HEAD: Kate Yoneyama
JAPAN: Ken Mikami Tel: +81 3 3267 8765
GREATER CHINA/SINGAPORE: Gloria To Tel: +852 2811 7191
INDIA: Vikas Chawla Tel: +91 124 288 1057

SPONSORSHIP
BUSINESS DEVELOPMENT MANAGER: David Bagshaw Tel: +1 212 726 9215
BUSINESS DEVELOPMENT MANAGER: Patrick Murphy Tel: +1 617 475 9216

NATUREJOBS naturejobs@nature.com
EUROPEAN HEAD OFFICE, LONDON: Tel: +44 (0)20 7843 4961
EUROPEAN SALES MANAGER: Nils Moeller (n.moeller@nature.com) **BUSINESS DEVELOPMENT MANAGER, MIDDLE EAST:** Jon Giuliani (j.giuliani@nature.com) **ADVERTISING PRODUCTION MANAGER:** Stephen Russell **NATUREJOBS ONLINE PRODUCTION:** Dennis Chu
US HEAD OFFICE, NEW YORK: naturejobs@naturenyc.com **US SALES MANAGER:** Ken Finnegan
JAPAN HEAD OFFICE, TOKYO: Tel: +81 3 3267 8765 **ASIA-PACIFIC HEAD:** Kate Yoneyama
ASIA-PACIFIC SALES & BUSINESS DEVELOPMENT MANAGER: Yuki Fujiwara **BUSINESS DEVELOPMENT MANAGER, GREATER CHINA, SINGAPORE:** Gloria To Tel: +852 2811 7191
INDIA: Vikas Chawla Tel: +91 1242881057 (v.chawla@nature.com)

MARKETING & SUBSCRIPTIONS

USA/CANADA/LATIN AMERICA subscriptions@us.nature.com
Tel: (USA/Canada)+1 866 363 7860; (outside USA/Canada) +1 212 726 9223
MARKETING: Sara Girard **FULFILMENT:** Karen Dawson

JAPAN/CHINA/KOREA subscriptions@natureasia.com
Tel: +81 3 3267 8751 **MARKETING:** Sachiyo Ikeda **FULFILMENT:** Masayo Tanaka

EUROPE/REST OF WORLD subscriptions@nature.com
Tel: +44 (0)1256 329242
MARKETING: Elena Woodstock, Marcus Parker, Hannah Phipps **FULFILMENT:** Jean Burrows

INDIA npgindia@nature.com
Tel: +91 124 2881053/54
HEAD OF BUSINESS DEVELOPMENT, INDIA: Debashish Brahmachari **MARKETING:** Harpal Singh Gill

ANNUAL SUBSCRIPTIONS (UK/Europe, including post and packing)
FULL RATE: £1,400
PERSONAL RATES: UK £135; Europe €209; Rest of World £210
STUDENT RATES: UK £79; Europe €122; Rest of World £125
Individual rates apply to payments by personal cheque or credit card. Back issues: £20.00.

ANNUAL SUBSCRIPTIONS (USA, including post and packing)
INSTITUTIONAL/CORPORATE RATE: $2,730 ; **PERSONAL RATE:** $199; **STUDENT RATE:** $99;
POSTDOC RATE: $119
Printed in USA. Individual rates available only to subscribers paying by personal check or credit card. Orders for student/postdoc subscriptions must be accompanied by a copy of student ID. Rates apply to USA, Canada, Mexico/Central & South America. Add 7% GST tax in Canada (Canadian GST number 140911595). **BACK ISSUES:** US$20.00.

ANNUAL SUBSCRIPTIONS (Asia, including post and packing)
JAPAN: 本間購読料金： *Nature* のみ 437,800 円 +21,890 円(消費税) =459,690 円(含む)
Nature + *Nature Digest* 466,550 円 +23,328 円(消費税) =489,878 (含む)
お問い合わせ 日本出版貿易株式会社 国内営業 1 部
〒101-0064 東京都千代田区猿楽町1-2-1 Tel: 03-3292-3767 Fax: 03-3292-8766
個人/学生購読について
NPG ネイチャー アジア・パシフィック フルフィルメント & カスタマーサービス
〒162-0843 東京都新宿区市谷田町2-37 千代田ビル Tel: 03-3267-8759 Fax: 03-3267-8752
CHINA: www.natureasia.com/cn/subscribe; **KOREA:** www.natureasia.com/korea/subscribe

NATURE ONLINE WWW.NATURE.COM/NATURE

CHIEF TECHNOLOGY OFFICER: Howard Ratner **ASSOCIATE DIRECTOR, NATURE.COM:** Daniel Pollock
PLATFORM DEVELOPMENT: Jeremy Macdonald **WEB PRODUCTION:** Alexander Thurrell, Deborah Anthony **WEB DESIGN:** Juan-Carlos Sobrino, Luke Stavenhagen **PLATFORM INTERFACES:** Amanda Ward

SITE LICENCES, FULFILMENT & CUSTOMER SERVICES

SITE LICENCES: npg.nature.com/libraries feedback@nature.com
CHIEF OPERATIONS OFFICER: John Carroll **ASSOCIATE DIRECTOR OF OPERATIONS:** Dominic Pettit
CUSTOMER SERVICE: Gerald Coppin **ORDER PROCESSING OPERATIONS:** Steve Poulter

NATURE PUBLISHING GROUP OFFICES

LONDON: The Macmillan Building, 4 Crinan Street, London N1 9XW Tel: +44 (0)20 7833 4000 Fax: +44 (0)20 7843 4596/7

BASINGSTOKE: Nature Publishing Group, Subscriptions, Brunel Road, Basingstoke, Hants RG21 6XS, UK Tel: +44 (0)1256 329242

WASHINGTON DC: 968 National Press Building, 529 14th St NW, Washington DC 20045-1938 Tel: +1 202 737 2355

NEW YORK: 75 Varick St, 9th Floor, New York, NY 10013-1917 Tel: +1 212 726 9200

BOSTON: 25 First Street, Suite 104, Cambridge, MA 02141 Tel: +1 617 475 9275

SAN FRANCISCO: 225 Bush Street, Suite 1453, San Francisco, CA 94104 Tel: +1 415 403 9027

MUNICH: Nymphenburger Strasse 14, D-80335 München Tel: +49 89 549057-13

PARIS: Moulin de Malicorne, Sainte Maure de Touraine, Paris 37800 Tel: +33 2 47 35 72 15

TOKYO: Chiyoda Building, 2-37 Ichigayatamachi, Shinjuku-ku, Tokyo 162-0843 Tel: +81 3 3267 8751

INDIA: Nature Publishing Group, 3A, 4th Floor, DLF Corporate Park, Gurgaon 122002 Tel: +91 124 2881053/54

Nature® (ISSN 0028-0836) is published by Nature Publishing Group, a division of Macmillan Publishers Ltd (The Macmillan Building, 4 Crinan Street, London N1 9XW). Registered as a newspaper at the British Post Office. North and South American orders to subscriptions@nature.com (Tel: +1 866 363 7860). Other orders to subscriptions@nature.com (Tel: +44 (0)1256 329242; Fax +44 (0)1256 812358). Authorization to photocopy material for internal or personal use, or internal or personal use of specific clients, is granted by *Nature* to libraries and others registered with the Copyright Clearance Center (CCC) Transactional Reporting Service, provided the relevant copyright fee is paid direct to CCC, 222 Rosewood Drive, Danvers MA 01923, USA. Identification code for *Nature*: 0028-0836/03. CPC PUB AGREEMENT #40032744. In the US, *Nature* (ISSN 0028-0836) is published weekly on Thursday, except the last week in December by Nature Publishing Group, 75 Varick St, 9th Fl, New York NY 10013-1917, USA. US Periodicals postage paid at New York NY, and additional mailing post offices. US POSTMASTER: send address changes to *Nature*, Subscription Dept, 75 Varick St, 9th Fl, New York NY 10013-1917, USA. Published in Japan by NPG Nature Asia-Pacific, Chiyoda Building, 2-37 Ichigayatamachi, Shinjuku-ku, Tokyo 162-0843, Japan. © 2012 Macmillan Publishers Limited. All rights reserved.

nature EDUCATION

ANNOUNCING

Principles of Biology

An interactive textbook solution by Nature Education

A learning solution designed to bridge students from the classroom to the lab.

200 customizable mini-chapters created by dozens of scientists, instructors, and editors	200+ online interactive exercises to give students a hands-on way to apply their knowledge	50 Science Techniques units cultivating real scientific skills, including data analysis	3000+ assessment questions integrated into lessons
Synopses and links to milestone research papers from *Nature* and other journals	Affordably priced for all students	Optional color print companion	Access on all devices:

Learn more at **www.nature.com/principles**

nature publishing group npg

NEW ENGLAND BioLabs Inc.
enabling technologies in the life sciences

Mix it up.

RE-Mix™ Restriction Enzyme Master Mixes

Restriction enzyme digests are now even easier! The same high quality restriction enzymes that you have come to trust from New England Biolabs are now available in master mix format; simply add your DNA and digest.

With RE-Mix Master Mixes take advantage of:

- Simplified and shortened protocols
- Fast digestion in 15 minutes (Time-Saver qualified)
- High product quality with reproducible results

RE-Mix Master Mixes – just add your DNA and mix

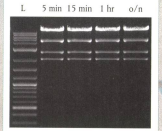

pXba DNA was digested with EcoRV-HF™ RE-Mix™ according to the recommended protocol. Lane L is the TriDye™ 2-Log DNA Ladder (NEB #N3270). The same results are obtained whether incubated for 5–15 minutes, 1 hour or overnight.

For more information, visit
www.NEBREMIX.com

Blue-footed Booby (Sula nebouxii)
© Tui De Roy

THIS WEEK

EDITORIALS

CLIMATE Dishonesty is a weapon not suited to scientists **p.440**

WORLD VIEW How Alan Turing managed to go from zero to hero **p.441**

GOING DOWN Madagascan jungle harbours smallest lizard **p.442**

Flu papers warrant full publication

Although more debate is needed, the benefits of publishing sensitive data outweigh the risks that have so far been made public.

"No one should presume to know all the ways in which influenza virus could be misused, and the motivations for doing so, but the consequences could be catastrophic. There are many scenarios to consider, ranging from mad lone scientists, desperate despots and members of millennial doomsday cults to nation states wanting mutually assured destruction options, bioterrorists or a single person's random acts of craziness. These are low-probability events, but they could introduce a new evolutionary H5N1 seed into the environment that seems not to exist in nature. This might not cause a pandemic instantly, but it could start the virus on a new path for pandemic evolution."

That is the rationale provided by Paul Keim, acting chair of the US National Science Advisory Board for Biosecurity (NSABB), in response to questions posed by *Nature* (P. S. Keim *Nature* **482,** 156–157; 2012) about the NSABB's recommendation that recent work on the transmissibility in mammals of artificial strains of avian H5N1 influenza virus should not be published in full. The work was conducted in ferrets — generally considered the best animal models for human transmission — and shows that avian H5N1 viruses have a greater potential to evolve into transmissible forms in mammals, including humans, than had been thought. The work is reported in two papers accepted but not yet published in *Nature* and *Science*.

Last week, a group of flu and public-health experts gathered at the World Health Organization (WHO) headquarters in Geneva, Switzerland, to discuss the matter (see go.nature.com/uyr1uu). And it was clear at the meeting that the above opening quote expresses the only rationale that attendees had received.

To its credit and that of the US government, the NSABB is the only body in the world set up to review these issues in a systematic fashion. It includes ex-officio representatives of all relevant government departments (including intelligence and security agencies), as well as independent researchers. The NSABB's guidance was an important first step in public consideration of the impacts and potential regulation of such research. The second step was last week's meeting at the WHO — again, like the NSABB, a body empowered only to make recommendations.

Some context is important in considering the issues surrounding publication. In 2003, *Nature* and many other journals met to establish editorial procedures for considering papers that have public-health and scientific benefits but that might also have biosecurity risks (see *Nature* **421,** 771; 2003). The statement that emerged from that meeting envisaged the possibility that a journal would reject a paper if it was clear that the risks of publication outweighed the benefits. *Nature* accordingly used independent advisers in considering the submission of the latest paper, and most of the advisers recommended publication in full. This is also the first paper submitted to any *Nature* journal for which recommendations have been made against publication on biosecurity grounds.

Rather than simply reject the papers, given also the NSABB's opinion, both *Nature* and *Science* decided to investigate another option: to publish a redacted version omitting key methods and data. But a condition of such an approach was that a method should exist for distributing a full version to those in need of the results for public-health reasons and those capable of pursuing the science. Both journals accordingly prepared full and redacted versions.

Those at the WHO meeting, under conditions of strict security, examined both versions of the two papers. It had already been said in blogs and news coverage that, because the methods used are not novel, and because one of the papers had been presented at an open meeting, redaction would be pointless. As one WHO participant said: "It was only when I'd seen both versions that I realized how ineffective redaction would be." What was also concluded was that a system for distributing the full paper only to selected individuals would be impossible to set up on any relevant timescale.

"There is already a substantial immediate risk to humans."

But what also became clear, partly from unpublished data, was that not only does the mammalian transmissibility threat seem greater than previously thought, but also that current avian viruses have some of the mutations identified in the new work. In other words, there is already a substantial immediate risk to humans. The meeting also concluded that the new data are of value for surveillance, and that the results should be built on to explore the mechanisms underlying transmissibility and the high fatality rate observed in humans infected by H5N1.

Given the inadequacy of redaction, and the immediate risks to global public health, the biosecurity objections expressed above seem too general and hypothetical to justify obstructing publication and further research. Moreover, with regard to the NSABB's recommendations and the recommendations of the WHO meeting (see go.nature.com/ky2skc), neither of the discussions that preceded them were sufficiently inclusive of the security, societal and research interests at stake.

Therefore, further discussion is essential. That must include a review of the safety regimes (lab equipment, buildings and practices) in which future work should be conducted. The two laboratories in which the latest research originated are categorized as 'BSL-3 enhanced' (see *Nature* **480,** 421–422; 2011), a classification that, although rigorous in these cases, is not well defined in general. The Public Health Agency of Canada has deemed the highest level of BSL-4 to be required (see page 447). Safety-standards committees in the United States and Europe are currently assessing required safety levels, and may report within a few weeks.

As was agreed by the journals and the lead authors at the meeting, publication of the papers must wait at least for the outcome of those discussions. There may yet be regulatory or legal obstacles to publication, or biosecurity or biosafety risks sufficient to outweigh the health risks. Otherwise, it is *Nature*'s view that the papers should ultimately be published in full. ■

Turing at 100

This year marks the centenary of the birth of Alan Turing. He deserves your attention.

Come the summer, many minds will turn to sport as the London Olympics kicks off. So it seems apt that, in a special issue this week, *Nature* invites its readers to embrace and celebrate a superb marathon runner — who also happened to be one of the brightest minds of all time.

Alan Turing, computer pioneer, wartime code-breaker and polymath, was born in London on 23 June 1912. But for injury, he would probably have joined the British Olympic team for the London games of 1948. (His personal best marathon time of 2 hours and 46 minutes was barely 11 minutes behind the gold medallist that year.) Yet, 100 years and one month after his birth, when the Olympics will return to the city, no official celebration of the connection is planned. An opportunity to bring an intellectual giant — and science itself — to the attention of the international public will be missed.

Turing's marathon time gives us an objective quantification of his physical excellence. His scientific genius and legacy, however, are much more difficult to measure — as his biographer, Andrew Hodges, a mathematician at the University of Oxford, UK, points out on page 441. Still, setting aside quarrels over his role in the development of the computer, the scientific world should stand together and relish the wonderful diversity of a universal mind. (See the special section starting on page 455 and www.nature.com/turing for more.)

The scope of Turing's achievements is extraordinary. Mathematicians will honour the man who cracked David Hilbert's *Entscheidungsproblem* or 'decision problem', and cryptographers and historians will remember him as the man who broke Nazi Germany's Enigma code and helped to shorten the Second World War. Engineers will hail the founder of the digital age and artificial intelligence. Biologists will pay homage to the theoretician of morphogenesis, and physicists will raise a glass to the pioneer of nonlinear dynamics. Philosophers, meanwhile, are likely to continue to frown over his one-liners on the limits of reason and intuition: "If a machine is expected to be infallible, it cannot also be intelligent," he said in a 1947 talk to the London Mathematical Society.

Turing demonstrated a terrific ability to combine first-hand experimentation, keen observation, rigorous theory and practical application. His multidisciplinary approach alone makes him of interest to this journal, yet questions still arise on whether the best papers in pure mathematics, computer science and artificial intelligence should be published in *Nature*. We certainly think so.

"Turing's mind was truly his own, and this contributed to the tragedy of his life."

So, too, do the researchers invited to decode Turing's legacy in a series of Comment articles, starting on page 459. They are thought-provoking pieces in their own right, but, more importantly, we hope that they will entice readers to seek out Turing's original work (see, for example, B. J. Copeland (ed.) *The Essential Turing*; Clarendon, 2004). His papers are models of accessibility and clarity, despite their extreme conceptual depth and intellectual rigour. Even his throwaway comments — about symmetry in physics versus biology, randomness in intelligence, learning in unorganized machines, or emotions in extrasensory perception, for example — are gems.

Turing's mind was truly his own, and this contributed to the tragedy of his life. Turing was persecuted by the British authorities for his homosexuality, and used cyanide to take his own life, aged 41.

That 2012 will see numerous events commemorating Turing worldwide (see, for example, www.turingcentenary.eu) is almost entirely down to volunteers, who have received little or no official help. This is in stark contrast to the World Year of Physics in 2005, when the German state helped to promote the centenary of Albert Einstein's 'miracle year', in which he published his four groundbreaking papers.

What could 2012, the Alan Turing year, be named? *Nature* suggests 'The Year of Intelligence'. Of the finest types of intelligence — human, artificial and military — Turing is perhaps the only person to have made a world-changing contribution to all three. Use this special issue, and the rest of 2012, to discover and make up your own mind about this extraordinary man. ■

Over the line

Dishonesty, however tempting, is the wrong way to tackle climate sceptics.

In a much-quoted Editorial in March 2010 (*Nature* **464,** 141; 2010), this publication urged researchers to acknowledge that they are involved in a street fight over the communication of climate science. So would it now be hypocritical to condemn Peter Gleick for fighting dirty? Gleick, a hydroclimatologist and president of the Pacific Institute for Studies in Development, Environment and Security in Oakland, California, admitted in a statement on news website *The Huffington Post* on 20 February that he had duped the Heartland Institute, a right-wing think tank based in Chicago, Illinois, into handing over documents that detailed its financial support for climate sceptics. Gleick had passed these documents on to the website DeSmogBlog.com, which made them public on 14 February.

Gleick's deception — using an e-mail address set up in someone else's name to request the documents from Heartland — is certainly in line with some of the tactics used to undermine climate science. When in November 2009 a hacker distributed thousands of e-mails stolen from climate researchers at the University of East Anglia in Norwich, UK, Heartland was prominent among those who criticized not the hacker, but the scientists who wrote the messages. However, Gleick, as he has admitted, crossed an important line when he acted in such a duplicitous way. It was a foolish action for a scientist, especially one who regularly engages with the public and critics. Society rightly looks to scientists for fairness and impartiality. Dishonesty, whatever its form and motivation, is a stain on the individual and the profession. Gleick does deserve credit for coming clean — but, it must be said, he did so only after he was publicly accused on the Internet of being involved.

The original accusation, incidentally, was more serious: that Gleick had deliberately forged a Heartland Institute memo that brought together, with suspicious convenience, the most incriminating sections of the other climate documents, which seem to have been presented to the Heartland board meeting in January. He denies doing so, and says that he received the memo, in which he is named and which Heartland says has been faked, separately from an anonymous source. The e-mail chicanery, he says, was an attempt to check whether it was genuine.

In his statement on Monday, Gleick said: "My judgment was blinded by my frustration with the ongoing efforts — often anonymous, well-funded, and coordinated — to attack climate science and scientists and prevent this debate, and by the lack of transparency of the organizations involved. Nevertheless I deeply regret my own actions in this case."

On 24 January, Gleick had published another article in *The Huffington Post*, entitled 'Climate Change: Sifting Truth From Lies in a Complex World'. As he now knows, the best way for scientists to help people find this truth is through open and honest debate. ■

➲ **NATURE.COM**
To comment online, click on Editorials at:
go.nature.com/xhnnqv

EPITOMICS®
BETTER ANTIBODIES • BETTER SCIENCE

SPECIAL OFFER
$129 AKT RABMABS
Find out more @
www.epitomics.com/akt

RabMAbs® = Better AKT Antibodies

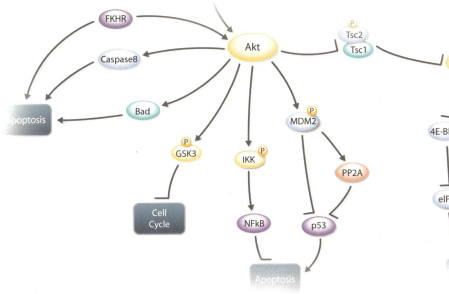

- **High quality antibodies to Akt and related proteins**
- **Validated in WB, IHC, IF, IP and FACS**
- **Over 7000 antibodies and counting**

At Epitomics, we provide a wide range of high quality antibodies to Akt and related proteins. Using our patented Rabbit Monoclonal Antibody (RabMAb®) technology, we have developed a collection of high quality Akt specific antibodies. Each Akt specific RabMAb offers superior antigen recognition of the rabbit immune system and the specificity of a monoclonal antibody.

Find out more @ www.epitomics.com/akt

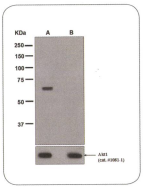

Akt1 Phospho (pT450)

Western blot analysis on NIH/3T3 cell lysate using anti-Akt1 Phospho (pT450) RabMAb (cat. #3188-1). Cells were either (A) untreated or (B) treated with Lambda Phosphatase.

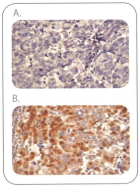

Akt1 Phospho (pS473)

Immunohistochemical staining of human cervical carcinoma tissue using anti-Phospho-Akt1 (pS473) RabMAb (cat. # 2118-1). Tissue was (A) phosphatase treated and (B) untreated.

Antibody Satisfaction Guarantee

www.epitomics.com

US & Canada | 1-877-772-2622
Outside NA | 650-583-6688
info@epitomics.com

Cellular & Molecular Immunology

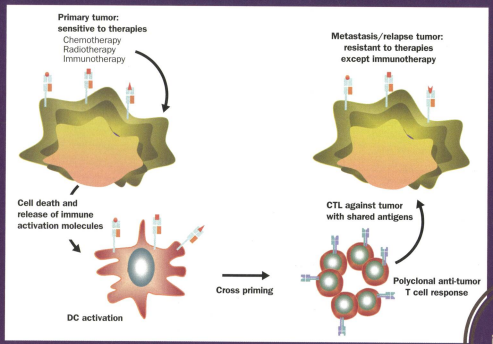

Special issue and Web Focus

Cancer Immunology

The January special issue of *Cellular & Molecular Immunology* presents two important strategies for generating potent and lasting anti-tumor immunity. Further background information on this important topic is available through the accompanying web focus which links to related articles from across Nature Publishing Group.

Featured articles include:

Bone marrow and the control of immunity
Ende Zhao, Huanbin Xu, Lin Wang, Ilona Kryczek, Ke Wu, Yu Hu, Guobin Wang and Weiping Zou

Targeting and utilizing primary tumors as live vaccines: changing strategies
Xuanming Yang, Eric D Mortenson and Yang-Xin Fu

Optimal culture conditions for the generation of natural killer cell-induced dendritic cells for cancer immunotherapy
Je-Jung Lee *et al.*

Anti-γδ TCR antibody-expanded γδ T cells: a better choice for the adoptive immunotherapy of lymphoid malignancies
Jianhua Zhou, Ning Kang, Lianxian Cui, Denian Ba and Wei He

To access the Special Issue and Web Focus on Cancer Immunology visit:
www.nature.com/CMI/focus/cancer_immunology/

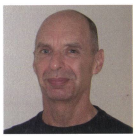

The man behind the machine

Alan Turing is famous for many reasons. **Andrew Hodges** *delves into why Turing's achievements took so long to be recognized.*

Alan Turing is always in the news — for his place in science, but also for his 1952 conviction for having gay sex (illegal in Britain until 1967) and his suicide two years later. Former Prime Minister Gordon Brown issued an apology to Turing in 2009, and a campaign for a 'pardon' was rebuffed earlier this month.

Must you be a great figure to merit a 'pardon' for being gay? If so, how great? Is it enough to break the Enigma ciphers used by Nazi Germany in the Second World War? Or do you need to invent the computer as well, with artificial intelligence as a bonus? Is that great enough?

Turing's reputation has gone from zero to hero, but defining what he achieved is not simple. Is it correct to credit Turing with the computer? To historians who focus on the engineering of early machines, Turing is an also-ran. Today's scientists know the maxim 'publish or perish', and Turing just did not publish enough about computers. He quickly became perishable goods. His major published papers on computability (in 1936) and artificial intelligence (in 1950) are some of the most cited in the scientific literature, but they leave a yawning gap. His extensive computer plans of 1946, 1947 and 1948 were left as unpublished reports. He never put into scientific journals the simple claim that he had worked out how to turn his 1936 "universal machine" into the practical electronic computer of 1945. Turing missed those first opportunities to explain the theory and strategy of programming, and instead got trapped in the technicalities of primitive storage mechanisms.

He could have caught up after 1949, had he used his time at the University of Manchester, UK, to write a definitive account of the theory and practice of computing. Instead, he founded a new field in mathematical biology and left other people to record the landscape of computers. They painted him out of it. The first book on computers to be published in Britain, *Faster than Thought* (Pitman, 1953), offered this derisive definition of Turing's theoretical contribution:

"Türing machine. In 1936 Dr. Turing wrote a paper on the design and limitations of computing machines. For this reason they are sometimes known by his name. The umlaut is an unearned and undesirable addition, due, presumably, to an impression that anything so incomprehensible must be Teutonic."

That a book on computers should describe the theory of computing as incomprehensible neatly illustrates the climate Turing had to endure. He did make a brief contribution to the book, buried in chapter 26, in which he summarized computability and the universal machine. However, his low-key account never conveyed that these central concepts were his own, or that he had planned the computer revolution.

The 1955 Royal Society's obituary of Turing, written by mathematician Max Newman, did him few favours when it claimed that computer designers were unaware of Turing's 1936 work. The Turing machines soon made a comeback, but Turing's image had become that of a pure mathematical logician, unrelated to practicality. It did not help that anyone looking into his story after his death would see dark hints that he had been *persona non grata* in an unmentionable manner — possibly excusable for a remote theorist from Cambridge University, but totally inappropriate for the founder of a mega-industry.

Yet the mid-1970s revealed Turing to have been highly practical: the chief scientific figure at code-breaking headquarters Bletchley Park, and in charge of methods and state-of-the-art machines for beating the German navy. Now it was clear why he had emerged as a computer builder in 1945 — he had gained experience he could never reveal. By the 1970s, there was also more room for his vision of computation. Software for "every known process", as he foresaw in 1946, was on the way. Turing's vision of mind and machine, which drew from his personal consciousness and experience, also became more acceptable. When in 1977 I started to investigate Turing's life, I found that his code-breaking was the hidden bridge between the 1936 theory and the "universal practical computing machine" he described in his unpublished 1948 work.

ANYONE LOOKING INTO HIS **STORY** AFTER HIS DEATH WOULD SEE **DARK HINTS** THAT HE HAD BEEN *PERSONA NON GRATA*.

On the question of individual reputation, in that 1948 report he wrote: "The isolated man does not develop any intellectual power. It is necessary for him to be immersed in an environment … He may then perhaps do a little research of his own and make a very few discoveries … the search for new techniques must be regarded as carried out by the human community as a whole, rather than by individuals." Science is like that, and he effaced himself in that spirit. But he was a star nonetheless.

What would Turing have thought of the campaign for his 'pardon'? When arrested, he was unrepentant and told police he expected a "Royal Commission to legalize it". Sixty years later, British law has caught up, not for him as a special case, but as a matter of principle. That practical action speaks louder than symbolic words, and is truer to his vision. I see the question not as whether the government should have pardoned Turing, but how on Earth Turing could ever have pardoned the government. ■

TURING AT 100
A legacy that spans science:
nature.com/turing

Andrew Hodges *is a mathematician at the University of Oxford, UK, and author of* Alan Turing: the Enigma.
e-mail: andrew.hodges@wadh.ox.ac.uk

RESEARCH HIGHLIGHTS

Selections from the scientific literature

BIOPHYSICS

Claustrophobic DNA in tug of war

When a long thin polymer such as DNA is forced into a confined space — say a small membrane channel — it loses some of its freedom, and hence its entropy. Regaining that entropy is a powerful driving force for escape.

Chia-Fu Chou at the Academia Sinica in Taipei and his colleagues used an electric pulse to force a single DNA molecule to extend from one microchannel to another through a restrictive gap just nanometres high. When the electric field was turned off, a tug-of-war lasting from seconds to minutes occurred as both ends of the DNA tried to pull out of the nanometre-sized space. Eventually, one side won and the DNA retracted.

The forces acting on the DNA depended only on the height of the confined passage between channels, and not on its length or the length of DNA passing through it. This understanding could aid applications from molecular filters to nanopore transporters, the authors say. ***Nano Lett.*** **http://dx.doi.org/10.1021/nl2045292 (2012)**

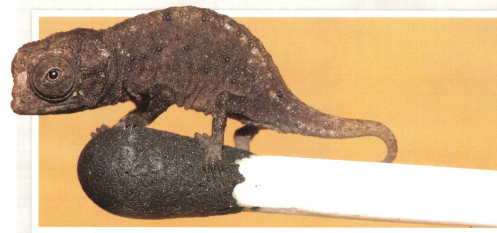

J. KOEHLER

EVOLUTION

Lilliputian lizards come to light

The forests of northern Madagascar harbour a dwarf chameleon that is the smallest lizard in the world in terms of total length. Adult males of the diminutive *Brookesia micra* reach a length of less than 24 millimetres.

B. micra and three other tiny lizard species were discovered in the region's rainforests and dry forests. Miguel Vences at the Technical University of Braunschweig in Germany and his group analysed tail length and head width, male genital morphology and gene sequences to place each species within the chameleon taxonomy. All occupy a small, discrete geographical range, and probably evolved some 10 million to 20 million years ago, the authors suggest. ***PLoS ONE*** **7, e31314 (2012)**

CELL SIGNALLING

Sideways activation

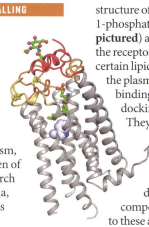

SCIENCE/AAAS

Elucidation of a cell receptor's crystal structure has revealed a unique lateral docking mechanism, report Hugh Rosen of the Scripps Research Institute in La Jolla, California, and his colleagues.

G-protein-coupled receptors (GPCRs) are signalling molecules that span the plasma membranes of cells and are generally activated by external molecules that pass through a channel-like opening into a binding site. However, the researchers determined the crystal structure of the sphingosine 1-phosphate receptor 1 ($S1P_1$, **pictured**) and showed that the receptor is triggered by certain lipids passing through the plasma membrane and binding through the lateral docking mechanism.

They also found that $S1P_1$ has atypical binding sites in less conserved regions of the docking site and that compounds that adhere to these activate $S1P_1$ more specifically than do lipids. ***Science*** **335, 851–855 (2012)**

BIOLOGY

Immunity's circadian link

Daily patterns in the body's biochemical and physiological processes called circadian rhythms may influence immune-system function. Erol Fikrig and his colleagues at Yale University in New Haven, Connecticut, have found that the expression of an immune protein called TLR9 rises and falls with the circadian cycle.

They induced sepsis in mice to examine whether pathogen recognition — a key part of the immune response — varies with circadian cycles. Higher TLR9 expression at the time of sepsis induction was linked to a worse outcome for mice. This suggests that daily fluctuations in biological processes may influence vulnerability to infections, as well as the efficacy of immune therapies such as TLR9 agonists, which are currently in development. ***Immunity*** **http://dx.doi.org/10.1016/j.immuni.2011.12.017 (2012)**

STEM-CELL BIOLOGY

Restore my beating heart

Infusions of a patient's own cardiac stem cells may reduce scar tissue and promote heart-muscle growth after a heart attack, according to a small safety study. Eduardo Marbán of the Cedars-Sinai Heart Institute in Los Angeles, California, and his colleagues harvested heart cells from 17 heart-attack patients. The cells were used to grow cardiac stem

cells that were then reinfused.

Six months later, patients had 28% less scar tissue mass than control patients who did not receive the infusion. Viable heart tissue mass also increased following the treatment, suggesting partial restoration of tissue lost during the heart attack. However, patients showed no improvement in several measurements of heart function, such as the volume pumped out of the left ventricle with each heartbeat.

Lancet **http://dx.doi.org/10.1016/S0140-6736(12)60195-0 (2012)**

GENOMICS

Loss-of-function found in droves

Genome-sequencing work has suggested that even healthy humans carry hundreds of 'loss of function' (LoF) mutations that seriously disrupt protein-coding genes. Daniel MacArthur at the Wellcome Trust Sanger Institute in Hinxton, UK, and his colleagues performed extensive analysis on 185 genomes and determined that a typical individual carries around 100 LoF variants, of which about 20 inactivate both copies of a gene.

Most of the common mutations occurred in non-essential genes and didn't seem to affect health. The team also identified many rare LoF variants found in less than 1% of the population, including 47 serious disease mutations in one copy of a gene. By studying differences between the harmful and neutral variants, the scientists developed an algorithm to prioritize mutations found in medical genome sequencing for further investigation.

Science **335, 823–828 (2012)**

ASTROPHYSICS

Zombie star rising

When a star suddenly brightened in 1961, many assumed it had died in a supernova — but it seems that the light has not yet gone out. Schuyler Van Dyk at the California Institute of Technology in Pasadena and Thomas Matheson at the National Optical Astronomy Observatory in Tucson, Arizona, examined ground- and space-based observations, and say that it still lives.

The duo reports that the star, designated 'Object 7', can be seen on the Hubble Space Telescope as a luminous blue variable (LBV) star. The authors suggest that the decades-old outburst could represent a 'supernova imposter', a type of explosion for which LBVs are known that doesn't destroy the parent star. Nevertheless, Object 7 may be on course to explode, and astronomers should look out for its stellar death rattle.

Astrophys. J. **746, 179 (2012)**

IMMUNOLOGY

Immune system master switch

The fetal immune system develops from stem cells in the liver, whereas the immune cells that protect adults form in the bone marrow. Moreover, early in life the immune system contains cells that quickly respond to only a limited number of foreign molecules; adult immune cells can recognize almost anything that might harm a host.

A 'master-switch' gene called *Lin28b* accounts for these differences, report Stefan Muljo and his team at the National Institute of Allergy and Infectious Diseases in Bethesda, Maryland. *Lin28b* — which blocks a class of gene-regulating RNA fragments called microRNAs — is active in the stem cells that form a mouse's immune system early in life, yet is absent from adult bone marrow. Marrow cells engineered to express a closely related gene, *Lin28*, and transplanted into adult mice form fetal-like immune cells.

Because the fetal-like immune cells are known to be effective against some pathogens, cancers and other diseases, coaxing transplanted bone marrow cells to take on fetal properties could be used to improve immune responses.

Science **http://dx.doi.org/10.1126/science.1216557 (2012)**

COMMUNITY CHOICE

The most viewed papers in science

CHEMISTRY

Simple solution for tricky chemistry

HIGHLY READ on pubs.acs.org in January

Chemists have invented a reagent to ease the addition of a desirable chemical group to many useful compounds. Pharmaceutical, medicinal and agricultural chemists add fluorine groups to molecules to improve certain properties — to lower toxicity, for example. However, adding a difluoromethyl group has proved complicated.

The process developed by Phil Baran at the Scripps Research Institute in La Jolla, California, and his colleagues does the job in a simple one-pot reaction. The authors used zinc difluoromethylsulphinate salt, a white powder that is soluble in water and stable in air, making it easy to handle. In water, this produces a reactive difluoromethyl radical that targets specific sites on other molecules.

In particular, Baran's reagent can add a difluoromethyl group to nitrogen-containing aromatic ring systems and onto some organic molecules containing sulphur.

J. Am. Chem. Soc. **134, 1494–1497 (2012)**

ZOOLOGY

Antifreeze's role in fish spread

Antifreeze proteins in the bodily fluids of Antarctic fishes are a crucial adaptation to life in the freezing waters — but their appearance alone is insufficient to explain the huge diversity of the region's fish species. Thomas Near of Yale University in New Haven, Connecticut, and his colleagues constructed a phylogeny of these notothenioid fishes (a sample **pictured**) and correlated it to both the appearance of the proteins and changes in global climate.

Contrary to the perception that the appearance of antifreeze proteins was the crucial factor driving evolution, they found that the most species-rich lineages diversified at least 10 million years after the proteins' appearance. This bout of evolution happened during a second cooling event in the Late Miocene (11.6 million to 5.3 million years ago), when ice activity in the Southern Ocean is thought to have increased. The authors suggest that the appearance of this new polar habitat, combined with the pre-existing antifreeze proteins, spurred the evolution of notothenioids.

T. J. NEAR

Proc. Natl Acad. Sci. USA **http://dx.doi.org/10.1073/pnas.1115169109 (2012)**

NATURE.COM

For the latest research published by *Nature* visit:
www.nature.com/latestresearch

POLICY

Flu work freed

Two studies that created ferret-transmissible strains of the highly pathogenic avian H5N1 influenza A virus should be published in full, a meeting of 22 experts convened by the World Health Organization in Geneva, Switzerland, concluded on 17 February. Last December, the US government and the US National Science Advisory Board for Biosecurity had asked that the research be censored. See pages 439 and 447 for more.

Climate politics

A high-profile water and climate scientist acknowledged on 20 February that he had dishonestly acquired internal budget documents from the Heartland Institute, a libertarian think tank in Chicago, Illinois, that aims to combat climate science. Peter Gleick, president of the Pacific Institute in Oakland, California, released the documents to environmental website DeSmogBlog. Heartland has not disputed the authenticity of most of the papers, but says that a strategy memo — which Gleick says he received anonymously — is fake. See go.nature.com/v1zrbu and page 440 for more.

Animal testing

Tens of millions of animals have been saved from use in chemical safety tests, after Europe's chemical regulator gave the go-ahead to a streamlined method for checking substances' effects on animals' reproductive systems. Toxicologists have been concerned that up to 54 million animals could be required for extra tests mandated by the European Union's sweeping 2007 chemicals legislation — with most of the increase down to reproductive-toxicity tests that have to be done in two generations of animals. But on 15 February, the European Chemical Agency, based in Helsinki, approved a test that uses only one generation. See go.nature.com/optzux for more.

AIDS budget cut

Health advocates said last week that they were dismayed by planned cuts to the US administration's global AIDS programme. According to the Kaiser Family Foundation, health-policy analysts headquartered in Menlo Park, California, President Barack Obama's 2013 budget request would cut 13% (US$543 million) from the US state department's support for HIV work, although it would add 27% ($350 million) to the Global Fund to Fight AIDS, Tuberculosis and Malaria. See go.nature.com/rcdhhv for more.

Iran concern

Iran has responded to tightened trade sanctions by claiming that it has made technical advances in its nuclear programme, including building a new generation of centrifuges to enable faster enrichment of uranium. Diplomats from the United States and Europe dismissed the pronouncements on 15 February as political bluster. As *Nature* went to press, inspectors from the International Atomic Energy Agency in Vienna were visiting Tehran to discuss Iran's nuclear programme for the second time in three weeks.

Drug trials rap

On 14 February, three senior Democrats in the US House of Representatives questioned the National Institutes of Health and the Food and Drug Administration over their apparent failure to enforce the public reporting of clinical-trial results. Under a 2007 act, sponsors must report the results of trials of already-approved drugs and devices on clinicaltrials.gov within a year of completion — or be fined. A study (A. P. Prayle *et al. Br. Med. J.* **344,** d7373; 2012)

S. MARAI/AFP/GETTY

The struggle against soot

An international coalition has launched a modest fund to curb emissions of methane, black carbon (soot) and other short-lived climate-affecting pollutants (see *Nature* **481,** 245–246; 2012). The United States, Canada, Sweden, Mexico, Bangladesh and Ghana founded the programme, which was unveiled in Washington DC on 16 February. With initial funding of US$15 million, it will aim to support projects such as cleaning up inefficient biomass stoves, brick kilns (pictured, in Kabul), diesel vehicles and coke ovens; and reducing gas leakage from rice paddies, landfills, wastewater systems and oil and gas extraction. See go.nature.com/nu3ak5 for more.

published in January found that results of only 22% of 738 trials completed in 2009 were reported in time.

RESEARCH

Fracking risks

There is little or no evidence that fracking — pumping high-pressure fluids into shale to force out natural gas — has contaminated groundwater, according to a university-funded report (see go.nature.com/sopiwm) from researchers assembled by the Energy Institute at the University of Texas at Austin. The report, released on 16 February at the meeting of the American Association for the Advancement of Science in Vancouver, Canada, found that harm ascribed to the controversial technique could usually be traced to above-ground chemical spills or problems common to all oil and gas drilling operations, such as casing failures.

Dioxin health risk

The US Environmental Protection Agency has released a long-delayed assessment of the health risks of dioxins — work that has taken more than two decades to produce. In line with its 2010 draft report, the agency recommends a safe consumption limit for the chemicals that is well below that proposed by the World Health Organization. But it also says that current exposure to dioxins "does not pose a significant health risk". See go.nature.com/dh3ary for more.

EVENTS

Greek robbery

Greece's economic suffering has been compounded by desecration of its archaeological heritage, with the robbery of 77 artefacts from the Museum of the History of the Olympic Games in Olympia on 17 February. Culture minister Pavlos Geroulanos offered to resign after the theft, which ministry officials said included a 3,300-year-old gold ring and a 2,400-year-old oil jar.

BUSINESS

Nanopore sequencer

Oxford Nanopore Technologies, a UK firm that promises its technology could theoretically sequence a human genome in 15 minutes, impressed scientists with the first public presentation of its data on 17 February, at the Advances in Genome Biology and Technology meeting in Marco Island, Florida. The technology identifies bases in real time by measuring electrical conductivity as a DNA strand is fed through a biological nanopore. The company expects to start selling its machine in the second half

of this year, and plans to sell a miniaturized, disposable sequencer (**pictured**) for less than US$900. See go.nature.com/evpc1e for more.

PEOPLE

Nobel laureate dies

Virologist Renato Dulbecco, who shared the 1975 Nobel Prize in Physiology or Medicine, died on 19 February, aged 97. Dulbecco won the Nobel for work in the 1950s and '60s showing that some viruses insert their genes into the genomes of the cells they infect, and that these changes can trigger cancer. Born in Italy, Dulbecco also worked in the United States and Britain. From 1988 to 1992 he was president of the Salk Institute for Biological Studies in San Diego, California.

MIT head resigns

The first female president of the Massachusetts Institute of Technology (MIT) in Cambridge has announced that she will resign the post, after seven years in charge. Susan Hockfield, a neuroscientist, has headed MIT since 2004; she previously spent two decades at Yale University in New Haven, Connecticut, including time as provost. On 16 February she said that she would step down when a successor was appointed, to pave the way for a new fund-raising effort.

Italy research head

Italy's multidisciplinary National Research Council (CNR), which runs more than 100 institutes and research centres, finally has a new president. It should now be able to implement a 2009 law intended to make the country's research system more transparent and meritocratic (see *Nature* **476**, 386; 2011). The reform has dragged on because outgoing CNR president Francesco Profumo, appointed last August, declined to resign the post after becoming national research minister last November. On 18 February, after Profumo was finally pressed into resignation, Luigi Nicolais, a chemical engineer who is also a member of parliament, was appointed as president of the CNR.

COMING UP

26–29 FEBRUARY
In Washington DC, scientists and policy-makers discuss research and political efforts on biodefence and bioterrorism, including work that created mutant influenza.
go.nature.com/xnsfjz

27 FEB–2 MARCH
Graphene, solar-energy technology and nanoscience remain hot topics at this year's American Physical Society meeting in Boston, Massachusetts.
go.nature.com/6m7ekb

TREND WATCH

A study of the careers of nearly 3,000 tenure-track science and engineering assistant professors in 14 US universities suggests that men and women are retained and promoted at about the same rate, spending a median time of 10.9 years at their first university. But in mathematics, women leave significantly sooner than men (see chart). A problem lies in hiring: only 27% of incoming academics are women, the authors point out. See go.nature.com/nn23z1 for more.

RETAINING SCIENCE TALENT

Men and women hired by US science and engineering faculties are retained at about the same rate — except in mathematics.

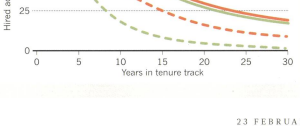

SOURCE: S. KAHN/BSKYABS

NATURE.COM
For daily news updates see:
www.nature.com/news

IBMS BoneKEy

BoneKEy Knowledge Environment

The premier online global network for bone health professionals

GET THE TAG READER FOR YOUR PHONE: GETTAG.MOBI
SCAN & REGISTER. FREE ACCESS TO REGISTERED USERS.

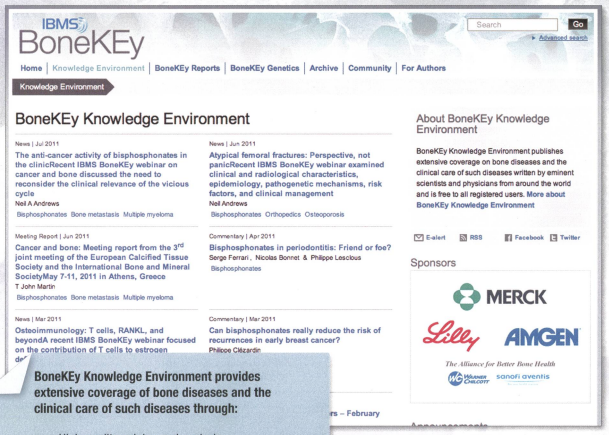
IBMS BoneKEy
Search
Go
Advanced search
Home | Knowledge Environment | BoneKEy Reports | BoneKEy Genetics | Archive | Community | For Authors
Knowledge Environment
BoneKEy Knowledge Environment
News | Jul 2011
The anti-cancer activity of bisphosphonates in the clinicRecent IBMS BoneKEy webinar on cancer and bone discussed the need to reconsider the clinical relevance of the vicious cycle
Neil A Andrews
Bisphosphonates Bone metastasis Multiple myeloma
News | Jun 2011
Atypical femoral fractures: Perspective, not panicRecent IBMS BoneKEy webinar examined clinical and radiological characteristics, epidemiology, pathogenetic mechanisms, risk factors, and clinical management
Neil Andrews
Bisphosphonates Orthopedics Osteoporosis
Meeting Report | Jun 2011
Cancer and bone: Meeting report from the 3rd joint meeting of the European Calcified Tissue Society and the International Bone and Mineral SocietyMay 7-11, 2011 in Athens, Greece
T John Martin
Bisphosphonates Bone metastasis Multiple myeloma
Commentary | Apr 2011
Bisphosphonates in periodontitis: Friend or foe?
Serge Ferrari, Nicolas Bonnet & Philippe Lesclous
Bisphosphonates
News | Mar 2011
Osteoimmunology: T cells, RANKL, and beyondA recent IBMS BoneKEy webinar focused on the contribution of T cells to estrogen
Commentary | Mar 2011
Can bisphosphonates really reduce the risk of recurrences in early breast cancer?
Philippe Clézardin
About BoneKEy Knowledge Environment
BoneKEy Knowledge Environment publishes extensive coverage on bone diseases and the clinical care of such diseases written by eminent scientists and physicians from around the world and is free to all registered users. More about BoneKEy Knowledge Environment
E-alert RSS Facebook Twitter
Sponsors
MERCK
Lilly AMGEN
The Alliance for Better Bone Health
Hologic Gen-Probe sanofi aventis

BoneKEy Knowledge Environment provides extensive coverage of bone diseases and the clinical care of such diseases through:

- High-quality opinion and analysis
- News & Commentaries
- Meeting Reports
- Webinars
- Web Portals: BoneKEy Genetics and BoneKEy Oncology (forthcoming in 2012)
- Multimedia article templates
- BoneKEy Community

Adhering to the highest standards of publication in the scientific community, all content on the *IBMS BoneKEy* platform is subject to rigorous peer review, copyediting and production procedures.

www.nature.com/bonekey

International Bone & Mineral Society
IBMS

nature publishing group npg

NEWS IN FOCUS

ETHICS Bioethicist signs on with controversial stem-cell company p.448

FUNDING NIH's top grant recipients will face extra scrutiny p.450

HIGH-ENERGY PHYSICS Vultures circle over the corpse of the Tevatron p.453

SPECIAL SECTION Sizing up science's debt to Alan Turing p.455

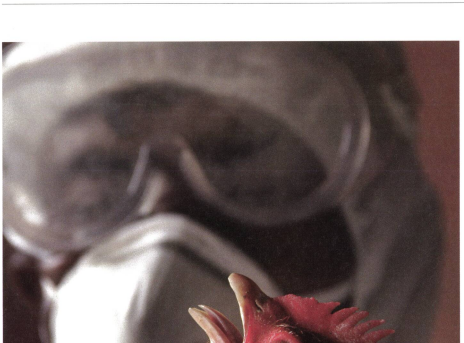

© DAS/AP PRESS ASSOCIATION IMAGES

Upgrading the biosafety level for studies on mutant avian influenza could put a stranglehold on the work.

BIOSECURITY

Flu meeting opts for openness

Controversial virus studies should be published and oversight of such work strengthened, conference concludes.

BY DECLAN BUTLER

After weeks of debate, two controversial papers describing forms of the H5N1 avian influenza virus capable of transmitting between mammals should be published in full. That was the unexpected outcome of a meeting convened last week in Geneva, Switzerland, by the World Health Organization (WHO), which also promised to create a more rigorous oversight system for such research.

The decision goes against a recommendation from the US National Science Advisory Board for Biosecurity (NSABB), which the US government has adopted as its official position. In December 2011, the board said that experimental details of the two studies should be redacted from any publications, because of concerns that the information could be used in a bioterror attack. The board also feared that publishing the details would prompt more laboratories to work on the viruses, making an accidental release more likely.

The studies, which created forms of H5N1 that can spread between ferrets through airborne transmission, are likely to be published in a few months. The 22 experts at the meeting, mainly flu researchers, believe that the delay is needed to explain the benefits of the work to the public, and allay concerns about its safety. Meanwhile, a 60-day moratorium on similar research will be extended until a system is put in place to review levels of biosafety and biosecurity. To that end, the WHO intends to convene international discussions among regulators and other bodies in the next few months.

The two researchers at the centre of the controversy say that they are pleased with the outcome. "I was pleasantly surprised by the fact that there were unanimous decisions about most issues, and strong consensus on the others," says Ron Fouchier, a flu virologist at Erasmus Medical Center in Rotterdam, the Netherlands, whose study has been accepted by the journal *Science*. Yoshihiro Kawaoka of the University of Wisconsin-Madison, lead researcher on the other study, adds that the meeting allowed him and Fouchier to explain their work, including the potential benefits for surveillance of emerging flu strains (*Nature* **481**, 417–418; 2012) and for vaccine preparation (*Nature* **482**, 142–143; 2012). "We presented why we did these experiments, what we did, what data we obtained, what these data contribute to public health and to the scientific field, and why we think the results should be shared," says Kawaoka, whose paper has been accepted by *Nature*. He adds that data he and Fouchier presented on the evolution of H5N1 in the wild clarified the threat from the virus, although he would not be drawn on the details, citing confidentiality.

Microbiologist Paul Keim, who chairs the NSABB and attended the meeting, did not respond to *Nature*'s request for an interview, but is reportedly "disappointed" by the recommendation to publish the papers.

NATURE.COM
For more, see *Nature*'s mutant flu special:
go.nature.com/mhmibi

Nature and *Science* last year agreed in principle to redact the papers, on the condition that the ▶

US government would develop a mechanism to disseminate the full papers to researchers and health officials on a need-to-know basis. But meeting participants concluded that this was impractical, and that the potential public-health benefits of the work outweighed any risk of publishing the papers in full.

BIOSAFETY FIRST

Many flu researchers have already seen the papers, so there was little to be gained by restricting their dissemination, says Richard Ebright, a molecular biologist and biodefence expert at Rutgers University in Piscataway, New Jersey. It is much more urgent, he says, to put in place strict biosafety, biosecurity and oversight provisions for such research.

David Fidler, an expert in international and national security law at Indiana University in Bloomington, points out that the meeting hasn't actually broken the publication deadlock, because Keim and representatives of the US government still do not agree with publishing the studies in full. "Most of the meeting's participants appear to have rejected the US position," says Fidler, "but [have] agreed to the extended moratorium and publication delay in the hope that the US government will change its mind."

Participants agreed that the mutant viruses should remain in their two containment facilities — rated at 'BSL-3 enhanced', the second-highest level of biosafety — and that both should be reviewed before any work restarts. Didier Houssin, president of the French Evaluation Agency for Research and Higher Education, says that the biosafety review of the work must consider whether studies of this kind should be conducted only in labs with the highest biosafety rating of BSL-4, a restriction imposed this month by Canada. Houssin, who attended the meeting, notes that imposing such a restriction globally would curtail similar work because there are just a few dozen BSL-4 labs worldwide. The safety level of BSL-3 labs is very variable, he says, and so any facilities working on such viruses would need to be rigorously assessed.

Fidler and other experts note that the meeting did not address the overall risks and benefits of the work, or how similar research might be overseen in future. Keiji Fukuda, WHO Assistant Director-General for Health Security and Environment, explains that later meetings will deal with these topics and will have wider participation.

Meanwhile, the meeting agreed that it was "critical" for the WHO to form a communications plan over the next few months to increase public awareness and understanding of the importance of the flu work, and to alleviate public anxieties. But Peter Sandman, a risk-communications consultant in Princeton, New Jersey, advises against any attempt by the WHO to "educate" the public out of its concerns. As a strategy, he says, it "is thoroughly discredited, because it doesn't work". ■ SEE EDITORIAL P.439

EPIDEMIOLOGY

Growing pains for children's study

Door-to-door recruitment abandoned for US project.

BY MEREDITH WADMAN

A proposed 15% budget cut is making for a troubled adolescence at the National Children's Study (NCS), an ambitious US government project that aims to chart biological, environmental and social influences on the health of 100,000 American children from before birth to age 21 years.

The study's managers at the National Institute of Child Health and Human Development (NICHD) in Bethesda, Maryland, say that they can cope with the White House's budget proposal, released on 13 February. This would cut funding for the programme by US$28 million, to $165 million in 2013 (see 'Belt tightening'). But their plan to save money, by recruiting study participants through health-care providers rather than by door-to-door recruitment, is worrying some of the study's scientists, who already feel shut out from its planning.

In 2010, a year after it started, the NCS's pilot phase had to expand from seven sites to 37 after recruitment rates fell well short of expectations. As the pilot winds down recruitment this year, it has enrolled only 4,000 subjects. The study, which could be used to probe the roots of conditions such as asthma, autism and diabetes, must therefore accelerate recruitment sharply after its main arm launches in 2013.

NICHD director Alan Guttmacher says that there was "understandable angst" among study-site directors the day the budget was made public. But NCS managers see room for savings, estimating that $30 million was spent on recruitment in 2011 alone. Although door-to-door recruitment is considered a gold standard in epidemiology, study managers believe that subjects can be recruited much more cheaply through health-care-providers' offices, where pilot-study data show that recruiters are much more likely to find eligible women who are pregnant or trying to become pregnant. The household recruitment has another downside, says Guttmacher: "It would take so long it would compromise the study." A "scientifically compelling" study with a budget of $165 million is still possible, he says.

According to one of the study's principal investigators (PIs), however, money is already too tight. "The idea that there are cost savings to be made here is absolutely absurd," says the researcher, who contends that many PIs have yet to receive funding for their data-management systems that was promised by NICHD managers last October. Some are coping by diverting funds from other parts of the study; others have simply stopped entering data for study subjects. The study's managers say that the PIs have been adequately funded.

Some PIs are also worried that recruitment at health-care-providers' offices would bias the study and render its findings inapplicable to the wider population. They point to a 2008 Institute of Medicine report that called the household-based sampling approach one of the study's main strengths.

And some scientists complain that they had no input into the decision to change the recruiting strategy, which many failed to hear about even after the budget was announced. "We don't have any full, thorough discussion of this," says Nigel Paneth, a paediatrician at Michigan State University in East Lansing who is PI at the NCS site in Wayne County. "What this study needs is full scientific input, not Bureaucratic Planning Central." Guttmacher notes that government officials cannot talk about White House budget proposals before they are released.

But with many congressional districts hosting study centres, the programme has proved resilient. The administration of former president George W. Bush repeatedly tried to cancel it, but Congress always restored full funding. ■

BELT TIGHTENING

Facing a proposed 15% cut, the US National Children's Study is seeking cheaper ways to recruit its cohort of more than 100,000 children.

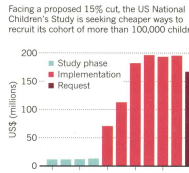

SOURCE: NIH

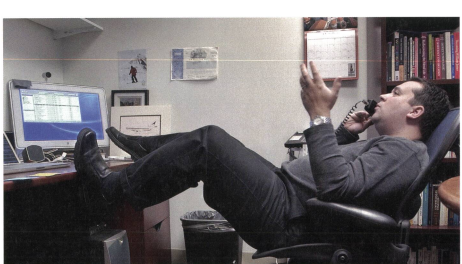

J. WILSON/KRT/NEWSCOM

Bioethicist Glenn McGee's new job raised questions of conflict of interest at the journal he founded.

ETHICS

Editor's move sparks backlash

Bioethicists are forced to consider their purpose as leading practitioner joins controversial stem-cell company.

BY DAVID CYRANOSKI

The field of bioethics is embroiled in a period of soul-searching, sparked by a startling career move by one of its biggest names.

Glenn McGee is the editor-in-chief of the *American Journal of Bioethics* (*AJOB*), the most cited bioethics journal, which he founded in 1999. Since December 2011, he has also been president for ethics and strategic initiatives at CellTex Therapeutics in Houston, Texas, a controversial company involved in providing customers with unproven stem-cell therapies. A CellTex press release says that "Dr McGee's responsibilities will include ensuring that all of the firm's work, centered on adult stem cells, will meet the highest ethical standards of the medical and scientific communities."

Although McGee has said he will leave the journal on 1 March, many bioethicists have criticized him, the journal's editorial board and its publisher, London-based Taylor and Francis. They argue that in holding both posts, McGee has a conflict of interest between his responsibilities to the journal and his new employer's desire to promote the clinical application of stem-cell treatments that are not approved by the US Food and Drug Administration.

"Imagine if the Editor of the *New England Journal of Medicine* took a job as Vice President at Merck, and the Mass Medical Society asked him to stay on as Editor, opining that the conflicts of interest would be manageable. One might rightly wonder, 'What are these people smoking?'," says John Lantos, director of the Children's Mercy Bioethics Center in Kansas City, Missouri, and a past president of the American Society for Bioethics and Humanities.

More broadly, bioethicists are questioning whether it can ever be acceptable to work for companies, which, they argue, may be using the appointment to present a veneer of ethical probity. The episode brings to a head concerns that have emerged among bioethicists over the past decade, says Insoo Hyun, a stem-cell bioethicist at Case Western Reserve University in Cleveland, Ohio. "It's a perfect storm," he says.

McGee is a leading voice on one side of the debate, arguing that bioethics must have practical relevance. For the past three years he has been chair of bioethics at the non-profit Center for Practical Bioethics in Kansas City, where he ran a course for those who might go on to chair hospital ethics committees or serve as ethical advisers to corporations.

But during McGee's tenure as editor-in-chief of the *AJOB*, four editors are known to have resigned from the editorial board because of differences in opinion over how the journal handles conflicts of interest. Two left this month, including Lantos, who wrote on his blog that he will no longer work with the journal because of McGee's simultaneous employment at the *AJOB* and CellTex, and frustration over the lack of a clear conflict-of-interest policy at the *AJOB*. In response to *Nature*'s questions about the situation, Taylor and Francis responded that it "is grateful for Dr McGee's editorship of AJOB" and "supportive of Glenn's decision to step down".

On 17 February, McGee announced that he is merely acting in an advisory capacity at the journal until 1 March, when its new editors-in-chief take over. They are David Magnus, director of the Center for Biomedical Ethics at Stanford University, California, and Summer Johnson McGee, director of graduate studies at the Center for Practical Bioethics and the journal's current executive editor. She is also Glenn McGee's wife.

Responding to questions from *Nature*, Summer Johnson McGee says that the journal has a conflict-of-interest policy that requires editors to withdraw from reviewing a manuscript if they perceive a conflict. She calls allegations that her appointment results from her relationship with her husband "baseless and sexist". "David Magnus and I were hired by our publisher, not by my husband." Magnus says that at least a dozen editorial board members have supported his and Summer Johnson McGee's appointments. Two even indicated that Glenn McGee should have been able to retain an advisory or editorial role.

Other bioethicists' blogs and Twitter feeds about the episode have expressed concerns, however. Leigh Turner of the University of Minnesota, Minneapolis, called on the entire editorial board of the *AJOB* to resign for allowing the situation to persist. And many say that McGee's move illustrates a broader problem. "Mainstream bioethics is no longer speaking truth to power," complains Jan Helge Solbakk at the University of Oslo. "Instead it has become the handmaiden of the medico-industrial complex, and of bioscience and technology."

"Mainstream bioethics is no longer speaking truth to power."

So how should companies get their advice on bioethics? Magnus never takes cash from industry for advising or speaking — "I'm a hardass about that" — but he believes that bioethicists can work for industry as long as they give up their academic positions, including posts on journal editorial boards. ▶

Working for a respected company may be acceptable to some bioethicists, but McGee's new employer comes with a great deal of baggage. CellTex, which was founded last year and as yet has no website, licenses stem-cell technology from Seoul-based RNL Bio. The South Korean company has made a business out of taking fat cells from people, processing them in a way that they say increases the number of mesenchymal stem cells, and then reinjecting them in an effort to treat conditions such as spinal cord injury.

McGee already had a connection with RNL Bio. In 2010, two patients died following injections of RNL's cells. McGee, working for stem-cell lobby group the International Cellular Medicine Society, based in Salem, Oregon, helped to conduct an investigation into the company. This concluded that only one of the two cases was likely to be related to the injections, and because the patient understood the risk the company was not culpable.

Jin Han Hong, the then president of RNL's US subsidiary, admitted in 2010 that there was no clinical-trial evidence proving that these treatments are effective (*Nature* **468,** 485; 2010). As treatment with RNL's stem cells is not approved in the United States or South Korea, for the procedures the company sends patients to China or Japan, where regulations are less strictly enforced. Using RNL's methods, CellTex is banking stem cells that have gone on to be used in a number of patients, including Rick Perry, governor of Texas (*Nature* **477,** 377–378; 2011). CellTex says that it does not conduct medical procedures itself.

When *Nature* contacted McGee to put the criticisms to him, he directed us to previous statements indicating that he wants to put CellTex on firmer ethical ground by having it conduct clinical trials that meet standards set by the International Society for Stem Cell Research, based in Deerfield, Illinois, which represents most mainstream stem-cell researchers around the world.

Hyun warns that working directly for business can be fraught with danger, however good a bioethicist's intentions. In 2005, he helped to craft the informed consent procedure for egg donations used in a cloning procedure by disgraced Korean stem-cell scientist Woo Suk Hwang. Following Hwang's claim, later proved fraudulent, that he had cloned human embryos and harvested stem cells from them, it emerged that he had ignored the consent procedure for egg donations (*Nature* **438,** 536–537; 2005), leading to embarrassment for Hyun.

"I know first hand how difficult it is to separate conflict of interest — to maintain the role of bioethicist," says Hyun. "I know you need to not be too chummy with enterprises trying to speed ahead in stem cells." ■

S. RYAN/NORTHWESTERN UNIV.

Researchers who, like Vadim Backman, top $1.5 million in NIH grants will face an extra layer of review.

FUNDING

Extra scrutiny for 'grandee grantees'

An analysis by Nature *reveals who holds the most grants from the US National Institutes of Health.*

BY ERIC HAND

Vadim Backman no longer relies on coffee to get him through the 100-hour weeks he puts in at his biomedical engineering laboratory at Northwestern University in Evanston, Illinois. Since giving up caffeine, he drops to the floor and does press-ups whenever he needs to clear his head. It certainly takes an alert mind to supervise 20 students, collaborate on clinical trials at 8 hospitals worldwide, and manage 7 grants worth a total of more than US$3 million from the US National Institutes of Health (NIH) in Bethesda, Maryland.

At 38, Backman is already a biomedical superstar. He is developing an imaging technology that could detect abnormal structures in cells during the earliest stages of cancer. And a *Nature* analysis has identified him as one of seven scientists whom the NIH supports with the most grants (see 'Seven lucky seven'). That puts him near the top of a larger group of NIH-supported researchers who will soon be targeted for extra scrutiny beyond the peer-review process.

As it released its 2013 budget proposal last week, the agency said that researchers who control more than $1.5 million in grants will undergo an extra layer of review from external advisers before further grants are approved. The decision comes as the agency tries to scrape money together for new grants in order to raise its current grant success rate of 18%, a historic low. But the countermeasure — potentially penalizing applicants on the basis of their previous success — is also historic.

The basic rule for giving out grants at the NIH has always been simple: to fund the best science. A retreat from pure meritocracy is "shocking", says Howard Garrison, director of public affairs at the Federation of American Societies for Experimental Biology in Bethesda, Maryland. "It's a huge sea change."

Nevertheless, Garrison supports the new rule because he is concerned about the vast number of researchers who are struggling to win, or hold, just one grant.

Nearly 1,500 principal investigators (PIs) — about 5% of those who held grants in 2011 — come in above the $1.5-million threshold and would be subject to the review. A $750,000 threshold for a similar layer of extra review has been in place since the 1990s at one NIH institute, the National Institute of General Medical Sciences, and has worked well, says the institute's former director Jeremy Berg, now at the University of Pittsburgh in Pennsylvania.

SHOPPING AROUND

Sally Rockey, the NIH deputy director for extramural research, says the agency isn't considering a hard cap based on the number of grants per scientist, nor extra review for those with many grants. She points out that a cap based on numbers of grants would have to be draconian to spread grants to a significantly greater number of researchers. An analysis she presented on her blog in October 2011 found that setting a maximum of two grants per PI would increase the grant success rate by just 2%.

In 2008, two NIH advisory panels tasked with reforming the peer-review process for grants recommended that PIs spend at least 20% of their time on any given grant — a de facto cap of five grants per researcher. Although most of the recommendations were ultimately adopted, the 20% rule was not. Berg, who was on one of the advisory panels, says he would still support a review threshold — although not a hard cap — for a certain number of grants. "You look at people with more than a certain number of grants and ask, 'Is this a good investment for the NIH?'" he says. There are concerns, he adds, that PIs could gain multiple grants by presenting similar experiments to different NIH institutes.

Berg has tried to measure the output of laboratories of different sizes, and found that the richest are not necessarily the most productive (see *Nature* **468,** 356–357; 2010). "There are some people who are definitely capable of running bigger operations while maintaining tremendous productivity per dollar," he says. "There are other people who are very well funded and aren't so productive."

Those questions are especially important for the very top grant winners, whom *Nature* identified on the basis of 'research project grants', an NIH-defined category composed mostly of the R-01 grants that provide bread-and-butter support to most PIs.

John Tainer, a structural biologist at the Scripps Research Institute in La Jolla, California, feels that the new rule will only further entrench a bias against those with multiple grants, and worries that it could restrict innovation by the elite. With 7 grants worth a combined sum of more than $5 million, it is hard to feel sorry for Tainer. But earlier this month, he lost a competitive renewal for a grant that he has held since 1985, to study the hair-like pili on the surface of bacteria that make them sticky and contribute to their pathogenicity. Because he relies on grants to pay the salaries of 18 lab members, as well as his own, this rejection could mean lay-offs.

Tainer suspects that the decision "reflects the fact that I have other projects". But, he continues, "The science hasn't changed. What we're doing now is better than what we've ever done."

"You look at people with more than a certain number of grants and ask, 'Is this a good investment?'"

The loss of the grant will extend beyond his own lab, he adds. "For the next decade, people will be publishing parts of things that I had done better. The cost to the NIH will be higher. If you're a leader and you have momentum and technology, the impact of taking that away and having other people do it at a different level is destructive."

Backman also dislikes the idea of capping the number of grants that an individual can win, but is more relaxed about the proposed $1.5-million threshold review. He is sympathetic to the plight of young researchers casting about for their first grant — he was in the same position just a few years ago — but says that the competition for established researchers must be based purely on the strength of their ideas. "I like the idea of meritocracy," he says. ■

SEVEN LUCKY SEVEN

Seven NIH-supported researchers are principal investigators on seven research project grants each.

Name	Grant total	Institution	Research
Ronald Davis	$6,986,908	Stanford University	Genomics
John Tainer	$5,069,800	Scripps Research Institute	Structural biology
Anjana Rao	$3,512,571	La Jolla Institute for Allergy & Immunology	Signalling and gene expression
George Koob	$3,365,229	Scripps Research Institute	Neurobiology of addiction
Vadim Backman	$3,054,165	Northwestern University	Biophotonics
Pier Pandolfi	$2,929,857	Beth Israel Deaconess Medical Center	Tumorigenesis
Pietro Sanna	$2,114,278	Scripps Research Institute	Neurobiology of addiction

Fiscal 2011 grant data were used. Grant totals reflect fractional shares of multi-PI grants. Analysis excludes grants made to large research centres. Grant supplements are included as part of original grant, rather than as a separate award.

WHAT'S THE FUTURE OF ENERGY? HERE'S WHAT YOU'RE TELLING US.

Shell is posing provocative questions to start a conversation about this important topic.

The Energy for the Future Poll measures global and regional opinions on where to place our energy and transportation priorities. Go online and tell us what you think.

Q Which area of the energy industry will advance the most in the next 10 years?

40% of global respondents thought that the solar industry offers the most potential technological progress. The wind, biofuels and nuclear industries each earned about 14% of the votes, though Asia and Australia respondents ranked nuclear as a clear second.

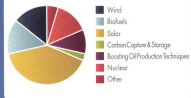

Q What policy option is the most effective as a solution to the energy challenge?

32% of global respondents saw mandating alternative energy as the most effective policy, while subsidizing renewable energy (18%) and carbon taxes (14%) were also strongly supported. In the lively online discussion, a number of respondents pointed out that controlling energy consumption and minimizing distribution waste are important steps we can take today.

Look for the Shell *Energy for the Future* Poll on **sciam.com/sponsored/energyforthefuture**

University of Dundee
College of Life Sciences

UNIVERSITY OF DUNDEE

Professorships & Lectureships

Dundee is situated in a spectacular Scottish landscape, framed by the sea and surrounded by rivers, lochs and mountains. The city has a dynamic, international outlook and a worldwide reputation as a crucible for pioneering life sciences research.

The College of Life Sciences is home to preeminent researchers from around the world working at the cutting-edge, across disciplines and consistently producing highly-cited papers in their fields.

We are seeking individuals with outstanding scientific credentials and exciting plans for ground-breaking research to become part of our thriving multi-disciplinary research community. Principal Investigator positions at lecturer to professorial level are available in:

- Biological Chemistry & Drug Discovery
- Cell and Developmental Biology
- Cell Signalling & Immunology
- Bioinformatics, Biophysics, Computational & Mathematical Biology
- Molecular Medicine
- Molecular Microbiology
- Plant Sciences
- Protein Phosphorylation & Ubiquitylation

We provide a fast-paced, collegiate and supportive environment where Principal Investigators can thrive through access to state-of-the-art technologies and collaborative opportunities in a single integrated complex.

Apply online at:
http://jobs.lifesci.dundee.ac.uk and find out more about our research, our exceptional facilities, and what it's like to live and work in Dundee.

The University of Dundee is committed to equal opportunities and welcomes applications from all sections of the community.

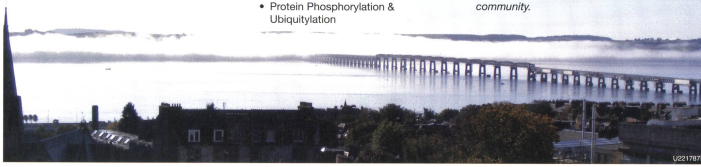

U221787R

Royal Botanic Garden Edinburgh

DIRECTOR OF SCIENCE

As a world-class plant biodiversity research institute with a long history in scientific exploration, horticulture and education, the Royal Botanic Garden Edinburgh has internationally important collections of living and preserved plants, modern laboratories and an extensive botanical library. With four gardens across Scotland, our mission is "exploring and explaining plants for a better future". RBGE is a Non-Departmental Public Body largely funded by the Scottish Government.

We are seeking a dynamic and well-qualified Director of Science to join the senior team reporting direct to and working closely with the Regius Keeper. He or she will lead the 75 people in our Science Division and contribute to developing and implementing strategies and policies across the organisation. This is an opportunity to make a difference in an organisation that contributes to tackling the challenges of the biodiversity crisis and climate change and is committed to engaging with people in wider society to inspire them about plants and the environment. The Director of Science will also be responsible for promoting our science nationally and internationally and further enhancing our links with universities and other research institutions. He or she will have a strong focus on increasing income from research grants and scientific consultancy and will maintain an active and innovative personal programme of research in an appropriate field. Applicants must be of high standing in scientific research, with an international reputation for leadership in their field. A PhD in a subject central to our scientific mission is essential, as is a strong track record in research evidenced by high quality research publications and the award of research grants.

They must also be able to demonstrate a successful record of scientific leadership, including the management of people and financial resources. Excellent interpersonal skills will be required, including the ability to articulate and communicate our science to Ministers, Scottish Government research committees, leaders of our partner institutions, the wider scientific community, and to the wider public.

To apply send your CV and a covering letter stating your motivation in applying and describing the skills and experience you would bring to the role to Gillian Oddie in our HR team (g.oddie@rbge.org.uk) by 16th March 2012. Interviews are expected to take place in the week commencing 26th March.

U221789R

To advertise here please contact – US tel. +1 800 989 7718, naturejobs@natureny.com or Europe/ROW tel. +44 20 7843 4961, naturejobs@nature.com

HIGH-ENERGY PHYSICS

Physicists raid Tevatron for parts

Fermilab icon plundered amid tight budgets and shifting scientific aims.

BY EUGENIE SAMUEL REICH

It is a 4,000-tonne edifice that stands three stories high, chock full of particle detectors, power supplies, electronics and photomultiplier tubes, all layered like a giant onion around a cylindrical magnet. During 26 years of operation at the Fermi National Accelerator Laboratory in Batavia, Illinois, this behemoth, the Collider Detector at Fermilab (CDF), helped to find the top quark and chased the Higgs boson. But since the lab's flagship particle collider, the Tevatron, was switched off in September 2011, the detector has been surplus stock — and it is now slowly being cannibalized for parts.

When the Tevatron closed, Fermilab announced that the CDF would become an educational display. Along with its companion experiment, D0, the detector was supposed to form the centrepiece of a tour through simulated control rooms and decommissioned accelerator tunnels. But tight budgets for experimental particle physicists — combined with their tendency to tinker and recycle — are pushing the outcome in a different direction, at least for the CDF.

"Some parts are worth pennies, but in this budgetary climate, even pennies are worth saving," says Rob Roser, who until recently was co-spokesman for the CDF and has now himself been recycled into a new position as head of scientific computing at Fermilab.

"Recycling equipment is as old as science itself," says Jonathan Lewis, the Fermilab scientist in charge of decommissioning the CDF. And thrift is in fashion. With most of the action in particle physics taking place at the Large Hadron Collider near Geneva in Switzerland, US researchers were preparing for hard times even before US President Barack Obama released his 2013 budget request on 13 February (see *Nature* **482,** 283–285; 2012). Although the Office of Science at the Department of Energy (DOE) got a 2.4% funding boost, the budget cut Fermilab's allotment by 5% and DOE funding for high-energy physics by 1.8%.

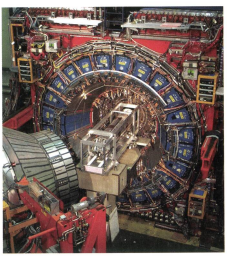

FERMILAB

The CDF, one of the Tevatron's two detectors, is slowly surrendering its parts to other experiments.

CANNIBALIZING THE TEVATRON

Parts at the Tevatron and its two main experiments, the CDF and D0, are being considered for recycling in the wake of the collider's closure in September 2011.

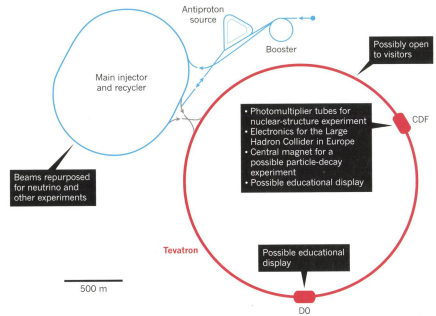

Looking for savings, Bogdan Wojtsekhowski, who leads three experiments to probe nuclear structure with an electron beam at the DOE's Jefferson Lab in Newport News, Virginia, convinced Fermilab to send him 600 photomultiplier tubes, which capture the light emitted as particles streak through detector materials. Buying them new would have cost $600,000.

The recycling reflects not only parsimony, but also a programmatic shift in US particle physics. With the shutdown of the Tevatron, researchers moved from the energy frontier, where physics is tested with particle collisions at the highest energies, to the intensity frontier, where the highest numbers of particles are collided. The fate of the CDF's parts mirrors this switch.

Some power supplies are going to Mu2e, an intensity-frontier experiment at Fermilab to look for the rare conversion of muons to electrons. Amplifier chips are going to g-2, another intensity-frontier experiment at Fermilab to measure a key magnetic parameter of the muon. Some scintillation materials, which emit light along the path of charged particles passing through them, are destined for the Long-Baseline Neutrino Experiment, which plans to send neutrinos 1,300 kilometres from Fermilab to the Homestake Mine in Lead, South Dakota.

Although most of the donations involve small items that would not stop the CDF from going on display, the most ambitious recycling request so far would see it gutted. A proposed experiment called ORKA, which would search for a predicted, but as yet unobserved, rare decay of kaon particles, needs a massive solenoid magnet like the one at the CDF's heart. ORKA has yet to be funded by the DOE, but the Physics Advisory Committee at Fermilab approved its scientific goals in December 2011.

Robert Tschirhart, co-spokesman for ORKA, says that adapting the magnet from the CDF by replacing some of its present detectors with a kaon detector may cost several million dollars. That would still be about half the cost of buying a new magnet.

Lab management will make a decision about whether ORKA can eviscerate the CDF in about 6 months' time. ■

PALAEOBOTANY

Wild flower blooms again after 30,000 years on ice

Fruits hoarded by ancient ground squirrels give new life to prehistoric plants.

BY SHARON LEVY

During the Ice Age, Earth's northern reaches were covered by chilly, arid grasslands roamed by mammoths, woolly rhinoceros and long-horned bison. That ecosystem, known by palaeontologists as the mammoth steppe, vanished about 13,000 years ago. It has no modern counterpart.

Yet one of its plants has reportedly been resurrected by a team of scientists who tapped a treasure trove of fruits and seeds, buried some 30,000 years ago by ground squirrels and preserved in the permafrost (S. Yashina *et al. Proc. Natl Acad. Sci. USA* http://dx.doi.org/10.1073/pnas.1118386109; 2012). The plant would be by far the most ancient ever revived; the previous record holder was a date palm grown from seeds roughly 2,000 years old.

The squirrels' burrows, 70 in all, were found on the banks of the lower Kolyma River in northeastern Siberia, 20–40 metres below the current surface of the tundra and surrounded by the bones of mammoths and other creatures. Some burrows contained hundreds of thousands of fruits and seeds, wonderfully preserved by the cold, dry environment.

Researchers had previously attempted to grow plants from seeds found in these ancient burrows, including sedge, Arctic dock, alpine bearberry and the herbaceous plant *Silene stenophylla*. Those seeds did begin to germinate, but then faltered and died back.

Tantalized, David Gilichinsky of the Russian Academy of Sciences' Institute of Physicochemical and Biological Problems in Soil Science in Pushchino decided to try a different approach (sadly, Gilichinsky passed away last week). He and his colleagues took samples of placental tissue from *S. stenophylla* fruits. The plant placenta — an example of which is the white matter inside a bell pepper — gives rise to and holds the seeds. The tissue produced shoots when it was cultivated *in vitro*, and the scientists used these to propagate more plants. They are the oldest living multicellular organisms on Earth, the team says.

A prehistoric plant resurrected from frozen tissue.

S. YASHINA *ET AL. PROC. NATL ACAD. SCI. USA*

The plants have already blossomed to produce fertile seeds, which were grown into a second generation of fertile plants. During propagation, the ancient form of the wild flower produced more buds but was slower to put out roots than modern *S. stenophylla*, which is found along the banks of the Kolyma. This suggests that the original has a distinct phenotype, adapted to the extreme environment of the Ice Age.

"I'm excited that someone has finally succeeded in doing this," says Grant Zazula of the Yukon Palaeontology Program in Whitehorse, Canada, who has investigated previous claims of ancient seed germination. "There is a good chance that extinct plant species could now be brought back to life from permafrost-preserved seeds."

Although some members of the mammoth steppe ecosystem survive, no place on Earth currently holds the same combination of grasses, sedge and wild flowers that have been found in the mummified guts of Ice Age mammoths or in the frozen hoards of squirrels (B. V. Gaglioti *et al. Quatern. Res.* **76,** 373–382; 2011). Zazula speculates that living plant tissue from much earlier — hundreds of thousands of years ago — might also be revived, revealing evolutionary change over a longer timescale, and helping scientists to understand the lost ecology of periods such as the Ice Age. ■

CLARIFICATION

The table in the News story 'Obama shoots for science increase' (*Nature* **482,** 283–285; 2012) was unclear about the make-up of the Food and Drug Administration's budget. Obama's request leaves the government's input nearly flat, but a rise in user fees from industry would lift the agency's overall 2013 budget to $4,486 million.

C. STRONG, S. DOUGLAS, G. MCGILL, NICOLE ZULAR MAYA & G. CAZENAVE

MORE ONLINE

TOP STORY

● DNA robot could kill cancer cells by seeking them out and delivering a deadly payload. go.nature.com/hzh4ya

MORE NEWS

● Tourette's-like disorder in New York school confounds experts. go.nature.com/b6dmq1

● Citizen science goes extreme. go.nature.com/7ghxol

● Kilogram conundrum on the road to resolution go.nature.com/u1dg1w

PODCAST

Alan Turing's birthday; the Y chromosome sticks around; and how cells sense pain. go.nature.com/qnk7uv

ANDY PITTS, TURING FAMILY

LEGACY OF A UNIVERSAL MIND

BY TANGUY CHOUARD

From the day he was born — 23 June 1912 — Alan Mathison Turing seemed destined to solitude, misunderstanding and persecution (see page 441). As his centenary year opens, *Nature* hails him as one of the top scientific minds of all time (see page 440). This special issue sweeps through Turing's innumerable achievements, taking us from his most famous roles — wartime code-breaker and founder of computer science (see page 459) — to his lesser known interests of botany, neural nets, unorganized machines, quantum physics and, well, ghosts (see page 562).

Everyone sees a different Turing. A molecular biologist might surprise you by saying that Turing's most important paper is his 1936 work on the 'Turing machine' because of its relevance to DNA-based cellular operations (see page 461). A biophysicist could instead point to his 1952 work on the formation of biological patterns — the first simulation of nonlinear dynamics ever to be published (see page 464).

NATURE.COM
For more on Turing, see:
nature.com/turing

Beneath it all, Turing was driven by the dream of reviving — possibly in the form of a computer program — the soul of Christopher Morcom, perhaps his only true friend, who died abruptly when they were both teenagers. I want to "build a brain", he said. So does electrophysiologist Henry Markram (see page 456). But it is still a matter of debate whether machine intelligence should faithfully simulate neuronal circuitry, or just emulate brain function using whatever expedient (see page 462).

Even when Turing was kept busy by wartime code-breaking and the practical implementation of his universal computer, he never forgot that he had, in 1936, discovered something even bigger: the 'incomputable' world. Contemporary physics hasn't even started to work out the implications of that discovery (see page 465).

It is typical of Turing's brilliance and playfulness that even as he gave so many fields the tools that allowed them to blossom, he planted a concept that pushes science as we know it — physical reality and Newtonian causality — towards the abyss. ■

Tanguy Chouard, *a biology editor at* Nature, *was the consulting editor for this special issue.*

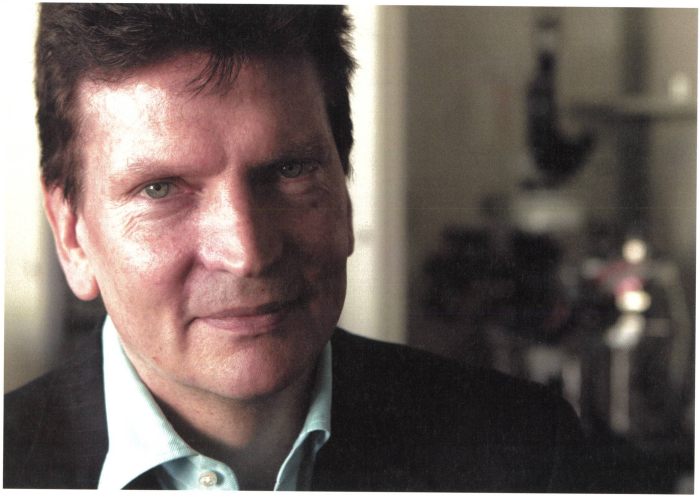

D. BALIBOUSE/REUTERS

BRAIN IN A BOX

Henry Markram wants €1 billion to model the entire human brain. Sceptics don't think he should get it.

BY M. MITCHELL WALDROP

TURING AT 100
A legacy that spans science:
nature.com/turing

It wasn't quite the lynching that Henry Markram had expected. But the barrage of sceptical comments from his fellow neuroscientists — "It's crap," said one — definitely made the day feel like a tribunal.

Officially, the Swiss Academy of Sciences meeting in Bern on 20 January was an overview of large-scale computer modelling in neuroscience. Unofficially, it was neuroscientists' first real chance to get answers about Markram's controversial proposal for the Human Brain Project (HBP) — an effort to build a supercomputer simulation that integrates everything known about the human brain, from the structures of ion channels in neural cell membranes up to mechanisms behind conscious decision-making.

Markram, a South-African-born brain electrophysiologist who joined the Swiss Federal Institute of Technology in Lausanne (EPFL) a decade ago, may soon see his ambition fulfilled. The project is one of six finalists vying to win €1 billion (US$1.3 billion) as one of the European Union's two new decade-long Flagship initiatives.

"Brain researchers are generating 60,000 papers per year," said Markram as he explained the concept in Bern. "They're all beautiful, fantastic studies — but all focused on their one little corner: this molecule, this brain region, this function, this map." The HBP would integrate these discoveries, he said, and create models to explore how neural circuits are organized, and how they give rise to behaviour and cognition — among the deepest mysteries in neuroscience. Ultimately, said Markram, the HBP would even help researchers to grapple with disorders such as Alzheimer's disease. "If we don't have an integrated view, we won't understand these diseases," he declared.

As the response at the meeting made clear, however, there is deep unease about Markram's vision. Many neuroscientists think it is ill-conceived, not least because Markram's idiosyncratic approach to brain

simulation strikes them as grotesquely cumbersome and over-detailed. They see the HBP as overhyped, thanks to breathless media reports about what it will accomplish. And they're not at all sure that they can trust Markram to run a project that is truly open to other ideas.

"We need variance in neuroscience," declared Rodney Douglas, co-director of the Institute for Neuroinformatics (INI), a joint initiative of the University of Zurich and the Swiss Federal Institute of Technology in Zurich (ETH Zurich). Given how little is known about the brain, he said, "we need as many different people expressing as many different ideas as possible" — a diversity that would be threatened if so much scarce neuroscience research money were to be diverted into a single endeavour.

Markram was undeterred. Right now, he argued, neuroscientists have no plan for achieving a comprehensive understanding of the brain. "So this is the plan," he said. "Build unifying models."

MARKRAM'S BIG IDEA

Markram has been on a quest for unity since at least 1980, when he began undergraduate studies at the University of Cape Town in South Africa. He abandoned his first field of study, psychiatry, when he decided that it was mainly about putting people into diagnostic pigeonholes and medicating them accordingly. "This was never going to tell us how the brain worked," he recalled in Bern.

His search for a new direction led Markram to the laboratory of Douglas, then a young neuroscientist at Cape Town. Markram was enthralled. "I said, 'That's it! For the rest of my life, I'm going to dig into the brain and understand how it works, down to the smallest detail we can possibly find.'"

That enthusiasm carried Markram to a PhD at the Weizmann Institute of Science in Rehovot, Israel; to postdoctoral stints at the US National Institutes of Health in Bethesda, Maryland, and at the Max Planck Institute for Medical Research in Heidelberg, Germany; and, in 1995, to a faculty position at Weizmann. He earned a formidable reputation as an experimenter, notably demonstrating spike-timing-dependent plasticity — in which the strength of neural connections changes according to when impulses arrive and leave (H. Markram *et al. Science* **275**, 213–215; 1997).

By the mid-1990s, individual discoveries were leaving him dissatisfied. "I realized I could be doing this for the next 25, 30 years of my career, and it was still not going to help me understand how the brain works," he said.

To do better, he reasoned, neuroscientists would have to pool their discoveries systematically. Every experiment at least tacitly involves a model, whether it is the molecular structure of an ion channel or the dynamics of a cortical circuit. With computers, Markram realized, you could encode all of those models explicitly and get them to work together. That would help researchers to find the gaps and contradictions in their knowledge and identify the experiments needed to resolve them.

Markram's insight wasn't original: scientists have been devising mathematical models of neural activity since the early twentieth century, and using computers for the task since the 1950s (see page 462). But his ambition was vast. Instead of modelling each neuron as, say, a point-like node in a larger neural network, he proposed to model them in all their multibranching detail — down to their myriad ion channels (see 'Building a brain'). And instead of modelling just the neural circuits involved in, say, the sense of smell, he wanted to model everything, "from the genetic level, the molecular level, the neurons and synapses, how microcircuits are formed, macrocircuits, mesocircuits, brain areas — until we get to understand how to link these levels, all the way up to behaviour and cognition".

The computer power required to run such a grand unified theory of the brain would be roughly an exaflop, or 10^{18} operations per second — hopeless in the 1990s. But Markram was undaunted: available computer power doubles roughly every 18 months, which meant that exascale computers could be available by the 2020s (see 'Far to go').

And in the meantime, he argued, neuroscientists ought to be getting ready for them.

Markram's ambitions fit perfectly with those of Patrick Aebischer, a neuroscientist who became president of the EPFL in 2000 and wanted to make the university a powerhouse in both computation and biomedical research. Markram was one of his first recruits, in 2002. "Henry gave us an excuse to buy a Blue Gene," says Aebischer, referring to a then-new IBM supercomputer optimized for large-scale simulations. One was installed at the EPFL in 2005, allowing Markram to launch the Blue Brain Project: his first experiment in integrative neuroscience and, in retrospect, a prototype for the HBP.

> "IT WILL BE LOTS OF EINSTEINS COMING TOGETHER TO BUILD A BRAIN."

Part of the project has been a demonstration of what a unifying model might mean, says Markram, who started with a data set on the rat cortex that he and his students had been accumulating since the 1990s. It included results from some 20,000 experiments in many labs, he says — "data on about every cell type that we had come across, the morphology, the reconstruction in three dimensions, the electrical properties, the synaptic communication, where the synapses are located, the way the synapses behave, even genetic data about what genes are expressed".

By the end of 2005, his team had integrated all the relevant portions of this data set into a single-neuron model. By 2008, the researchers had linked about 10,000 such models into a simulation of a tube-shaped piece of cortex known as a cortical column. Now, using a more advanced version of Blue Gene, they have simulated 100 interconnected columns.

The effort has yielded some discoveries, says Markram, such as the as-yet unpublished statistical distribution of synapses in a column. But its real achievement has been to prove that unifying models can, as promised, serve as repositories for data on cortical structure and function. Indeed, most of the team's efforts have gone into creating "the huge ecosystem of infrastructure and software" required to make Blue Brain useful to every neuroscientist, says Markram. This includes automatic tools for turning data into simulations, and informatics tools such as http://channelpedia.net — a user-editable website that automatically collates structural data

BUILDING A BRAIN

The Blue Brain simulation — a prototype for the Human Brain Project — constructs simulated sections of cortex from the bottom up, starting from detailed models of individual neurons.

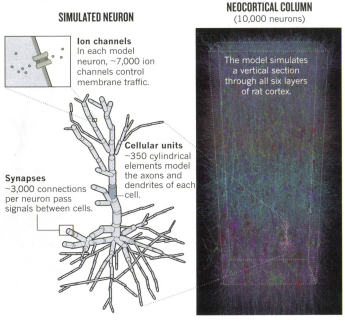
SIMULATED NEURON
Ion channels
In each model neuron, ~7,000 ion channels control membrane traffic.
Cellular units
~350 cylindrical elements model the axons and dendrites of each cell.
Synapses
~3,000 connections per neuron pass signals between cells.
NEOCORTICAL COLUMN
(10,000 neurons)
The model simulates a vertical section through all six layers of rat cortex.

SOURCE: BBP/EPFL

FAR TO GO

The Blue Brain Project has steadily increased the scale of its cortical simulations through the use of cutting-edge supercomputers and ever-increasing memory resources. But the full-scale simulation called for in the proposed Human Brain Project (red) would require resources roughly 100,000 times larger still.

SOURCE: BBP/EPFL

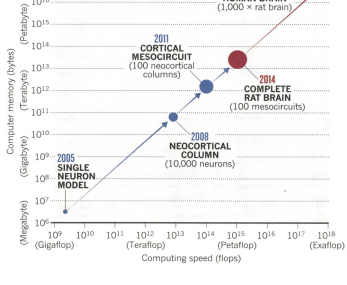

on ion channels from publications in the PubMed database, and currently incorporates some 180,000 abstracts.

The ultimate goal was always to integrate data across the entire brain, says Markram. The opportunity to approach that scale finally arose in December 2009, when the European Union announced that it was prepared to pour some €1 billion into each of two high-risk, but potentially transformational, Flagship projects. Markram, who had been part of the 27-member advisory group that endorsed the initiative, lost no time in organizing his own entry. And in May 2011, the HBP was named as one of six candidates that would receive seed money and prepare a full-scale proposal, due in May 2012.

If the HBP is selected, one of the key goals will be to make it highly collaborative and Internet-accessible, open to researchers from around the world, says Markram, adding that the project consortium already comprises some 150 principal investigators and 70 institutions in 22 countries. "It will be lots of Einsteins coming together to build a brain," he says, each bringing his or her own ideas and expertise.

BOTTOM TO TOP

The description of the HBP as an open user facility sparked interest and enthusiasm at the Bern meeting. But much more vocal were Markram's critics, many of whom focused on the perceived inadequacies of the Blue Brain model — and of Markram's approach to data integration.

At the heart of that approach is Markram's conviction that a good unifying model has to assimilate data from the bottom up. In his view, modellers should start at the most basic level — he focuses on ion channels because they determine when a neuron fires — and get everything working at one level before proceeding to the next. This requires a lot of educated guesses, but Markram argues that the admittedly huge gaps in knowledge about the brain can be filled with data as experiments are published — the Blue Brain model is updated once a week. The alternative approach, approximating and abstracting away the biological detail, leaves no way to be sure that the model's behaviour has anything to do with how the brain works, said Markram.

This is where other computational neuroscientists gnash their teeth. Most of them are already using simple models of individual neurons to explore high-level functions such as pattern recognition. Markram's bottom-up approach risks missing the wood for the trees, many of them argued in Bern: the model could be so detailed that it is no easier to understand than the real brain. And that is if Markram can build it at all. Judging by what Blue Brain has accomplished in the past six years, critics said, that seems unlikely. The tiny swathe of simulated rat cortex has no inputs from sensory organs or outputs to other parts of the brain, and produces almost no interesting behaviour, pointed out Kevan Martin, co-director of the INI, in an e-mail. It is "certainly not the case" that Markram has simulated the column as it works in a whole animal, he said.

Markram's response to such criticisms in Bern was that more capabilities are always being added to the Blue Brain simulation. But Martin remained unimpressed. "I cannot imagine how this level of detail, which is still very incomplete even after Henry's considerable labours, is ever going to be obtained from more than a few regions of the rodent brain in the next decade, let alone brains of *Drosophila*, zebrafish, songbird, mouse or monkey," his e-mail continued.

"Of course," Martin added, "all this would be but a storm in the professors' teacups" if the HBP hadn't come along and raised the stakes enormously. It is all too easy to imagine other areas of neuroscience research being starved for resources by the HBP — especially in Switzerland, which as host country will have to provide a substantial, but still-undetermined, fraction of the funding. Douglas asks: should Europe be spending €1 billion to support the passionate quest of one man? He concedes that visionaries are sometimes necessary to drive progress. "But what if they're passionately wrong?"

Also fuelling anxiety — and irritation — is the widespread sense that Markram has been making his case through the news media, not through publishing, conferences and the other conventional channels of science. Reporters see much to like: Markram is tall, striking and explains his ideas with the clarity, quotability and urgency of a South African version of the late Carl Sagan. He has "a hypnotic effect", says Richard Hahnloser, a computational neuroscientist at the INI. But critics say that this results in too many news accounts that leave the impression that the HBP will, say, eliminate the need for experimental animals.

"The whole neuroscience community will be in trouble ten years from now" when the implied predictions don't come true, says another INI researcher, who worries that the politicians will be right there saying, "But you promised!"

MARCH OF PROGRESS

In Bern, Markram bristled at accusations that he has deliberately cultivated hype. "I have never said that the HBP would replace animal experiments," he shot back at one questioner. "I said that simulation helps you choose the experiments that will best add value."

Markram was also at pains to insist that the HBP will be open to other modelling approaches. "This concern is unfounded because they simply have not bothered to find out what is being proposed," he told *Nature* after the meeting. The final facility "will allow anyone to build models at a range of levels of biological detail with as much data as possible from anywhere".

Markram seems to be building support. Last year, the board that oversees both the ETH and the EPFL enthusiastically endorsed the Blue Brain Project after a rigorous review by a four-member panel that included two outspoken sceptics of Markram's approach. The board asked the Swiss parliament to commit 75 million Swiss francs (US$81 million) to the project for 2013–16 — more than ten times Blue Brain's current budget. Parliament's decision is expected next month.

Markram is optimistic that the European Union will come to much the same conclusion about the HBP. However, if the project isn't endorsed, says Markram, "we'll just continue with Blue Brain" — although it may take a lot longer to reach a full brain simulation.

Markram clearly feels that history is on his side. "Simulation-based research is an inevitability," he declared in Bern. "If I get stopped from doing this, it's going to happen. It has happened already in many areas of science. And it is going to happen in life science." ■

M. Mitchell Waldrop *is a features editor for* Nature *based in Washington DC.*

COMMENT

INTELLIGENCE Four experts compare brains with machines **p.462**

MATHEMATICS What lies beyond the limits of computability? **p.465**

THEATRE How actors use empathy to seduce an audience **p.466**

VIROLOGY Three books explore 30 years of developments in HIV/AIDS research **p.468**

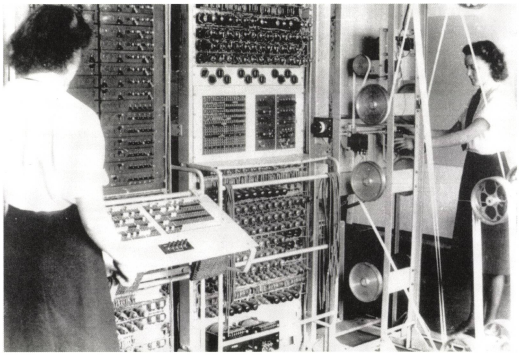

BLETCHLEY PARK TRUST/SSPL/GETTY

Using techniques developed by Alan Turing, the Colossus was able to decode German wartime communications.

The dawn of computing

Alan Turing's bridging of logic and machines laid the foundation for digital computers, says **George Dyson**.

The history of digital computing can be divided into an old testament and a new testament. The prophets of the old testament, led by Gottfried Wilhelm Leibniz in the 1670s, supplied the logic; those of the new testament, led by John von Neumann in the 1940s, built the machines. Alan Turing, born on 23 June 1912, falls in between. His paper 'On computable numbers, with an application to the *Entscheidungsproblem*', written in 1936 while he was a fellow at the University of Cambridge's King's College, UK, and published shortly after his arrival as a graduate student at Princeton University, New Jersey, in October 1936, led the way to the implementation of mathematical logic in machines[1].

Turing was aiming to solve German mathematician David Hilbert's 1928 *Entscheidungsproblem* — the 'decision problem' of whether a mechanical procedure could determine the validity of any logical statement in a finite number of steps. Turing took the 1930s concept of a computer — a person equipped with pencil, paper and instructions — and deconstructed it by removing all traces of intelligence except for the ability to follow instructions and read and write a finite alphabet of symbols on an unbounded paper tape.

The result was the Turing machine: a mathematical black box that obeys preset instructions, represented by symbols encoded on the tape or stored in the machine's internal 'state of mind'. At any moment, the machine can read, write or erase a symbol from a square; move a square to the right or left; or change its state of mind. Complex symbols can be represented by strings of simpler ones, the limit being the binary distinction between two symbols (or the presence or absence of a hole in the tape). These 'bits' of information can take two forms: patterns in space that are transmitted across time, termed memory; or patterns in time that are transmitted across space, called code. For a Turing machine, time exists not as a continuum, but as a sequence of changes of state.

Turing then demonstrated the existence of a single machine that could "compute any computable" sequence[1]. Such a 'universal computing machine' could mimic any ▶

TURING AT 100
A legacy that spans science:
nature.com/turing

▶ other machine by executing an encoded description of it. Thus, he foresaw the concept of software.

Finally, Turing answered Hilbert's conundrum. He identified a question that could not be answered by any machine in a finite number of steps: will a given encoded description come to a halt or run forever when executed by the universal computing machine? The answer to the *Entscheidungsproblem* was, therefore, no.

"You can build an organ which can do anything that can be done," explained von Neumann, paraphrasing Turing, in a lecture in 1949, "but you cannot build an organ which tells you whether it can be done"[2]. Sensing the limits of deterministic machines, Turing began to explore non-deterministic computation by 'oracle' machines. These proceed step-by-step, but occasionally make unpredictable leaps by consulting "a kind of oracle as it were"[3].

CODE BREAKING

Having completed his PhD, Turing returned to England in July 1938. The outbreak of the Second World War soon sparked demand for his ideas, and he was sequestered at the Government Code & Cypher School at Bletchley Park. There, Turing and his colleagues, including his mentor, topologist Maxwell 'Max' Newman, deciphered enemy communications, including messages encrypted by the German Enigma machine — a Turing machine with an internal mechanism that shifted through 10^{20} possible configurations to scramble the input text.

Starting with a set of electromechanical devices called bombes, each of which could emulate 36 suspected Enigma configurations at a time, the researchers at Bletchley Park, assisted by engineer Thomas Flowers at the General Post Office Research Station in Dollis Hill, London, developed a machine called Colossus — a sophisticated electronic digital computer. A 1,500-vacuum-tube internal memory provided Colossus with a programmable state of mind that searched for clues in coded sequences scanned from punched paper tape.

Colossus was swiftly improved and duplicated, producing a second generation of 2,400-tube machines that influenced the outcome of the war and the development of modern computers, although Britain's Official Secrets Act kept the details embargoed for more than 30 years. When the war ended, the push for more powerful computers shifted from cryptanalysis to the design of nuclear weapons, and the United States, which had declassified its wartime computer, the ENIAC (Electronic Numerical Integrator and Computer), in February 1946, assumed the lead.

At the Institute for Advanced Study in Princeton, and with funding from the US Army, the Office of Naval Research and the US Atomic Energy Commission, von Neumann set out to build an electronic version of Turing's universal computing machine. He wanted a Turing machine with a memory that was accessible at the speed of light, and he decided to build it himself. The US government wanted to know whether a hydrogen bomb was feasible, so von Neumann promised it a machine, with 5 kilobytes of storage, that could run the required hydrodynamic codes. The computer's design was made public so that copies could be freely duplicated — and commercialized by IBM. "Words coding the orders are handled in the memory just like numbers," von Neumann announced at the first project meeting, on 12 November 1945 (ref. 4). This mingling of data and instructions was central to Turing's model. Most computers today are the direct offspring, in terms of their logical architecture, of a Turing machine built from war-surplus components in an outbuilding on a former New Jersey farm.

Turing and von Neumann first met in Cambridge in 1935, and subsequently spent two years together in Princeton, where Newman joined them for 6 months. How much Turing and von Neumann collaborated during the war remains unknown, but we do know that Turing was in the United States between November 1942 and March 1943, and that von Neumann was in England between February and July 1943. During the war, British physicists, in consultation with von Neumann, made important contributions to the atomic bomb project at Los Alamos in New Mexico; and US cryptanalysts, in consultation with Turing, contributed to the effort at Bletchley Park. Although they could not communicate them openly in writing, Turing, von Neumann and Newman probably shared their ideas verbally, both during and after the war.

"Most computers today are the direct offspring of a Turing machine built from war-surplus components."

Turing's model was one-dimensional: a string of symbols encoded on a tape. von Neumann's implementation was two-dimensional: the random-access address matrix that underlies most computers today. The Internet — many Turing machines with concurrent access to a shared tape — has made the landscape three-dimensional. Yet the way in which computers work has remained fundamentally unchanged since 1946.

LEARNING FROM MISTAKES

Both Turing and von Neumann were conscious of processing errors in their machines. Early codes could be fully debugged, but the hardware was more unreliable, giving inconsistent results — a problem that has since been reversed. Both men knew that biology relied on statistical, fault-tolerant methods for processing information (such as pulse-frequency coding in the brain) and assumed that technology would follow nature's lead. If "every error has to be caught, explained and corrected, a system of the complexity of the living organism would not run for a millisecond", von Neumann commented[5].

"If a machine is expected to be infallible, it cannot also be intelligent," Turing noted in 1947 (ref. 6). When Turing joined Newman's group at the University of Manchester, UK, the following year and began designing the Manchester Mark 1 (a prototype for the Ferranti Mark 1, the first commercial stored-program electronic digital computer), he included a random-number generator, which allowed the computer to make guesses and learn from its mistakes.

Turing's deterministic universal machine receives the most attention, but his non-deterministic oracle machines are closer to the way in which intelligence really works: intuition bridging the gaps between logical sequences. Turing's oracle machines are no longer theoretical abstractions — an Internet search engine, for instance, operates deterministically until a person clicks on a link, adding non-deterministically to the search engine's map of where the meaningful information is.

Turing wanted to know how molecules were able to collectively self-organize, and whether machines could think. Von Neumann wanted to know how the brain worked and whether machines could reproduce. Turing, who died at the age of 41, left behind an unfinished theory of morphogenesis, and von Neumann, who died aged 53, left an unfinished theory of self-reproduction — a model inspired by the Turing machine's ability to generate copies of itself.

Had Turing and von Neumann lived longer, we can only imagine how their ideas might have merged. Their lives were both cut short just as the mechanism underlying the translation between sequence and structure in biology was revealed. ■

George Dyson *is a writer based in Bellingham, Washington, and author of* Turing's Cathedral.
e-mail: Gdyson@ias.edu

1. Turing, A. M. *Proc. Lond. Math. Soc.* **s2-42,** 230–265 (1936–37).
2. von Neumann, J. In: *Theory of Self-Reproducing Automata* (ed. Burks, A. W.) 42–56 (Univ. Illinois Press, 1966).
3. Turing, A. M. *Proc. Lond. Math. Soc.* **s2-45,** 161–228 (1939).
4. Minutes of the Institute for Advanced Study Electronic Computer Project, Meeting 1, 12 November 1945.
5. von Neumann, J. In: *Theory of Self-reproducing Automata* (ed. Burks, A. W.) Univ. Illinois Press, 1966).
6. Turing, A. M. Lecture to London Mathematical Society 20 February 1947. Turing archive held at King's College, Cambridge.

Life's code script

Turing machines and cells have much in common, argues **Sydney Brenner**.

Biological research is in crisis, and in Alan Turing's work there is much to guide us. Technology gives us the tools to analyse organisms at all scales, but we are drowning in a sea of data and thirsting for some theoretical framework with which to understand it. Although many believe that 'more is better', history tells us that 'least is best'. We need theory and a firm grasp on the nature of the objects we study to predict the rest.

Three of Turing's papers are relevant to biology. In 1952, 'The chemical basis of morphogenesis'[1] explored the hypothesis that patterns are generated in plants and animals by "chemical substances called morphogens, reacting together and diffusing through a tissue". Using differential equations, Turing set out how instabilities in a homogeneous medium could produce wave patterns that might account for processes such as the segregation of tissue types in the developing embryo.

Yet biological support for Turing's idea has been marginal. The pre-ordered patterns found in *Drosophila* development do not fit the instability theory, which, until recently, could describe only chemical systems. Skin patterning has, however, been shown to follow a broader interpretation of Turing's terms[2], where cell-to-cell signalling pathways, rather than individual molecules, are considered. The ion channels postulated by Alan Lloyd Hodgkin and Andrew Huxley[3], also in 1952, were discovered more immediately by molecular biology.

Turing published another biology-related paper, in 1950. 'Computing machinery and intelligence'[4] introduced the Turing test as an imitation game in which an outside interrogator tries to distinguish between a computing machine and a human foil through their responses to questions. But the Turing test does not say whether machines that match humans have intelligence, nor does it simulate the brain. For that, we need a theory for how the brain works.

The most interesting connection with biology, in my view, is in Turing's most important paper: 'On computable numbers with an application to the *Entscheidungsproblem*'[5], published in 1936, when Turing was just 24.

Computable numbers are defined as those whose decimals are calculable by finite means. Turing introduced what became known as the Turing machine to formalize the computation. The abstract machine is provided with a tape, which it scans one square at a time, and it can write, erase or omit symbols. The scanner may alter its mechanical state, and it can 'remember' previously read symbols. Essentially, the system is a set of instructions written on the tape, which describes the machine. Turing also defined a universal Turing machine, which can carry out any computation for which an instruction set can be written — this is the origin of the digital computer.

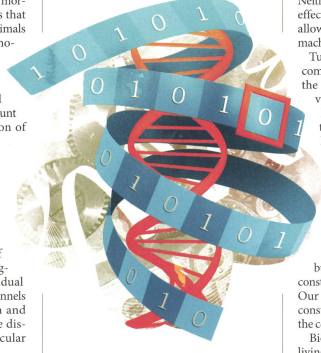

ILLUSTRATION BY ANDY POTTS

Turing's ideas were carried further in the 1940s by mathematician and engineer John von Neumann, who conceived of a 'constructor' machine capable of assembling another according to a description. A universal constructor with its own description would build a machine like itself. To complete the task, the universal constructor needs to copy its description and insert the copy into the offspring machine. Von Neumann noted that if the copying machine made errors, these 'mutations' would provide inheritable changes in the progeny.

Arguably the best examples of Turing's and von Neumann's machines are to be found in biology. Nowhere else are there such complicated systems, in which every organism contains an internal description of itself. The concept of the gene as a symbolic representation of the organism — a code script — is a fundamental feature of the living world and must form the kernel of biological theory.

Turing died in 1954, one year after the discovery of the double-helical structure of DNA by James Watson and Francis Crick, but before biology's subsequent revolution. Neither he nor von Neumann had any direct effect on molecular biology, but their work allows us to discipline our thoughts about machines, both natural and artificial.

Turing invented the stored-program computer, and von Neumann showed that the description is separate from the universal constructor. This is not trivial. Physicist Erwin Schrödinger confused the program and the constructor in his 1944 book *What is Life?*, in which he saw chromosomes as "architect's plan and builder's craft in one". This is wrong. The code script contains only a description of the executive function, not the function itself.

Thus, Hodgkin and Huxley's equations represent properties of the nerve impulse as an electrical circuit, but the required channels and pumps are constructed from specifications in the genes. Our problems reside in understanding the constructor part of the machinery, and here the cell is the right level of abstraction[6].

Biologists ask only three questions of a living organism: how does it work? How is it built? And how did it get that way? They are problems embodied in the classical fields of physiology, embryology and evolution. And at the core of everything are the tapes containing the descriptions to build these special Turing machines. ■

Sydney Brenner *is a senior fellow at the Janelia Farm Research Campus, Howard Hughes Medical Institute, Ashburn, Virginia, 20147, USA.*

1. Turing, A. M. *Phil. Trans. R. Soc. Lond. B* **237,** 37–72 (1952).
2. Kondo, S. & Miura, T. *Science* **329,** 1616–1620 (2010).
3. Hodgkin, A. L. & Huxley, A. F. *J. Physiol.* **117,** 500–544 (1952).
4. Turing, A. M. *Mind* **49,** 433–460 (1950).
5. Turing, A. M. *Proc. Lond. Math. Soc.* **s2-42,** 230–265 (1936–37).
6. Brenner, S. *Phil. Trans. R. Soc. B* **365,** 207–212 (2010).

TURING AT 100
A legacy that spans science:
nature.com/turing

ILLUSTRATION BY ANDY POTTS

Is the brain a good model for machine intelligence?

To celebrate the centenary of the year of Alan Turing's birth, four scientists and entrepreneurs assess the divide between neuroscience and computing.

RODNEY BROOKS
Avoid the cerebral blind alley

Emeritus professor of robotics, Massachusetts Institute of Technology

I believe that we are in an intellectual cul-de-sac, in which we model brains and computers on each other, and so prevent ourselves from having deep insights that would come with new models.

The first step in this back and forth was made by Alan Turing. In his 1936 paper[1] laying the foundations of computation, Turing used a person as the basis for his model. He abstracted the actions of a human 'computer' using paper and pencil to perform a calculation (as the word meant then) into a formalized machine, manipulating symbols on an infinite paper tape.

But there is a worry that his version of computation, based on functions of integers, is limited. Biological systems clearly differ. They must respond to varied stimuli over long periods of time; those responses in turn alter their environment and subsequent stimuli. The individual behaviours of social insects, for example, are affected by the structure of the home they build and the behaviour of their siblings within it.

Nevertheless, for 70 years, those people working in what is now called computational neuroscience have assumed that the brain is a computer — a machine that is equivalent to Turing's finite-state machine with an infinite tape and a finite symbol set, and that does computation.

In 1943, Warren McCulloch and Walter Pitts[2] noted the "all-or-none" nature of the firing of neurons in a nervous system, and suggested that networks of neurons could be modelled as logical propositions. They modelled a network of neurons as circuits of logic gates, noting that these may "compute only such numbers as can a Turing machine". But more, they proposed that everything at a psychological level happens in these networks. Over the decades, such ideas begat more studies in neural networks, which in turn begat computational neuroscience. Now those metaphors and models pervade explanations of how the brain 'computes'. But these binary abstractions do not capture all the complexities inherent in the brain.

So now I see circles before my eyes. The brain has become a digital computer; yet we are still trying to make our machines intelligent. Should those machines be modelled on the brain, given that our models of the brain are performed on such machines? That will probably not be enough.

When you are stuck, you are stuck. We will get out of this cul-de-sac, but it will take some brave and bright souls to break out of our circular confusions of models.

DEMIS HASSABIS
Model the brain's algorithms

Neuroscientist, computer-game producer and chess master, University College London

Alan Turing looked to the human brain as the prototype for intelligence. If he were alive today, he would surely be working at the intersection of natural and artificial intelligence.

Yet to date, artificial intelligence (AI) researchers have mostly ignored the brain as a source of algorithmic ideas. Although in Turing's time we lacked the means to look inside this biological 'black box', we now have a host of tools, from functional magnetic resonance imaging to optogenetics, with which to do so.

Neuroscience has two key contributions to make towards progress in AI. First, the many structures being discovered in the brain — such as grid cells used for navigation, or hierarchical cell layers for vision processing — may inspire new computer

TURING AT 100
A legacy that spans science:
nature.com/turing

algorithms and architectures. Second, neuroscience findings may validate the plausibility of existing algorithms being integral parts of a general AI system.

To advance AI, we need to better understand the brain's workings at the algorithmic level — the representations and processes that the brain uses to portray the world around us. For example, if we knew how conceptual knowledge was formed from perceptual inputs, it would crucially allow for the meaning of symbols in an artificial language system to be grounded in sensory 'reality'.

AI researchers should not only immerse themselves in the latest brain research, but also conduct neuroscience experiments to address key questions such as: "How is conceptual knowledge acquired?" Conversely, from a neuroscience perspective, attempting to distil intelligence into an algorithmic construct may prove to be the best path to understanding some of the enduring mysteries of our minds, such as consciousness and dreams.

DENNIS BRAY

Brain emulation requires cells

Department of Physiology, Development and Neuroscience, University of Cambridge

Machines can match us in many tasks, but they work differently from networks of nerve cells. If our aim is to build machines that are ever more intelligent and dexterous, then we should use circuits of copper and silicon. But if our aim is to reproduce the human brain, with its quirky brilliance, capacity for multitasking and sense of self, we have to look for other materials and different designs.

Computers outperform us in complex mathematical calculations and are better at storing and retrieving data. We accept that they can beat us at chess — once regarded as the apogee of human intellect. But the success of a computer called Watson in US television quiz show *Jeopardy!* in 2011 was a nail in the coffin of human superiority. The machine beat two human contestants by answering questions posed in colloquial English, making sense of cultural allusions, metaphors, puns and jokes. If Alan Turing had been given a transcript of the show, would he have spotted the odd one out?

Watson may be the latest vindication of Turing's view of intellectual processes as a series of logical states. But its internal workings are not based on the human brain. Broad similarities in organization might be imposed by the nature of the task, but most software engineers neither know nor care about anatomy or physiology. Even biologically inspired approaches such as cellular automata, genetic algorithms and neural networks have only a tenuous link to living tissue.

In 1944, Turing confessed his dream of building a brain, and many people continue in that endeavour to this day. Yet any neurobiologist will view such attempts as naive. How can you represent a neuronal synapse — a complex structure containing hundreds of different proteins, each a chemical prodigy in its own right and arranged in a mare's nest of interactions — with a single line of code? We still do not know the detailed circuitry of any region of the brain well enough to reproduce its structure. Brains are special. They steer us through the world, tell us what to do or say, and perform myriad vital functions. Brains are the source of our emotions, motivation, creativity and consciousness. Because no one knows how to reproduce any of these features in an artificial machine, we must consider that something important is missing from the canonical microchip.

Brains differ from computers in a number of key respects. They operate in cycles rather than in linear chains of causality, sending and receiving signals back and forth. Unlike the hardware and software of a machine, the mind and brain are not distinct entities. And then there is the question of chemistry.

Living cells process incoming sensory information and generate not just electrical signals but subtle biochemical changes. Cells are soft, malleable and built from an essentially infinite variety of macromolecular species quite unlike silicon chips. Organisms encode past experiences in distinct cellular states — in humans these are the substrate of goal-oriented movements and the sense of self. Perhaps machines built from cell-like components would be more like us.

AMNON SHASHUA

Speed will trump brain's advantages

Sachs Professor of Computer Science, Hebrew University of Jerusalem, and co-founder and chairman of Mobileye

The saying that "people who are really serious about software should make their own hardware", attributed to computer scientist Alan Kay in the 1980s, still rings true today. The idea that the function and form of computing architecture should serve each other is at the root of algorithms in signal processing, image rendering, gaming, video compression and streaming. I believe that it is also true for the human brain — meaning that the brain does not implement 'intelligence' in the same way as a computer.

Two of the many fundamental differences between the brain and the computer are memory and processing speed. The analogue of long-term memory in a computer is the hard disk, which can store practically unlimited amounts of data. Short-term information is held in its random access memory (RAM), the capacity of which is astronomical compared with the human brain. Such quantitative differences become qualitative when considering strategies for intelligence.

"Signals in the brain are transmitted at a snail's pace."

Intelligence is manifested by the ability to learn. Machine-learning practitioners use 'statistical learning' which requires a very large collection of examples on which to generalize. This 'frequentist' approach to probabilistic reasoning needs vast memory capacity and algorithms that are at odds with available data on how the brain works. For example, IBM computer Watson needed to consume terabytes of reference material to beat human contestants on *Jeopardy!*. Volvo's pedestrian-detection system (developed by Mobileye) learned to identify people by using millions of pictures. In both cases, the human brain is considerably more parsimonious in the reliance on data — something that does not constrain the computer.

In terms of processing power, the brain can reach about 10–50 petaflops — equivalent to hundreds of thousands of the most advanced Intel Core i7 CPUs. Yet signals in the brain are transmitted at a snail's pace — five or six orders of magnitude slower than modern CPUs. This huge difference in communication speed drives vastly different architectures.

The brain compensates for the slow signal speed by adopting a hierarchical parallel structure, involving successive layers with increasing receptive field and complexity. By comparison, a computer architecture is usually flat and, because of its much faster clock rate, can employ brute-force techniques. Computer chess systems such as Deep Blue use pattern-recognition strategies, such as libraries of opening moves and completely solved end-games, complemented by their ability to evaluate the outcomes of some 200 million moves per second. This is way beyond the best grandmaster.

An intimate understanding of how cognitive tasks are performed at an algorithmic level would allow artificial intelligence to grow in leaps and bounds. But we must bear in mind that the vastly different architecture of the computer favours strategies that make optimal use of its practically unlimited memory capacity and brute-force search. ■

1. Turing, A. M. *Proc. Lond. Math. Soc.* **s2-42**, 230–265 (1936–37).
2. McCulloch, W. S. & Pitts, W. H. *Bull. Math. Biophys.* **5**, 115–133 (1943).

ILLUSTRATION BY ANDY POTTS

Pattern formation

We are only beginning to see the impact of Turing's influential work on morphogenesis, says **John Reinitz**.

Alan Turing's 1952 paper on the origin of biological patterning[1] solved an intellectual problem that had seemed so hopeless that it caused a great developmental biologist, Hans Driesch, to give up science and turn to the philosophy of vitalism.

In the late nineteenth century, Driesch, and later Hans Spemann, demonstrated that animal bodies develop from a patternless single cell, rather than growing from a microscopic, preformed version of the adult body — in humans, the 'homunculus'. But such self-organization, Driesch realized, could not be understood with the ideas of that century. Before the invention of computers, applied mathematics dealt only with linear differential equations, which can amplify a pattern but not generate it.

In 'The chemical basis of morphogenesis', Turing showed that a pattern can indeed form *de novo*. In considering how an embryo's development unfolds instant by instant from its molecular and mechanical state, Turing was using a modern approach. Developmental biologists today similarly investigate how molecular determinants and forces exerted by cells control embryonic patterning.

Turing's focus was on chemical patterns: he coined the term 'morphogen' as an abstraction for a molecule capable of inducing tissue differentiation later on. This concept will be familiar to any molecular biologist: the protein products of the *HOX* gene cluster, for example, which are essential for body patterning throughout the animal kingdom, are morphogens in Turing's sense. (Confusingly, the term has been more narrowly defined since.)

At the heart of pattern-making is symmetry-breaking. Turing considered an idealized embryo beginning with a uniform concentration of morphogens, which have translational symmetry that is lost as specific tissues emerge. He raised deep questions that are still unsolved, noting for instance that all physical laws known at the time had mirror-image symmetry, but biological systems did not. Turing speculated that the asymmetry of organisms originated from that of biological molecules. His point is still relevant to life's origins.

Turing's argument involved a mathematical trick: he created a nonlinear system by turning on diffusion discontinuously in an otherwise linear system at a specific instant. Without diffusion, the system is stable and homogeneous, but with diffusion, it becomes unstable and forms spatial pattern. The brilliance of the trick is that the nonlinearity is confined to a single point in time, so that at all other times, only the theory of linear equations is needed. Turing cleverly arranged to have diffusion generate pattern, rather than blur it, as it usually does.

The influence of Turing's paper is difficult to overstate. It was a transition point from the era of analytical mathematics to that of computational mathematics. Although his proof was constructed analytically, Turing's paper contains the first computer simulations of pattern formation in the presence of stochastic fluctuations, and is possibly the first openly published case of computational experimentation.

Turing used analytical arguments of the nineteenth century to point the way towards the computational science of the twenty-first century. He was well aware, however, that nonlinear science and developmental biology would require more advanced computational methods. "Most of the organism, most of the time, is developing from one pattern into another, rather than from homogeneity into a pattern," he stated[1]. He realized that even though an embracing theory for such processes might not be possible, individual cases could be modelled with a digital computer.

Yet Turing's work is frequently misinterpreted, perhaps because he died tragically in 1954, before he could correct the record. His analytical arguments are often mistaken for biological predictions, although Turing did not intend them as such. His hypothetical system, based on two substances, was a simplification. For the pattern-forming trick to work, one substance should catalyse synthesis of both substances while diffusing slowly; the other should catalyse destruction of both substances while diffusing rapidly. For patterns that shift over time, three substances would be required. A field of investigation of these models has sprung up[2], but credit or blame for the results rests with those authors, not Turing.

What Turing should receive credit for is opening the door to a new view of developmental biology, in which we deal directly with the chemical reactions and mechanical forces embryos use to self-organize their bodies from a single cell. He was well ahead of his time. It was three decades before the work on *Drosophila* embryos by Lewis[3], Wieschaus and Nüsslein-Volhard[4] led to the discovery of real morphogens. It is the young researchers of today who will benefit most from reading Turing's work — seeing his ideas about morphogenesis not as speculation but as the conceptual framework for concrete problems. ■

John Reinitz *is in the departments of statistics, ecology and evolution, and molecular genetics and cell biology at the University of Chicago, Chicago, Illinois 60637, USA.*
reinitz@galton.uchicago.edu

1. Turing, A. M. *Phil. Trans. R. Soc. Lond. B* **237,** 37–72 (1952).
2. Kondo, S. & Miura, T. *Science* **329,** 1616–1620 (2010).
3. Lewis, E. B. *Nature* **276,** 565–570 (1978).
4. Nüsslein-Volhard, C. & Wieschaus, E. *Nature* **287,** 795–801 (1980).

TURING AT 100
A legacy that spans science:
nature.com/turing

The incomputable reality

The natural world's interconnectivity should inspire better models of the Universe, says **Barry Cooper**.

Alan Turing put bounds on what is computable in a famous 1936 paper[1]. The Turing machines he presented implement finite algorithms, handling data coded as real numbers. They are deterministic, but give some bizarre results. You can build a universal machine that can simulate any other Turing machine. But not every question you can ask of it has a computable answer: you cannot predict, for example, whether it ever spits out a given number or series of numbers.

By coincidence, our Newtonian view of physics faltered at about the same time as our computable view of mathematics. Lingering problems in classical physics, such as the unpredictable trajectories of three bodies following a collision, may involve incomputability. Albert Einstein's theory of general relativity opens up a new world of computation with exotic objects such as spinning black holes. Quantum mechanics tells us that measurements are inherently uncertain.

The concept of computability is basic to modern science, from quantum gravity to artificial intelligence. It is also relevant in the everyday world, where it is useful to distinguish problems that are merely difficult to compute in practice from those that are intrinsically impossible with any machine. Incomputability should trouble economists, because breakdowns of control in chaotic markets can wreak havoc.

But disciplinary boundaries are preventing us from getting a full view of its role. Cosmetic differences may hide revealing parallels.

ILLUSTRATION BY ANDY POTTS

EMERGENT PHENOMENA

Turing was interested in the mathematics of computing and also in its embodiment — the material environment that houses it. This theme links all of his work, from machines to the brain and morphogenesis. Although many mathematicians and software engineers today see it as irrelevant, embodiment is key to explaining the physical world.

Take turbulence: a river swollen by recent rain occasionally erupts into surprising formations that we would not expect from the basic dynamics of the water flow. The reason is coherence — non-local connectivity affects the water's motion. Turbulence, and other 'emergent' nonlinear phenomena, may not be computable with a Turing machine. Zebra stripes and tropical-fish patterns, which Turing described in 1952–54 with his differential equations for morphogenesis, arise similarly.

TURING AT 100
A legacy that spans science:
nature.com/turing

Even in nonlinear systems, such high-order behaviour is causal — one phenomenon triggers another. Levels of explanation, from the quantum to the macroscopic, can be applied. But modelling the evolution of the higher-order effects is difficult in anything other than a broad-brush way. Such problems infiltrate all our models of the natural world.

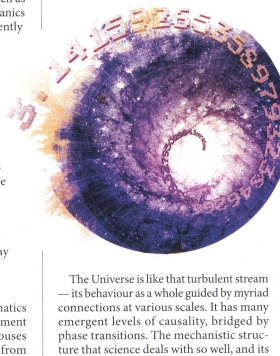

The Universe is like that turbulent stream — its behaviour as a whole guided by myriad connections at various scales. It has many emergent levels of causality, bridged by phase transitions. The mechanistic structure that science deals with so well, and its invariant laws, are hard to explain in terms of the quantum level. Biology emerges from the quantum world, but is not computable from it. We are part of an organic whole — fragmented but coherent.

Across these boundaries, higher-level relations can feed back into lower ones. But looking up from a lower level, the causality will not be computable. For example, the uncertainty principle prevents the quantum world from fully describing the state of a particle at any instant. A measurement produces a full description, but we cannot compute how it does it. In Turing's world, a description of reality is not always enough for a computable prediction.

Nature presents us with new ways of computing, from the Universe to the brain. Turing went on to build logical hierarchies to better understand real-world computation, which includes intuitive or unpredictable leaps[2]. Researchers experimenting with intelligent machines today see the possibilities in such an approach. But problems of control of higher-order behaviours still present formidable challenges to implementing it.

BRIDGE BUILDING

It took nature millions of years to build a human brain. Meanwhile, we have to live with the stupidity of purely algorithmic processes. We need to embrace more experimental approaches to computation, and a renewed respect for embodied computing — as anticipated in Turing's late work in the 1950s on artificial intelligence and morphogenesis.

Bridges between mathematicians and physicists are important if we are to do this. It is a long time since Kurt Gödel and Albert Einstein chatted in the halls of Princeton University in New Jersey. Mathematicians can bring to the table Turing's model of basic causal structure. This would help physicists to discover more complete descriptions of the Universe — making redundant Hugh Everett's many-worlds interpretation and related multiverse hypotheses — and fix the arbitrariness of parts of the standard model of particle physics.

Samson Abramsky, a computer scientist at the University of Oxford, UK, recently asked: "Why do we compute?" Turing computation does not create anything that is not there already in the initial data. Can information increase in computation?

If we look at the world with new eyes, allowing computation full expression, we may come to startling conclusions. ■

Barry Cooper *is in the School of Mathematics, University of Leeds, Leeds LS2 9JT, UK.*
e-mail: pmt6sbc@leeds.ac.uk

1. Turing, A. M. *Proc. Lond. Math. Soc.* **s2-42,** 230–265 (1936–37).
2. Turing, A. M. *Proc. Lond. Math. Soc.* **s2-45,** 161–228 (1939).

M. KINGWILL/ARENAPAL

Our brains recreate the emotions of actors such as Geraldine James when we watch them perform.

NEUROSCIENCE

Powerful acts

Giovanni Frazzetto explores how theatre exerts its psychological effects on the emotions.

From rage and grief to exquisite tenderesse, emotion is laid bare in theatre. Few art forms electrify or illuminate as powerfully as stage acting. But how have theatrical greats such as John Gielgud or Vanessa Redgrave cast their spell? Acting may be one of the most ancient arts, but science is only just beginning to get to grips with it.

Science started to seep into theatre in the late nineteenth and early twentieth centuries, with the Russian actor and theatre director Constantin Stanislavski. Founder of the influential Moscow Art Theatre, Stanislavski turned to physiologist Ivan Pavlov's research on conditioned reflexes to improve his acting method. The aim was to create performance that united psychological experience and physical action.

➲ NATURE.COM
A review of Danny Boyle's staging of *Frankenstein*: go.nature.com/wqxsbt

Stanislavski sought a way to consciously trigger an actor's emotional expression. Science had begun to discover that neural pathways underlie complex behaviour and emotions, which can be conditioned in response to a changing environment. By practising key physical actions pertinent to the character and the play, Stanislavski realized, the actor could learn, by reflex, how to express the psychological experience of the emotion — with help from the imagination. A particular posture or movement would trigger a particular emotion. So by working hard on small actions such as clenching the fists and tensing the neck muscles, the actor could trigger anger, or they could awaken feelings of despair by shuffling, drooping and bowing the shoulders.

But, as we now know, the psychology of performance is more complex than this. To deliver a believable performance, actors need to remember not just emotions, body postures and expressions, but also their cues and lines. And, more importantly, they must seek ways of engaging with their audience to evoke empathy — the recognition or sharing of emotional states.

German philosopher Theodor Lipps was the first to use the term empathy (*Einfühlung*, literally 'feeling into') in the early twentieth century as a way of describing the relationship between artwork and observer in the psychology of aesthetic experience. In the 1990s, Italian neurophysiologists Giacomo Rizzolatti, Vittorio Gallese and their colleagues at the University of Parma in Italy offered a neurological framework for studying empathy through their discovery of mirror neurons — cells that fire both when we perform an action, and when we observe someone else performing it. They showed that our visual-motor system is activated as if we were executing an action that we are simply watching: the brain simulates that action.

These discoveries have resonated widely among theatrical professionals. They extend to intentionality (thinking of a way of doing some action), imitation (the replication of an action) and action understanding (grasping the import of an action) — all central to acting technique.

The actor must also demand something else of the audience: a suspension of disbelief. The phrase was coined in 1817 by English poet and philosopher Samuel Taylor Coleridge to describe how weaving enough facts into a fantastical narrative will help readers to accept the story, rather than judge it as implausible. Film-makers suspend disbelief by exploiting the power of moving images in a darkened room, which lures an audience into their simulacrum of reality. In theatre, suspension of disbelief hinges on the switch between two realities — the set and the cast of actors, and the places and characters they represent. In the prologue to *Henry V*, Shakespeare asks the audience to transform the bare stage by seeing it as the world of the king at war with France: "Piece out our imperfections with your thoughts … and make imaginary puissance."

"Acting is predicated on technique and craft, but remains visceral and intuitive."

Twentieth-century German playwright Bertolt Brecht deliberately turned this tactic on its head in his 'epic theatre' system. By using techniques such as having the actors suddenly sing out of character, he ensured that his audiences became

emotionally detached from the characters. The audience members then became aware that they were witnessing fiction and were able to critically question the social realities represented in the play.

The cognitive processes underlying the suspension of disbelief have been the subject of several scientific studies. In 2010, Marie-Noëlle Metz-Lutz of the University of Strasbourg, France, and her colleagues used functional magnetic resonance imaging (fMRI) to scan the brains of people watching a play to pinpoint when they were transported into another reality. This was defined as when the subject's brain response tallied with a passage in the script intended to elicit such a response. The brain regions that fired at those moments included two areas involved in processing language and, specifically, in understanding metaphor, denoting the power of language to capture a spectator's attention. Both regions are also involved in processes of social and aesthetic judgements, probably governing appreciation of the writing style, plot or characterization.

The French team also found that the subjects' heart rates slowed during transportation, and that brain activity fell in areas involved in building consciousness about the self and the external world. Without activity in these regions, an observer will take the fictionalized reality of the play at face value, despite the sensory perception of the stage, set and actors. Such results point to complete absorption in a play as a sort of hypnotic state involving the temporary loss of self-reference, and a disconnection from immediate sensory information — a distinct feeling of being 'carried away'.

In theory, such scanning experiments might help playwrights to identify specific language and theatrical devices that trigger audiences to become as absorbed as possible, and so enrich acting as an art and theatre as a vehicle of meaning and 'enchantment'. With a nod to Stanislavski, playwrights could focus on what movements or expressions are the most poignant, and which are most effective at conveying grief, compassion or joy. Such studies could also reveal which metaphors express an action or thought with the most brevity and wit, and what elements of plot device or vocal emphasis can make a difference in the brain.

Yet fMRI images and statistics will never replace the unpredictability and revelatory power of what is born in the rehearsal room. Acting is predicated on technique and craft, but remains visceral and intuitive. ■

Giovanni Frazzetto *is a visiting research fellow in the School of Science and Social Policy at King's College London, Strand, London WC2R 2LS, UK.*
e-mail: gio@giovannifrazzetto.com

Books in brief

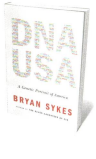

DNA USA: A Genetic Portrait of America
Bryan Sykes W. W. NORTON *320 pp. £19.99 (2012)*
The US human population is a bouillabaisse of DNA. Geneticist Bryan Sykes took on the challenge of identifying its ingredients on an epic cross-country trip. He recounts the detective work — including interviews with genealogists and fellow geneticists — and methodology behind the findings. How did European genes appear in the DNA of Native Americans some 10,000 years ago, for instance? And why does the southwestern Hispanic population contain genes typically found in Jewish people? Ultimately, Sykes suggests, the country is an even richer human mix than we thought.

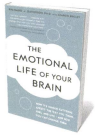

The Emotional Life of Your Brain: How Its Unique Patterns Affect the Way You Think, Feel, and Live — And How You Can Change Them
Richard J. Davidson and Sharon Begley HUDSON STREET PRESS *279 pp. $25.95 (2012)*
Why do some people plod stoically through crises while others collapse? Science writer Sharon Begley and neuropsychologist Richard Davidson argue that each of us has an 'emotional style': a pattern of responses to life's events that is allied to underlying brain systems. Looking at dimensions from social intuition to context sensitivity, the authors suggest that we can achieve better equilibrium by rewiring our emotional style through research-inspired exercises.

Game Changer: Animal Rights and the Fate of Africa's Wildlife
Glen Martin UNIVERSITY OF CALIFORNIA PRESS *243 pp. £20.95 (2012)*
Africa's wild megafauna are caught in the crossfire between animal-welfare campaigners and conservationists, argues environmental reporter Glen Martin. In this pacy, unsentimental account, Martin interviews seasoned conservation biologists, zoologists and game wardens, focusing on practice in Kenya, Namibia and Tanzania. He concludes that holistic strategies incorporating habitat conservation, controlled hunting and respect for local people's needs are workable — and points out that measures such as ecotourism and protection for iconic species have backfired dramatically.

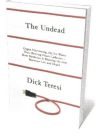

The Undead: Organ Harvesting, the Ice-Water Test, Beating Heart Cadavers — How Medicine Is Blurring the Line Between Life and Death
Dick Teresi PANTHEON *368 pp. $26.95 (2012)*
The moment of death, suggests science writer Dick Teresi, is harder to pin down than ever. He introduces us to those who work at this borderline: cell biologists, specialist doctors, undertakers and people who have recovered from comas. Charting historical definitions of death, the thinking of research greats and debates over near-death experiences, Teresi notes that the ethical challenges are immense, asking, for instance, whether all organ donors are unrevivable.

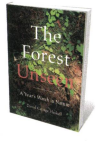

The Forest Unseen: A Year's Watch in Nature
David George Haskell VIKING *288 pp. $25.95 (2012)*
Training a biologist's eye on ecology, geology and climate, David Haskell visited a square metre of old-growth forest in southeastern Tennessee nearly every day for a year. His observations — of lichens, snowflakes, salamanders and more — are deftly interwoven with the science. His account is fascinating, whether he's stripping off in January to experience the physiological effects of severe cold, describing the symphonic sounds of trees in a high wind, or wondering at the bacteriocidal properties of a vulture's digestive tract.

INFECTIOUS DISEASE

Chronicles of a killer virus

Just over 30 years after HIV/AIDS was first recognized, three accounts of its ravages intrigue **Robin Weiss**.

The AIDS Conspiracy: Science Fights Back
NICOLI NATTRASS
Columbia University Press: 2012. 240 pp. $34.50, £24

The Origins of AIDS
JACQUES PÉPIN
Cambridge University Press: 2011. 310 pp. £45, $28.99

AIDS at 30: A History
VICTORIA A. HARDEN
Potomac Books: 2012. 304 pp. $29.95

As a frightening pandemic associated with sex, blood and death, AIDS was bound to evoke a rich mythology. Nicoli Nattrass's *The AIDS Conspiracy* deals with those myths and how scientific arguments counteract them. Jacques Pépin's *The Origins of AIDS* looks back at the emergence of HIV in the era before the syndrome was recognized, and Victoria Harden's *AIDS at 30* covers the period after its identification in 1981.

The AIDS Conspiracy is essential reading for anyone who is curious about why some people will not accept scientific facts about the nature, origin and lethality of HIV. As an HIV researcher, I used to divide people's strange beliefs about AIDS into myths of denial, and of blame and conspiracy. But Nattrass, who directs the AIDS and Society Research Unit at the University of Cape Town in South Africa, explains how HIV denialism has also become a conspiratorial attack on science and medicine — one that aims to convince people that antiretroviral therapy is more harmful than the 'blameless' virus.

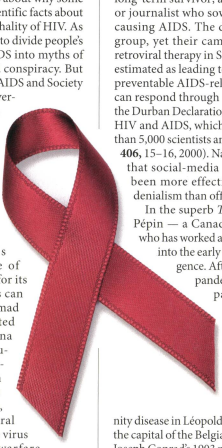

OCEAN/CORBIS

Even when HIV is accepted as the cause of AIDS, Africa is blamed for its origin. Yet new diseases can arise anywhere: BSE or 'mad cow disease' in the United Kingdom, SARS in China and the 2009 H1N1 influenza pandemic in Mexico. Some AIDS creation myths continue to have an allure — for example, that HIV came out of oral polio vaccines, or that the virus is a man-made germ-warfare agent that was deliberately released in Africa by the United States.

Nattrass identifies four types of HIV denialist: the dissident scientist who lends credibility; the 'cultropreneur' who peddles quack therapies; the living icon or long-term survivor; and the praise-singer or journalist who sows doubt about HIV causing AIDS. The dissidents are a tiny group, yet their campaign against antiretroviral therapy in South Africa has been estimated as leading to more than 300,000 preventable AIDS-related deaths. Science can respond through mechanisms such as the Durban Declaration on the link between HIV and AIDS, which was signed by more than 5,000 scientists and physicians (*Nature* **406,** 15–16, 2000). Nattrass also points out that social-media activists have often been more effective at tackling HIV denialism than official bodies.

In the superb *The Origins of AIDS*, Pépin — a Canadian epidemiologist who has worked across Africa — delves into the early phases of HIV emergence. After the ancestor of the pandemic HIV-1 group M passed from a chimpanzee to a human in southeast Cameroon about 100 years ago, a few infected people travelled down the River Congo. AIDS became a community disease in Léopoldville (now Kinshasa), the capital of the Belgian Congo depicted in Joseph Conrad's 1903 novella *Heart of Darkness*. HIV began to thrive in its new host, Pépin shows, for several reasons.

There was a surge in medical injections using non-sterile syringes in mid-twentieth-century Africa, giving the transmission of HIV (and hepatitis viruses) a crucial helping hand — a theory previously postulated by US epidemiologist Ernest Drucker. No Congolese physicians were trained under colonial rule, and when Belgium abandoned the Congo in 1960, few colonial or missionary doctors remained. Pépin describes a society in turbulent transition, with 'free women' and migrants swelling the capital. HIV became a mainly sexually transmitted infection. After the unsuccessful war of secession in Katanga in southeast Congo, Haitians among the United Nations troops brought HIV to the West. Homosexual men went to Haiti for sex, and Luckner Cambronne, leader of the country's Tonton Macoutes paramilitary force, sold more than 6,000 litres of blood plasma a month to the United States.

One question that Pépin skirts is why HIV prevalence in Kinshasa since 1980 remained relatively stable and low while it exploded elsewhere in Africa, spreading widely in southern Africa only in the 1990s. That mystery drives home the point that where a virus first enters the human population isn't necessarily where it blooms; roots are not shoots. Another puzzle is why HIV-1 group M has been so successful compared with the other cross-species infections of HIV-1 groups N, O and P from apes, and of HIV-2 from monkeys. Pépin rightly argues that, apart from social factors promoting HIV spread, inherent properties of the virus must determine its fitness to become pandemic. He also provides the best analysis I have read of the declining HIV-2 epidemic in West Africa.

> *"Where a virus first enters the human population isn't necessarily where it blooms; roots are not shoots."*

AIDS at 30 begins where Pépin leaves off, with the appearance of AIDS in the United States. Harden, the retired doyenne of medical history at the US National Institutes of Health, draws extensively on that agency's archives for her narrative of the scientific advances in understanding HIV/AIDS, its treatment and prevention. She is particularly strong on the challenges of formulating US public-health policies for AIDS.

With 34 million people living with HIV, besides the 30 million it has already killed, seeking to understand the myths and the history of AIDS is surely important — although not as pressing as developing a safe and efficacious HIV vaccine. ■

Robin A. Weiss *is professor of viral oncology in the Division of Infection & Immunity, University College London, UK. e-mail: r.weiss@ucl.ac.uk*

D. TREVAS

Q&A Peter Diamandis

The eternal optimist

Peter Diamandis is the founder of the non-profit X Prize Foundation, which aims to kick-start research and development to solve humanity's biggest challenges. On the publication this week of his book Abundance, *co-authored with journalist Steven Kotler, he explains how technological and social progress will enable us to provide enough food, water and energy for all.*

Your book is optimistic about humanity's future. But aren't we already exceeding our planet's carrying capacity?

The carrying capacity for Earth is a relative number. If I have an orange grove and I can reach only the lowest oranges on my trees, I need five trees to feed my family. If I can build a ladder, then I need only one tree. If humanity were to run out of food, our 'ladder' might be genetic engineering, or growing food hydroponically inside skyscrapers. It's not as if water is leaving the planet, or energy is not shining down, or we're not recycling food. These are all replenishable resources once we are able to use them more efficiently.

How can we use resources better?

We're living on a water planet; the challenge is that 98% is salt water. But there are technologies that can purify it — such as the Slingshot, a device the size of a mini refrigerator that can run on cow dung, which the Coca-Cola Company is helping to trial in Africa. With food, we now have the ability to go from evolution by natural selection to evolution by intelligent direction using genetic engineering. We will make cleaner energy through solar and nuclear approaches, which are the only ones that can scale to meet our needs. Mobile-phone use is growing exponentially, and soon more than 70% of the world will have one; the Qualcomm Tricorder X Prize is asking teams to build a mobile app that allows users to diagnose themselves as well as a physician can.

Abundance: The Future Is Better Than You Think
PETER H. DIAMANDIS AND STEVEN KOTLER
Free Press: 2012. 400 pp. $26.99

How quickly can such technologies develop?

The world is full of exponential technologies. When the Human Genome Project started in 1990, people said that it would take 50 years and would consume every scientist on the planet. These things can happen much more quickly. And now there are new forces making them happen. Through the X Prize Foundation, I've witnessed individuals and small teams do things that, in the past, only governments could do. There is the DIY innovator: the person or team empowered by extraordinary technology, such as parents of sick children who create biolabs in their own kitchens. There are the techno-philanthropists: 'centimillionaires' who are being created younger and younger and tackling global challenges — just as Bill Gates has tackled malaria. In 2010 there were some 2 billion people online; by 2020 that is going to rise to 5 billion. These people are going to join the global economy, and innovate on a zero-cost basis.

Are things better now than in the past?

Over the twentieth century, lifespan has doubled. We're living in the most peaceful time ever. Every generation thinks that their problems are the biggest, but eventually we get around them. That was an important insight for me. People idealize the past but they forget how horrible it really was. Seeing problems is an evolutionary survival trait. The easiest way to survive is to be hypervigilant for problems.

What about the growing gap between rich and poor?

That's immaterial at some point. In the United States, happiness correlates with income only up to about US$75,000. It's about providing for your needs. If someone in Africa can have first-tier [basic] health and education and access to abundant energy, food and water, they might still have little income, but those changes represent a huge step forward.

You write of fulfilling basic needs for free and automating menial tasks. How would that affect the future economy?

I don't know. 'Work' as a defined activity in society didn't exist for the first 100,000 years of our species. It was invented. If I own a nanobot that can create my food, a shelter, a car and anything else, I have everything I need. But what do you do with all your spare time? Does everyone become an artist? A thinker? An explorer? It is going to be interesting.

Do you plan to live long enough to find out?

When I was a first-year medical student I saw a television show about some turtles that might live as long as 700 years. So I asked, if they can, why can't I? We are on the edge of a revolution in health. We're designing an organogenesis X Prize for spare body parts. I'm staying in touch with the smartest researchers and physicians I know. ■

INTERVIEW BY NICOLA JONES

Correspondence

Mutant flu: preparing for a pandemic

We at the global humanitarian organization Save the Children agree that controversy over lab-created H5N1 avian influenza virus should not detract from the larger concern of global preparedness for a flu pandemic (*Nature* **482,** 131; 2012).

In a pandemic flu situation, when all countries and responding organizations are stricken, we think it is unrealistic to hope that the most resource-poor communities around the world will receive adequate supplies of vaccine, antivirals or antibiotics. We believe in preparing now so that community leaders, and the organizations working with them, can mitigate the effects of a severe wave of flu in the absence of substantial outside resources.

As the World Health Organization has noted, non-pharmaceutical interventions such as quarantine are crucial for an effective response, and may sometimes be the only means of delaying the spread of flu. Yet most national plans lack practical operational considerations (see go.nature.com/mi9sr3).

Detailed authoritative guidance on reducing flu transmission at household and community levels, and on the home-based care of flu patients, in low-resource settings is the most important, and needs to be published. Support should also be provided to governments in developing countries to adapt this guidance for their settings.

We believe that such efforts should be an urgent priority, and are concerned about this apparent gap in the most basic level of pandemic preparedness.

Eric S. Starbuck *Save the Children, Westport, Connecticut, USA. estarbuck@savechildren.org*

Mutant flu: assessing biosecurity risks

In the ongoing controversy over the mutant H5N1 avian influenza research (*Nature* **481,** 9–10, 2012), we should be wary of reducing biosecurity measures merely to assigning access rights to sensitive information and materials. A national security body made up of military and law-enforcement officials that puts confidentiality stamps on dual-use research is not in the long-term interest of scientific progress.

Biosecurity in research needs to be integrated into a more comprehensive strategy if it is to be effective and avoid harming public-health interests.

As a member and chair of several ethics-review panels of dual-use research for the European Union, I believe that these research projects, and their clearly foreseeable implications, should have undergone a proper risk–benefit assessment before funding. They could then have been modified to accommodate additional risk-management procedures.

For example, threats to biosecurity could have been minimized by developing diagnostic kits for early detection and surveillance of the new genetic variants, and by testing possible treatment strategies. It seems that none of this was done.

Johannes Rath *University of Vienna, Austria. johannes.rath@univie.ac.at*

Questionable use of chimpanzees

By conducting their experiments at US chimpanzee centres, foreign scientists have been circumventing their own nations' bans on chimpanzee research since 2005 (*Nature* **482,** 132; 2012). It is important to point out that those scientists are almost all employed by foreign-based drug companies — as reported by a US National Institutes of Health representative at the Institute of Medicine (IOM) public hearing in May 2011.

The US Food and Drug Administration's Office of New Drugs reported to the IOM committee in June 2011 that chimps are never required for preclinical drug testing in the United States, and that the agency discourages the use of chimps for this purpose. The IOM's report *Chimpanzees in Biomedical and Behavioral Research*, released in December 2011, also concludes that chimps are unnecessary for preclinical drug testing.

The use of chimps for preclinical drug trials in US centres by foreign drug companies is therefore contrary to US practice and should be banned.

John J. Pippin *Physicians Committee for Responsible Medicine, Washington DC, USA. jpippin@pcrm.org*

Sugar: there's more to the obesity crisis

To describe sugar as "toxic" is extreme, as is its ludicrous comparison with alcohol (*Nature* **482,** 27–29; 2012). Such sensationalism could damage the livelihoods of thousands of people working in the sugar industry worldwide, and will be felt in countries such as Australia, the United States, Fiji, Mauritius, Indonesia and India.

As the senator for Queensland, Australia, where sugar is the most significant agricultural crop, I wish to voice the industry's concerns. Consumers should be assured that sugar is a safe ingredient and suitable for consumption as part of a balanced diet.

Nutritionist Jennie Brand-Miller of the University of Sydney is not alone in her disgust that you published this opinion piece (*The Australian*, 4 February 2012). The Dietitians Association of Australia believes that it is simplistic and unhelpful to blame sugar alone for the obesity crisis.

Alan Barclay of the Australian Diabetes Council notes in the same article in *The Australian* that sugar consumption in Australia has dropped by 23% since 1980. But he adds that during that time, the number of overweight or obese people has doubled, while diabetes has tripled.

A literature review by Australia's National Health Medical Research Council, together with its draft dietary guidelines of December 2011, found that the evidence to support advice on added sugar and obesity was "limited, inconclusive or contradictory".

Robert Lustig *et al.* have stimulated debate, yet have unnecessarily tarnished the image of sugar. There is no evidence to suggest that reducing sugar consumption will halt the rise in obesity. The contributing factors are far more complex.

Ron Boswell *Brisbane, Queensland, Australia. senator.boswell@aph.gov.au*

Sugar: fruit fructose is still healthy

Robert Lustig and colleagues argue that sugar is "toxic" (*Nature* **482,** 27–29; 2012), focusing on the "deadly effect" of the fructose moiety of sucrose. But they are directing attention away from the problem of general overconsumption.

Guidelines on healthy eating encourage fruit consumption, and fruit and fruit products are the third-largest source of fructose in the US diet.

Our meta-analyses of controlled feeding trials indicate a net metabolic benefit, with no harmful effects, from fructose at a level of intake obtainable from fruit (J. L. Sievenpiper *et al. Br. J. Nutr.*, in the press).

John L. Sievenpiper, Russell J. de Souza, David J. A. Jenkins *St Michael's Hospital, Toronto, Ontario, Canada. john.sievenpiper@utoronto.ca*

Sugar: a problem of developed countries

The contribution of sugar towards chronic disease is more relevant to developed countries than to the developing world (*Nature* **482,** 27–29; 2012). In Asia, for example, up to 10% of the population is obese and/or diabetic (see go.nature.com/qmmoha), even though the daily energy contribution from sugar is less than 837 kilojoules per person. It is more likely that a high consumption of starch-based foods is to blame for this statistic (see go.nature.com/2hoimi) .

Overconsumption of foods that have a high glycaemic index (that trigger a rapid and sharp increase in blood glucose), such as wheat, potatoes and certain types of rice, also contributes to obesity and diabetes. Emphasis on sugar alone is therefore too narrow a basis for devising policies to curb these problems.

Christiani Jeyakumar Henry, Viren Ranawana *Clinical Nutrition Research Centre, Singapore Institute for Clinical Sciences, Singapore.*
jeya_henry@sics.a-star.edu.sg

Sugar: other 'toxic' factors play a part

Regulating products based on a scientific risk analysis is a worthy goal, but I contend that Robert Lustig and colleagues oversimplify the "toxic" truth about refined carbohydrates (*Nature* **482,** 27–29; 2012). Rather than demonizing sugar, the authors would have better served public health with recommendations to manage a balanced diet with exercise.

The authors also downplay other complex factors that could contribute to non-communicable disease burdens. These include relatively recent changes in exercise patterns, and pollutants and additives that affect metabolic activity.

Putting sugars in a regulatory league with alcohol and tobacco is misleading. Sugars do not cause behavioural intoxication, nor do they have the second-hand proximity impact of tobacco smoking — key factors in their regulation.

Saleem H. Ali *University of Vermont, Burlington, USA.*
saleem.ali@uvm.edu

Australia: small steps to control invasives

We believe that there are more obvious and less destructive options for controlling gamba grass and other invasive weeds in Australia than introducing mega-herbivores such as elephants (*Nature* **482,** 30; 2012).

Biological control using carefully screened host-specific arthropods or pathogens, combined with quarantine and spread-prevention measures, is a more balanced approach, and one with which Australia has considerable experience.

The world is littered with examples of generalist vertebrate species (cane toads, foxes, mynas, mosquito fish and so on) that were introduced in the misguided hope of controlling a pest species, only to have a substantial undesired impact on native biodiversity.

Credible solutions to these problems are more likely to come from small things done well, rather than through elephantine, rhinocerine, or even asinine fixes.

Bruce L. Webber, John K. Scott, Raphael K. Didham *CSIRO Ecosystem Sciences, Floreat, Australia; and University of Western Australia, Crawley, Australia.*
bruce.webber@csiro.au

Australia: better solutions to wildfires

Among David Bowman's more outlandish suggestions for dealing with Australia's massive problems of wildfires, feral animals and weeds, there are some workable ideas (*Nature* **482,** 30; 2012).

Some of these are already being implemented, such as the reinstatement of Aboriginal fire management in the north of the country. The Australian Wildlife Conservancy's prescribed-burn programme in the Kimberley region is having great success.

These innovations are radical, but they are based on a sound ecological understanding.

Richard J. Hobbs *University of Western Australia, Crawley, Australia.*
richard.hobbs@uwa.edu.au

Australia: a case for Aboriginal rangers

David Bowman makes a strong case for employing Aboriginal people to manage their own land and to reinstate traditional fire practices in Australia (*Nature* **482,** 30; 2012). This strategy could form the basis of a coordinated, long-term conservation service.

It would also provide desperately needed employment for landowners, as well as supplying them with a reliable source of protein from hunting feral animals (N. Collier *et al. Hum. Ecol.* **39,** 155–164; 2011).

In addition, the Aboriginal people, who have a deep spiritual connection to land, would be able to remain on their traditional territories and so maintain close functional relationships with their ancestors.

Clive R. McMahon *Charles Darwin University, Darwin, Northern Territory, Australia.*
clive.mcmahon@cdu.edu.au

Australia: no price on cutting fire risk

David Bowman proposes that elephants should be introduced into Australia as a cost-effective way to control invasive gamba grass, a major source of wildfire fuel (*Nature* **482,** 30; 2012). But managing the elephants could be more expensive than, say, launching a fleet of harvesters every year to reduce fire risk. We should start by asking what is likely to work best, regardless of the cost.

To combat the problems caused by invasive aliens, we should implement ecologically sound control mechanisms that have a reasonable probability of success. We can worry about the bill later.

P. J. Nico de Bruyn, Andrew B. Davies *University of Pretoria, Hatfield, South Africa.*
pjndebruyn@zoology.up.ac.za

APS | Acta Pharmacologica Sinica

Obesity
Special Feature and Web Focus

The February 2012 issue of *APS* (*Acta Pharmacologica Sinica*) contains a special feature on Obesity including articles by leading experts on several topics that relate to obesity etiology, animal models, therapeutics and clinical implications. Further background information on this important topic is available through the accompanying web focus which links to related articles from across Nature Publishing Group.

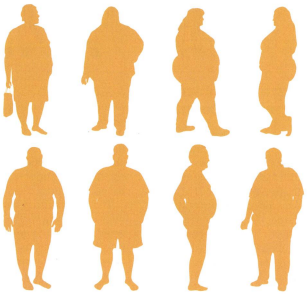

Featured articles include:

Why do anti-inflammatory therapies fail to improve insulin sensitivity?
Zhan-guo Gao and Jian-ping Ye

Rare adipose disorders (RADs) masquerading as obesity
Karen Herbst

Effects of liraglutide and sibutramine on food intake, palatability, body-weight and glucose tolerance in the gubra DIO-rat
Gitte Hansen, Niels Vrang and Jacob Jelsing

A continued saga of Boc5, the first non-peptidic glucagon-like peptide-1 receptor agonist
Ming-Wei Wang, Min He, Ni Guan, Weiwei Gao, Qing Liu, Xiaoyan Wu, Dawei Ma, Dafang Zhong, Guangbo Ge, Chuan Li, Xiaoyan Chen and Ling Yang

Laboratory animals as surrogate models of human obesity
Cecilia Nilsson, Kirsten Raun, Feifei Yan, Marianne Larsen and Mads Tang-Christensen

To access the Special Feature and Web Focus on Obesity visit:
www.nature.com/aps/focus/obesity

nature publishing group npg

RESEARCH

NEW ONLINE

Papers published this week at Nature.com/nature

NEWS & VIEWS ESA's Planck satellite discovers islands of cold gas in the Milky Way **p.475**

PERSPECTIVE Why computer codes should be part of the publishing package **p.485**

ARTICLE The structural tricks that keep ribosomes recycling **p.501**

PUBLISHED 19 FEBRUARY 2012

PHYSIOLOGY

A signal for obesity

GPR120 is a G-protein-coupled receptor that binds to free fatty acids and is involved in fat-cell generation and appetite regulation. Here, Atsuhiko Ichimura *et al.* show that without GPR120, mice on a high-fat diet develop obesity, glucose intolerance and a fatty liver. They also show that people who are obese have high levels of GPR120 expression in adipose tissue, and that some carry a mutation that inhibits GPR120 signalling.

Dysfunction of lipid sensor GPR120 leads to obesity in both mouse and human
A Ichimura *et al.*
doi:10.1038/nature10798

ECOLOGY

Destabilized by complexity

Writing in *Nature* 40 years ago, Robert May questioned a central belief in ecology — that complex ecosystems are more stable than simple ones. He proved that sufficiently large or complex networks can become unstable. Later work in theoretical ecology centred on finding out why some networks are stable. Stefano Allesina and Si Tang analyse stability criteria for various realistic networks, and find key differences between predator–prey interactions, which are stabilizing, and competitive and mutualistic interactions, which are destabilizing.

Stability criteria for complex ecosystems
S Allesina & S Tang
doi:10.1038/nature10832

NEUROSCIENCE

Opposite effects of fear conditioning and extinction on dendritic spine remodelling
C S W Lai *et al.*
doi:10.1038/nature10792

Repetitive motor learning induces coordinated formation of clustered dendritic spines *in vivo*
M Fu *et al.*
doi:10.1038/nature10844

The role of *Drosophila* Piezo in mechanical nociception
S E Kim *et al.*
doi:10.1038/nature10801

Piezo proteins are pore-forming subunits of mechanically activated channels
B Coste *et al.*
doi:10.1038/nature10812

PUBLISHED 22 FEBRUARY 2012

PHYSIOLOGY

Male-specific sirtuin action

The role of the sirtuin deacetylases in the regulation of lifespan of yeast, nematodes and fruitflies is controversial, and the role of the mammalian sirtuins SIRT1 to SIRT7 in regulating lifespan is unclear. Here, Yariv Kanfi *et al.* show that transgenic male — but not female — mice that overexpress exogenous SIRT6 have a significantly longer lifespan than do their wild-type littermates. They conclude that SIRT6 is an important regulator of mammalian longevity, and suggest that it might be possible to treat age-related diseases by manipulating SIRT6 levels.

The sirtuin SIRT6 regulates lifespan in male mice
Y Kanfi *et al.*
doi:10.1038/nature10815

Sorting out the sirtuins
D B Lombard & R A Miller
doi:10.1038/nature10950

EVOLUTION

The fate of the Y chromosome

The human X and Y chromosomes evolved from a pair of autosomes (non-sex chromosomes), but as a result of genetic decay, the male-specific region of the human Y chromosome retains only 3% of the ancestral autosomal genes. Here, Jennifer Hughes and colleagues sequence the corresponding region of the rhesus macaque Y chromosome and reconstruct the trajectory of its evolution through comparison of the rhesus, human and chimpanzee Y chromosomes. They show that initial rapid loss was followed by strict conservation through purifying selection, which runs counter to the view that the human Y chromosome is destined for extinction.

Strict evolutionary conservation followed rapid gene loss on human and rhesus Y chromosomes
J F Hughes *et al.*
doi:10.1038/nature10843

MATERIALS SCIENCE

Second act for iron superconductors

Reports of superconductivity at up to 32 K have stimulated interest in iron chalcogenide superconductors. Liling Sun and colleagues now report that superconductivity vanishes in iron chalcogenides as the pressure in a system increases, but that it reappears, with a higher transition temperature, at pressures of greater than 11.5 GPa. This phenomenon could be useful in the manipulation of the electronic and structural properties of materials without altering the chemistry.

Re-emerging superconductivity at 48 kelvin in iron chalcogenides
L Sun *et al.*
doi:10.1038/nature10813

NEUROSCIENCE

Gain control by layer six in cortical circuits of vision
S R Olsen *et al.*
doi:10.1038/nature10835

MOLECULAR BIOLOGY

Circadian rhythms govern cardiac repolarization and arrhythmogenesis
D Jeyaraj *et al.*
doi:10.1038/nature10852

CANCER

Sequencing of neuroblastoma identifies chromothripsis and defects in neuritogenesis genes
J J Molenaar *et al.*
doi:10.1038/nature10910

The translational landscape of mTOR signalling steers cancer initiation and metastasis
A C Hsieh et al.
doi:10.1038/nature10912

BIOCHEMISTRY

The mechanism of OTUB1-mediated inhibition of ubiquitination
R Wiener *et al.*
doi:10.1038/nature10911

BRIEF COMMUNICATIONS ARISING

Arising from 'Species–area relationships always overestimate extinction rates from habitat loss' by *F He & S P Hubbell* Nature ***473,*** *368–371 (2011)*

Geometry and scale in species–area relationships
H M Pereira *et al.*
doi:10.1038/nature10857

Extinction and climate change
C D Thomas & M Williamson
doi:10.1038/nature10858

***Reply* — F He & S P Hubbell**
doi:10.1038/nature10859

CELL BIOLOGY

Collagen secretion explained

Cells package proteins into vesicles for secretion to the extracellular milieu. A study has now identified an enzyme that modifies the packaging machinery to encapsulate unusually large proteins, such as collagen. SEE ARTICLE P.495

DAVID J. STEPHENS

Together with other extracellular proteins, collagen provides the structural framework on which tissues develop and function. It is synthesized in the endoplasmic reticulum, an intracellular organelle, as a rigid, rod-like precursor (procollagen) about 300 nanometres in length. Procollagen — like nearly all secreted proteins — is then packaged into transport vesicles for delivery to another organelle, the Golgi apparatus, before its secretion to the cell's surroundings. Transport vesicles, however, are typically smaller than 100 nm, as they are generated from the endoplasmic reticulum by a group of proteins (the COPII coat) that co-assemble as a structurally defined polyhedral cage[1]. On page 495 of this issue, Jin *et al.*[2] reveal that modification of one of the COPII proteins allows the formation of vesicles that are large enough to hold procollagen.

The outer layer of the COPII coat is assembled using structural elements comprised of the proteins SEC13 and SEC31 (Fig. 1a). Although it was thought that the hinges between these elements are flexible enough to allow vesicles of various sizes to form[3,4], little was known about how vesicle size is controlled. Jin and colleagues[2] show that SEC31 can be modified by ubiquitination — the attachment of one or more copies of a small protein called ubiquitin. Although ubiquitination can 'mark' a protein for degradation, it is becoming increasingly clear that it can also affect protein function[5].

Specifically, the authors[2] report that, in mouse cells, the enzyme CUL3–KLHL12 adds a single ubiquitin to a small pool of SEC31 molecules, and that this modification is required to drive the secretion of collagen. Using high-resolution electron microscopy, they found that overexpression of CUL3–KLHL12 leads to the production of large COPII structures, up to 500 nm in diameter — sufficient to accommodate procollagen. The simplest explanation for these observations is that ubiquitin attachment to SEC31 results in a structural change in the COPII cage that alters coat flexibility, and allows procollagen to be encapsulated in a nascent vesicle (Fig. 1b).

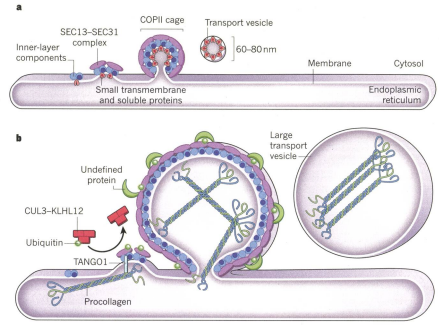

Figure 1 | Big vesicles for collagen secretion. a, Soluble proteins targeted for secretion, together with small transmembrane proteins, are packaged at the endoplasmic reticulum into vesicles that are coated by the COPII protein cage. Proteins that will form the inner layer of the COPII coat associate in an ordered fashion and then recruit the proteins SEC13 and SEC31, which form the outer layer. This leads to membrane deformation and ultimately to scission of 60–80-nm transport vesicles. **b**, Large proteins such as procollagen (the collagen precursor) do not fit into these typical vesicles. Jin *et al.*[2] report that, to encapsulate such large cargoes, the enzyme CUL3–KLHL12 attaches one copy of the small protein ubiquitin to SEC31 within the SEC13–SEC31 complex, and that this process facilitates collagen export. An additional, unknown protein might further stabilize lateral SEC13–SEC31 interactions. Although it is not known whether collagen synthesis directly triggers CUL3–KLHL12 activity, the transmembrane protein TANGO1 — which couples collagen in the endoplasmic reticulum to the assembling coat on the cytosolic face — might have a role in the process.

Jin and colleagues' observation that only some SEC31 molecules are modified indicates strongly that the addition of ubiquitin does not directly modulate the mechanics of COPII coat assembly. Instead, SEC31 ubiquitination might lead to recruitment of an additional, unknown protein to perform this role — for example, by further stabilizing lateral SEC13–SEC31 interactions. Identification of the additional factor and a more detailed molecular explanation of the modified geometry of the vesicle coat are challenges for the future.

Ubiquitination of some SEC31 molecules could be an ongoing process that facilitates the formation of large COPII vesicles as a routine cell function; alternatively, large vesicles might be formed only on demand. In the latter case, however, it is not immediately obvious how CUL3–KLHL12, located in the cytoplasm, would sense the presence of newly synthesized procollagen in the endoplasmic reticulum. A potential candidate for relaying this information across the endoplasmic reticulum membrane is the transmembrane protein TANGO1, which forms part of a packaging receptor that is essential for

procollagen secretion[6,7]. TANGO1, however, does not make contact with SEC31 directly, nor is it found in fully formed vesicles, and so its possible connection to CUL3–KLHL12 is unclear.

Other questions remain. Does collagen become entirely encapsulated in a large COPII cage during vesicle formation (Fig. 1b), or does COPII somehow aid collagen export indirectly, without the need for a complete cage? And how does the addition of ubiquitin change the geometry of the COPII coat? Jin and colleagues' findings[2] might aid the development of a cell-free system for studying COPII-dependent packaging of collagen that would help to address these issues. Moreover, is SEC31 ubiquitination relevant to the packaging of other large secreted macromolecules, such as lipoproteins?

These questions are relevant to our understanding not only of the fundamental mechanisms of cellular secretion, but also of diseases in which secretion (particularly of collagen) is defective because of gene mutation[8]. Furthermore, manipulation of the CUL3–KLHL12 ubiquitination pathway might be used to increase collagen secretion from cells for applications in stem-cell culture, for growth of tissue components in regenerative medicine, or perhaps for ameliorating age-related degeneration of connective tissue. ■

David J. Stephens *is in the Cell Biology Laboratories, School of Biochemistry, University of Bristol, Bristol BS8 1TD, UK.*
e-mail: david.stephens@bristol.ac.uk

1. Zanetti, G., Pahuja, K. B., Studer, S., Shim, S. & Schekman, R. *Nature Cell Biol.* **14,** 20–28 (2011).
2. Jin, L. *et al. Nature* **482,** 495–500 (2012).
3. Stagg, S. M. *et al. Cell* **134,** 474–484 (2008).
4. Fath, S., Mancias, J. D., Bi, X. & Goldberg, J. *Cell* **129,** 1325–1336 (2007).
5. Komander, D. *Biochem. Soc. Trans.* **37,** 937–953 (2009).
6. Saito, K. *et al. Cell* **136,** 891–902 (2009).
7. Wilson, D. G. *et al. J. Cell Biol.* **193,** 935–951 (2011).
8. De Matteis, M. A. & Luini, A. *N. Engl. J. Med.* **365,** 927–938 (2011).

ASTROPHYSICS

First results from Planck observatory

Early data from the Planck space satellite provide information about dust in distant galaxies, as well as in the Milky Way, and on the properties of gas in some of the largest clusters of galaxies in the Universe.

UROŠ SELJAK

Astronomers have long known[1] that most of the stars in the Universe are born in messy environments containing dusty clouds. Young stars in such dust-enshrouded regions are not visible to optical telescopes; thus, multi-wavelength studies, from the radio to the X-ray regime, are used to better understand how stars form in our Galaxy. But for more distant galaxies, including some of the first galaxies in the Universe, such dusty expanses are essentially invisible across most wavelengths. One exception is the wavelengths in the far-infrared and microwave regimes, which are roughly 1,000 times longer than those of visible light. Stars heat up the dust surrounding them to temperatures of roughly 20 kelvin — much lower than that of the stars themselves, but nevertheless high enough for the dust to radiate microwave and far-infrared light. This warm-dust signature, called the cosmic infrared background, has now been observed[2] by a large team of astronomers working with data from the Planck space observatory. The results are part of a series of studies that form a collection of 26 papers, published by the Planck team in *Astronomy & Astrophysics* (see go.nature.com/au8vap).

The Planck satellite's measurement of the cosmic infrared background[2] improves on previous measurements, including data[3] obtained by Herschel, a twin observatory to Planck launched by the European Space Agency aboard the same rocket in 2009. The rocket carried them to the Earth–Sun Lagrangian point L2 (1.5 million kilometres from Earth in the opposite direction from the Sun), where the satellites can be stationary relative to both the Sun and Earth, allowing for shielding from the Sun's radiation.

Planck detects microwave light in several wavelength bands in which the warm-dust emission can be observed (Fig. 1). Because the Universe is expanding and the wavelength of light stretches with the expansion, the light that we observe has a longer wavelength than it

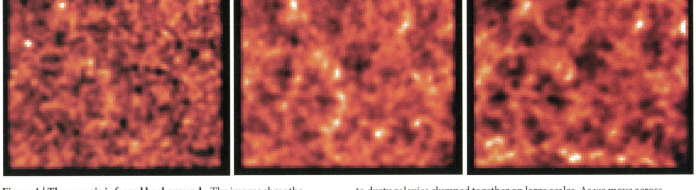

Figure 1 | The cosmic infrared background. The images show the anisotropies, or irregularities, of the cosmic infrared background in three of the frequency channels (217 gigahertz, 353 GHz and 857 GHz) probed by the Planck observatory[2] over a 26° × 26° patch of the sky. The anisotropies are visible as globular structures and correspond to dusty galaxies clumped together on large scales. As we move across frequency channels, different epochs of cosmic time become visible: observations at 217 GHz offer a glimpse of some of the oldest galaxies in the Universe, which formed when the Universe was less than 2 billion years old.

FLUID MECHANICS

Mist opportunities

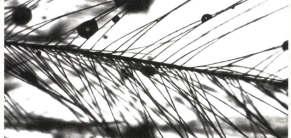

C. DUPRAT & S. PROTIÈRE

From the fixative properties of hairsprays to the stickiness of filaments on beetles' feet, the wetting of flexible fibres with droplets of liquid is a universal phenomenon — but one we know surprisingly little about. On page 510 of this issue, Duprat *et al.* formulate rules to describe how mists of droplets interact with flexible fibre arrays (C. Duprat, S. Protière, A. Y. Beebe & H. A. Stone *Nature* **482,** 510–513; 2012).

The researchers began with the simplest possible model: the interactions of water droplets with a pair of closely aligned, flexible glass fibres that were clamped at one end but free to bend at the other. They observed that a droplet deposited close to the clamped ends adopts one of three forms: it could remain as a tight, spherical bridge between the filaments, or, depending on the conditions, it could either partially or completely spread along the fibres, in the latter case causing them to coalesce.

On further investigation, Duprat *et al.* found that six physical parameters control droplet shape and spreading; they include fibre geometry, the distance between the fibres, and the fibres' mechanical properties. The authors also identified a critical droplet volume above which fibres do not coalesce, and a second critical volume at which droplet capture by fibres is maximized.

The team went on to explore the wetting of a natural fibre array by spraying a goose feather with oil droplets and observing the effects on the barbules (filaments projecting from each barb of a feather). They found that their theoretical model held up — small droplets spread along the barbules and caused barbule clumping, whereas larger droplets did not spread and could be easily dislodged — despite the roughness of the feather's barbules and the chemical affinity between the droplet and the barbules' surfaces.

Duprat and colleagues' discoveries suggest that the mechanical properties and spatial organization of biological fibre arrays may have evolved to optimize interactions with liquid droplets, and so enhance functions such as adhesion, dew collection and self-cleaning. The work also offers opportunities for improving the performance of technological wetting systems — for example, droplet volumes in sprays could be engineered to fine-tune their wetting interactions with relevant fibres. **Rosamund Daw**

had at its source. This means that, for the same dust temperature, observing the dust emission at the longer wavelengths corresponds to observing an epoch when the Universe was smaller, and hence younger. By measuring the dust at different wavelengths, Planck can track the emission from star-forming galaxies as a function of cosmic time. Planck's observations[2] suggest that most of the emission in the longer-wavelength bands comes from galaxies that formed at a time when the Universe was less than 2 billion years old (the age of the Universe today is approximately 14 billion years).

To achieve this measurement, the Planck team performed[2] a sophisticated software analysis called component separation. This was required because these wavelength bands contain radiation from many other sources, mostly the Milky Way, but also the cosmic microwave background (CMB, relic radiation from the early Universe glowing at 2.7 K). The strengths of these sources vary differently as a function of wavelength. By combining Planck's nine wavelength bands with additional external measurements, the team was able to separate the cosmic-infrared-background component from the other sources of radiation. The authors found[2] a broad agreement in results between different areas in the sky, which had been specially chosen for having low radiation from our Galaxy, suggesting that the component separation was successful.

The emission from the Milky Way is not just a contaminant of the cosmic infrared background; it also contains some surprises of its own. One of these relates to the 'anomalous microwave emission' at centimetre wavelengths. This has been known about for a few years, but its origin has been controversial. In particular, although this radiation has been observed[4] to correlate with the emission from small dust grains in the Galaxy, simple models of thermal emission from dust could not explain its wavelength dependence. However, if the dust particles are spinning at high rates, they can radiate at a wavelength that relates to their spinning frequency and size. In this spinning-dust model, the emission occurs over a relatively narrow range of wavelengths that happens to coincide with the longest-wavelength band of the Planck observatory. Planck's observations of emission from the Milky Way provide[5] strong support for the spinning-dust model.

Not all of the results from Planck are related to dust radiation. Light propagating through hot gas can be scattered off electrons zooming around these high-temperature regions. The result of this process, named the Sunyaev–Zeldovich (SZ) effect after the two Russian scientists who first proposed[6] it, is that longer-wavelength light is shifted to shorter wavelengths. When viewed against the background provided by the CMB radiation, this effect leads to a dark hole at longer wavelengths at the position of a gas clump on the sky. Similarly, it causes a bright peak of light at shorter wavelengths at the same position.

With Planck's many wavelength bands, both of these features can be observed, leading to a convincing detection of the SZ effect. The sources most likely to provide a detectable SZ signal are the most massive galaxy clusters, which contain huge amounts of some of the hottest gas in the Universe. The Planck team found[7] nearly 200 cluster candidates with this technique, of which about 20 were previously unknown. Most of these have subsequently been confirmed as real clusters by follow-up studies, including X-ray observations[8] with the XMM-Newton satellite. Combined analysis of these data provides detailed information about the gas density and temperature distribution in the clusters, resulting in a better understanding of the processes that led to their formation.

These new results[7] demonstrate that it is possible to find clusters of galaxies with the SZ technique even for surveys looking at the entire sky, in contrast to previous SZ detections — by the South Pole Telescope[9] and Atacama Cosmology Telescope[10] — that searched smaller patches of the sky. Ultimately, the SZ method will allow clusters to be observed at a much larger distance from Earth than is possible with other methods, such as X-ray emission. One exciting application of the SZ approach would be to probe the growth of the largest (and thus rarest) structures at early times. Such observations would provide a measurement of the different components that make up the Universe and of the size of the initial density fluctuations that eventually

grew to become galaxies and galaxy clusters.

The early results from Planck demonstrate that the observatory is working flawlessly, and provide a first glimpse of its scientific potential. However, the best is yet to come. The main mission of Planck is to map the CMB radiation and its polarization with unprecedented precision. This measurement will provide a window onto the early Universe and offer clues as to what created the first seeds of structure. Planck may also detect the relic gravity waves from the Big Bang through the observations of CMB polarization. The task is complicated by the relative faintness of the CMB compared with other sources of radiation, such as dust emission, in most of the wavelength bands. Careful separation of components is thus needed to isolate the CMB signal, a task that has proved challenging and is the main reason that these early results do not include any primary CMB data. These CMB results are expected to be announced in early 2013. Given the spectacular instrument performance of Planck shown by its early findings[2,5,7], the cosmology community is eagerly awaiting more results. ■

Uroš Seljak *is in the Physics and Astronomy Department and Lawrence Berkeley National Laboratory, University of California, Berkeley, California 94720, USA, and at the Institute for Theoretical Physics, University of Zurich, Switzerland.*
e-mail: useljak@berkeley.edu

1. Shu, F. H., Adams, F. C. & Lizano, S. *Annu. Rev. Astron. Astrophys.* **25,** 23–81 (1987).
2. Planck Collaboration *Astron. Astrophys.* **536,** A18 (2011).
3. Amblard, A. *et al. Nature* **470,** 510–512 (2011).
4. Finkbeiner, D. P., Schlegel, D. J., Frank, C. & Heiles, C. *Astrophys. J.* **566,** 898–904 (2002).
5. Planck Collaboration *Astron. Astrophys.* **536,** A20 (2011).
6. Sunyaev, R. A. & Zeldovich, Y. B. *Comments Astrophys. Space Phys.* **4,** 173–178 (1972).
7. Planck Collaboration *Astron. Astrophys.* **536,** A8 (2011).
8. Planck Collaboration *Astron. Astrophys.* **536,** A9 (2011).
9. Carlstrom, J. E. *et al. Publ. Astron. Soc. Pacif.* **123,** 568–581 (2011).
10. Marriage, T. A. *et al. Astrophys. J.* **737,** 61 (2011).

MATERIALS SCIENCE

Cell environments programmed with light

A combination of two light-induced reactions has been used to attach peptides to a polymeric gel, and then to detach them from it. This feat opens up opportunities for studying the effects of signalling molecules on cell behaviour *in vitro*.

MATTHIAS P. LUTOLF

The ability to use light to precisely control the activity of cells has transformed the way many experiments in biology are performed. In particular, optogenetic techniques — in which light is used to manipulate cells that have been genetically engineered to be light responsive — have revolutionized neuroscience by providing a completely new way to modulate cell signalling, even in live animals[1]. Writing in *Angewandte Chemie*, DeForest and Anseth[2] report that light can be used to dynamically manipulate not only the intrinsic cellular regulatory machinery, but also the external microenvironment of a cell. Specifically, they showcase a class of 'optobiomaterial' whose biochemical properties can be changed to influence cellular activity simply by having different sources of light shone on it.

Far from being intrinsically determined, cell behaviour such as proliferation, differentiation and migration are tightly regulated by spatio-temporally complex signals originating from the surrounding milieu (the extracellular matrix, ECM). For instance, the microenvironments (known as niches) surrounding rare adult stem cells in human tissues regulate stem-cell behaviour using a combination of local cell–cell interactions, ECM-derived signals and soluble signalling molecules. Together, these niche signals are crucial for ensuring lifelong maintenance of stem-cell function[3]. An understanding of how stem cells respond to signals from their extracellular environment is therefore essential, especially for realizing the therapeutic potential of stem cells.

Biologists have a variety of *in vitro* model systems at hand to study such complex cell–ECM interactions, and this enables them to uncover cell-signalling mechanisms in near-physiological, three-dimensional contexts. These models have been generated from crosslinked networks of protein components of the ECM such as collagen, or from ECM glycoproteins (polypeptides that have sugars attached) such as laminin. They have provided vital insight into extrinsic cell regulation, and in some cases have even made possible the formation of entire tissues from single stem cells *in vitro*[4]. Unfortunately, these biomatrices tend to suffer from uncontrollable batch-to-batch variability and are unable to modulate the availability of extrinsic signalling molecules — and thus cell function — controllably in space and time.

To recreate the dynamics of cellular microenvironments in three dimensions, researchers have sought strategies in materials chemistry that permit the biophysical and biochemical properties of matrices to be selectively modulated in a tailor-made fashion. Most approaches rely on well-characterized, cross-linked, synthetic polymers known as hydrogels that have ECM-like biophysical properties.

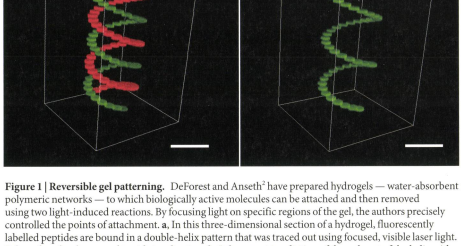

Figure 1 | Reversible gel patterning. DeForest and Anseth[2] have prepared hydrogels — water-absorbent polymeric networks — to which biologically active molecules can be attached and then removed using two light-induced reactions. By focusing light on specific regions of the gel, the authors precisely controlled the points of attachment. **a**, In this three-dimensional section of a hydrogel, fluorescently labelled peptides are bound in a double-helix pattern that was traced out using focused, visible laser light. False colour has been used to aid visualization. **b**, Subsequent irradiation of the red part of the helix with ultraviolet light has caused the peptides in that region to detach. Scale bars, 200 micrometres. (Images reproduced from ref. 2.)

But, in contrast to ECMs, most synthetic hydrogels are biologically inert because their polymer 'backbones' contain no biologically active components. This allows researchers to design very 'clean' experimental systems: biologically active molecules can be attached to hydrogels to perturb cell activity in a well-controlled fashion, without interference from the hydrogel itself.

Several research groups have carried out work in which light-sensitive molecular building blocks were attached to hydrogel networks to generate artificial ECMs in which the properties of microenvironments could be specifically modulated by light exposure[5]. For example, the introduction of chemical groups that can be cleaved by ultraviolet light has led to hydrogels that soften on light exposure[6]. Conversely, the incorporation of groups that form crosslinks between polymer chains when irradiated with ultraviolet light has resulted in materials that stiffen upon such irradiation[7].

Systems in which light triggers the coupling[8,9] or removal[6] of biologically active molecules to or from hydrogel polymer networks have also been devised. These light-mediated approaches to modifying hydrogels have been used to control some aspects of the basic three-dimensional behaviour of cells embedded in the materials, such as adhesion to the artificial ECM or migration. But because the modifications involved are irreversible, they allow only one-way manipulation of cell activity.

DeForest and Anseth's work[2] now demonstrates fully reversible modulation of biologically active building blocks within light-sensitive hydrogels. They synthesized small peptides that can act as signals for cell adhesion, to which a short linker section was attached. The free end of the linker was a chemical group that can react with alkene groups in a hydrogel when irradiated with visible light, thereby attaching the peptide to the gel (Fig. 1). Another part of the linker was a group that breaks apart when irradiated with ultraviolet light; by shining this light on a hydrogel that had been decorated with the peptides, the authors could detach the peptides from the gel.

Crucially, both light-activated reactions are cell-compatible, which allowed DeForest and Anseth to attach (or detach) the peptides to (or from) their hydrogel in the presence of mouse embryonic fibroblast cells. By controlling precisely when and where the cell-adhesive peptides bound in the gel, the authors could control the duration and locations in which the cells attached and spread.

In a first gel-patterning step, DeForest and Anseth used visible light to create small 'islands' of peptides to which fibroblasts grown in culture with the gel adhered. In a second step, conducted after one day of culture, the authors removed peptides from areas of the islands using ultraviolet light. This caused rapid, selective detachment of cells from those areas. The authors showed that the removed cells could then be grown again in culture, or analysed in other assays. As DeForest and Anseth suggest[2], this kind of protocol could be widely used to manipulate and study subsets of cells (or even individual cells) of larger cell populations.

One long-term goal of work such as this is the development of materials to act as scaffolds for tissue regeneration. Can we expect this and/or similar techniques to transform tissue engineering in the same way that optogenetics is transforming neuroscience? This is, of course, difficult to predict. For DeForest and Anseth's hydrogel to be fully physiologically relevant, the ability to attach and release full-length proteins[3] — rather than short peptides — to the material needs to be developed. And it remains to be seen whether their approach is directly translatable to tissue regeneration *in vivo*. Furthermore, it could be argued that these methods will be valuable for tissue regeneration in only a relatively few cases, such as those in which much simpler scaffolds fail, because the spatial arrangement of ECM signals is necessary for driving regeneration.

Nevertheless, the reversible, dynamic control of chemical and physical gel properties should allow previously impossible experiments to be performed in cell culture. For example, it might be used to investigate how individual stem cells differentiate or renew themselves in response to changes in signals from an artificial microenvironment that spatially resembles natural stem-cell niches. Alternatively, three-dimensional environments for stem cells could be made in which the display or release of molecular signals is graded, to mimic processes that occur during the embryonic development of an organism. DeForest and Anseth's optobiomaterials therefore represent a major contribution to a nascent field in stem-cell bioengineering. ■

Matthias P. Lutolf *is at the School of Life Sciences and the Institute of Bioengineering, École Polytechnique Fédérale de Lausanne, Lausanne 1015, Switzerland.*
e-mail: matthias.lutolf@epfl.ch

1. Fenno, L., Yizhar, O. & Deisseroth, K. *Annu. Rev. Neurosci.* **34,** 389–412 (2011).
2. DeForest, C. A. & Anseth, K. S. *Angew. Chem. Int. Edn* **51,** 1816–1819 (2012).
3. Morrison, S. J. & Spradling, A. C. *Cell* **132,** 598–611 (2008).
4. Sato, T. *et al. Nature* **459,** 262–265 (2009).
5. Khetan, S. & Burdick, J. A. *Soft Matter* **7,** 830–838 (2011).
6. Kloxin, A. M., Kasko, A. M., Salinas, C. N. & Anseth, K. S. *Science* **324,** 59–63 (2009).
7. Khetan, S. & Burdick, J. A. *Biomaterials* **31,** 8228–8234 (2010).
8. Hahn, M. S., Miller, J. S. & West, J. L. *Adv. Mater.* **18,** 2679–2684 (2006).
9. Wylie, R. G. *et al. Nature Mater.* **10,** 799–806 (2011).

QUANTUM COMPUTING

A topological route to error correction

Quantum computing is plagued by noise and small errors. An approach based on topological techniques reduces the sensitivity to errors and boosts the prospects for building practical quantum computers. SEE ARTICLE P.489

JAMES D. FRANSON

Quantum computers have the potential to solve numerical problems that would be impossible on a classical computer. Roughly speaking, the superposition principle of quantum mechanics allows a quantum computer to perform many calculations simultaneously on a single processor, and entanglement (non-classical correlations) provides an exponential increase in its memory capacity. Unfortunately, the same properties that enhance the computational power of a quantum computer also make it sensitive to errors produced by interactions with the environment or by imperfect logic operations. In this issue, Yao *et al.*[1] (page 489) describe the first experimental demonstration of a technique that uses topological effects to reduce the sensitivity of a quantum computer to errors.

The bits in a quantum computer, commonly referred to as qubits, can be represented by a two-state quantum system, such as the two quantized energy levels of an atom (Fig. 1a). One state represents a logical value of '0' and the other state represents a '1' — meaning that, like a classical computer, a quantum computer is a digital device. But unlike classical physics, quantum mechanics allows situations in which both possibilities (0 or 1) exist simultaneously. The probability of finding the system in the 0 or 1 state is equal to the square of a complex number known as the probability amplitude. As a result, the information stored in a qubit corresponds to a continuous range of

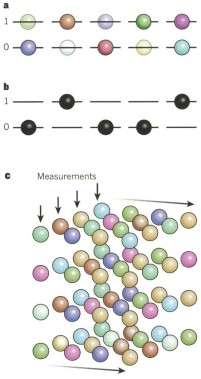

Figure 1 | Measuring quantum bits. a, Five qubits represented by the energy levels of five atoms (spheres). The ground state encodes the logical value '0', whereas the excited state encodes the value '1'. Because of their quantum nature, the atoms can be in both states simultaneously. The intensity of the spheres' colour denotes the probability that an energy level is occupied, and the colours indicate the phase of the oscillating probability amplitude associated with the energy level. **b**, After a measurement, the qubits collapse to classical states with a specific value of 0 or 1, and the phase information is destroyed, as illustrated by the black colour. **c**, A three-dimensional array of qubits can be used to implement topological error correction, which reduces the sensitivity of quantum computing to errors. The calculation consists of a series of measurements that proceeds from all of the qubits in the plane that forms the left side of the array through the adjacent planes to the right. Yao *et al.*[1] demonstrated topological error correction using an ensemble of eight qubits.

probability amplitudes. According to quantum mechanics, the probability amplitudes of both the 0 and 1 states have wave-like properties, and their relative position in an oscillatory cycle corresponds to an additional degree of freedom known as their phase. In addition, the qubits can be entangled with one another in many different ways. Thus a qubit can contain much more information than a classical bit, which can have only a specific value of 0 or 1.

Measuring the value of a qubit causes it to collapse to a specific value of 0 or 1, reducing it to a classical bit (Fig. 1b). Because measuring a qubit destroys its quantum-mechanical properties, it was not initially apparent whether there was any way to correct for errors in qubits without destroying them. It was subsequently shown[2] that error correction was possible if a 'logical' qubit was constructed from a combination of multiple physical qubits (Fig. 1a). For example, the value of the logical qubit can be taken to be the parity of the ensemble of physical qubits, where parity is defined to be 0 if the sum of the qubit values is even and 1 if the sum is odd. But there are more efficient ways of encoding the logical information. Quantum logic operations on the qubit ensemble can be used to correct the errors in the individual qubits without measuring the value of the logical qubit, and thus without destroying the information it encodes. This allows the errors in a quantum computer to be made arbitrarily small — although additional errors will be introduced during the error-correction process itself, so the average error rate must be below a threshold on the order of 10^{-4} for conventional error-correction techniques.

In the type of topological error correction[3,4] used by Yao *et al.*[1], the logical qubits are distributed over a lattice of physical qubits in such a way that the information is automatically protected against most forms of error. This type of error correction is theoretically expected to increase the tolerance for errors to above 1%. The authors[1] demonstrated topological error correction by combining topological techniques with cluster-state quantum computing[5], in which a three-dimensional array, or cluster, of qubits is prepared with a carefully chosen form of entanglement between nearest neighbours in the array.

Their approach begins with measurement of all the qubits in the plane that forms the left side of the array (Fig. 1c). The results of those measurements are then used to decide what kind of measurements to perform on the next layer of adjacent qubits. No active logic operations are performed — instead, the calculation depends on choosing the measurements in such a way that the collapse of the quantum state produces the desired logical operations[6,7]. The calculation proceeds until the final layer of qubits on the far right side of the array — the values of which give the desired output of the calculation — is reached. The authors reduced the sensitivity of the calculations to environmental noise and small errors in the logical operations by optimizing the spatial arrangement, or topology, of the qubits and the measurements.

Yao and colleagues[1] performed their experiment using an eight-qubit cluster, in which the value of each qubit (0 or 1) was represented by the polarization of a single photon (the direction of the photon's electric field). An optical route to quantum computing has the advantage that optical fibres can be readily used to transfer qubits from one location to another. The greatest challenge of an optical approach

50 Years Ago

Although the annual figures for carriage-rates of all pathogenic staphylococci follow no particular course, evidence from many sources in industrialized countries shows that this is not the case with regard to the proportions of penicillin-resistant organisms … These findings raise many questions about the origin and spread of resistant strains. They are certainly consistent with the general impression of a relationship between the increased use of penicillin and the growth of resistant strains … It has to be borne in mind that penicillin, with other antibiotics, is being used on a large scale for preserving food and controlling animal diseases in many countries. It is increasingly present in milk and cheese, and quite large numbers of hospital, veterinary and farm workers are intermittently or continuously exposed to small concentrations of the antibiotic. These are all factors likely to promote the emergence of resistant strains in man.

From *Nature* 24 February 1962

100 Years Ago

By the death of Lord Lister, the world has lost one of its greatest men … it was his work which gave the main impulse to the development of the great science of bacteriology, a science which bids fair to occupy the most prominent place in medical work … Until Pasteur's time the existence of bacteria and their life-history had been looked on as only an interesting but not very important study … As soon as Lister showed that the exclusion of these organisms from wounds meant the disappearance of a variety of diseases to which man had been previously subject, the study of these organisms naturally advanced with great rapidity.

From *Nature* 22 February 1912

is developing an efficient mechanism for generating large numbers of entangled photons on demand. The authors were able to enhance the efficiency of their entangled-photon source using quantum-interference techniques, but further improvements in photon sources will be necessary.

Topological error correction could also be performed using qubits based on other physical systems, such as superconducting devices or trapped ions, which, like optical approaches, have allowed strong progress to be made in quantum computing. Other forms of topological error correction[8] may be able to further reduce the sensitivity to experimental errors beyond that achieved by the authors. For example, it is possible to produce a change in the phase of a probability amplitude that depends only on the number of times that the trajectory of a quantum system circles a specific point in a complex mathematical space known as Hilbert space, regardless of the exact shape of the trajectory. Topological error correction can increase the tolerance for experimental errors to the point that it is consistent with experimental capabilities, and greatly increases the prospects for building large-scale quantum computers. The experiment by Yao *et al.* represents an essential first step in that direction. ■

James D. Franson *is in the Physics Department, University of Maryland, Baltimore County, Baltimore, Maryland 21250, USA.*
e-mail: jfranson@umbc.edu

1. Yao, X.-C. *et al. Nature* **482,** 489–494 (2012).
2. Shor, P. W. *Phys. Rev. A* **52,** R2493–R2496 (1995).
3. Dennis, E., Kitaev, A., Landahl, A. & Preskill, J. *J. Math. Phys.* **43,** 4452–4505 (2002).
4. Barrett, S. D. & Stace, T. M. *Phys. Rev. Lett.* **105,** 200502 (2010).
5. Raussendorf, R. & Briegel, H. J. *Phys. Rev. Lett.* **86,** 5188–5191 (2001).
6. Knill, E., Laflamme, R. & Milburn, G. J. *Nature* **409,** 46–52 (2001).
7. Pittman, T. B., Jacobs, B. C. & Franson, J. D. *Phys. Rev. Lett.* **88,** 257902 (2002).
8. Nayak, C., Simon, S. H., Stern, A., Freedman, M. & Das Sarma, S. *Rev. Mod. Phys.* **80,** 1083–1159 (2008).

STRUCTURAL BIOLOGY

Muscarinic receptors become crystal clear

Muscarinic acetylcholine receptors mediate many physiological responses of the nervous system. Structures of two of these receptors yield insight into how they bind drugs and their mechanism of action. SEE LETTERS P.547 & P.552

REBECCA L. KOW & NEIL M. NATHANSON

G-protein-coupled receptors (GPCRs) are the darling drug targets of many pharmaceutical and biotech companies. This largest superfamily of cell-membrane receptors affects many aspects of life, including mood and behaviour, the immune system and the senses. In this issue, Haga *et al.*[1] and Kruse and colleagues[2] describe the crystal structures of two GPCRs — the M2 and M3 muscarinic acetylcholine receptors, which belong to the same GPCR family but couple to different effector proteins. The results not only advance our understanding of the structure and molecular pharmacology of this receptor family, but also contribute to our knowledge of GPCRs and membrane proteins in general.

Muscarinic acetylcholine receptors (mAChRs) are expressed on most target organs of the autonomic branch of the peripheral nervous system, which controls unconscious physiological responses such as heart rate, digestion, respiration and urination. They are also expressed in the central nervous system, where they modulate circuits that control movement and contribute to processes such as learning and memory. Drugs that target these receptors are being used and/or tested for conditions that include abnormal heart rate, asthma, overactive bladder, Alzheimer's disease, Parkinson's disease and schizophrenia.

Mammals have five subtypes of mAChR (M1–M5), which are divided into two functional groups: M2 and M4 preferentially couple to the G_i family of G proteins, whereas M1, M3 and M5 couple to the G_q family. The receptors affect different aspects of body function. For instance, M2 decreases heart rate by controlling certain potassium-ion membrane channels, and M3 stimulates hormone secretion and relaxes airway smooth muscle. Understanding the intricate structural details of these receptors should help in the design of drugs that target specific mAChRs without producing undesirable side effects.

Solving crystal structures of GPCRs is notoriously difficult because of the proteins' natural flexibility. A trademark of these receptors is their seven transmembrane domains (TM1–TM7), which give rise to intracellular and extracellular loops. Of these, the third intracellular loop is particularly large and mobile. To solve the structures of M2 and M3, respectively, Haga *et al.* (page 547) and Kruse *et al.* (page 552) replaced this loop with phage T4 lysozyme, a protein that promotes crystal formation. As with other GPCRs previously crystallized by this approach, the modification did not alter the receptors' ability to bind agonist ligands (molecules that activate the receptors, such as the neurotransmitter acetylcholine) or antagonist ligands (molecules that block receptor activation).

Haga *et al.*[1] describe the structure of M2 bound to the muscarinic blocker 3-quinuclidinyl benzilate. They report that the structure of inactive M2 is similar to that of other inactive

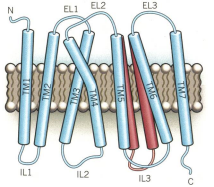

Figure 1 | Differences between receptor subtypes. G-protein-coupled receptors have seven transmembrane (TM) domains that span the cell membrane, giving rise to three intracellular loops (IL1–IL3) and three extracellular loops (EL1–EL3). Haga *et al.*[1] and Kruse and colleagues[2] report the crystal structures of two such receptors, M2 and M3, which are muscarinic acetylcholine receptors. The intracellular ends of TM5 and TM6 are farther apart in M2 (blue) and other G_i-coupled receptors than in M3 (red) and other G_q-coupled receptors. This and other structural differences between M2 and M3 may contribute to variations in the association and dissociation rates of drugs targeted to the two receptors.

GPCRs, particularly in the transmembrane domains. But M2 differs most from other GPCRs at its extracellular surface and in having a 33-ångström channel that contains the ligand binding pocket and extends beyond it. The ligand is oriented in the binding pocket by an aspartate amino-acid residue in TM3 and an asparagine residue in TM6. It also interacts with a lid formed by an 'aromatic cage' consisting of multiple tyrosine and tryptophan residues (located in TM3, TM6 and TM7). The authors found similar aromatic cages in three non-GPCR proteins that bind acetylcholine, which suggests that the aromatic cage is a common motif for binding this ligand.

Kruse *et al.*[2] determine the structure of M3 bound to tiotropium — a bronchodilator and mAChR blocker. Overall, the structures of inactive M3 and M2 are similar. For instance,

a characteristic of mAChRs seems to be an outward bend in TM4, which is not seen in other GPCRs. But the authors also identify a few notable differences in the structures of inactive M2 and M3. One is the presence of a phenylalanine residue (rather than, as in M2, a leucine) in the second extracellular loop of M3, which creates a space in the receptor's binding pocket. This small difference in the structure of the binding pocket may facilitate the development of drugs that have increased selectivity for a specific mAChR subtype. The relative position of TM7 in the two receptors also varies, possibly due to a difference in the TM2 amino acids with which TM7 interacts.

Another difference between M2 and M3 is in the position of TM5, especially at the cytoplasmic end of this domain. Specific TM6 residues that interact with TM5 at the cytoplasmic end determine the receptor's coupling selectivity for various G proteins. This difference may be a factor in the coupling selectivity of other GPCRs, as the TM5–TM6 distance in the M2 receptor is longer than that in M3 and similar to that in other G_i-coupled GPCRs, whereas in M3 this distance is similar to that in other G_q-coupled GPCRs (Fig. 1).

Kruse *et al.* used molecular-dynamics simulations to investigate the binding of tiotropium to mAChRs. Although this blocker binds to the acetylcholine binding site, the simulations indicate that it pauses at a separate (allosteric) site during both association and dissociation from the mAChR. Tiotropium dissociation from M3 is slower than from M2, perhaps because the second extracellular loop in M3 is less mobile. Exploiting such differences in the extracellular surfaces of mAChRs may again contribute to the development of subtype-specific drugs, an endeavour that has previously been impeded by the close structural similarity of the ligand binding regions in the transmembrane core of mAChRs.

These latest advances inevitably raise further questions. For example, what are the differences in the receptors' structure on binding to antagonists, full agonists and 'biased' agonists (which elicit only a subset of physiological responses[3])? Also, for the G-protein-interacting regions of GPCRs to be sufficiently ordered for crystallization, the receptor must be bound to its G protein[4]. Yet replacement of the third intracellular loop with the phage T4 lysozyme eliminates receptor coupling to G proteins. The conformational changes involved on binding to the G protein are therefore unclear. Crystallization of more intact mAChRs in complex with their cognate G proteins is thus required for detailed information about the pathways of receptor–G-protein coupling. These are some of the challenges we face in our attempts to better understand mAChRs. ■

Rebecca L. Kow *and* **Neil M. Nathanson**
are in the Department of Pharmacology, University of Washington, Seattle, Washington 98195-7750, USA.
e-mail: nathanso@u.washington.edu

1. Haga, K. *et al. Nature* **482,** 547–551 (2012).
2. Kruse, A. C. *et al. Nature* **482,** 552–556 (2012).
3. Reiter, E., Ahn, S., Shukla, A. K. & Lefkowitz, R. J. *Annu. Rev. Pharmacol. Toxicol.* **52,** 179–197 (2012).
4. Rasmussen, S. G. F. *et al. Nature* **477,** 549–555 (2011).

CANCER GENETICS

Evolution after tumour spread

A genetic study of brain cancers in mice and humans reveals distinct mutations in primary tumours and their metastases, suggesting that the two disease 'compartments' may require different treatments. SEE LETTER P.529

STEVEN C. CLIFFORD

The spread of a primary tumour to secondary sites in the body is a key step in the development of many cancers, and treatment of these secondary metastatic tumours represents one of the foremost challenges in oncology. On page 529 of this issue, Wu *et al.*[1] describe two new mouse strains that serve as models of metastasis in the childhood brain cancer medulloblastoma*. In the mice, primary and metastatic tumours seem to occupy two genetically distinct 'compartments', which arise from divergent DNA-sequence mutations that occur after metastasis. The authors also detect similar differences in human medulloblastoma tumours — a finding that may influence the development of anticancer therapies.

Wu *et al.* used an experimental system called Sleeping Beauty mutagenesis[2,3] to introduce random genetic mutations into cerebellar progenitor cells in the developing brains of two strains of mice. These two new strains were derived by breeding the existing $Tp53^{mut}$ and $Ptch^{+/-}$ strains, which are predisposed to brain tumours[3,4], with a strain that expresses the Sleeping Beauty mutagen in cerebellar progenitors. This system leaves a unique genetic 'footprint' at each mutation site, which allows mutated genes to be identified by DNA sequencing. Such mutagenesis experiments are used to identify genes in which mutations frequently arise, because the likelihood of these being involved in tumour development is reasoned to be above average[2,3].

As in mouse models of other cancer types[2,3], Wu and colleagues' Sleeping Beauty mutagenesis accelerated the development of medulloblastoma in both mouse strains. The authors identified a range of new and established cancer-related genes that had mutations, including some that have previously been implicated in medulloblastoma. They also observed that, following mutagenesis, mice of both strains developed metastases around a type of brain tissue called the leptomeninges, in patterns that are reminiscent of metastatic human medulloblastoma[5]. The two mouse models thus provided an opportunity to track mutations present in the primary and metastatic disease, and to investigate their genetic provenance.

Wu *et al.* found that there were, in general, only a few mutations common to primary and metastatic tumours from the same mouse, but that the mutations in different metastases from the same mouse tended to be more similar to each other. Moreover, certain mutations observed in metastases were detected at only low levels within the primary tumour, and some mutations were unique to one or the other tumour type. The authors conclude that their findings are consistent with a model in which metastases originate from rare cells in the primary tumour, and that, following metastasis, additional mutations accumulate independently — both in the primary tumour (post-dispersion events) and in metastases (post-metastasis events) (Fig. 1).

Turning our attention away from mice, an obvious question is whether primary and metastatic tumours in the human disease also show 'bi-compartmental' genetics. Approximately 30% of patients with medulloblastoma already have metastases when they are first diagnosed, and this is associated with a poor prognosis[5]. However, few previous studies have compared the biology of human primary tumours with their associated metastases, mainly because metastases are not routinely biopsied. Despite the limited sample availability, Wu *et al.*[1] show initial evidence of differing genetics in primary and metastatic tumours from seven human patients.

Further investigation is required to establish whether the authors' findings are broadly relevant to human medulloblastoma. The

*This article and the paper[1] under discussion were published online on 15 February 2012.

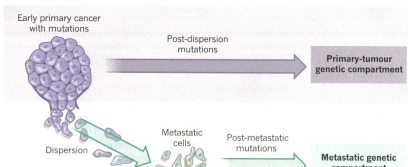

Figure 1 | A bi-compartmental genetic model of cancer metastasis. By analysing the tumours from two strains of mice that model the brain cancer medulloblastoma, Wu *et al.*[1] found differences in the DNA-sequence mutations present in primary and metastatic tumours. They propose that rare cells in the primary tumour that are capable of metastasizing disperse to other sites in the brain, where they form metastases. The cells of the primary tumour and the metastases then continue to accumulate mutations, generating two distinct genetic compartments.

human disease exhibits[5] more complex patterns of metastases than are observed in mice, and is classified into four molecular subgroups (WNT, SHH, Group 3 and Group 4), which each display distinct biological and clinical characteristics[6]. The *Ptch*$^{+/-}$ mice used by Wu *et al.*[1] develop SHH-associated medulloblastomas[4]; similar mutagenesis-driven approaches using existing mouse models of other medulloblastoma disease groups, such as WNT[7], might prove informative.

Perhaps the most urgent question arising from this study[1] is whether the genetic differences between the two disease compartments lead to distinct biological features that make them respond differently to treatment. In mice, these compartments remain genomically characterized entities, the biological and therapeutic importance of which is untested. In humans, clinical-trial data show[5] that primary and metastatic sites respond similarly to current therapies (with cure achieved at both sites) in around 60% of children with metastatic disease, but a more objective assessment of treatment response is confounded by the fact that primary tumours are mostly removed by surgery prior to treatment. Wu *et al.* provide initial evidence that the tumour compartments may respond differently to current therapies in certain patients, but they rightly caution that these effects could also relate to clinical factors such as radiotherapy being delivered at different intensities to different tumour sites.

Some of the mutations identified by Wu and colleagues' experiments may also reveal biological processes or pathways that could offer drug targets for the improved treatment of primary tumours, metastases, or both. The new mouse strains provide excellent models in which to test this possibility. The multitude and variety of mutations described by Wu *et al.*[1] are noteworthy, but the next challenge is to determine which of them can drive tumour development, which are therapeutically relevant, and which occur at sufficient frequency in the human disease to warrant their pursuit as potential targets. The authors justifiably reason that targets that are common to primary tumours and metastases, in both humans and mice, are those most attractive for further development. However, only one cellular pathway, insulin-dependent signalling, meets these criteria on the basis of their current data.

Providing answers to all these questions will require further biological investigation across species, as well as clinical studies. An additional challenge is posed by the fact that there are fewer than 700 cases of medulloblastoma per year in Europe. More routine biopsy and characterization of human metastases will be essential, and the impetus and ethical justification for such a fundamental change to clinical practice will, at least in part, come from experimental studies such as those presented here. Time will tell whether this tale of Sleeping Beauty and mice develops into a clinically relevant human paradigm. ■

Steven C. Clifford *is at the Northern Institute for Cancer Research, Newcastle University, Newcastle upon Tyne NE1 4LP, UK.*
e-mail: steve.clifford@ncl.ac.uk

1. Wu, X. *et al. Nature* **482,** 529–533 (2012).
2. Collier, L. S., Carlson, C. M., Ravimohan, S., Dupuy, A. J. & Largaespada, D. A. *Nature* **436,** 272–276 (2005).
3. Copeland, N. G. & Jenkins, N. A. *Nature Rev. Cancer* **10,** 696–706 (2010).
4. Goodrich, L. V., Milenković, L., Higgins, K. M. & Scott, M. P. *Science* **277,** 1109–1113 (1997).
5. Pizer, B. L. & Clifford, S. C. *Br. J. Neurosurg.* **23,** 364–375 (2009).
6. Taylor, M. D. *et al. Acta Neuropathol.* http://dx.doi.org/10.1007/s00401-011-0922-z (2011).
7. Gibson, P. *et al. Nature* **468,** 1095–1099 (2010).

CLIMATE CHANGE

Shrinking glaciers under scrutiny

Melting glaciers contribute to sea-level rise, but measuring their mass loss over time is difficult. An analysis of satellite data on Earth's changing gravity field does just that, and delivers some unexpected results. SEE LETTER P.514

JONATHAN BAMBER

Glaciers and ice caps are pivotal features of both water resources and tourism. They are also a significant contributor to sea-level rise. About 1.4 billion people are dependent on the rivers that flow from the Tibetan plateau and Himalayas[1]. Yet significant controversy[2] and uncertainty surround the recent past and future behaviour of glaciers in this region. This is not so surprising when one considers the problem in hand. There are more than 160,000 glaciers and ice caps worldwide. Fewer than 120 (0.075%) have had their mass balance (the sum of the annual mass gains and losses of the glacier or ice cap) directly measured, and for only 37 of these are there records extending beyond 30 years. Extrapolating this tiny sample of observations to all glaciers and ice caps is a challenging task that inevitably leads to large uncertainties.

On page 514 of this issue, Jacob and colleagues[3] describe a study based on satellite data for Earth's changing gravity field that tackles this problem*. Their results have surprising implications for both the global contribution of glaciers to sea level and the changes occurring in the mountain regions of Asia.

Melting glaciers are an iconic symbol of climate change. On the basis of the limited data mentioned above, they seem to have been receding, largely uninterrupted, almost

*This article and the paper[3] under discussion were published online on 8 February 2012.

everywhere around the world for several decades[4]. Scaling up the small sample of ground-based observations to produce global estimates is, however, fraught with difficulty. Size, local topography, altitude range, aspect and micro-climate all affect the response of individual glaciers in complex ways. Even the seasonality of changes in temperature and precipitation strongly influence the glaciers' response, and those that terminate in a lake or ocean behave differently again.

Nonetheless, until recently there was little alternative to some form of extrapolation of the terrestrial observations to large regions and numbers of glaciers. One such high-profile assessment[5] concluded that, during the period 1996–2006, the mass loss from glaciers and ice caps (GICs) increased steadily, contributing a sea-level rise of 1.1 ± 0.24 millimetres per year by 2006. In this study[5], the authors concluded that GICs had been the dominant mass contributor to sea-level rise over the study period, and they extrapolated their results forward to argue that this would also be the case in the future.

Then along came the Gravity Recovery and Climate Experiment (GRACE), which consists of a pair of satellites that have been making global observations of changes in Earth's gravity field since their launch in 2002. They have been used in various studies to examine the changing mass of the great ice sheets of Antarctica and Greenland[6] and several other large glaciated regions[7]. But, so far, the data have not been analysed simultaneously and consistently for all areas.

The difficulty with doing this is that GRACE measures the gravity field of the complete Earth system. This includes mass exchange and/or mass redistribution in the oceans, atmosphere, solid Earth and land hydrology, in addition to any changes in GIC volume. To determine the latter, it is clearly essential to be able to separate it from the other sources of mass movement that affect the gravity field. A second, related issue is the effective resolution of the observations. The GRACE satellites are sensitive to changes in the gravity field over distances of a few hundred kilometres. They cannot 'see' the difference between the signal from one glacier or small ice cap and another.

To isolate the GIC signal from others at the surface, Jacob and colleagues defined units of mass change — called mass concentrations, or mascons — within each of their 18 GIC regions (including the European Alps; Fig. 1). Each region might have many tens of mascons defining the geographic extent of significant ice volume within the sector[3]. Combined with global models of land hydrology and atmospheric-moisture content, the authors were able to isolate the GIC mass trends over the eight-year (2003–10) period of the observations. What they found was unexpected.

First, the contribution of GICs (excluding the Antarctica and Greenland peripheral GICs) to sea-level rise was less than half the value of the most recent, comprehensive estimate[8] obtained from extrapolation of *in situ* measurements for 2001–05 (0.41 ± 0.08 compared with 1.1 mm yr^{-1}). Second, losses for the High Mountain Asia region — comprising the Himalayas, Karakoram, Tianshan, Pamirs and Tibet — were insignificant. Here, the mass-loss rate was just 4 ± 20 gigatonnes per year (corresponding to 0.01 mm yr^{-1} of sea-level rise), compared with previous estimates that were well over ten times larger. By a careful analysis, the authors discounted a possible tectonic origin for the huge discrepancy, and it seems that this region is more stable than previously believed.

What is the significance of these results[3]? Understanding, and closing, the sea-level budget (the relative contributions of mass and thermal expansion to ocean-volume change) is crucial for testing predictions of future sea-level rise. Estimates of the future response of GICs to climate change are, in general, based on what we know about how they have responded in the past. A better estimate of past behaviour, such as that obtained by Jacob and colleagues, will therefore result in better estimates of future behaviour. Discussion of the demise of the Himalayan glaciers has been mired in controversy, partly because of basic errors[2], but also because of the dearth of reliable data on past trends. Given their role as a water supply for so many people[1], this has been a cause for concern and an outstanding issue.

Of course, eight years is a relatively short observation period. Some of the regions, such as the Gulf of Alaska, experience large inter-annual variations in mass balance that are mainly due to variability in precipitation[7]. This is also true for the High Mountain Asia region[3], and, as a consequence, a different measurement period could significantly alter the estimated trend for this sector. Furthermore, some areas, such as the European Alps and Scandinavia, have been relatively well monitored, and thus constrained, using other approaches. Nonetheless, Jacob and colleagues have dramatically altered our understanding of recent global GIC volume changes and their contribution to sea-level rise. Now we need to work out what this means for estimating their future response. ■

J. BALOG/EXTREME ICE SURVEY

Figure 1 | The Leschaux and Talèfre glaciers in the French Alps. The photograph highlights the complex and intricate topographic setting of these mountain glaciers and the difficulty in extrapolating observations from one glacier to others. Jacob and colleagues[3] avoided these difficulties by using the area-integrated signal from satellite gravity data.

Jonathan Bamber *is at the Bristol Glaciology Centre, School of Geographical Sciences, University of Bristol, Bristol BS8 1SS, UK.*
e-mail: j.bamber@bristol.ac.uk

1. Immerzeel, W. W., van Beek, L. P. H. & Bierkens, M. F. P. *Science* **328,** 1382–1385 (2010).
2. Cogley, J. G., Kargel, J. S., Kaser, G. & van der Veen, C. J. *Science* **327,** 522 (2010).
3. Jacob, T., Wahr, J., Pfeffer, W. T. & Swenson, S. *Nature* **482,** 514–518 (2012).
4. Kaser, G., Cogley, J. G., Dyurgerov, M. B., Meier, M. F. & Ohmura, A. *Geophys. Res. Lett.* **33,** L19501 (2006).
5. Meier, M. F. *et al. Science* **317,** 1064–1067 (2007).
6. Velicogna, I. *Geophys. Res. Lett.* **36,** L19503 (2009).
7. Luthcke, S. B., Arendt, A. A., Rowlands, D. D., McCarthy, J. J. & Larsen, C. F. *J. Glaciol.* **54,** 767–777 (2008).
8. Cogley, J. G. *Ann. Glaciol.* **50,** 96–100 (2009).

nature

23 February 2012 / Vol 482 / Issue No. 7386

Publication policies, author guidelines and information

This is a summary of *Nature*'s guide to authors, publication policies and other author information, available in full on the web via our main author information page at www.nature.com/nature/authors.

Getting published in *Nature*

Please read www.nature.com/nature/authors/get_published before finalizing any original scientific research manuscripts you intend to submit. This section explains *Nature*'s editorial criteria, and how manuscripts are handled by the editors after submission and before acceptance for publication.

Formatting guide

Please read www.nature.com/nature/authors/gta before finalizing and submitting your contribution. This section provides instructions for preparing, formatting and writing all types of contribution published by *Nature*.

Publication policies

This section, at www.nature.com/authors, describes *Nature*'s conditions of publication, including policies on authorship; competing financial interests; duplicate publication; prepublicity and embargoes; materials and data availability; research on animal (including human) subjects; referees; corrections, retractions, errata and addenda to published papers; the complaints procedure and refutations; and copyright/licence to publish. All contributions, for whatever section of the journal, are considered for publication and published on the condition that authors agree to these policies.

Submissions

These sections, at www.nature.com/nature/authors/submissions, contain our online service for presubmission enquiries and submission and tracking of Articles, Letters and Review-type manuscripts. Authors should read the formatting guide before using this service. Authors who cannot submit online can submit by post, but *Nature* strongly recommends the online service. **Authors must not submit by both methods.** Authors experiencing operational difficulty in using the online submission service can send an enquiry to mtshelp@nature.com, with a brief explanation of the problem.

Editorial contacts and author services

This section, at www.nature.com/nature/about/contact, provides the addresses of *Nature*'s editorial offices; names of editorial staff; and contact details for advice, reprints, permissions, press office (press@nature.com), and other author-related contact information, including postal addresses for mailed submissions. Short biographies of editors are also available at www.nature.com/nature/about/editors.

Final submissions

This section, at www.nature.com/nature/authors/submissions/final, applies only if an Article or Letter has been accepted in principle for publication and the author has been asked by the editor for a final version. Authors will need to upload electronic files of the text, production-quality figures and supplementary information (if any) to our database. Authors must include a completed manuscript checklist and all relevant signed forms and declarations as requested by the editor.

Short version of guide to authors

See www.nature.com/nature/authors for full version. Contributors not used to *Nature*'s format are advised to read some papers in published issues before submission, to familiarize themselves with *Nature*'s style. *Nature*'s main formats for original research are Articles and Letters.

ARTICLES are original reports whose conclusions represent a substantial advance in understanding of an important problem and have immediate, far-reaching implications. They do not normally exceed **5 pages** of *Nature* and have **no more than 50** references. (One page of undiluted text is about 1,300 words.)

Articles have a summary for readers outside the discipline, separate from the main text and containing no references, of up to 150 words. The summary does not contain numbers, abbreviations, acronyms or measurements unless essential. It contains a brief account of the background and rationale of the work, followed by a statement of the main conclusions, introduced by the phrase 'Here we show' or its equivalent.

The Article itself typically has about 3,000 words of text, beginning with up to 500 words of referenced text expanding on the background to the work, followed by a concise, focused account of the findings, and ending with one or two short paragraphs of discussion. The text can contain a few short subheadings consisting of about 20 but no more than 40 characters (including spaces) each.

LETTERS are short reports of original research focused on an outstanding finding whose importance means that it will be of interest to scientists in other fields. They do not normally exceed **4 pages** of *Nature*, and have **no more than 30** references. They begin with a **fully referenced paragraph** of not more than 300 words, aimed at readers in other disciplines. This paragraph contains a summary of the background and rationale for the work, followed by a one-sentence statement of the main conclusions introduced by the phrase 'Here we show' or its equivalent, and ending with two to three sentences describing the implications in context.

The main text which follows is typically up to 1,500 words long. This text can, if the author requires, start with a further brief paragraph of introductory material. A description of the research then follows. Any discussion at the end of the text should be as succinct as possible.

FIGURES in both Articles and Letters are as small as possible: Articles typically have 5 or 6 figures, Letters typically have 3 or 4 figures. Legends and/or methods are additional to the main text. Methods Summaries (which are published in print only) are no longer than 300 words; Methods sections (which are published online) can be up to 1,000 words; legends should not exceed 100 words each and start with a one-sentence title for the figure, followed by a brief explanation of the parts and symbols.

See www.nature.com/nature/authors/gta/others.html for details of other types of contribution to *Nature*, including Brief Communications Arising; Reviews and Perspectives (presubmission enquiries to reviewsandinsights@nature.com); and Correspondence (submit to corres@nature.com).

See Authors and Referees @ NPG (www.nature.com/authors) for details of Nature journals' publication policies, author and referee services, author benefits and for links to Nautilus and Peer to Peer blogs.

PERSPECTIVE

doi:10.1038/nature10836

The case for open computer programs

Darrel C. Ince[1], Leslie Hatton[2] & John Graham-Cumming[3]

Scientific communication relies on evidence that cannot be entirely included in publications, but the rise of computational science has added a new layer of inaccessibility. Although it is now accepted that data should be made available on request, the current regulations regarding the availability of software are inconsistent. We argue that, with some exceptions, anything less than the release of source programs is intolerable for results that depend on computation. The vagaries of hardware, software and natural language will always ensure that exact reproducibility remains uncertain, but withholding code increases the chances that efforts to reproduce results will fail.

The rise of computational science has led to unprecedented opportunities for scientific advance. Ever more powerful computers enable theories to be investigated that were thought almost intractable a decade ago, robust hardware technologies allow data collection in the most inhospitable environments, more data are collected, and an increasingly rich set of software tools are now available with which to analyse computer-generated data.

However, there is the difficulty of reproducibility, by which we mean the reproduction of a scientific paper's central finding, rather than exact replication of each specific numerical result down to several decimal places. We examine the problem of reproducibility (for an early attempt at solving it, see ref. 1) in the context of openly available computer programs, or code. Our view is that we have reached the point that, with some exceptions, anything less than release of actual source code is an indefensible approach for any scientific results that depend on computation, because not releasing such code raises needless, and needlessly confusing, roadblocks to reproducibility.

At present, debate rages on the need to release computer programs associated with scientific experiments[2–4], with policies still ranging from mandatory total release to the release only of natural language descriptions, that is, written descriptions of computer program algorithms. Some journals have already changed their policies on computer program openness; *Science*, for example, now includes code in the list of items that should be supplied by an author[2]. Other journals promoting code availability include *Geoscientific Model Development*, which is devoted, at least in part, to model description and code publication, and *Biostatistics*, which has appointed an editor to assess the reproducibility of the software and data associated with an article[6].

In contrast, less stringent policies are exemplified by statements such as[7] "*Nature* does not require authors to make code available, but we do expect a description detailed enough to allow others to write their own code to do similar analysis." Although *Nature*'s broader policy states that "...authors are required to make materials, data and associated protocols promptly available to readers...", and editors and referees are fully empowered to demand and evaluate any specific code, we believe that its stated policy on code availability actively hinders reproducibility.

Much of the debate about code transparency involves the philosophy of science, error validation and research ethics[8,9], but our contention is more practical: that the cause of reproducibility is best furthered by focusing on the dissection and understanding of code, a sentiment already appreciated by the growing open-source movement[10]. Dissection and understanding of open code would improve the chances of both direct and indirect reproducibility. Direct reproducibility refers to the recompilation and rerunning of the code on, say, a different combination of hardware and systems software, to detect the sort of numerical computation[11,12] and interpretation[13] problems found in programming languages, which we discuss later. Without code, direct reproducibility is impossible. Indirect reproducibility refers to independent efforts to validate something other than the entire code package, for example a subset of equations or a particular code module. Here, before time-consuming reprogramming of an entire model, researchers may simply want to check that incorrect coding of previously published equations has not invalidated a paper's result, to extract and check detailed assumptions, or to run their own code against the original to check for statistical validity and explain any discrepancies.

Any debate over the difficulties of reproducibility (which, as we will show, are non-trivial) must of course be tempered by recognizing the undeniable benefits afforded by the explosion of internet facilities and the rapid increase in raw computational speed and data-handling capability that has occurred as a result of major advances in computer technology[14]. Such advances have presented science with a great opportunity to address problems that would have been intractable in even the recent past. It is our view, however, that the debate over code release should be resolved as soon as possible to benefit fully from our novel technical capabilities. On their own, finer computational grids, longer and more complex computations and larger data sets—although highly attractive to scientific researchers—do not resolve underlying computational uncertainties of proven intransigence and may even exacerbate them.

Although our arguments are focused on the implications of *Nature*'s code statement, it is symptomatic of a wider problem: the scientific community places more faith in computation than is justified. As we outline below and in two case studies (Boxes 1 and 2), ambiguity in its many forms and numerical errors render natural language descriptions insufficient and, in many cases, unintentionally misleading.

The failure of code descriptions

The curse of ambiguity

Ambiguity in program descriptions leads to the possibility, if not the certainty, that a given natural language description can be converted into computer code in various ways, each of which may lead to different numerical outcomes. Innumerable potential issues exist, but might include mistaken order of operations, reference to different model versions, or unclear calculations of uncertainties. The problem of ambiguity has haunted software development from its earliest days.

Ambiguity can occur at the lexical, syntactic or semantic level[15] and is not necessarily the result of incompetence or bad practice. It is a natural consequence of using natural language[16] and is unavoidable. The

[1]Department of Computing Open University, Walton Hall, Milton Keynes MK7 6AA, UK. [2]School of Computing and Information Systems, Kingston University, Kingston KT1 2EE, UK. [3]83 Victoria Street, London SW1H 0HW, UK.

BOX 1

The United Kingdom Meteorological Office produces (in conjunction with the University of East Anglia's Climatic Research Unit) the downloadable and widely used gridded temperature anomaly data sets known as HadCRUT and CRUTEM3. Yet even such a high-profile data set, developed by an organization with a good standard of software development[34], contained errors that would have been more quickly identified and rectified had the underlying code been readily available.

In 2009, on examining the available data sets and the description of the algorithm[35], J.G.-C. identified a number of errors (the software he used to check the meteorological database is available upon request). One set of errors was procedural, and involved incorrect computation of historical average temperatures in a number of records in New Zealand and Australia. The Meteorological Office confirmed the errors, showed that they had resulted in errors up to 0.2 °C (either warmer or cooler) in the average temperature for Australia and New Zealand in some years before 1900, and issued an update to CRUTEM3. Two other errors occurred in the coding of the calculation of station errors (an estimate of the error in any average temperature reading). When corrected, a minor reduction in station errors resulted, improving the accuracy of the data. So, although these implementation problems did not lead to serious errors in the temperature data sets, they highlight the difficulty of translating a natural-language description (even with some formulae expressed mathematically) into code.

These errors do not in any way reflect badly on the original authors. The code rewriting simply plays the part of peer review and it is normal to find such errors. Indeed, the discovery of such errors in 'working' software is exceedingly common in all computing, even when the software has been in use for a considerable time. This was emphatically demonstrated in a seminal IBM study[36], demonstrating that fully a third of all the software failures in the study took longer than 5,000 execution years (execution time indicates the total time taken executing a program) to fail for the first time.

BOX 2

As discussed, unambiguous descriptions are no guarantee of reproducibility. One example from the geological literature makes the point[37]. This study compared nine different commercial implementations of the same seismic data-processing algorithms, developed independently. Several sources of ambiguity were successfully excluded, the same data set was used, the signal-processing algorithms used were unambiguously specified in mathematics, and the same programming language was used (Fortran 77). The individual companies followed industry standards in code implementation.

Approximately 200,000 lines of code were exercised in each of the packages in a 14-stage pipeline for which the output of each stage was the input to the next. The signal-processing algorithms used would be familiar to many scientists—such as Wiener deconvolution, acoustic wave equation solutions, fast Fourier transforms and numerous common statistical procedures.

The initial stage involved reading 32-bit pressure data from tapes recorded in a marine environment. During the processing pipeline, the agreement between the results of each package declined from the six significant figures present in the input data to only between one and two in the final output. These data, however, were used by geologists to site extremely expensive marine drilling rigs and could "fundamentally affect the conclusions reached as to the nature of potential hydrocarbon accumulations" [37]. Furthermore "it seems reasonable to infer that the primary source of disagreement is indeed software error"[37]. Even porting other seismic software between different architectures using the same input data lost two out of six significant places[12]. On the positive side, correction of the programming errors found during developer feedback led to considerably improved agreement.

Although conducted some years ago, the study is just as relevant today. Fortran 77 is still in use in one dialect or another in scientific research, the same software assurance procedures are still widely used, and scientific programmers are still people, subject to human fallibility.

problem is regarded as so axiomatic that its avoidance or minimization is routinely taught at the undergraduate level in computing degrees. Nor is the study of ambiguity confined to the classroom. Active research continues on the use of tools for the detection of ambiguity[17], the avoidance of ambiguity in major projects[18], and the clarification of the intended functions of computer programs[15].

One proposed solution to the problem of ambiguity is to devote a large amount of attention to the description of a computer program, perhaps expressing it mathematically or in natural language augmented by mathematics. But this expectation would require researchers to acquire skills that are only peripheral to their work (set theory, predicate calculus and proof methods). Perhaps worse, investment of effort or resources alone cannot guarantee the absence of defect[19]. A recent study[20] of a tightly specified, short, simply expressed algorithm whose semi-mathematical specification was supplemented by example outputs showed that major problems still arose with large numbers of programs individually implemented to this specification. In short, natural language descriptions cannot hope to avoid ambiguous program implementations, with unpredictable effects on results.

Errors exist within 'perfect' descriptions

Let us assume for a moment that a researcher, perhaps trained—as are computer scientists—to think of computer algorithms as mathematical objects, and fully versed in the formal semantics of software description, has managed to describe a computer program perfectly in some notation. Unfortunately, even such a description would not ensure direct or indirect reproducibility, because other forms of error or ambiguity (unrelated to natural language) are likely to creep in, leading to potentially serious uncertainties (Box 2).

First, there are programming errors. Over the years, researchers have quantified the occurrence rate of such defects to be approximately one to ten errors per thousand lines of source code[21].

Second, there are errors associated with the numerical properties of scientific software. The execution of a program that manipulates the floating point numbers used by scientists is dependent on many factors outside the consideration of a program as a mathematical object[22]. Rounding errors can occur when numerous computations are repeatedly executed, as in weather forecasting[23]. Although there is considerable research in this area, for example in arithmetic and floating point calculations[24–27], algorithms[28], verification[29] and fundamental practice[30], much of it is published in outlets not routinely accessed by scientists in generic journals, such as *Computers & Mathematics with Applications*, *Mathematics in Computer Science* and the *SIAM Journal on Scientific Computing*.

Third, there are well-known ambiguities in some of the internationally standardized versions of commonly used programming languages in scientific computation[13]. Monniaux[23] describes an alarming example relating to implementation of software features:

"More subtly, on some platforms, the exact same expression, with the same values in the same variables, and the same compiler, can be evaluated to different results, depending on seemingly irrelevant statements (printing debugging information or other constructs that do not openly change the values of variables)."

This is known as an order-of-evaluation problem and many programming languages are subject to its wilful ways. Ironically, such execution

ambiguity is quite deliberate and is present to allow a programming language compiler more flexibility in its optimization strategy. And even when programs are simple, or developed by the largest software companies, such errors remain surprisingly common: numerical ambiguity led Microsoft to declare in 2010 and reaffirm in September 2011, that the treatment of floating point numbers in its popular Excel spreadsheet "...may affect the results of some numbers or formulas due to rounding and/or data truncation." (http://support.microsoft.com/kb/78113).

Perfection is no guarantee of reproducibility

Finally, even if a computer program could be unambiguously described and implemented without error, other problems can arise in machine deployment whereby the results from identical code often diverge when hardware and software configurations are changed[22]. So even perfection in one's own software environment does not guarantee reproducibility. As a result, to maximize the chances of reproducibility and consistency, not only would we urge code release, but also a description of the hardware and software environment in which the program was executed and developed.

Challenges are no excuse for closed code

Nature's policy on code release implies that algorithmic descriptions using mathematical specifications, equations, formal algorithmic descriptions or pseudocode (simplified version of complete code) may be required. But there is no guarantee that such tools can avoid ambiguity[20], and even if they could, we have shown above that implementation and numerical errors—possibly compounded by differences in machine architecture—will still arise. So, even if complete code is made available, exact replication or even reproduction of central results may fail. A reasonable observer might therefore ask why code should be made available at all. Our response is that the alternative is far worse. Keeping code closed ensures that potential uncertainties or errors in a paper's conclusions cannot be traced to ambiguity, numerical implementation, or machine architecture issues and prevents testing of indirect reproducibility. Although it is true that independent efforts to reproduce computational results without recourse to the original source code constitute an important approach, the all-too-common treatment of code as a black box unnecessarily slows and impedes valid efforts to evaluate model results. We therefore regard the non-availability of code as a serious impediment to reproducibility.

Potential barriers and proposed solutions

There are a number of barriers to the release of code. These include a shortage of tools that package up code and data in research articles; a shortage of central scientific repositories or indexes for program code; an understandable lack of perception of the computational problems with scientific code leading to the faulty assumption that program descriptions are adequate (something we address in this article); and finally that the development of program code is a subsidiary activity in the scientific effort.

A modest proposal

An effective step forward would be for journals to adopt a standard for declaring the degree of source code accessibility associated with a scientific paper. A number of simple categories illustrate the idea:

- Full source code: full release of all source code used to produce the published results along with self-tests to build confidence in the quality of the delivered code, as is the case with Perl modules in the CPAN archive, for example (http://cpan.org).
- Partial source code: full release of source code written by the researcher accompanied by associated documentation of ancillary packages used, for example commercial scientific subroutine libraries.
- Marginal source code: release of executable code and an application programming interface to allow other researchers to write test cases.
- No source code: no code at all provided.

This hierarchy of disclosure would alert both the readers and authors of a journal article to the fact that the issue is important and would highlight the degree to which results might be reproduced independently. There remain, however, some potential stumbling blocks, a number of which can easily be resolved using existing facilities.

Intellectual property rights

Clearly, if there is evidence of commercial potential or use, such as a patent or some copyright, then there is a problem. It is difficult to see how a journal might deal with this without substantial financial commitment to independent testing under a non-disclosure agreement or possibly even the purchase of commercial rights. Perhaps the simplest solution is for a journal to flag the software as 'No source code' (ideally giving the reasons) until such time as the source code can be included, either because the code goes into the public domain or is released under some free licence. Such a designation simply says that, for the moment, the results are not reproducible with the authors' own source code, and that testing of the main results must proceed with independent approaches.

Limited access

Researchers may not have access to at least some of the software packages that are used for development. We suggest that this would not be a problem for most researchers: their institutions would normally provide such software. If it were to be a problem, then a journal could mark a publication as 'Partial source code'. The release of the code, even without the software environment required for compilation and execution, would still be valuable in that it would address issues such as dissection and indirect reproducibility (see above) and would enable rewriting using other programming languages.

Procedure

Adopting the simple disclosure of the availability of source code will help make it clear to the readership of a journal that this is an important issue, while also giving them an idea of the degree of code release. However, we would further suggest that journals adopt a standard that specifies that supplementary material supporting a research article must describe each of the released modular components of any software used. *Nature* editors and referees are already empowered to include an appraisal of code in their judgement about the publication potential of the article, and this practice should be more widely advertised and supported. A good example of this approach is the way that the journal *Geoscientific Model Development* asks authors to describe their program code.

Logistics

Over the past two decades, the open-source community has solved the logistics of releasing and storing code while maintaining a cooperative development environment. SourceForge (http://www.sourceforge.net/) is an excellent example. Founded in 1999, it is a web-based source-code repository which acts as a free centralized location for developers working on open-source projects. It currently hosts around 300,000 projects and has over two million registered users. Not only does it store source code but also it provides access to version control information, project wikis (websites that are easily modifiable by its users) and database access. We urge funding agencies to investigate and adopt similar solutions.

Packaging

There are a number of tools that enable code, data and the text of the article that depends on them to be packaged up. Two examples here are *Sweave* associated with the programming language R and the text-processing systems LaTeX and LyX, and *GenePattern-Word RRS*, a system specific to genomic research[31]. *Sweave* allows text documents, figures, experimental data and computer programs to be combined in such a way that, for example, a change in a data file will result in the regeneration of all the

research outputs. *GenePattern-Word RRS* is similar in that it enables an author to link text, tables and figures to the analysis and data that yielded the results, reported in a word-processed document; it also allows further experimentation (for example, additional analyses can be carried out). It is still early days, however, and localized solutions are emerging at the grassroots level. Donoho and co-workers, for example, have developed software packages that allow anyone with access to the *Matlab* programming language and development environment to reproduce figures from their harmonic analysis articles, inspect source code, change parameters and access data sets[32].

Steps to implementation

Our thesis is that journal and funding body strictures relating to code implementations of scientific ideas are now largely obsolete. We have suggested one modest path to code availability in this article. There are a number of further steps that journals, academies and educational organizations might consider taking:

- Research funding bodies should commission research and development on tools that enable code to be integrated with other elements of scientific research such as data, graphical displays and the text of an article.
- Research funding bodies should provide metadata repositories that describe both programs and data produced by researchers. The Australian National Data Service (http://www.ands.org.au/) which acts as an index to data held by Australian research organizations, is one example of this approach.
- Journals should expect researchers to provide some modular description of the components of the software that support a research result; referees should take advantage of their right to appraise software as part of their reviewing task. An example of a modular description can be seen in a recent article published in *Geoscientific Model Development*[33].
- Science departments should expand their educational activities into reproducibility. Clearly such teaching should be relevant to the science at hand; however, courses on statistics, programming and experimental method could be easily expanded and combined to include the concept of reproducibility.

Received 9 May 2011; accepted 5 January 2012.

1. Schwab, M., Karrenbach, M. & Claerbout, J. Making scientific computations reproducible. *Comput. Sci. Eng.* **2**, 61–67 (2000).
2. Barnes, N. Publish your computer code: it is good enough. *Nature* **467,** 753 (2010).
3. McCafferty, D. Should code be released? *Commun. ACM* **53,** 16–17 (2010).
4. Merali, Z. . . *Error. Nature* **467,** 775–777 (2010).
5. Hanson, B., Sugden, A. & Alberts, B. Making data maximally available. *Science* **331,** 649 (2011).
6. Peng, R. D. Reproducible research and biostatistics. *Biostatistics* **10,** 405–408 (2009).
   This work provides a succinct and convincing argument for reproducibility—*Biostatistics* is at the forefront of ensuring that code and data are provided for other researchers.
7. Devil in the details. *Nature* **470,** 305–306 (2011).
8. Pedersen, T. Empiricism is not a matter of faith. *Comput. Linguist.* **34,** 465–470 (2008).
9. Donoho, D. L. An invitation to reproducible computational research. *Biostatistics* **11,** 385–388 (2010).
10. Raymond, E. S. *The Cathedral and the Bazaar* (O'Reilly, 2001).
11. He, Y. & Ding, C. H. Q. Using accurate arithmetics to improve numerical reproducibility and stability in parallel applications. *J. Supercomput.* **18,** 259–277 (2001).
12. Hatton, L. *et al.* The seismic kernel system—a large scale exercise in Fortran 77 portability. *Softw. Pract. Exper.* **18,** 301–329 (1988).
13. Hatton, L. The T experiments: errors in scientific software. *IEEE Comput. Sci. Eng.* **4,** 27–38 (1997).
14. Hey, T., Tansley, S. & Tolle, K. (eds) *The Fourth Paradigm: Data-Intensive Scientific Discovery* (Microsoft Press, 2009).
15. Gervasi, V. & Zowghi, D. On the role of ambiguity in RE. In *Requirements Engineering: Foundation for Software Quality* (eds Wieringa, R. & Persson, A) 248–254 (Springer, 2010).
16. van Deemter, K. *Not Exactly: In Praise of Vagueness* (Oxford University Press, 2010).
17. Yang, H., Willis, A., De Roeck, A. & Nuseibeh, B. Automatic detection of nocuous coordination ambiguities in natural language requirements. In *Proc. IEEE/ACM Intl Conf. on Automated Software Engineering* 53–62 (ACM, 2010).
18. de Bruijn, F. & Dekkers, H. L. Ambiguity in natural language software requirements: a case study. In *Requirements Engineering: Foundation for Software Quality* (eds Wieringa, R & Persson, A.) 233–247 (Springer, 2010).
19. Pfleeger, S. L. & Hatton, L. Investigating the influence of formal methods. *IEEE Computer* **30,** 33–43 (1997).
20. van der Meulen, M. J. P. & Revilla, M. A. The effectiveness of software diversity in a large population of programs. *IEEE Trans. Softw. Eng.* **34,** 753–764 (2008).
21. Boehm, B., Rombach, H. D. & Zelkowitz, M. V. (eds) *Foundations of Empirical Software Engineering: the Legacy of Victor R. Basili* (Springer, 2005).
22. Monniaux, D. The pitfalls of verifying floating-point computations. *ACM Trans. Programming Languages Systems* **30** (3), 1–41 (2008).
23. Thomas, S. J., Hacker, J. P., Desagne, M. & Stull, R. B. An ensemble analysis of forecast errors related to floating point performance. *Weather Forecast.* **17,** 898–906 (2002).
24. Revol, N. Standardized interval arithmetic and interval arithmetic used in libraries. *Proc. 3rd Intl Congr. Mathematical Software* 337–341 (2010).
25. Rump, S. M., Ogita, T. & Oishi, S. Accurate floating point summation. Part 1: Faithful rounding. *SIAM J. Sci. Comput.* **31,** 189–224 (2009).
26. Rump, S. M. Accurate and reliable computing in floating-point arithmetic. *Proc. 3rd Intl Congr. Mathematical Software* 105–108 (2010).
27. Badin, M., Bic, L., Dillencourt, M., & Nicolau, A. Improving accuracy for matrix multiplications on GPUs. *Sci. Prog.* **19,** 3–11 (2011).
28. Pan, V. Y., Murphy, B., Qian, G. & Rosholt, R. E. A new error-free floating-point summation algorithm. *Comput. Math. Appl.* **57,** 560–564 (2009).
29. Boldo, S. & Muller, J.-M. Exact and approximated error of the FMA. *IEEE Trans. Comput.* **60,** 157–164 (2011).
30. Kahan, W. Desperately needed remedies for the undebuggability of large floating-point computations in science and engineering. *IFIP/SIAM/NIST Working Conf. Uncertainty Quantification in Scientific Computing* (Springer, in the press).
31. Mesirov, J. P. Accessible reproducible research. *Science* **327,** 415–416 (2010).
32. Donoho, D. L., Maleki, A., Rahman, I. U., Shahram, M. & Stodden, V. Reproducible research in computational harmonic analysis. *Comput. Sci. Eng.* **11,** 8–18 (2009).
    Donoho and fellow researchers have been at the forefront of reproducibility for many years; this article reviews their work, including facilities for code presentation.
33. Yool, A., Popova, E. E. & Anderson, T. R. Medusa-1.0: a new intermediate complexity plankton ecosystem model for the global domain. *Geosci. Model Develop.* **4,** 381–417 (2011).
    An example of an article from a journal that asks for code release for model description papers and encourages code release for other categories of paper.
34. Easterbrook, S. M. & Johns, T. C. Engineering the software for understanding climate change. *Comput. Sci. Eng.* **11,** 65–74 (2009).
35. Brohan, P., Kennedy, J. J., Harris, I., Tett, S. F. B. & Jones, P. D. Uncertainty estimates in regional and global observed temperature changes: a new dataset from 1850. *J. Geophys. Res.* **111,** D12106 (2006).
36. Adams, E. N. Optimizing preventive service of software products. *IBM J. Res. Develop.* **28,** 2–14 (1984).
37. Hatton, L. & Roberts, A. How accurate is scientific software? *IEEE Trans. Softw. Eng.* **20,** 785–797 (1994).

Acknowledgements We thank D. Hales of the Department of Design at the Open University and P. Piwak of the Department of Computing for pointing out some reproducibility work outside computing. J.G.-C. is grateful to I. Goz for pointing out the calculation errors in the CRUTEM data from the Meteorological Office.

Author Contributions D.C.I., L.H. and J.G.-C. contributed to all aspects of this article.

Author Information Reprints and permissions information is available at www.nature.com/reprints. The authors declare no competing financial interests. Readers are welcome to comment on the online version of this article at www.nature.com/nature. Correspondence and requests for materials should be addressed to D.C.I. (d.c.ince@open.ac.uk).

ARTICLE

doi:10.1038/nature10770

Experimental demonstration of topological error correction

Xing-Can Yao[1], Tian-Xiong Wang[1], Hao-Ze Chen[1], Wei-Bo Gao[1], Austin G. Fowler[2], Robert Raussendorf[3], Zeng-Bing Chen[1], Nai-Le Liu[1], Chao-Yang Lu[1], You-Jin Deng[1], Yu-Ao Chen[1] & Jian-Wei Pan[1]

Scalable quantum computing can be achieved only if quantum bits are manipulated in a fault-tolerant fashion. Topological error correction—a method that combines topological quantum computation with quantum error correction—has the highest known tolerable error rate for a local architecture. The technique makes use of cluster states with topological properties and requires only nearest-neighbour interactions. Here we report the experimental demonstration of topological error correction with an eight-photon cluster state. We show that a correlation can be protected against a single error on any quantum bit. Also, when all quantum bits are simultaneously subjected to errors with equal probability, the effective error rate can be significantly reduced. Our work demonstrates the viability of topological error correction for fault-tolerant quantum information processing.

Quantum computers exploit the laws of quantum mechanics and can solve many problems exponentially more efficiently than their classical counterparts[1–3]. However, in the laboratory the ubiquitous decoherence of quantum states makes it notoriously hard to achieve the required high degree of quantum control. To overcome this problem, quantum error correction has been invented[4–6]. The principal result in quantum error correction, the threshold theorem[7,8], states that as long as the error rate, p, per gate in a quantum computer is smaller than a threshold value, p_c, arbitrarily long and accurate quantum computation is efficiently possible. However, most methods of fault-tolerant quantum computing with a high threshold error rate (10^{-4}–10^{-2}) require strong and long-range interactions[7–9], and are thus difficult to implement. Local architectures are normally associated with much lower thresholds. For traditional concatenated codes on a two-dimensional lattice of quantum bits (qubits) with nearest-neighbour gates, the highest threshold known at present[10] is 2.02×10^{-5}.

In such lattices, it is advantageous to use topological error correction[11–15] (TEC) in the framework of topological cluster-state quantum computing. This scheme makes use of the topological properties in three-dimensional (3D) cluster states, which form an inherently error-robust 'fabric' for computation. Local measurements drive the computation and, at the same time, implement the error correction. Active error correction and topological methods are combined, yielding a high error threshold[12,13] of 0.7–1.1% and tolerating loss rates[15] up to 24.9%. This allows for the unavoidable imperfections of physical devices, and makes our implementation of TEC close to the experimental state of the art. For practical quantum computation with TEC, a larger cluster state of more qubits would be needed. The 3D architecture can be further mapped onto a local setting in two spatial dimensions plus time[14], also with nearest-neighbour interactions only. Two detailed architectures have already been proposed[16,17]. We note that a different topological scheme has been proposed in which quantum computation is driven by non-Abelian anyons[18,19] and fault tolerance is achieved through passive stabilization afforded by a ground-state energy gap.

Some simple quantum error correction codes have been experimentally demonstrated in nuclear magnetic resonance[20,21], ion traps[22,23] and optical systems[24,25]. However, the experimental realization of topological quantum error correction methods remains challenging. At present, multipartite cluster states can be generated with up to six photons and work is under way to create non-Abelian anyons for topological quantum computing[18,19]. Here we develop an ultrabright entangled-photon source by using an interferometric Bell-type synthesizer. With this and a noise-reduction interferometer, we generate a polarization-encoded eight-photon cluster state, which is shown to possess the required topological properties for TEC. In accordance with the TEC scheme, we measure each photon (qubit) locally. Error syndromes are constructed from the measurement outcomes, and one topological quantum correlation is protected. We demonstrate that if only one physical qubit suffers an error, the faulty qubit can be located and corrected, and that if all qubits are simultaneously subjected to errors with equal probability, the effective error rate is significantly reduced by error correction. This constitutes a proof-of-principle experiment that demonstrates the viability of TEC, a central ingredient in topological cluster-state computing.

Cluster states and quantum computing

In cluster-state quantum computing[26], projective one-qubit measurements replace unitary evolution as the elementary process driving a quantum computation. The computation begins with a highly entangled multi-qubit state, the 'cluster state' $|G\rangle$ (ref. 27), which is specified by an interaction graph, G, and can be created from a product state through the pairwise Ising interaction over the edges in G. For each vertex $i \in G$, we define a stabilizer as $K_i \equiv X_i \otimes_{e_{ij}} Z_j$ where the product is over all the interaction edges, e_{ij}, connecting vertex i to its nearest-neighbouring vertices, j. The symbols X_i and Z_j denote the bit- and phase-flip Pauli operators, respectively, acting on qubits i and j. State $|G\rangle$ is the unique joint eigenstate of a complete set of stabilizers K_i such that $K_i|G\rangle = |G\rangle$ for all $i \in G$.

Cluster states in $d \geq 3$ dimensions are resources for universal fault-tolerant quantum computing[12], in which the TEC capability—shared with Kitaev's toric code[11,28] and the colour code[29]—is combined with the capability to process quantum information.

[1]Shanghai Branch, National Laboratory for Physical Sciences at Microscale and Department of Modern Physics, University of Science and Technology of China, Shanghai 201315, China. [2]CQC2T, School of Physics, University of Melbourne, Victoria 3010, Australia. [3]Department of Physics and Astronomy, University of British Columbia, Vancouver, British Columbia V6T 1Z1, Canada.

Topological error correction

Quantum error correction and fault-tolerant quantum computing are possible with cluster states whenever the underlying interaction graph can be embedded in a 3D cell structure known as a cell complex[30], which consists of volumes, faces, edges and vertices. Qubits are encoded on the edges and faces of a cell complex. The associated interaction graph connects the qubit on each face to the qubits on its surrounding edges through the interaction edges. Consider the elementary cell complex in Fig. 1a, shown by the dashed lines: it has one cubic volume, six square faces, twelve edges and eight vertices. The interaction edges, represented by the solid lines, form an 18-qubit cluster state, $|G_{18}\rangle$. There are six face stabilizers, K_f ($f = 1, 2, \ldots, 6$). It follows that multiplication of these stabilizers cancels out all Z operators in K_f and thus yields a unit expectation value: $\langle X_1 X_2 \cdots X_6 \rangle = 1$. This leads to the straightforward but important observation that despite the X measurement on each individual face qubit having the random outcome ± 1, the product of all the outcomes on any closed surface, F, is $+1$. That is, any closed surface has the topological quantum correlation $C_F \equiv \langle \otimes_{f \in F} X_f \rangle = 1$, where f is a face of F.

A larger cell complex is displayed in Fig. 1b, which encodes and propagates a logical qubit. It consists of $5 \times 5 \times T$ cells, where T specifies a span of simulated time (t). A 'defect' along the t direction (Fig. 1b, line of green dots) is first produced by performing local Z measurements. Then the topological quantum correlation, $C_{F_D} = 1$, on a defect-enclosing closed surface (F_D), combined with the boundary, is used to encode a logical qubit. The evolution of the logical state from t_1 to t_2 is achieved by local X measurements on all other physical qubits between t_1 and t_2 (see ref. 31 for details). Quantum computing requires a much larger cell complex and more defects, where quantum algorithms are realized by appropriate braiding-like manipulation of defects (a sketch of the logical controlled-NOT gate is shown in Supplementary Information).

The quantum computation is possible because the topological quantum correlation $C_{F_D} = 1$ holds on defect-enclosing closed surfaces. The TEC capability arises from the $\mathbf{Z}_2$ homology, a topological feature, of a sufficiently large 3D cell complex (Supplementary Information). For a given F_D, there exist many homologically equivalent closed surfaces with the same topological correlation ($C_{F_D} = 1$). This redundancy leads to the topological protection of the correlation[12].

Remarkably, in TEC it is sufficient to deal with Z errors, because an X error either has no effect, if it occurs immediately before an X measurement, or is equivalent to multiple Z errors. Finally, as TEC is implemented in topological cluster-state quantum computing—a measurement-based process—corrections suggested by TEC are not applied to the remaining cluster state but rather to the classical outcomes of X measurements.

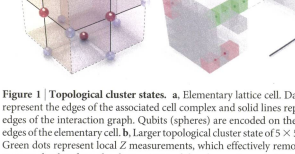

Figure 1 | Topological cluster states. a, Elementary lattice cell. Dashed lines represent the edges of the associated cell complex and solid lines represent the edges of the interaction graph. Qubits (spheres) are encoded on the faces and edges of the elementary cell. **b**, Larger topological cluster state of $5 \times 5 \times T$ cells. Green dots represent local Z measurements, which effectively remove the measured qubits from the cluster state and thereby create a non-trivial topology capable of supporting a single correlation. Red dots represent Z errors. Red cells indicate the ends of error chains where $C_F = -1$. One axis of the cluster can be regarded as simulating the 'circuit time', t. The evolution of logical states from t_1 to t_2 is achieved by performing local X measurements on all physical qubits between t_1 and t_2.

Simpler topological cluster state

The cell complex in Fig. 1b encodes a propagating logical qubit in terms of one topological correlation, $C_{F_D} = 1$, and is robust against a local Z error. However, it contains 25 elementary cells and 180 physical qubits for each layer of complex over a unit time span, which is beyond the capacity of available experimental techniques. We design a simpler graph state, $|G_8\rangle$ (Fig. 2a), to mimic the cell complex of Fig. 1b.

The topological feature of $|G_8\rangle$ can be seen from its association with the 3D cell complex in Fig. 2b, which consists of four elementary volumes, $\{v, w, y, z\}$; six faces, $\{f_1, f_2, f_3, f_4, f_5, f_6\}$; two edges, $\{e_7, e_8\}$; and two vertices, $\{s, t\}$. All six faces have the same boundary, $e_7 \cup e_8$, and any two of them form a closed surface, F. The centre volume is removed to resemble the defect in Fig. 1b, and the topological correlation to be protected, C_{F_D}, reads

$$C_{F_D} \equiv \langle X_5 X_6 \rangle = 1 \tag{1}$$

In this simple cell complex, the topological correlation $C_{F_D} = 1$ is already multiply encoded: it is represented by any expectation $\langle X_i X_j \rangle$ with $i \in \{1, 2, 5\}$ and $j \in \{3, 4, 6\}$. Moreover, there exist four other closed surfaces, corresponding to the respective boundaries of the volumes $\{v, w, y, z\}$, that do not enclose the defect. The 'redundant' topological correlations are

$$\langle X_1 X_2 \rangle = \langle X_2 X_5 \rangle = \langle X_3 X_6 \rangle = \langle X_3 X_4 \rangle = 1 \tag{2}$$

These can be used as error syndromes in TEC, which makes one or more of them equal to -1. As shown in Table 1, a single Z error on any physical qubit can be located and corrected.

Therefore, from the aspect of TEC capability, the cluster state $|G_8\rangle$ is analogous to the cell complex in Fig. 1b. Each protects one topological correlation and is robust against a single Z error, despite the cell complex in Fig. 2b being too small to propagate a logical qubit (see Supplementary Information for details).

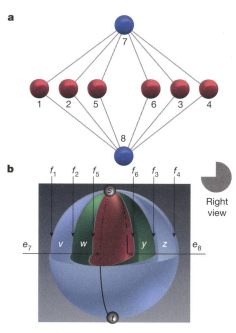

Figure 2 | Cluster state $|G_8\rangle$ and its cell complex. a, G_8, the interaction graph of $|G_8\rangle$. **b**, The corresponding 3D cell complex, with volumes $\{v, w, y, z\}$, faces $\{f_1, f_2, f_3, f_4, f_5, f_6\}$, edges $\{e_7, e_8\}$ and vertices $\{s, t\}$. The exterior and the centre volume are not in the complex. For better illustration, the cell complex is cut open and the foreground quarter is removed (silhouette view from right is shown for clarity).

Table 1 | G_8⟩ and the syndromes $\langle X_iX_j\rangle$

Qubit with Z error	$\langle X_1X_2\rangle$	$\langle X_2X_3\rangle$	$\langle X_3X_4\rangle$	$\langle X_5X_6\rangle$
1	−1	1	1	1
2	−1	−1	1	1
3	1	1	−1	−1
4	1	1	1	−1
5	1	−1	1	1
6	1	1	−1	1

Preparation of the eight-photon cluster state

In our experiment, we create the desired eight-photon cluster state using spontaneous parametric down-conversion and linear optics. The first step is to develop an ultrabright, high-fidelity entangled-photon source. As shown in Fig. 3a, an ultraviolet mode-locked laser pulse (power, 915 mW) passes through a β-barium borate crystal, generating a pair of polarization-entangled photons in the state $|\phi\rangle = (|HH\rangle + |VV\rangle)/\sqrt{2}$. Using an interferometric Bell-state synthesizer[33], we guide photons of different bandwidths (Fig. 3a, red and blue dots, respectively) along separate paths. This disentangles the temporal information from the polarization information. By contrast with the conventional narrowband filtering technique, this process does not result in photon loss and we thus achieve ultrahigh brightness. Four pairs of such entangled photons are prepared and labelled as 1–2, 3–4, 5–6 and 7–8 (Fig. 3b). Then we generate two graph states, each of four photons. The first is a Greenberger–Horne–Zeilinger state, $(|H^{\otimes 4}\rangle_{1-4} + |V^{\otimes 4}\rangle_{1-4})/\sqrt{2}$, obtained by superposing photons 2 and 4 on a polarizing beam splitter (PBS_1), which transmits horizontal polarization (H) and reflects vertical polarization (V). At the same time, photons 6 and 8 are interfered on a polarization-dependent beam splitter (PDBS) and then separately pass through two other PDBSs. The first PDBS has transmitting probabilities $T_H = 1$ and $T_V = 1/3$, and the second and third have $T_H = 1/3$ and $T_V = 1$. The combination of these three PDBSs acts as a controlled-phase gate[33,34]. With a success probability of one-ninth, there is twofold coincidence in paths 6′ and 8′, yielding a four-photon cluster state[34] $(|HH\rangle_{56}(|HH\rangle_{78} + |VV\rangle_{78}) + |VV\rangle_{56}(|HH\rangle_{78} - |VV\rangle_{78}))/2$. Finally, photons 4′ and 6′ are superposed on PBS_2. When eight photons come out of the output ports simultaneously, we obtain an entangled eight-photon cluster state:

$$|\psi\rangle = \frac{1}{2}\left[|H^{\otimes 6}\rangle_{1-6}(|HH\rangle_{78} + |VV\rangle_{78}) + |V^{\otimes 6}\rangle_{1-6}(|HH\rangle_{78} - |VV\rangle_{78})\right] \quad (3)$$

This is exactly the cluster state $|G_8\rangle$ shown in Fig. 2a under Hadamard operations $H^{\otimes 8}$ on all qubits. We note that the photons, which are interfered on the PBSs or the PDBS, have the same bandwidth, and that a star topology of the eight-photon interferometer[32] leads to an effective noise reduction.

To ensure good spatial and temporal overlap, the photons are also spectrally filtered, with full-widths at half-maximum of $\Delta\lambda_{FWHM} = 8$ nm for photons 1, 3, 5 and 7 and $\Delta\lambda_{FWHM} = 2.8$ nm for photons 2, 4, 6 and 8, and are coupled by single-mode fibres. We obtain an average twofold coincidence count of $\sim 3.4 \times 10^5\ s^{-1}$ and a visibility of ~94% in the $\{|H\rangle, |V\rangle\}$ basis as well as in the $\{|+\rangle, |-\rangle\}$ basis, where $|\pm\rangle = (|H\rangle \pm |V\rangle)/\sqrt{2}$. Fine adjustments of the delays between the different paths are tuned to ensure that all the interfering photons arrive at the PBSs and the PDBS simultaneously.

Measurement of each photon is made using a polarization analyser, which contains a combination of a QWP, a HWP and a PBS together

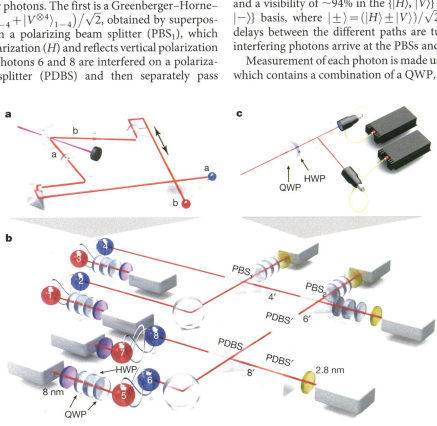

Figure 3 | Experimental set-up for the generation of the eight-photon cluster state and the demonstration of topological error correction. **a**, Creation of ultrabright entangled-photon pairs. An ultraviolet laser pulse passes through a 2-mm, nonlinear β-barium borate crystal, creating an entangled photon pair {a, b} with density matrix $\rho = (|H_a^o\rangle|V_b^e\rangle\langle V_a^e|\langle H_b^o| + |V_a^e\rangle|H_b^o\rangle\langle H_b^o|\langle V_a^e|)/2$ by parametric down-conversion, where o and e indicate ordinary and extraordinary polarizations, respectively perpendicular and parallel relative to the V-polarized pump. After both photons pass through compensators, which include a 45° half-wave plate (HWP) and a 1-mm β-barium borate crystal, one of the photons' polarizations is rotated by another 45° HWP. Then we re-overlap the two photons on a PBS, creating an entangled photon pair in a state $|\phi_{ab}\rangle = (|H\rangle|H\rangle + e^{i\varphi}|V\rangle|V\rangle)\otimes|e_A\rangle|o_b\rangle/\sqrt{2}$, where $|e_A\rangle$ is a state in which all photons in path a have extraordinary polarization and $|o_b\rangle$ is a state in which all photons in path b have ordinary polarization. **b**, To create the desired cluster state, we combine photons from paths 6 and 8 at the first PDBS and let each photon pass through another PDBS (PDBS′), resulting a controlled-phase operation between the two photons. At the same time, photons 2 and 4 are interfered on PBS_1. Then photons 4′ and 6′ are overlapped on PBS_2. On coincidence detection, we create the eight-photon cluster state (equation (3)) for topological error correction. **c**, Polarization analyser for each individual photon, containing a quarter-wave plate (QWP), a HWP, a PBS and two single-mode, fibre-coupled single-photon detectors.

with a single-mode, fibre-coupled single-photon detectors in each output of the PBS (Fig. 3c). The complete set of all 256 possible combinations of eight-photon coincidence events is registered by a home-made programmable coincidence logic unit based on a field-programmable gate array. We obtain an eightfold coincidence rate of 3.2 per hour. On the basis of the measurements for the 256 possible polarization combinations in the $\{|H\rangle, |V\rangle\}$ basis (Fig. 4a), we obtain a signal-to-noise ratio, defined as the ratio of the average number of desired components to that of non-desired components, of about 200:1. This indicates that we have been successful in preparing the desired eight-photon cluster state.

To characterize the cluster state more precisely, we use the entanglement witness method to determine its fidelity. For this purpose, we construct a witness that allows for the lower bound on the state fidelity and requires only eight measurement settings (Supplementary Information):

$$\mathcal{W}_8 = \frac{1}{2} - (|\psi\rangle\langle\psi| - |\psi'\rangle\langle\psi'|)$$

$$= \frac{1}{2} - \left[\frac{1}{4}\left(|H\rangle\langle H|^{\otimes 6} - |V\rangle\langle V|^{\otimes 6}\right)_{1-6} \otimes \langle X_7X_8 - Y_7Y_8\rangle + \frac{1}{12}\left(\sum_{k=0}^{5}(-1)^k M_k^{\otimes 6}\right)_{1-6} \otimes \left(|H\rangle\langle H|^{\otimes 2} - |V\rangle\langle V|^{\otimes 2}\right)_{78}\right]$$

Here $\langle\psi'|\psi\rangle = 0$ and $M_k = \cos(k\pi/6)X + \sin(k\pi/6)Y$. The measured expectation value of each measurement setting in $\mathcal{W}_8$ is shown in Fig. 4b. These yield the witness $\langle\mathcal{W}_8\rangle = -0.105 \pm 0.023$, which is negative by 4.5 s.d. The state fidelity is $F > 0.5 - \langle\mathcal{W}_8\rangle = 0.605 \pm 0.023$. This confirmed the presence of genuine eight-photon entanglement.

Experimental topological error correction

Given such a cluster state, topological error correction is implemented using a series of single-qubit measurements and classical correction operations. In the laboratory, operations are performed on state $|\psi\rangle$ (equation (3)), which differs from $|G_8\rangle$ in Fig. 2a by the Hadamard operation $H^{\otimes 8}$. Therefore, the correlation to be protected in equation (1), $\langle X_5X_6\rangle$, corresponds to $\langle Z_5Z_6\rangle$ in the experiment; similarly, each $\langle X_iX_j\rangle$ in equation (2) corresponds to $\langle Z_iZ_j\rangle$. Furthermore, X errors are simulated instead of Z errors.

In the experiment, the noisy quantum channels on polarization qubits are simulated by one HWP positioned between two QWPs, which are set at 90° relative to the horizontal. By randomly setting the HWP axis to be oriented at $\pm\theta$ with respect to the horizontal direction, the noisy quantum channel can be simulated with a bit-flip error probability of $p = \sin^2(2\theta)$.

We first study the case in which only a single X error occurs on one of the six photons $\{1, \ldots, 6\}$. The syndrome correlations are measured (Fig. 5). For comparison, in Fig. 4c we plot the correlations without any simulated error. This comparison, together with Table 1, makes it possible to locate precisely the physical qubit undergoing an X error.

We then consider the case in which all six photons are simultaneously subject to a random X error with equal probability $0 < p < 1$ and study the rate of errors, $\langle Z_5Z_6\rangle = -1$, for the topological quantum correlation $\langle Z_5Z_6\rangle$. Without error correction, the error rate of correlation $\langle Z_5Z_6\rangle$ is $P = 1 - (1-p)^2 - p^2$. With error correction, the residual error becomes

$$P = 1 - \left[(1-p)^6 + p^6\right] - \left[6p(1-p)^5 + 6(1-p)p^5\right] - \left[9p^2(1-p)^4 + 9(1-p)^2p^4\right]$$

For small p, the residual error rate after error correction is significantly reduced relative to the unprotected case. As shown in Fig. 6, the experimental results are in good agreement with these theoretical predictions. Considerable improvement of the robustness of the correlation $\langle Z_5Z_6\rangle$ can be seen both in theory and in practice.

In the experiment, the whole measurement takes about 80 days. This requires our set-up to be extremely stable. The imperfections in the experiment are mainly due to the undesired components in the $\{|H\rangle, |V\rangle\}$ basis, which arise from higher-order emissions of entangled photons, and the imperfect photon overlapping at the PBSs and the PDBS. In spite of these issues, the viability of TEC is successfully demonstrated in the experiment.

Discussion

In this work, we have experimentally demonstrated TEC with an eight-photon cluster state. This state represents the current state of the art for preparation of cluster states in qubit systems and is of particular interest in studying multipartite entanglement and quantum information processing. The scalable construction of cluster

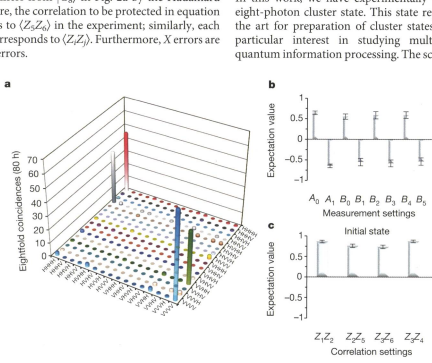

Figure 4 | Experimental results for the created eight-photon cluster state. **a**, Measured eightfold coincidence in the $\{|H\rangle, |V\rangle$ basis. **b**, The expectation values for different witness measurement settings. The measurement settings are $A_0 = (|H\rangle\langle H|^{\otimes 6} - |V\rangle\langle V|^{\otimes 6})_{1-6}X_7X_8$, $A_1 = (|H\rangle\langle H|^{\otimes 6} - |V\rangle\langle V|^{\otimes 6})_{1-6}Y_7Y_8$ and $B_i = M_i^{\otimes 6}(|H\rangle\langle H|^{\otimes 2} - |V\rangle\langle V|^{\otimes 2})_{78}$ with $i = 0, \ldots, 5$. The measurement of each setting takes 50 h for the first two settings and 30 h for the remaining settings. **c**, Correlations for the initial state without any simulated error. Error bars, 1 s.d., deduced from propagated Poissonian counting statistics of the raw detection events.

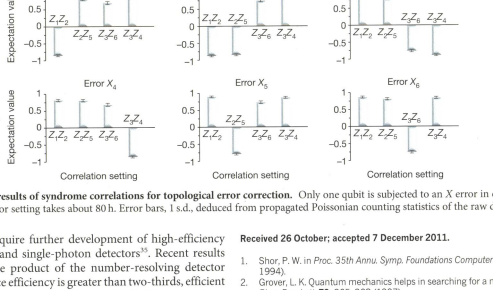

Figure 5 | Experimental results of syndrome correlations for topological error correction. Only one qubit is subjected to an X error in each plot. The measurement for each error setting takes about 80 h. Error bars, 1 s.d., deduced from propagated Poissonian counting statistics of the raw detection events.

states in future will require further development of high-efficiency entanglement sources and single-photon detectors[35]. Recent results have shown that if the product of the number-resolving detector efficiency and the source efficiency is greater than two-thirds, efficient linear optical quantum computation is possible[36]. There has been technical progress towards this goal, such as deterministic, storable, single-photon sources[37] and photon-number-resolving detectors[38]. Our demonstration of TEC is a further step towards fault-tolerant quantum computation. In the scheme, given sufficient qubits and physical error rates below 0.7–1.1%, arbitrary quantum computations can be performed arbitrarily reliably. The high threshold error rate is especially remarkable given that only nearest-neighbour interactions are required. Owing to these advantages, TEC is especially well suited for physical systems geometrically constrained to nearest-neighbour interactions, such as quantum dots[39], Josephson junction qubits[40], ion traps[41], cold atoms in optical lattices[42] and photonic modules[17]. A quantum gate with an error rate below the threshold required in TEC is within reach of present technology[43]. It would be interesting in future work to exploit cluster states of the maximum achievable size, to implement topologically error-protected quantum algorithms using local measurements.

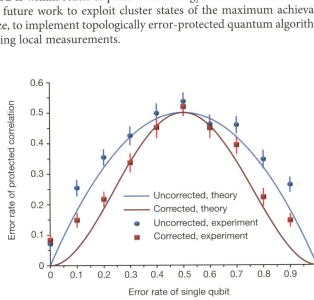

Figure 6 | Experimental results of topological error correction. All physical qubits are simultaneously subject to an X error with equal probability ranging from 0 to 1. The blue circles and blue lines represent the experimental and, respectively, theoretical values of the error rate for the protected correlation without TEC, and the red squares and red lines similarly represent the error rate with TEC. The agreement between the experimental and the theoretical results demonstrates the viability of TEC. The measurement of each data point takes 80 h. Error bars, 1 s.d., deduced from propagated Poissonian counting statistics of the raw detection events.

Received 26 October; accepted 7 December 2011.

1. Shor, P. W. in *Proc. 35th Annu. Symp. Foundations Computer Sci.* 124–134 (IEEE, 1994).
2. Grover, L. K. Quantum mechanics helps in searching for a needle in a haystack. *Phys. Rev. Lett.* **79,** 325–328 (1997).
3. Feynman, R. P. Simulating physics with computers. *Int. J. Theor. Phys.* **21,** 467–488 (1982).
4. Calderbank, A. R. & Shor, P. W. Good quantum error-correcting codes exist. *Phys. Rev. A* **54,** 1098–1105 (1996).
5. Steane, A. M. Error correcting codes in quantum theory. *Phys. Rev. Lett.* **77,** 793–797 (1996).
6. Gottesman, D. Theory of fault-tolerant quantum computation. *Phys. Rev. A* **57,** 127–137 (1998).
7. Knill, E. Quantum computing with realistically noisy devices. *Nature* **434,** 39–44 (2005).
8. Aliferis, P., Gottesman, D. & Preskill, J. Quantum accuracy threshold for concatenated distance-3 code. *Quantum Inf. Comput.* **6,** 97–165 (2006).
9. Kitaev, A. Y. Quantum computations: algorithms and error correction. *Russ. Math. Surv.* **52,** 1191–1249 (1997).
10. Spedalieri, F. & Roychowdhury, V. P. Latency in local, two-dimensional, fault-tolerant quantum computing. *Quantum Inf. Comput.* **9,** 666–682 (2009).
11. Dennis, E., Landahl, A., Kitaev, A. & Preskill, J. Topological quantum memory. *J. Math. Phys.* **43,** 4452–4505 (2002).
12. Raussendorf, R., Harrington, J. & Goyal, K. A fault-tolerant one-way quantum computer. *Ann. Phys.* **321,** 2242–2270 (2006).
13. Wang, D. S., Austin, A. G. & Hollenberg, L. C. L. Quantum computing with nearest neighbor interactions and error rates over 1%. *Phys. Rev. A* **83,** 020302(R) (2011).
14. Raussendorf, R. & Harrington, J. Fault-tolerant quantum computation with high threshold in two dimensions. *Phys. Rev. Lett.* **98,** 190504 (2007).
15. Barrett, S. D. & Stace, T. M. Fault tolerant quantum computation with very high threshold for loss errors. *Phys. Rev. Lett.* **105,** 200502 (2010).
16. Stock, R. & James, D. F. V. A scalable, high-speed measurement-based quantum computer using trapped ions. *Phys. Rev. Lett.* **102,** 170501 (2009).
17. Devitt, S. J. *et al.* Topological cluster state computation with photons. *N. J. Phys.* **11,** 083032 (2009).
18. Nayak, C., Simon, S. H., Stern, A., Freedman, M. & Sarma, S. D. Non-abelian anyons and topological quantum computation. *Rev. Mod. Phys.* **80,** 1083–1159 (2008).
19. Wilczek, F. *Fractional Statistics and Anyon Superconductivity* (World Scientific, 1990).
20. Cory, D. G. *et al.* Experimental quantum error correction. *Phys. Rev. Lett.* **81,** 2152–2155 (1998).
21. Knill, E., Laflamme, R., Martinez, R. & Negrevergne, C. Benchmarking quantum computers: the five-qubit error correcting code. *Phys. Rev. Lett.* **86,** 5811–5814 (2001).
22. Chiaverini, J. *et al.* Realization of quantum error correction. *Nature* **432,** 602–605 (2004).
23. Schindler, P. *et al.* Experimental repetitive quantum error correction. *Science* **332,** 1059–1061 (2011).
24. Lu, C.-Y. *et al.* Experimental quantum coding against qubit loss error. *Proc. Natl Acad. Sci. USA* **105,** 11050–11054 (2008).
25. Aoki, T. *et al.* Quantum error correction beyond qubits. *Nature Phys.* **5,** 541–546 (2009).
26. Raussendorf, R. & Briegel, H. J. A one-way quantum computer. *Phys. Rev. Lett.* **86,** 5188–5191 (2001).
27. Schlingemann, D. & Werner, R. F. Quantum error-correcting codes associated with graphs. *Phys. Rev. A* **65,** 012308 (2001).
28. Kitaev, A. Y. Fault-tolerant quantum computation by anyons. *Ann. Phys.* **303,** 2–30 (2003).
29. Bombin, H. & Martin-Delgado, M. A. Topological quantum distillation. *Phys. Rev. Lett.* **97,** 180501 (2006).
30. Hatcher, A. *Algebraic Topology* (Cambridge Univ. Press, 2002).

31. Fowler, A. G. & Goyal, K. Topological cluster state quantum computing. *Quantum Inf. Comput.* **9,** 727–738 (2009).
32. Yao, X.-C. *et al.* Observation of eight-photon entanglement. *Nature Photon.* (in the press); preprint at (http://arxiv.org/abs/1105.6318) (2011).
33. Hofmann, H. F. & Takeuchi, S. Quantum phase gate for photonic qubits using only beam splitters and postselection. *Phys. Rev. A* **66,** 024308 (2002).
34. Kiesel, N. *et al.* Experimental analysis of a four-qubit photon cluster state. *Phys. Rev. Lett.* **95,** 210502 (2005).
35. O'Brien, J. L. Optical quantum computing. *Science* **318,** 1567–1570 (2007).
36. Varnava, M., Browne, D. E. & Rudolph, T. How good must single photon sources and detectors be for efficient linear optical quantum computation? *Phys. Rev. Lett.* **100,** 060502 (2008).
37. Chen, S. *et al.* Deterministic and storable single-photon source based on quantum memory. *Phys. Rev. Lett.* **97,** 173004 (2006).
38. Kardynał, B. E., Yuan, Z. L. & Shields, A. J. An avalanche-photodiode-based photon-number-resolving detector. *Nature Photon.* **2,** 425–428 (2008).
39. Press, D. *et al.* Complete quantum control of a single quantum dot spin using ultrafast optical pulses. *Nature* **456,** 218–221 (2008).
40. Hime, T. *et al.* Solid-state qubits with current-controlled coupling. *Science* **314,** 1427–1429 (2006).
41. Hensinger, W. K. *et al.* T-junction ion trap array for two-dimensional ion shuttling, storage, and manipulation. *Appl. Phys. Lett.* **88,** 034101 (2006).
42. Jaksch, D. *et al.* Entanglement of atoms via cold controlled collisions. *Phys. Rev. Lett.* **82,** 1975–1978 (1999).
43. Benhelm, J., Kirchmair, G., Roos, C. F., & Blatt, R. Towards fault-tolerant quantum computing with trapped ions. *Nature Phys.* **4,** 463–466 (2008).

Supplementary Information is linked to the online version of the paper at www.nature.com/nature.

Acknowledgements We acknowledge discussions with M. A. Martin-Delgado and O. Gühne. We are grateful to X.-H. Bao for his original idea of the ultrabright entanglement and to C.-Z. Peng for his idea of reducing high-order emission. We would also like to thank C. Liu and S. Fölling for their help in designing the figures. This work has been supported by the NNSF of China, the CAS, the National Fundamental Research Program (under grant no. 2011CB921300) and NSERC.

Author Contributions W.-B.G., A.G.F., R.R., Z.-B.C., Y.-J.D. and J.-W.P. had the idea for and initiated the experiment. A.G.F., R.R. and Y.-J.D. contributed to the general theoretical work. X.-C.Y., C.-Y.L., Y.-A.C. and J.-W.P. designed the experiment. X.-C.Y., T.-X.W. and H.-Z.C. carried out the experiment. X.-C.Y. and Y.-A.C. analysed the data. X.-C.Y., A.G.F., R.R., N.-L.L., C.-Y.L., Y.-J.D., Y.-A.C. and J.-W.P. wrote the manuscript. N.-L.L., Y.-A.C. and J.-W.P. supervised the whole project.

Author Information Reprints and permissions information is available at www.nature.com/reprints. The authors declare no competing financial interests. Readers are welcome to comment on the online version of this article at www.nature.com/nature. Correspondence and requests for materials should be addressed to Y.-A.C. (yuaochen@ustc.edu.cn) or J.-W.P. (pan@ustc.edu.cn).

ARTICLE

doi:10.1038/nature10822

Ubiquitin-dependent regulation of COPII coat size and function

Lingyan Jin[1]*, Kanika Bajaj Pahuja[1,2]*, Katherine E. Wickliffe[1], Amita Gorur[1,2], Christine Baumgärtel[1], Randy Schekman[1,2] & Michael Rape[1]

Packaging of proteins from the endoplasmic reticulum into COPII vesicles is essential for secretion. In cells, most COPII vesicles are approximately 60–80 nm in diameter, yet some must increase their size to accommodate 300–400 nm procollagen fibres or chylomicrons. Impaired COPII function results in collagen deposition defects, cranio-lenticulo-sutural dysplasia, or chylomicron retention disease, but mechanisms to enlarge COPII coats have remained elusive. Here, we identified the ubiquitin ligase CUL3–KLHL12 as a regulator of COPII coat formation. CUL3–KLHL12 catalyses the monoubiquitylation of the COPII-component SEC31 and drives the assembly of large COPII coats. As a result, ubiquitylation by CUL3–KLHL12 is essential for collagen export, yet less important for the transport of small cargo. We conclude that monoubiquitylation controls the size and function of a vesicle coat.

The extracellular matrix provides a scaffold for cell attachment and binding sites for membrane receptors, such as integrins, making it essential for the development of all metazoans[1,2]. When engaged with the extracellular matrix, integrins trigger signalling cascades that regulate cell morphology and division, yet in the absence of a functional extracellular matrix, integrins are removed from the plasma membrane by endocytosis[3]. The proper interplay between integrins and the extracellular matrix is particularly important during early development[4], as stem cells depend on integrin-dependent signalling for division and survival[5].

The establishment of the extracellular matrix requires secretion of several proteins, including its major constituent collagen. Following its synthesis in the endoplasmic reticulum, the export of collagen from cells depends on COPII vesicles[6–9], and mutations in genes encoding COPII proteins lead to collagen deposition defects, skeletal aberrations and developmental diseases, such as cranio-lenticulo-sutural dysplasia[10,11].

COPII vesicles are surrounded by a coat consisting of the SAR1 GTPase, SEC23–SEC24 adaptors, and an outer layer of SEC13–SEC31 heterotetramers[12]. These coat proteins self-assemble into cuboctahedral structures with a diameter of approximately 60–80 nm, which are too small to accommodate a procollagen fibre with a length of 300–400 nm[13–15]. Thus, collagen transport in cells must involve factors that are absent from *in vitro* self-assembly reactions. Indeed, TANGO1 (also known as MIA3) and its partner cTAGE5 interact with collagen and SEC23–SEC24, thereby recruiting collagen to nascent COPII coats[16,17]. The deletion of *Tango1* in mice resulted in collagen deposition defects similar to those caused by loss of COPII[18], and mutations in human TANGO1 are associated with premature myocardial infarction[19]. However, TANGO1 is not known to regulate the size of COPII coats and mechanisms that permit the COPII coat to accommodate a large cargo remain poorly understood.

By analysing mouse embryonic stem (ES) cell division, we have identified CUL3–KLHL12 as a regulator of COPII coat formation. CUL3–KLHL12 monoubiquitylates SEC31 and drives assembly of large COPII coats. As a result, ubiquitylation by CUL3–KLHL12 is essential for collagen export, a step that is required for integrin-dependent mouse ES cell division. We conclude that monoubiquitylation determines the size and function of a vesicle coat.

CUL3 regulates mouse ES cell morphology

To provide insight into stem cell-specific division networks, we depleted ubiquitylation enzymes from mouse ES cells and scored for effects on proliferation and morphology. We found that loss of the ubiquitin ligase CUL3 caused mouse ES cells to form tightly packed cell clusters with prominent actin cables and aberrant adhesions, as seen by confocal microscopy analysis of actin and vinculin localization (Fig. 1a). A similar phenotype was observed upon depletion of UBA3, a component of the NEDD8 pathway that activates CUL3 (Supplementary Fig. 1a). CUL3-depleted mouse ES cells were delayed in proliferation (Supplementary Fig. 1b, d), yet retained their pluripotency, as seen by OCT4- and alkaline phosphatase-staining and the absence of differentiation markers in expression analyses (Supplementary Figs 1c, e, f and 2b). In contrast to mouse ES cells, depletion of CUL3 had weaker consequences in fibroblasts (Fig. 1a), although a previously reported increase in multinucleation was observed (Supplementary Fig. 1g; ref. 20).

Several observations show that the mouse ES cell phenotypes were caused by specific depletion of CUL3. First, several short interfering RNAs targeting distinct regions of the *Cul3* messenger RNA had the same effects on mouse ES cells, with a close correlation between knockdown efficiency and strength of phenotype (Supplementary Fig. 2a). Second, microarray analysis showed a strong reduction in *Cul3* mRNA upon siRNA treatment, whereas no other gene was significantly and reproducibly affected (Supplementary Fig. 2b). Third, siRNAs that target closely related proteins, such as other cullins, did not disturb the morphology of mouse ES cells (Supplementary Fig. 2c).

The aberrant morphology of CUL3-depleted mouse ES cells was reminiscent of increased RhoA GTPase activity, which triggers actin filament bundling[21]. Accordingly, a reduction in RhoA levels or inhibition of the RhoA effector kinase ROCK1 rescued CUL3-depleted mouse ES cells from compaction (Supplementary Fig. 3a). Among several possibilities, higher RhoA activity in the absence of CUL3 could result from RhoA stabilization or defective integrin signalling. Stabilization

[1]Department of Molecular and Cell Biology, University of California at Berkeley, California 94720, USA. [2]Howard Hughes Medical Institute, University of California at Berkeley, California 94720, USA.
*These authors contributed equally to this work.

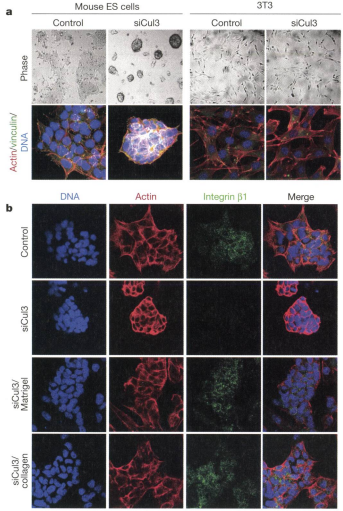

Figure 1 | CUL3 regulates mouse ES cell morphology. a, Left, D3 mouse ES cells were plated on gelatin and transfected with siRNAs targeting *Cul3* (siCul3), which resulted in cell clustering (phase microscopy; upper panel) and compaction (confocal microscopy: vinculin, green; actin, red; DNA, blue). Right, Depletion of CUL3 from mouse 3T3 fibroblasts did not cause cell compaction. Phase images original magnification was ×10, fluorescence images ×40. **b**, CUL3 is required for integrin localization to the mouse ES cell plasma membrane. D3 mouse ES cells were plated on gelatin (top two rows), growth-factor-depleted Matrigel or collagen IV. Following CUL3 depletion, cell compaction and integrin-targeting to the plasma membrane were analysed by confocal microscopy (actin, red; integrin β1, green; DNA, blue). Original magnification ×40.

of RhoA by co-depletion of all RhoA-specific CUL3 adaptors, the BACURDs[22], did not affect mouse ES cell morphology (data not shown). By contrast, depletion of components of integrin signalling pathways phenocopied the loss of CUL3 in mouse ES cells (Supplementary Fig. 3b); partial reduction in CUL3 levels showed synthetic lethality with dasatinib, an inhibitor of the SRC kinase that acts downstream of integrin activation (Supplementary Fig. 3c); and integrin β1 was absent from the plasma membrane of CUL3-depleted mouse ES cells (Fig. 1b).

CUL3 could regulate integrin synthesis and trafficking, or it could allow for efficient deposition of extracellular matrix proteins to prevent integrin internalization[3]. To distinguish between these possibilities, we grew mouse ES cells on growth-factor-depleted Matrigel to provide an exogenous extracellular matrix. Strikingly, under these conditions, integrin β1 was found at the plasma membrane of CUL3-depleted mouse ES cells and no cell clustering was observed (Fig. 1b). Thus, CUL3 controls integrin signalling in mouse ES cells, most likely by supporting the establishment of a functional extracellular matrix.

KLHL12 is a key CUL3 adaptor in mouse ES cells

CUL3 recruits substrates through adaptors with BTB domains[23–26], yet siRNA approaches did not yield roles for BTB proteins in ES cells. As an alternative strategy to isolate CUL3 adaptors, we made use of the observation that stem cell regulators are highly expressed in ES cells, but downregulated upon differentiation[27]. Using affinity purification and mass spectrometry, we identified 31 BTB proteins that interact with CUL3 in mouse ES cells (Supplementary Fig. 4a; Supplementary Table 1). When analysed by quantitative polymerase chain reaction with reverse transcription (qRT–PCR) and immunoblot, we found that three adaptors, KLHL12, KBTBD8 and IBTK, were highly expressed in mouse ES cells, but downregulated upon differentiation (Fig. 2a, b and Supplementary Fig. 3d). Next, we depleted these adaptors from mouse ES cells that were sensitized for changes in integrin signalling by treatment with dasatinib. Importantly, depletion of KLHL12, but no other BTB protein, resulted in mouse ES cell compaction, as seen with loss of CUL3 (Fig. 2c). Accordingly, endogenous KLHL12 effectively binds CUL3 in mouse ES cells (Supplementary Fig. 4b). These experiments, therefore, identify KLHL12 as a key substrate-adaptor for CUL3 in mouse ES cells and the CUL3–KLHL12 ubiquitin ligase as an important regulator of mouse ES cell morphology.

CUL3 monoubiquitylates SEC31

To isolate the substrates of CUL3–KLHL12, we constructed 293T cell lines that allowed for the inducible expression of Flag–KLHL12. By affinity chromatography and mass spectrometry, we identified the

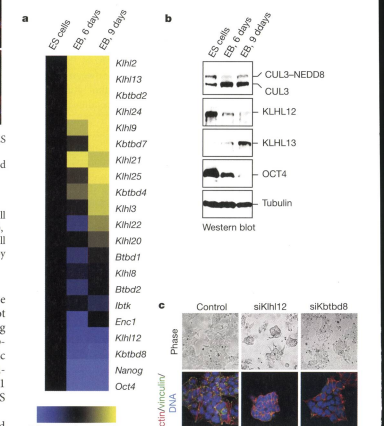

Figure 2 | KLHL12 is a substrate adaptor for CUL3 in mouse ES cells. a, D3 mouse ES cells were subjected to differentiation, and mRNA levels of indicated proteins were measured by qRT–PCR. EB, embryoid bodies. **b**, KLHL12 protein is downregulated upon differentiation, as observed by immunoblot of above samples. **c**, KLHL12 is a critical CUL3-adaptor in mouse ES cells. D3 mouse ES cells were sensitized towards altered integrin-signalling with dasatinib and monitored for compaction by phase (upper panel) or confocal microscopy (actin, red; vinculin, green; DNA, blue). Original magnification ×40.

COPII proteins SEC13 and SEC31 as specific binding partners of KLHL12 (Fig. 3a and Supplementary Table 2). Immunoblotting confirmed retention of endogenous SEC13 and SEC31 in KLHL12 purifications, but not in precipitates of other BTB proteins (Supplementary Fig. 5a). As seen in pull-down assays, KLHL12 directly bound SEC31, but not SEC13 (Supplementary Fig. 5c, d), and this interaction was mediated by the amino terminus of SEC31 (Supplementary Fig. 6a) and the Kelch domain of KLHL12 (Supplementary Fig. 6b). In cells, approximately 30% of endogenous KLHL12 was associated with SEC13–SEC31 (Fig. 3b and Supplementary Fig. 5b). Consistent with such a prominent interaction, SEC13–SEC31 and KLHL12 colocalized in punctae, which are likely to represent endoplasmic reticulum exit sites of COPII vesicles (Fig. 3c; [28]). Importantly, siRNAs that compromise COPII resulted in mouse ES cell compaction (Fig. 3d), indicating that CUL3–KLHL12 and the COPII coat act in the same pathway.

In vitro, CUL3–KLHL12 catalysed the monoubiquitylation of SEC31 (Fig. 3e), which was not observed if a KLHL12 mutant with a defective SEC31-binding interface was used (Fig. 3f). SEC31 was also monoubiquitylated in cells, which was strongly increased upon expression of KLHL12 (Fig. 3g). KLHL12 mutants unable to bind SEC31 abolished its monoubiquitylation (Fig. 3h), which is likely to be due to dimerization with and inactivation of endogenous KLHL12 (Fig. 3a and Supplementary Fig. 6c). SEC31 monoubiquitylation was also strongly diminished upon expression of dominant-negative CUL3 (Fig. 3g) or depletion of CUL3–KLHL12 by siRNA (Fig. 3i). As seen upon expression of lysine-free ubiquitin, SEC31 was monoubiquitylated at one preferred and an alternative, less prominently used lysine (Fig. 3g), consistent with proteomic analyses that identified Lys 647 and Lys 1217 in SEC31A as ubiquitylation sites[29,30]. However, neither mutation of these residues nor any other of the 65 lysine residues of SEC31 blocked ubiquitylation by CUL3–KLHL12 (data not shown), revealing flexibility in the actual modification site.

Co-expression of KLHL12 and CUL3 triggered SEC31 multiubiquitylation and degradation (Figs 3g, 4e and Supplementary Fig. 6d), which was not observed with lysine-free ubiquitin (Fig. 3g). However, whereas SEC31 was monoubiquitylated by endogenous CUL3–KLHL12, its multiubiquitylation was only seen when CUL3 and KLHL12 were overexpressed. Depletion of CUL3–KLHL12 or proteasome inhibition did not change SEC31 levels in untransfected cells (Fig. 3i and Supplementary Fig. 6e), and blockade of ubiquitin chain formation or proteasome inhibition did not impair CUL3–KLHL12 function (see Fig. 5). Thus, multiubiquitylation of SEC31 is unlikely a key outcome of CUL3–KLHL12 activity in mouse ES cells. Instead, it seems that CUL3–KLHL12 acts by catalysing monoubiquitylation, with the COPII protein SEC31 as a major substrate.

CUL3 regulates the size of COPII coats

To identify a role for monoubiquitylation by CUL3–KLHL12, we induced KLHL12 expression in cells and followed the fate of SEC31 by microscopy. Shortly after KLHL12 induction, the majority of KLHL12 and SEC31 colocalized in small punctae (Fig. 4a). Over time, these punctae grew into much larger structures that contained most of SEC31, as well as other COPII components, such as SEC13 or SEC24C (Fig. 4a, b). As seen by high-resolution confocal imaging, the large structures were hollow and spherical with a diameter of 200–500 nm, and they were decorated with the proteins of the COPII coat and with KLHL12 (Fig. 4c). Accordingly, thin-section electron microscopy revealed large, crescent-shaped tubules, possibly of endoplasmic reticulum origin, in cells transfected with KLHL12 (Fig. 4d). Immunogold-labelling electron microscopy showed comparable structures of

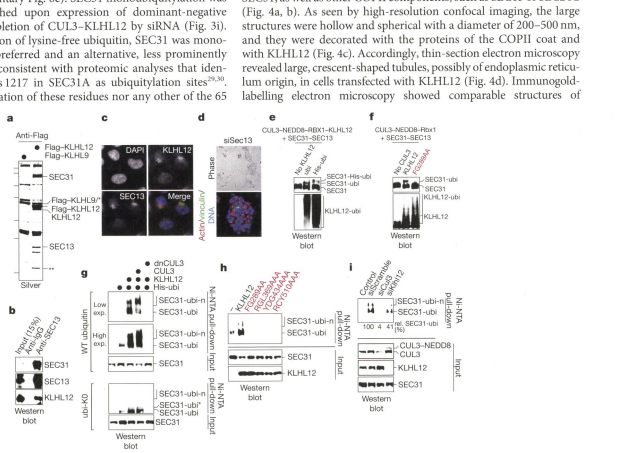

Figure 3 | CUL3–KLHL12 monoubiquitylates SEC31.
a, Immunoprecipitates of Flag–KLHL12 or Flag–Klhl9 were analysed by silver staining and mass spectrometry. Asterisk, non-specific band; double asterisk, breakdown product of KLHL12. **b**, SEC13 was immunoprecipitated from HeLa cell lysates, and SEC31 and KLHL12 were detected by immunoblot. **c**, KLHL12 colocalizes with COPII, as seen by confocal microscopy (KLHL12, green; SEC13, red; DNA, blue). Original magnification ×60. **d**, D3 mouse ES cells grown on gelatin and depleted of SEC13 were analysed for compaction by phase (top) or confocal microscopy (actin, red; vinculin, green; DNA, blue). Original magnification ×40. **e**, CUL3–KLHL12 monoubiquitylates SEC31. CUL3–NEDD8–RBX1 was incubated with KLHL12, SEC13/31 and ubiquitin (ubi) or His-ubiquitin (His-ubi). **f**, *In vitro* ubiquitylation of SEC31 by CUL3–KLHL12 or CUL3–KLHL12(FG289AA) (FG289AA) was performed as above. **g**, SEC31 is monoubiquitylated *in vivo*. Upper panels, ubiquitin conjugates were purified under denaturing conditions from MG132-treated 293T cells expressing His–ubiquitin, haemagglutinin–SEC31, KLHL12, CUL3 or dominant-negative CUL3 (dnCUL3), and analysed by anti-SEC31 Western blot. Lower panels, the same experiment was performed with lysine-free His–ubiquitin, which only allowed SEC31-monoubiquitylation on at least two sites (SEC31-ubi and SEC31-ubi*). SEC31-ubi-n denotes multiubiquitylated SEC31. **h**, Ubiquitin conjugates were purified from 293T cells expressing KLHL12 or SEC31-binding deficient KLHL12 mutants. **i**, CUL3 is essential for SEC31 ubiquitylation *in vivo*. 293T cells were transfected with His–ubiquitin and siRNAs, and ubiquitin conjugates were analysed for SEC31 by Western blot.

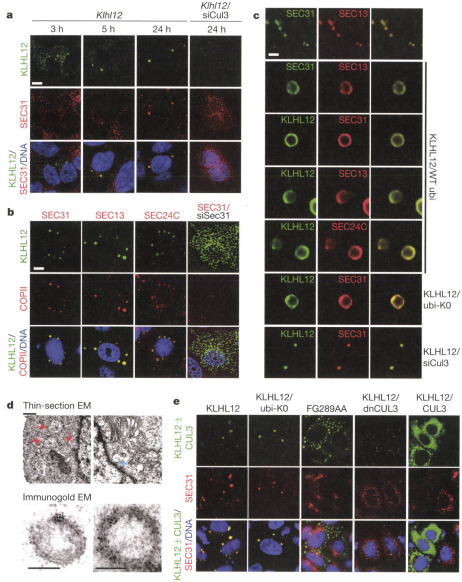

Figure 4 | CUL3–KLHL12-dependent monoubiquitylation enlarges COPII-structures. **a**, Localization of doxycycline (dox)-induced Flag–KLHL12 (dox:*Klhl12*, green) and SEC31 (red) in 293T cells, monitored by confocal microscopy. Scale bar, 3 μm. **b**, KLHL12-expressing HeLa cells were analysed for KLHL12 (green) and SEC31, SEC13 or SEC24C (red) by confocal microscopy. Scale bar, 3 μm. **c**. COPII-structures in HeLa cells transfected with Flag–KLHL12, lysine-free ubiquitin (ubi-K0) or *Cul3*-siRNA, analysed by confocal microscopy. Scale bar, 500 nm. **d**, Upper panel, thin-section electron microscopy (EM) of KLHL12-expressing or control HeLa cells (red arrow, KLHL12-dependent structures; blue arrow, small control vesicles). Scale bar, 500 nm. Lower panel, immunogold-EM of KLHL12 in transiently transfected HeLa (left) or stable 293T cells (right). Scale bar, 200 nm. **e**, HeLa cells transfected with Flag–KLHL12, lysine-free ubiquitin, Flag–KLHL12(FG289AA), Flag–CUL3(1–250) or Flag–CUL3 were analysed for localization of KLHL12/CUL3 (green) and SEC31 (red) by confocal microscopy. Original magnification ×40.

200–500 nm that were decorated with KLHL12 (Fig. 4d). The KLHL12-dependent structures neither contained a *cis*-Golgi protein; ERGIC-53, which is absent from procollagen transport vesicles[31]; endoplasmic reticulum membrane markers that do not accumulate at endoplasmic reticulum exit sites[32]; nor endosomal or autophagosomal markers (Supplementary Fig. 7a–c). Importantly, SEC31-binding deficient mutants, including KLHL12(FG289AA), neither colocalized with SEC31 nor induced formation of large structures (Fig. 4e and Supplementary Fig. 7d), and depletion of SEC31 blocked formation of large structures by KLHL12 (Fig. 4b). Thus, binding of KLHL12 to SEC31 triggers formation of large COPII-containing structures.

When KLHL12 was expressed with a CUL3 mutant that blocks SEC31 ubiquitylation (CUL3(1–250)), COPII structures were not enlarged (Fig. 4e). In addition, depletion of CUL3 by siRNAs, which also abolishes SEC31 monoubiquitylation, prevented formation of large COPII structures by KLHL12 (Fig. 4a, c). By contrast, if KLHL12 was expressed with lysine-free ubiquitin to allow mono-, but not multiubiquitylation, large COPII structures were readily detected (Fig. 4c, e), and these structures were enriched for ubiquitin, consistent with monoubiquitylation being non-proteolytic (Supplementary Fig. 7e). Thus, monoubiquitylation by CUL3–KLHL12 promotes formation of large COPII structures, which probably represent a mixture of nascent coats at endoplasmic reticulum exit sites and budded coats on large COPII vesicles or tubules.

CUL3 is required for collagen export

Our screen linked CUL3–KLHL12 to the establishment of the stem cell extracellular matrix, which requires collagen secretion. Thus, the CUL3–KLHL12-dependent increase in COPII size might function to promote collagen export from the endoplasmic reticulum. To test this hypothesis, we expressed KLHL12 in IMR90 cells, which at steady state accumulate collagen in the endoplasmic reticulum due to inefficient export. Strikingly, KLHL12, but not KLHL12(FG289AA) or unrelated BTB proteins, triggered depletion of procollagen I from intracellular endoplasmic reticulum pools (Fig. 5a). As a result, increased collagen levels were detected in the supernatant of cells expressing KLHL12, but not KLHL12(FG289AA) (Fig. 5b). When secretion was inhibited with brefeldin A, or if collagen folding in the endoplasmic reticulum was impaired by removal of ascorbate from the medium, procollagen remained within KLHL12-expressing cells (Fig. 5a). Time-resolved experiments showed that KLHL12 strongly accelerated collagen export from IMR90 cells (Fig. 5c). Shortly after inducing secretion, KLHL12 and collagen were detected at overlapping locations (Supplementary Fig. 7f), all of which indicates that CUL3–KLHL12 facilitates collagen traffic from the endoplasmic reticulum.

Blockade of SEC31 ubiquitylation by dominant-negative CUL3 interfered with the KLHL12-dependent export of collagen from IMR90 cells (Supplementary Fig. 8a). Similarly, depletion of CUL3–KLHL12 from engineered HT1080 fibrosarcoma cells severely

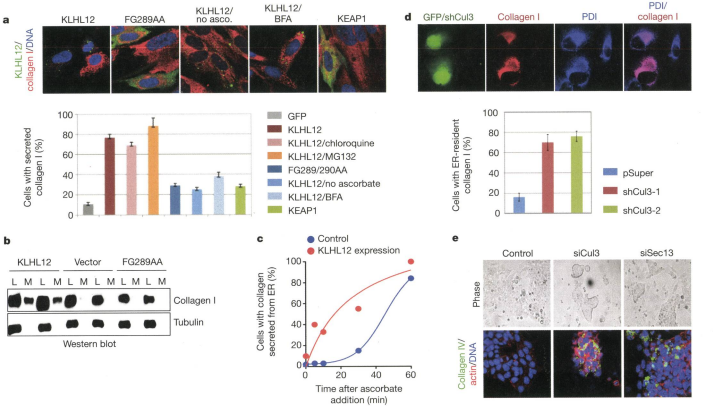

Figure 5 | CUL3–KLHL12 promotes collagen export. a, IMR90 cells transfected with Flag–KLHL12, Flag–KLHL12(FG289AA) or Flag–KEAP1 were analysed by confocal microscopy (BTB, green; collagen-I, red; DNA, blue). When noted, cells were treated with chloroquine, MG132, brefeldin A (BFA) or dialysed medium lacking ascorbate. Errors bars, standard deviation $n = 3$. Original magnification ×60. **b**, Cell lysate (L) or culture medium (M) of IMR90 cells transfected with Flag–KLHL12 or Flag–KLHL12(FG289AA) was analysed by immunoblotting. **c**, Collagen I localization was analysed in IMR90 cells expressing KLHL12, after re-addition of ascorbate. Original magnification ×40. **d**, HT1080 cells stably expressing collagen I were transfected with shRNAs against *Cul3* and analysed by confocal microscopy (transfection control green fluorescent protein (GFP), green; protein disulphide isomerase (PDI), blue; collagen I, red). Error bars, standard deviation $n = 3$. Original magnification ×60. **e**, D3 mouse ES cells were treated with control siRNAs or siRNAs targeting *Cul3* or *Sec13* and analysed by confocal microscopy (collagen IV, green; actin, red; DNA, blue). Original magnification ×40.

impaired collagen export, and most cells retained high levels of collagen in their endoplasmic reticulum (Fig. 5d and Supplementary Fig. 8b). In contrast, smaller COPII cargoes, such as fibronectin or EGF receptor, were properly localized in the absence of CUL3 (Supplementary Fig. 8c, d). Similar observations were made in mouse ES cells, where depletion of CUL3 led to a strong intracellular accumulation of collagen IV, comparable to the effects observed upon loss of SEC13 (Fig. 5e and Supplementary Fig. 8e). Thus, CUL3–KLHL12 is required for collagen export, whereas it is less important for the trafficking of smaller COPII cargo.

If promoting collagen export were the key role of CUL3 in mouse ES cells, the phenotypes of CUL3 depletion might be mitigated by addition of collagen *in trans*. Indeed, this was the case: when mouse ES cells were plated on purified collagen IV, depletion of CUL3 did not cause cell clustering, and integrin β1 was detected at the plasma membrane (Fig. 1b). We conclude that promoting collagen secretion is a key a function of CUL3, in agreement with its role in driving the assembly of large COPII coats.

Discussion

In this study, we have identified CUL3–KLHL12 as an essential regulator of collagen export, which is required for mouse ES cell division. Deletion of *Cul3* in mice results in early embryonic lethality with completely disorganized extraembryonic tissues[33], a phenotype that can in part be attributed to its role in collagen secretion. Moreover, KLHL12 has been identified as an autoantigen in the connective tissue disorder Sjogren's syndrome[34], raising the possibility that aberrant function of CUL3–KLHL12 might be related to disease.

CUL3–KLHL12 monoubiquitylates SEC31 and promotes formation of large COPII coats that can accommodate unusually shaped cargo. As a result, CUL3 is essential for the secretion of procollagen fibres, whereas it is not required for the transport of smaller or more flexible molecules, such as fibronectin, EGF receptor or integrin β1. Thus, CUL3–KLHL12 seems to be specifically required for the COPII-dependent transport of large cargo.

How ubiquitylation affects COPII coat size or structure is not known. None of the 65 lysine residues of SEC31 was essential for ubiquitylation by CUL3–KLHL12, showing that CUL3 can target alternative lysine residues if the primary site is blocked. Despite this flexibility, CUL3–KLHL12 does not stoichiometrically ubiquitylate SEC31. Thus, if SEC31 ubiquitylation performs a structural role, then few ubiquitylated molecules must suffice to produce large COPII coats, and these vesicles must tolerate considerable variation in the modification site. Alternatively, as often seen with monoubiquitylated proteins, modified SEC31 might recruit an effector that delays COPII budding or promotes coat polymerization. As CUL3–KLHL12 ubiquitylates other proteins[35], SEC31 may not be its only substrate in the secretory pathway. Identification of the complete set of CUL3–KLHL12 substrates and potential effector molecules should reveal the mechanism underlying the ubiquitin-dependent regulation of vesicle size.

Our findings have the potential to be translated into therapeutic strategies. We envision that agonists of CUL3–KLHL12 function mitigate consequences of *Sec23A* mutations in cranio-lenticulo-sutural dysplasia or *Sar1* mutations in chylomicron retention disease[10,11]. By contrast, interfering with CUL3 activity may counteract increased collagen

deposition during fibrosis or keloid formation[36]. Given the strong clustering phenotypes observed in CUL3-depleted mouse ES cells, inhibition of CUL3–KLHL12 might impair the proliferation of metastatic cells, which display features of undifferentiated cells[37,38]. Thus, our identification of CUL3–KLHL12 as a regulator of COPII size and function provides an exciting starting point to understand and therapeutically exploit key events in protein trafficking.

METHODS SUMMARY

For stem cell culture, mouse D3 ES cells were maintained in GIBCO Dulbecco's Modified Eagle ES cell medium containing 15% FBS, 1× sodium pyruvate, 1× non-essential amino acids, 1 mM β-mercaptoethanol and 1,000 U ml^{-1} leukaemia inhibitory factor (Millipore), and grown on gelatin-coated culture plates. Doxycycline-inducible 293T Trex Flag–BTB stable cell lines were made with the Flp-In T-REx 293 Cell Line system (Invitrogen) and maintained with blasticidin and hydromycin B.

For screening, two siRNA oligonucleotides were designed against 40 mouse ubiquitin ligases (Qiagen). siRNA oligonucleotides (10 pmol) and Lipofectamine 2000 were pre-incubated in a gelatin-coated 96-well plate. D3 mouse ES cells were seeded at 15,000 cells per well on top of the siRNA mixture, and the morphology of ES cell colonies was examined by bright-field microscopy 48 h after transfection.

To identify CUL3–KLHL12 substrates, doxycycline-inducible 239T cell lines expressing Flag–KLHL12 or Flag–KLHL9 were induced for 48 h. Cleared lysate was subjected to anti-Flag M2 affinity gel (Sigma), and precipitations were eluted with 3×Flag peptide (Sigma). Concentrated eluates were analysed by SDS–PAGE, and specific bands were identified by mass spectrometry analysis by the Vincent J. Coates Proteomics/Mass Spectrometry Laboratory.

For *in vitro* ubiquitylation reactions, CUL3/RBX1 purified from Sf9 cells was conjugated to NEDD8 using recombinant APPBP1–UBA3, UBC12 (also known as UBE2M) and NEDD8. KLHL12 purified from *Escherichia coli* and SEC31A–SEC13 complexes from Sf9 cells were added together with energy mix, E1, UBCH5C (also known as UBE2D3) and ubiquitin and incubated at 30 °C for 1 h.

For confocal microscopy, cells fixed in paraformaldehyde and permeabilized with Triton X-100 were incubated with primary antibodies for 2 h and Alexa-labelled secondary antibodies (Invitrogen) for 1 h. Pictures were taken on Zeiss LSM 510 and 710 confocal microscopes and analysed with LSM image browser and Imaris 3D imaging processing software. Images were processed for contrast enhancement to remove noise.

Full Methods and any associated references are available in the online version of the paper at www.nature.com/nature.

Received 3 August 2011; accepted 3 January 2012.

1. Leitinger, B. Transmembrane collagen receptors. *Annu. Rev. Cell Dev. Biol.* **27,** 265–290 (2011).
2. Wickström, S. A., Radovanac, K. & Fassler, R. Genetic analyses of integrin signaling. *Cold Spring Harb. Perspect. Biol.*. doi:10.1101/cshperspect.a005116 (30 December 2010).
3. Caswell, P. T., Vadrevu, S. & Norman, J. C. Integrins: masters and slaves of endocytic transport. *Nature Rev. Mol. Cell Biol.* **10,** 843–853 (2009).
4. Stephens, L. E. *et al.* Deletion of beta 1 integrins in mice results in inner cell mass failure and peri-implantation lethality. *Genes Dev.* **9,** 1883–1895 (1995).
5. Chen, S. S., Fitzgerald, W., Zimmerberg, J., Kleinman, H. K. & Margolis, L. Cell-cell and cell-extracellular matrix interactions regulate embryonic stem cell differentiation. *Stem Cells* **25,** 553–561 (2007).
6. Lang, M. R., Lapierre, L. A., Frotscher, M., Goldenring, J. R. & Knapik, E. W. Secretory COPII coat component Sec23a is essential for craniofacial chondrocyte maturation. *Nature Genet.* **38,** 1198–1203 (2006).
7. Townley, A. K. *et al.* Efficient coupling of Sec23-Sec24 to Sec13-Sec31 drives COPII-dependent collagen secretion and is essential for normal craniofacial development. *J. Cell Sci.* **121,** 3025–3034 (2008).
8. Sarmah, S. *et al.* Sec24D-dependent transport of extracellular matrix proteins is required for zebrafish skeletal morphogenesis. *PLoS ONE* **5,** e10367 (2010).
9. Ohisa, S., Inohaya, K., Takano, Y. & Kudo, A. *sec24d* encoding a component of COPII is essential for vertebra formation, revealed by the analysis of the medaka mutant, *vbi. Dev. Biol.* **342,** 85–95 (2010).
10. Boyadjiev, S. A. *et al.* Cranio-lenticulo-sutural dysplasia is caused by a *SEC23A* mutation leading to abnormal endoplasmic-reticulum-to-Golgi trafficking. *Nature Genet.* **38,** 1192–1197 (2006).
11. Fromme, J. C. *et al.* The genetic basis of a craniofacial disease provides insight into COPII coat assembly. *Dev. Cell* **13,** 623–634 (2007).
12. Jensen, D. & Schekman, R. COPII-mediated vesicle formation at a glance. *J. Cell Sci.* **124,** 1–4 (2011).
13. Stagg, S. M. *et al.* Structural basis for cargo regulation of COPII coat assembly. *Cell* **134,** 474–484 (2008).
14. Fath, S., Mancias, J. D., Bi, X. & Goldberg, J. Structure and organization of coat proteins in the COPII cage. *Cell* **129,** 1325–1336 (2007).
15. Fromme, J. C. & Schekman, R. COPII-coated vesicles: flexible enough for large cargo? *Curr. Opin. Cell Biol.* **17,** 345–352 (2005).
16. Saito, K. *et al.* TANGO1 facilitates cargo loading at endoplasmic reticulum exit sites. *Cell* **136,** 891–902 (2009).
17. Saito, K. *et al.* cTAGE5 mediates collagen secretion through interaction with TANGO1 at endoplasmic reticulum exit sites. *Mol. Biol. Cell* **22,** 2301–2308 (2011).
18. Wilson, D. G. *et al.* Global defects in collagen secretion in a *Mia3/TANGO1* knockout mouse. *J. Cell Biol.* **193,** 935–951 (2011).
19. Kathiresan, S. *et al.* Genome-wide association of early-onset myocardial infarction with single nucleotide polymorphisms and copy number variants. *Nature Genet.* **41,** 334–341 (2009); corrigendum **41,** 762 (2009).
20. Sumara, I. *et al.* A Cul3-based E3 ligase removes Aurora B from mitotic chromosomes, regulating mitotic progression and completion of cytokinesis in human cells. *Dev. Cell* **12,** 887–900 (2007).
21. Shaw, L. M., Rabinowitz, I., Wang, H. H., Toker, A. & Mercurio, A. M. Activation of phosphoinositide 3-OH kinase by the α6β4 integrin promotes carcinoma invasion. *Cell* **91,** 949–960 (1997).
22. Chen, Y. *et al.* Cullin mediates degradation of RhoA through evolutionarily conserved BTB adaptors to control actin cytoskeleton structure and cell movement. *Mol. Cell* **35,** 841–855 (2009).
23. Furukawa, M. & Xiong, Y. BTB protein Keap1 targets antioxidant transcription factor Nrf2 for ubiquitination by the Cullin 3-Roc1 ligase. *Mol. Cell. Biol.* **25,** 162–171 (2005).
24. Geyer, R., Wee, S., Anderson, S., Yates, J. & Wolf, D. A. BTB/POZ domain proteins are putative substrate adaptors for cullin 3 ubiquitin ligases. *Mol. Cell* **12,** 783–790 (2003).
25. Pintard, L. *et al.* The BTB protein MEL-26 is a substrate-specific adaptor of the CUL-3 ubiquitin-ligase. *Nature* **425,** 311–316 (2003).
26. Xu, L. *et al.* BTB proteins are substrate-specific adaptors in an SCF-like modular ubiquitin ligase containing CUL-3. *Nature* **425,** 316–321 (2003).
27. Young, R. A. Control of the embryonic stem cell state. *Cell* **144,** 940–954 (2011).
28. Hughes, H. *et al.* Organisation of human ER-exit sites: requirements for the localisation of Sec16 to transitional ER. *J. Cell Sci.* **122,** 2924–2934 (2009).
29. Kim, W. *et al.* Systematic and quantitative assessment of the ubiquitin-modified proteome. *Mol. Cell* **44,** 325–340 (2011).
30. Emanuele, M. J. *et al.* Global identification of modular cullin-RING ligase substrates. *Cell* **147,** 459–474 (2011).
31. Stephens, D. J. & Pepperkok, R. Imaging of procollagen transport reveals COPI-dependent cargo sorting during ER-to-Golgi transport in mammalian cells. *J. Cell Sci.* **115,** 1149–1160 (2002).
32. Zhu, W. *et al.* Bcl-2 mutants with restricted subcellular location reveal spatially distinct pathways for apoptosis in different cell types. *EMBO J.* **15,** 4130–4141 (1996).
33. Singer, J. D., Gurian-West, M., Clurman, B. & Roberts, J. M. Cullin-3 targets cyclin E for ubiquitination and controls S phase in mammalian cells. *Genes Dev.* **13,** 2375–2387 (1999).
34. Uchida, K. *et al.* Identification of specific autoantigens in Sjogren's syndrome by SEREX. *Immunology* **116,** 53–63 (2005).
35. Angers, S. *et al.* The KLHL12-Cullin-3 ubiquitin ligase negatively regulates the Wnt–β-catenin pathway by targeting Dishevelled for degradation. *Nature Cell Biol.* **8,** 348–357 (2006).
36. Schäfer, M. & Werner, S. Cancer as an overhealing wound: an old hypothesis revisited. *Nature Rev. Mol. Cell Biol.* **9,** 628–638 (2008).
37. Nguyen, D. X., Bos, P. D. & Massague, J. Metastasis: from dissemination to organ-specific colonization. *Nature Rev. Cancer* **9,** 274–284 (2009).
38. Zhang, X. H. *et al.* Latent bone metastasis in breast cancer tied to Src-dependent survival signals. *Cancer Cell* **16,** 67–78 (2009).

Acknowledgements We thank B. Schulman for advice and gifts of cDNAs and proteins. We are grateful to J. Schaletzky for critically reading the manuscript and many discussions. We thank the members of the Rape and Schekman labs for advice and suggestions, L. Lim for providing *Cul3*-shRNAs, C. Glazier for contributions on BTB protein cloning, and A. Fischer and M. Richner for tissue culture support. This work was funded by grants from the Pew Foundation (M.R.), the NIH (NIGMS-RO1, M.R.; NIH Director's New Innovator Award, M.R.), and the Howard Hughes Medical Institute (R.S.). L.J. was funded by a CIRM predoctoral fellowship; she is a Tang fellow. K.B.P. is an HFSP long term post-doctoral fellow.

Author Contributions Experiments were designed by L.J., K.B.P., R.S. and M.R.; L.J. performed the mouse ES cell screen, identified KLHL12 and SEC31, and analysed the role of CUL3 in COPII formation in cells and in collagen export in mouse ES cells; K.B.P. analysed collagen export in fibroblasts; K.E.W. analysed COPII formation in cells; C.B. identified inactive KLHL12; A.G. performed electron microscopy; L.J., K.B.P. and M.R. prepared the manuscript.

Author Information Reprints and permissions information is available at www.nature.com/reprints. The authors declare no competing financial interests. Readers are welcome to comment on the online version of this article at www.nature.com/nature. Correspondence and requests for material should be addressed to M.R. (mrape@berkeley.edu).

ARTICLE

doi:10.1038/nature10829

Structural basis of highly conserved ribosome recycling in eukaryotes and archaea

Thomas Becker[1]*, Sibylle Franckenberg[1]*, Stephan Wickles[1], Christopher J. Shoemaker[2], Andreas M. Anger[1], Jean-Paul Armache[1], Heidemarie Sieber[1], Charlotte Ungewickell[1], Otto Berninghausen[1], Ingo Daberkow[3], Annette Karcher[1,4], Michael Thomm[5], Karl-Peter Hopfner[1], Rachel Green[2] & Roland Beckmann[1]

Ribosome-driven protein biosynthesis is comprised of four phases: initiation, elongation, termination and recycling. In bacteria, ribosome recycling requires ribosome recycling factor and elongation factor G, and several structures of bacterial recycling complexes have been determined. In the eukaryotic and archaeal kingdoms, however, recycling involves the ABC-type ATPase ABCE1 and little is known about its structural basis. Here we present cryo-electron microscopy reconstructions of eukaryotic and archaeal ribosome recycling complexes containing ABCE1 and the termination factor paralogue Pelota. These structures reveal the overall binding mode of ABCE1 to be similar to canonical translation factors. Moreover, the iron–sulphur cluster domain of ABCE1 interacts with and stabilizes Pelota in a conformation that reaches towards the peptidyl transferase centre, thus explaining how ABCE1 may stimulate peptide-release activity of canonical termination factors. Using the mechanochemical properties of ABCE1, a conserved mechanism in archaea and eukaryotes is suggested that couples translation termination to recycling, and eventually to re-initiation.

Recycling of ribosomes for a new round of translation initiation is an essential part of protein synthesis. In archaea and eukaryotes recycling has been shown to require the highly conserved and essential ABC-type ATPase ABCE1 (Rli1p in *Saccharomyces cerevisiae* with 46.7% identity to archaeal (a)ABCE1 in *Pyrococcus furiosus*)[1–4]. ABCE1 can dissociate ribosomes into subunits either after canonical termination by release factors* or after recognition of stalled ribosomes by messenger RNA surveillance factors such as Pelota (Dom34p in *S. cerevisiae*, aPelota in *P. furiosus*)[5]. Crystal structures of aABCE1 revealed two nucleotide-binding domains (NBDs) in a typical head-to-tail orientation as observed for most of the other members of the ABC protein family[6–8]. Additional unique structural features of ABCE1 proteins are a helix–loop–helix (HLH) motif, a highly conserved hinge domain and an iron–sulphur cluster domain (FeS) containing two $[4Fe\text{–}4S]^{2+}$ clusters[6,9].

In eukaryotes ABCE1 can be found associated with ribosomes and small ribosomal subunits, but also with release factors and initiation factors (eRF1, eIF2, eIF3 and eIF5)[10,11]. Notably, ABCE1 physically interacts with eRF1 and directly influences its function in stop-codon recognition and peptidyl-transfer RNA (tRNA) hydrolysis[12,13]. During recycling ABCE1 can split post-termination complexes obtained with eRF1 and eRF3 into free 60S subunits and tRNA- and mRNA-bound 40S subunits[4]. A similar role for ABCE1 was found in an archaeal translation system in which aABCE1 together with aRF1 was shown to dissociate ribosomes into subunits upon ATP binding[8].

ABCE1 also acts together with the eRF1 paralogue Pelota[5]. In *S. cerevisiae*, Dom34 and the eRF3 paralogue Hbs1 were described as mRNA surveillance factors recognizing stalled elongating ribosomes[14]. Such stalls can occur on mRNAs with stable secondary structures, truncations or lacking a stop codon, so that further elongation or canonical termination is prevented. In the so called no-go mRNA decay (NGD) or non-stop mRNA decay (NSD) pathways, such stalled ribosomes are recognized by Dom34 and Hbs1 (NGD and NSD, respectively)[14] or by another eRF3 paralogue Ski7 (NSD), eventually triggering mRNA degradation[14–18]. A cryo-electron microscopy (cryo-EM) structure of a stalled ribosome bound to Dom34–Hbs1 shows that Dom34 occupies the ribosomal A site, whereas Hbs1 binds the ribosome similar to other translational GTPases, such as elongation factor Tu (EF-Tu)[19]. Dom34–Hbs1 alone shows ribosome dissociation activity and splits stalled reconstituted ribosomes that contain P-site peptidyl-tRNA[20]. In a mammalian system, however, ABCE1 is strictly required for ribosome disassembly of both programmed and vacant ribosomes by Pelota and Hbs1l5 (ref. 5). Taken together, ABCE1 is probably the general ribosome recycling factor in archaea and eukaryotes. In contrast to the analogous bacterial system, however, ABCE1 acts not only after canonical release-factor-dependent termination but also after Pelota-dependent recognition of stalled ribosomes.

It is not known how ABCE1 functions on the ribosome in concert with Pelota or release factors, and how the mechanochemical properties of ABCE1 are used for ribosome recycling. To address these questions, we determined cryo-EM structures of eukaryotic and archaeal recycling complexes containing Pelota and ABCE1.

Model of Pelota–ABCE1–ribosome complexes

Recycling complexes were obtained by *in vitro* reconstitution of the 70S and 80S ribosomes with purified Pelota and ABCE1 orthologues.

[1]Gene Center and Center for integrated Protein Science Munich (CiPSM), Department of Biochemistry, University of Munich, Feodor-Lynen-Straße 25, 81377 Munich, Germany. [2]Howard Hughes Medical Institute, Department of Molecular Biology and Genetics, Johns Hopkins University School of Medicine, Baltimore, Maryland 21205, USA. [3]Tietz Video and Image Processing Systems GmbH, Eremitenweg 1, 82131 Gauting, Germany. [4]Rainer-Maria-Rilke-Gymnasium Icking, Ulrichstraße 1-7, 82057 Icking, Germany. [5]NWF III/Biology and Preclinical Medicine, Department of Microbiology, University of Regensburg, Universitätsstraße 31, 93053 Regensburg, Germany.
*These authors contributed equally to this work.

For the generation of a *S. cerevisiae* 80S ribosome–Dom34–Rli1 complex we used ribosome nascent chain complexes (RNCs) stalled by an mRNA with a synthetic stem loop (SL)[14,21], a complex used previously for an 80S–Dom34–Hbs1 cryo-EM reconstruction[19]. For archaeal (*P. furiosus*) 70S–aPelota–aABCE1 complexes, 70S ribosomes were purified from a translation extract[22]. Simultaneous ribosome binding of Pelota and ABCE1 in the presence of non-hydrolysable ADPNP was shown by pelleting assays in the yeast and archaeal systems (Supplementary Fig. 1a, b). Notably, aABCE1-dependent splitting of archaeal ribosomes was not detectable with ADPNP, but strictly required ATP (Supplementary Fig. 1c, d).

Using cryo-EM in combination with single-particle analysis, we determined the structures of the SL–RNC–Dom34–Rli1 complex from yeast and the 70S–aPelota–aABCE1 complex from *P. furiosus*. Computational sorting was performed to generate homogeneous populations of ribosomal complexes containing Pelota, ABCE1 and P-site tRNA. The resolution of the final maps was determined to be 7.2 Å for the yeast complex and 6.6 Å for the archaeal complex (Supplementary Fig. 2). In both reconstructions we observed density for Pelota in the ribosomal A site, for ABCE1 in the GTPase translation factor binding site, and for tRNA in the P site (Fig. 1a, b). Additional E-site tRNA density is present in the archaeal ribosome. Both reconstructions are remarkably similar with respect to conformation and the ribosomal interaction patterns of the ABCE1 and Pelota orthologues. Using available crystal structures we could unambiguously assign and position the individual domains of Pelota—divided into amino-terminal domain (NTD), central domain and carboxy-terminal domain (CTD)—and ABCE1—divided into the N-terminal FeS, NBD1 containing a HLH motif, NBD2 and the hinge domain (Fig. 1c and Supplementary Fig. 3).

Notably, the two electron dense $[4Fe–4S]^{2+}$ clusters of ABCE1 can be clearly resolved as distinct spheres at high contour levels in both the yeast and archaeal maps reconstructions, validating the positioning of crystal structures in the EM maps (Fig. 1d). For molecular analysis we used the crystal structure of the yeast 40S subunit[23], the model of the yeast 80S ribosome[24,25] and, in addition, we built a homology-based molecular model of the archaeal 70S ribosome.

Ribosome–ABCE1 interaction

ABCE1 binds to ribosomes in the intersubunit space, where canonical translational GTPases such as EF-Tu, EF-G/eEF2 or Hbs1 also interact with the ribosome (Fig. 2a)[19,26–29]. ABCE1 excludes these factors from binding at the same time, and we thus conclude that dissociation of Hbs1 or aEF1α or, in the case of termination, eRF3 or aEF1α, has to precede ABCE1 binding. Similar to these GTPases, the ATPase ABCE1 contacts the small ribosomal subunit, specifically ribosomal RNA helices h5, h8, h14 and h15 (Supplementary Tables 1 and 2). The h5–h15 region interacts with domain II of the translational GTPases, whereas the h8–h14 junction is the most proximal region to the GTPase switch regions[30,31] (Supplementary Fig. 4). Interestingly, the same regions are contacted by ABCE1 via two specific, up to now unexplained, structural features of ABCE1-type ABC-ATPases. The HLH motif of ABCE1 contacts the h5–h15 junction, whereas the hinge region establishes extensive contacts with the h8–h14 junction. In contrast to translational GTPases that engage in close interaction with the sarcin-ricin loop (SRL) of the rRNA helix, H95, contacts of ABCE1 with the large subunit are essentially limited to L9 in both species. Despite the overall marked similarity between Rli1 and aABCE1 in their ribosome interaction mode, additional minor contacts are present in the yeast complex: Rli1 contacts rpS6e and rpS24e on the small subunit, and, on the large subunit, rpP0 and a small region of the SRL (H95), which is different from the binding region of translational GTPases (Fig. 2b, c). Unexpectedly, the FeS cluster domain of ABCE1 does not directly bind the ribosome but instead interacts with Pelota only. These interactions are conserved between yeast and archaea.

In summary, ABCE1 establishes multiple contacts with both small and large ribosomal subunits as well as with the release factors (and

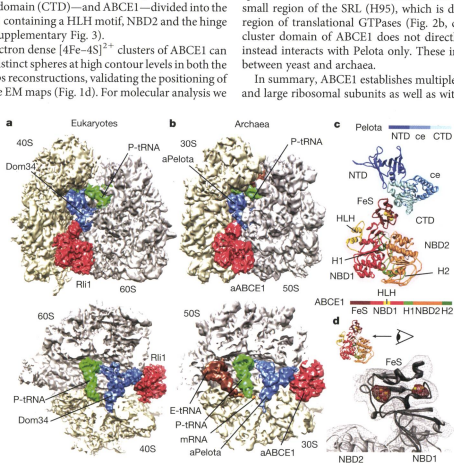

Figure 1 | The ribosome-bound Pelota–ABCE1 complex. a, **b**, Cryo-EM reconstructions of the eukaryotic SL–RNC–Dom34–Rli1 and the archaeal 70S–aPelota–aABCE1 complexes at 7.2 Å and 6.6 Å resolution, respectively. Extra densities were observed for Dom34/aPelota and Rli1/aABCE1 in the canonical factor binding site as well as for P-site tRNA, E-site tRNA and mRNA. The top section represents side views, the bottom section top views, where large and small subunits were cut. **c**, Homology model for ribosome-bound Pelota and ABCE1 in transparent density. The individual domains are colour-coded as in the schematic representation of domain organization. The NTD, central domain (ce) and CTD are indicated. H1 and H2 indicate hinge 1 and hinge 2 domains. **d**, Zoom on the FeS domain of aABCE1. The density for the two $[4Fe–4S]^{2+}$ clusters is displayed in red mesh at high contour level.

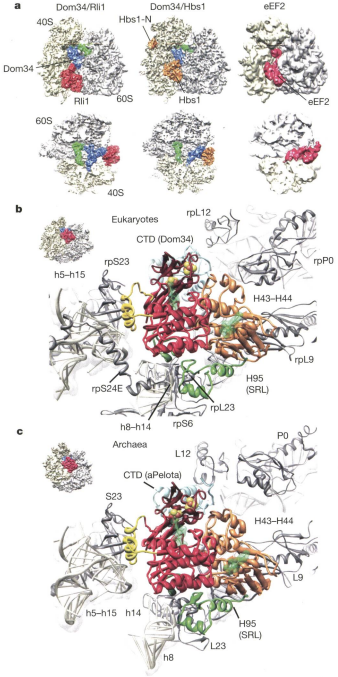

Figure 2 | Interaction of Pelota and ABCE1 with the ribosome. **a**, Comparison of the SL–RNC–Dom34–Rli1 cryo-EM map with the SL–RNC–Dom34–Hbs1 and the 80S–eEF2 maps. Views are as in Fig. 1a, b. **b**, **c**, Interactions of ABCE1 with the eukaryotic (**b**) and the archaeal (**c**) ribosome. The view is indicated by a thumbnail. The domain colour code is as in Fig. 1c.

their paralogues) and these interactions involve all domains of ABCE1. Such tight recognition provides a rationale for direct mechanochemical coupling of ATP-driven conformational changes in ABCE1 with structural changes in the ribosome that are critical for termination and release.

ABCE1-stabilized conformational switch of Pelota

The FeS domain of ABCE1 binds to the CTD of Pelota and we observe a large-scale conformational change in the central domain and CTD compared to the Dom34 structure in the Hbs1-bound state[19] (Fig. 3). By contrast, the NTD of Pelota is essentially unchanged in these two structures where they are located in the A site contacting rRNA helices h18, h28, h31, h34 and h44, and additionally the ribosomal protein rpS30 in yeast. The β3–β4 loop reaches deeply into the A site and at the given resolution we observed additional contacts of this loop of aPelota with the ribosomal protein S5 (Supplementary Fig. 3c). The most marked rearrangements, however, occur in the central domain of both Pelota orthologues: the central domain of Dom34 bound to Hbs1 in the yeast ribosome is tightly packed against Hbs1 (ref. 19), very similar to the domain arrangement in the crystal structure of an aPelota–aEF1α complex[32] (Fig. 3b); in the presence of ABCE1, however, the central domain of Dom34 or aPelota is rotated by approximately 140° towards the P-site tRNA (Supplementary Movies 1 and 2). In this conformation it establishes numerous new contacts to rRNA in domain IV and V of the large subunit (Supplementary Tables 1 and 2). The positively charged loop β10–α3 directly contacts the P-site tRNA acceptor stem and the ribosomal protein L10e in archaea. In the closely related RF1 proteins, this loop contains the GGQ motif that is essential for catalysing the hydrolysis of peptide from peptidyl-tRNA[33,34]. When modelling ribosome-bound eRF1 on the basis of the Pelota conformation observed in the presence of ABCE1, the GGQ motif of eRF1 would be ideally positioned to interact with the CCA-end of the P-site peptidyl-tRNA in the peptidyl transferase centre (Fig. 3c). This may explain how ABCE1 can stimulate termination activity *in vivo* and *in vitro*[12,13].

As the CTD of Pelota establishes the only contact site with ABCE1 via the FeS cluster domain, the interaction surface is rather small (440 Å^2) compared to that between ribosome-bound Dom34 and Hbs1 trapped in the GTP state (1,940 Å^2)[19]. In the ABCE1-bound conformation, the CTD is rotated downwards by approximately 15° together with a movement of the ribosomal stalk base (H43–H44, rpL12), similar to that induced by eEF2 binding (Supplementary Fig. 5)[28,29]. Both the stalk base and the CTD of Dom34 move closer towards the SRL of H95 and a strong contact between the CTD of Dom34 (helix α7) and the SRL is established (Fig. 3d). Very similar conformations of the stalk base, as well as of the central domain and CTD, were observed for aPelota on the archaeal ribosome, although some molecular details of domain fold and ribosome interaction pattern also differ between Dom34 and aPelota. Interestingly, helices α5, α6 and α7, which link the central domain and the CTD of aPelota, establish one long α-helix with a kink between α5 and α6 in the presence of aABCE1 that reaches from the SRL deeply into the A site (Fig. 3e).

In summary, in both species the presence of ABCE1 stabilizes an alternative conformation of Pelota on the ribosome, primarily affecting the central domain that reaches through the A site to contact the P-site tRNA. An analogous behaviour of the closely related release factors would ideally position the conserved GGQ loop for catalysing peptidyl-tRNA hydrolysis.

Mechanochemical activity of ABCE1 on the ribosome

Typically, ABC proteins generate mechanochemical work by nucleotide-driven clamp-like motions of the two NBDs: in the apo or ADP-bound state, NBDs adopt an open conformation often linked to a higher affinity for the given substrate of the ABC enzyme. ATP binding triggers a closed state, by binding to Walker A and B motifs of one NBD and the opposing conserved LSGGQ loop (signature motif) of the other NBD that coordinates the γ-phosphate of ATP for subsequent hydrolysis[35]. ATP binding or subsequent ATP hydrolysis leads to a 'power stroke' that usually causes concomitant conformational changes in connected domains or binding partners.

To analyse the mechanochemical function of ABCE1 in ribosome splitting, we compared the ribosome-bound conformation of ABCE1 with the open ADP-bound form as observed in the crystal[6–8] and with a model for the closed ATP-bound state (Fig. 4a). The model for the closed state is derived by individually superimposing the NBDs of ABCE1 to NBDs crystallized in the ATP-bound state[36]. Interestingly,

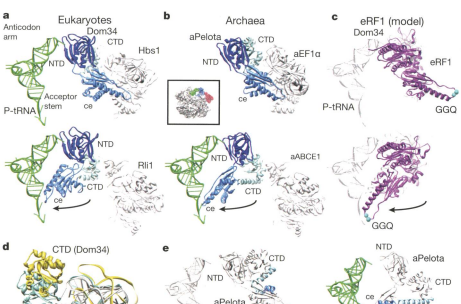

Figure 3 | Domain movements in Pelota and eRF1. **a**, Comparison of the ribosome-bound Dom34 conformation in complex with Hbs1 (top) and Rli1 (bottom). **b**, Comparison of the aPelota–aEF1α crystal structure[35] with the ribosome-bound aPelota in complex with aABCE1. The central domain (ce) of Pelota swings out towards the P-site tRNA. The inset shows a thumbnail indicating the view. **c**, Models for eRF1 before and after the suggested movement of the central domain. The arrows indicate the movement of the central domains. **d**, Conformation of the Dom34 CTD and the stalk base rRNA (H43–H44) when bound to Hbs1 (yellow) and to Rli1 (blue). rRNA conformation without factors bound is shown in grey. **e**, In aPelota three separate small helices refold into a long α-helix during movement of the central domain bridging the CTD and the central domain.

neither the open nor the closed model can be easily modelled into the electron density in the reconstructions. In both reconstructions, we observe an intermediate, half-open state of the two NBDs: NBD2 rotates by approximately 17° towards NBD1 and the FeS cluster domain. However, an additional upward movement by 8 Å of NBD2 would be required to obtain the fully closed conformation, in which the signature motif of one NBD domain contacts the nucleotide-binding pocket of the other NBD domain (Supplementary Movie 3). Notably, in the observed half-open state of ABCE1 we find a contact between the NBD2 domain and the FeS cluster domain that is not seen in the crystal structures of the open state. Adoption of the fully closed ATP-bound conformation would therefore require a substantial shift of the FeS cluster domain, also of about 8 Å (Fig. 4a), to avoid a steric clash. Although the limited resolution of the reconstruction does not allow for any conclusions regarding the nature of the bound nucleotide, the conformations of the individual lobes within the NBD1 and NBD2 domains more closely resemble those of the ADP-bound crystal structures. The similarity of the 'intermediate' conformation in both reconstructions suggests that binding to the ribosome induces an allosteric change in ABCE1, perhaps related to allosteric control of the ABC transporter by substrate binding[37].

The finding that ATP hydrolysis[4,5] is required for full splitting activity strongly suggests that ABCE1 indeed has to undergo a conversion from the observed half-open pre-splitting conformation to the fully closed ATP state to efficiently dissociate ribosomes. Therefore, we analysed the effect of ATP-dependent NBD domain closure by superimposing the half-open ribosome-bound state of ABCE1 with the model for the closed state. ABCE1 in the closed conformation would not sterically clash with the ribosomal subunits

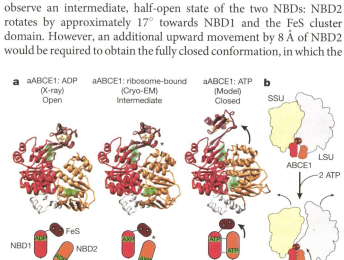

Figure 4 | Mechanochemical activity of ABCE1 on the ribosome. **a**, Crystal structure of the open (ADP-bound) aABCE1, the cryo-EM structure of the ribosome-bound aABCE1 and homology model of the closed (ATP-bound) aABCE1 including schematic drawings. An asterisk indicates a contact between NBD2 and the FeS domain of aABCE1. **b**, Ribosomal subunits may be dissociated by following the trajectory of aABCE1 domain closure upon ATP binding. **c**, Interactions of the aPelota NTD and central domain within the ribosome. **d**, ABCE1 domain closure could lead to an allosteric cascade with the FeS domain acting as a bolt on the CTD of Pelota to rearrange the NTD and central domain of Pelota. This mechanism would be analogous to the splitting reaction in bacteria by RRF and EF-G as depicted in **e**.

to induce splitting. One possibility is that the small and large ribosomal subunits follow the trajectory of NBD1 and NBD2 of ABCE1, respectively. In this case the ribosomal subunits would sufficiently rotate away from each other so as to affect the intersubunit bridges and, thus, the overall ribosome stability (Fig. 4b).

It is more likely, however, that the transition of ABCE1 through the closed conformation triggers an allosteric cascade affecting Pelota: the FeS cluster domain of ABCE1 contacts the NBD2 domain already in the half-open state and has to follow the movement of the NBD2 during closure. This conformational change of the FeS cluster domain towards the intersubunit space is likely to be transmitted to Pelota via the close interaction with its CTD. A shift of the CTD would in turn be transmitted to both the NTD and the central domain of Pelota. These Pelota domains establish a network of contacts with the small and the large ribosomal subunit as well as with the P-site tRNA (Fig. 4c). Indeed, numerous mutations underline the functional importance of these domains for the activity of Pelota (Supplementary Tables 1 and 2). A conformational shift can be easily envisaged to cause dissociation of the ribosome by destabilizing intersubunit bridges and the P-site tRNA. A function of the FeS cluster domain of ABCE1 as a structural bolt to remodel Pelota by transmitting ATP-induced changes from the NBDs is in good agreement with the finding that deletion of this domain abolishes splitting activity[8]. The enhanced stability of the domain provided by the FeS cluster may be required in the transmission of the mechanochemical power of ABCE1 for ribosome splitting.

Although using an entirely different cast of characters, this scenario is structurally reminiscent of bacterial ribosome recycling by ribosome recycling factor (RRF) and elongation factor G (EF-G). In this case, an EF-G-based GTP-dependent conformational switch positions RRF to clash with the small ribosomal subunit, inevitably promoting subunit dissociation[8] (Fig. 4d, e).

Conclusion

We provide a structural basis and a universal mechanistic model for eukaryotic and archaeal ribosome recycling in which ABCE1 actively coordinates rescue (or translation termination) with recycling and re-initiation (Fig. 5):

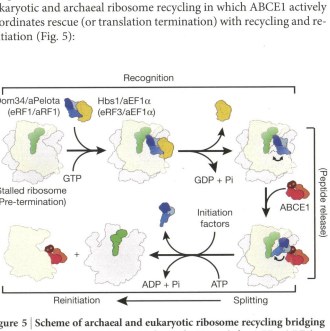

Figure 5 | Scheme of archaeal and eukaryotic ribosome recycling bridging termination with initiation. A translational GTPase (Hbs1/aEF1α/eRF3) delivers the factor, which recognizes stalled ribosomes (Pelota) or pre-termination complexes (eRF1/aRF1). After GTP hydrolysis, the GTPase dissociates and ABCE1 can bind. ABCE1 induces or stabilizes the swung-out conformation of Pelota (or RF1), which would lead to peptide release in case of termination. Ribosome splitting is induced after ATP binding to ABCE1 and hydrolysis. In eukaryotes, initiation factors can bind during the splitting reaction, coupling ribosome recycling with re-initiation. After splitting ABCE1 stays associated with the small ribosomal subunit.

In the first stage, the recognition stage, the sensing factors Pelota (for rescue) or RF1 (for termination) are delivered to stalled ribosomes or pre-termination complexes by EF-Tu-like GTPases. In the next step, the GTPase dissociates to allow ABCE1 binding to the ribosome. ABCE1 interacts with the CTD of Pelota (or of RF1 in termination) to stabilize the extended conformation of the central domain. In the case of translation termination, the GGQ motif of RF1 will be positioned proximal to the CCA-end of the P-site tRNA to catalyse peptide release; in the case of ribosome rescue, the central domain will be tightly accommodated proximal to the peptidyl transferase centre. Subsequently, in both cases, ABCE1 triggers ribosome disassembly into subunits by a power stroke upon NBD domain closure and ATP hydrolysis[8]. Our biochemical and structural data suggest a universal role of ATP hydrolysis in the mechanism of ABCE1-driven recycling. The conformational switch of ABCE1 could cause either a direct disruption of the ribosomal intersubunit bridges or, more likely, further conformational changes via an allosteric cascade from the FeS cluster domain of ABCE1 to the central domain and NTD of Pelota. In the archaeal system ABCE1 remains bound to the small ribosomal subunit after splitting[8] and it has been also found on the small subunit in eukaryotes[10,11]. Notably, ribosome recycling is coupled in eukaryotes with re-initiation when initiation factors such as eIF3, eIF1 and eIF1A bind the small ribosomal subunit as recycling is completed[38]. An initial recruitment of eIF3 to the 80S ribosome may even occur directly via ABCE1 interaction with the eIF3 subunit eIF3j (Hcr1p in yeast), even before recycling is completed[13,39,40]. In contrast, the analogous bacterial recycling system consisting of RRF and EF-G acts only after termination is completed and the participation of initiation factors is less clear[41].

In conclusion, the archaeal and eukaryotic kingdoms have maintained an extremely conserved general ribosome recycling system with an ABC-type ATPase at the core: the mechanochemical properties of ABCE1 are used through a still somewhat enigmatic FeS cluster domain. This domain triggers an allosteric cascade that actively coordinates translation termination or rescue with recycling[12], and eventually with re-initiation. It remains a puzzle as to why a complex FeS cluster domain is apparently used for a structural role only and has not been replaced by a simpler structure over billions of years of evolution. Thus, it is highly desirable to seek deeper insight into additional functions of ABCE1 in processes such as translation initiation and ribosome assembly.

METHODS SUMMARY

Programmed yeast SL–RNCs were prepared from cell-free extracts as described[19,42]. Archaeal ribosomes were purified from cell-free extracts[22] by sucrose density centrifugation. Ribosome binding partners (Dom34, aPelota, ABCE1, aRF1 and aIF6) were expressed in *E. coli* or *S. cerevisiae* (Rli1) and purified using affinity chromatography. Ligands were reconstituted *in vitro* with SL–RNCs or 70S ribosomes, and binding was analysed by SDS–PAGE after pelleting of ribosome-bound fractions. Splitting activity was monitored in sucrose gradients using ultraviolet profiles. For cryo-EM, yeast and archaeal recycling complexes were vitrified and data were collected on a Titan Krios electron microscope (FEI Company). Single-particle analysis and three-dimensional reconstruction was done using the SPIDER software package[43]. Homology models were generated using HHPRED[44] and MODELLER[45].

Full Methods and any associated references are available in the online version of the paper at www.nature.com/nature.

Received 18 August 2011; accepted 5 January 2012.

1. Winzeler, E. A. *et al.* Functional characterization of the *S. cerevisiae* genome by gene deletion and parallel analysis. *Science* **285,** 901–906 (1999).
2. Coelho, C. M. *et al.* Growth and cell survival are unevenly impaired in pixie mutant wing discs. *Development* **132,** 5411–5424 (2005).
3. Estevez, A. M., Haile, S., Steinbuchel, M., Quijada, L. & Clayton, C. Effects of depletion and overexpression of the *Trypanosoma brucei* ribonuclease L inhibitor homologue. *Mol. Biochem. Parasitol.* **133,** 137–141 (2004).
4. Pisarev, A. V. *et al.* The role of ABCE1 in eukaryotic posttermination ribosomal recycling. *Mol. Cell* **37,** 196–210 (2010).

5. Pisareva, V. P., Skabkin, M. A., Hellen, C. U., Pestova, T. V. & Pisarev, A. V. Dissociation by Pelota, Hbs1 and ABCE1 of mammalian vacant 80S ribosomes and stalled elongation complexes. *EMBO J.* **30,** 1804–1817 (2011).
6. Karcher, A., Schele, A. & Hopfner, K.-P. X-ray structure of the complete ABC enzyme ABCE1 from *Pyrococcus abyssi*. *J. Biol. Chem.* **283,** 7962–7971 (2008).
7. Karcher, A., Buttner, K., Martens, B., Jansen, R. P. & Hopfner, K. P. X-ray structure of RLI, an essential twin cassette ABC ATPase involved in ribosome biogenesis and HIV capsid assembly. *Structure* **13,** 649–659 (2005).
8. Barthelme, D. *et al.* Ribosome recycling depends on a mechanistic link between the FeS cluster domain and a conformational switch of the twin-ATPase ABCE1. *Proc. Natl. Acad. Sci. USA* **108,** 3228–3233 (2011).
9. Barthelme, D. *et al.* Structural organization of essential iron-sulfur clusters in the evolutionarily highly conserved ATP-binding cassette protein ABCE1. *J. Biol. Chem.* **282,** 14598–14607 (2007).
10. Dong, J. *et al.* The essential ATP-binding cassette protein RLI1 functions in translation by promoting preinitiation complex assembly. *J. Biol. Chem.* **279,** 42157–42168 (2004).
11. Andersen, D. & Leevers, S. The essential *Drosophila* ATP-binding cassette domain protein, Pixie, binds the 40S ribosome in an ATP-dependent manner and is required for translation initiation. *J. Biol. Chem.* **282,** 14752–14760 (2007).
12. Shoemaker, C. J. & Green, R. Kinetic analysis reveals the ordered coupling of translation termination and ribosome recycling in yeast. *Proc. Natl Acad. Sci. USA* **108,** E1392–E1398 (2011).
13. Khoshnevis, S. *et al.* The iron-sulphur protein RNase L inhibitor functions in translation termination. *EMBO Rep.* **11,** 214–219 (2010).
14. Doma, M. & Parker, R. Endonucleolytic cleavage of eukaryotic mRNAs with stalls in translation elongation. *Nature* **440,** 561–564 (2006).
15. Atkinson, G., Baldauf, S. & Hauryliuk, V. Evolution of nonstop, no-go and nonsense-mediated mRNA decay and their termination factor-derived components. *BMC Evol. Biol.* **8,** 290 (2008).
16. Lee, H. H. *et al.* Structural and functional insights into Dom34, a key component of no-go mRNA decay. *Mol. Cell* **27,** 938–950 (2007).
17. Frischmeyer, P. *et al.* An mRNA surveillance mechanism that eliminates transcripts lacking termination codons. *Science* **295,** 2258–2261 (2002).
18. van Hoof, A., Frischmeyer, P. A., Dietz, H. C. & Parker, R. Exosome-mediated recognition and degradation of mRNAs lacking a termination codon. *Science* **295,** 2262–2264 (2002).
19. Becker, T. *et al.* Structure of the no-go mRNA decay complex Dom34-Hbs1 bound to a stalled 80S ribosome. *Nature Struct. Mol. Biol.* **18,** 715–720 (2011).
20. Shoemaker, C. J., Eyler, D. E. & Green, R. Dom34:Hbs1 promotes subunit dissociation and peptidyl-tRNA drop-off to initiate no-go decay. *Science* **330,** 369–372 (2010).
21. Hosoda, N. *et al.* Translation termination factor eRF3 mediates mRNA decay through the regulation of deadenylation. *J. Biol. Chem.* **278,** 38287–38291 (2003).
22. Endoh, T., Kanai, T. & Imanaka, T. A highly productive system for cell-free protein synthesis using a lysate of the hyperthermophilic archaeon, *Thermococcus kodakaraensis*. *Appl. Microbiol. Biotechnol.* **74,** 1153–1161 (2007).
23. Rabl, J., Leibundgut, M., Ataide, S. F., Haag, A. & Ban, N. Crystal structure of the eukaryotic 40S ribosomal subunit in complex with initiation factor 1. *Science* **331,** 730–736 (2011).
24. Armache, J. P. *et al.* Localization of eukaryote-specific ribosomal proteins in a 5.5-Å cryo-EM map of the 80S eukaryotic ribosome. *Proc. Natl Acad. Sci. USA* **107,** 19754–19759 (2010).
25. Armache, J. P. *et al.* Cryo-EM structure and rRNA model of a translating eukaryotic 80S ribosome at 5.5-Å resolution. *Proc. Natl Acad. Sci. USA* **107,** 19748–19753 (2010).
26. Schmeing, T. M. *et al.* The crystal structure of the ribosome bound to EF-Tu and aminoacyl-tRNA. *Science* **326,** 688–694 (2009).
27. Gao, Y. G. *et al.* The structure of the ribosome with elongation factor G trapped in the posttranslocational state. *Science* **326,** 694–699 (2009).
28. Taylor, D. J. *et al.* Structures of modified eEF2 80S ribosome complexes reveal the role of GTP hydrolysis in translocation. *EMBO J.* **26,** 2421–2431 (2007).
29. Spahn, C. M. *et al.* Domain movements of elongation factor eEF2 and the eukaryotic 80S ribosome facilitate tRNA translocation. *EMBO J.* **23,** 1008–1019 (2004).
30. Villa, E. *et al.* Ribosome-induced changes in elongation factor Tu conformation control GTP hydrolysis. *Proc. Natl Acad. Sci. USA* **106,** 1063–1068 (2009).
31. Connell, S. R. *et al.* Structural basis for interaction of the ribosome with the switch regions of GTP-bound elongation factors. *Mol. Cell* **25,** 751–764 (2007).
32. Kobayashi, K. *et al.* Structural basis for mRNA surveillance by archaeal Pelota and GTP-bound EF1α complex. *Proc. Natl Acad. Sci. USA* **107,** 17575–17579 (2010).
33. Frolova, L. *et al.* Mutations in the highly conserved GGQ motif of class 1 polypeptide release factors abolish ability of human eRF1 to trigger peptidyl-tRNA hydrolysis. *RNA* **5,** 1014–1020 (1999).
34. Song, H. *et al.* The crystal structure of human eukaryotic release factor eRF1—mechanism of stop codon recognition and peptidyl-tRNA hydrolysis. *Cell* **100,** 311–321 (2000).
35. Hopfner, K. P. & Tainer, J. A. Rad50/SMC proteins and ABC transporters: unifying concepts from high-resolution structures. *Curr. Opin. Struct. Biol.* **13,** 249–255 (2003).
36. Smith, P. C. *et al.* ATP binding to the motor domain from an ABC transporter drives formation of a nucleotide sandwich dimer. *Mol. Cell* **10,** 139–149 (2002).
37. Locher, K. P. Structure and mechanism of ATP-binding cassette transporters. *Phil. Trans. R. Soc. Lond. B* **364,** 239–245 (2009).
38. Pisarev, A. V., Hellen, C. U. & Pestova, T. V. Recycling of eukaryotic posttermination ribosomal complexes. *Cell* **131,** 286–299 (2007).
39. Kispal, G. *et al.* Biogenesis of cytosolic ribosomes requires the essential iron–sulphur protein Rli1p and mitochondria. *EMBO J.* **24,** 589–598 (2005).
40. Yarunin, A. *et al.* Functional link between ribosome formation and biogenesis of iron–sulfur proteins. *EMBO J.* **24,** 580–588 (2005).
41. Pavlov, M. Y., Antoun, A., Lovmar, M. & Ehrenberg, M. Complementary roles of initiation factor 1 and ribosome recycling factor in 70S ribosome splitting. *EMBO J.* **27,** 1706–1717 (2008).
42. Beckmann, R. *et al.* Architecture of the protein-conducting channel associated with the translating 80S ribosome. *Cell* **107,** 361–372 (2001).
43. Frank, J. *et al.* SPIDER and WEB: processing and visualization of images in 3D electron microscopy and related fields. *J. Struct. Biol.* **116,** 190–199 (1996).
44. Soding, J., Biegert, A. & Lupas, A. N. The HHpred interactive server for protein homology detection and structure prediction. *Nucleic Acids Res.* **33,** W244–W248 (2005).
45. Eswar, N., Eramian, D., Webb, B., Shen, M. Y. & Sali, A. Protein structure modeling with MODELLER. *Methods Mol. Biol.* **426,** 145–159 (2008).

Supplementary Information is linked to the online version of the paper at www.nature.com/nature.

Acknowledgements We thank A. Schele and A. Gilmozzi for technical assistance, and D. Wilson for critical discussions. This work was supported by grants from the Deutsche Forschungsgemeinschaft, SFB594 (to R.B.), SFB646 (to T.B., R.B. and K.-P.H.), National Institutes of Health U19 AI083025 (to K.-P.H.) and by the Fonds der chemischen Industrie (to S.F.).

Author Contributions T.B. and R.B. designed the study, T.B. processed the yeast SL–RNC–Dom34–Rli1 complex and interpreted the cryo-EM structures, S.F. purified archaeal proteins and reconstituted the archaeal 70S-aPelota–aABCE1 sample, processed all archaeal data sets and interpreted the cryo-EM structures, S.W. developed an automated workflow for data processing from the Titan Krios microscope, C.J.S. purified yeast Rli1p, A.M.A. built the archaeal 70S ribosome rRNA model, J.-P.A. built the archaeal 70S ribosome protein models, H.S. reconstituted the SL–RNC–Dom34–Rli1 sample, C.U. prepared cryo-EM grids and assisted in data collection, O.B. optimized and performed cryo-EM data collection, I.D. implemented software for automated data collection on the Titan Krios microscope, A.K. purified archaeal ABCE1, M.T. provided *P. furiosus* and *Thermococcus kodakaraensis* cells, T.B., S.F., K.-P.H., R.G. and R.B. interpreted results.

Author Information EM density maps are deposited in the 3D-EM database (EMD-2008 and EMD-2010 for yeast maps, EMD-2009 for the archaeal map) and the coordinates for EM-based models are deposited in the Protein Data Bank (3J15 and 3J16). Reprints and permissions information is available at www.nature.com/reprints. The authors declare no competing financial interests. Readers are welcome to comment on the online version of this article at www.nature.com/nature. Correspondence and requests for materials should be addressed to R.B. (beckmann@lmb.uni-muenchen.de) or T.B. (becker@lmb.uni-muenchen.de).

LETTER

doi:10.1038/nature10793

Abrupt acceleration of a 'cold' ultrarelativistic wind from the Crab pulsar

F. A. Aharonian[1,2], S. V. Bogovalov[3] & D. Khangulyan[4]

Pulsars are thought to eject electron–positron winds that energize the surrounding environment, with the formation of a pulsar wind nebula[1]. The pulsar wind originates close to the light cylinder, the surface at which the pulsar co-rotation velocity equals the speed of light, and carries away much of the rotational energy lost by the pulsar. Initially the wind is dominated by electromagnetic energy (Poynting flux) but later this is converted to the kinetic energy of bulk motion[2]. It is unclear exactly where this takes place and to what speed the wind is accelerated. Although some preferred models imply a gradual acceleration over the entire distance from the magnetosphere to the point at which the wind terminates[3,4], a rapid acceleration close to the light cylinder cannot be excluded[5,6]. Here we report that the recent observations of pulsed, very high-energy γ-ray emission from the Crab pulsar[7–9] are explained by the presence of a cold (in the sense of the low energy of the electrons in the frame of the moving plasma) ultrarelativistic wind dominated by kinetic energy. The conversion of the Poynting flux to kinetic energy should take place abruptly in the narrow cylindrical zone of radius between 20 and 50 light-cylinder radii centred on the axis of rotation of the pulsar, and should accelerate the wind to a Lorentz factor of (0.5–1.0) × 10^6. Although the ultrarelativistic nature of the wind does support the general model of pulsars, the requirement of the very high acceleration of the wind in a narrow zone not far from the light cylinder challenges current models.

The Crab pulsar is one of the brightest γ-ray sources in the sky. Both the light curve and the energy spectrum have been studied[10] in great detail by the Large Area Telescope on board NASA's Fermi Gamma-ray Space Telescope (Fermi). The phase-averaged spectrum is best fitted by a power law with a photon index of $\alpha = 1.97$ and an exponential cut-off at $E_c = 5.8$ GeV (Fig. 1). Although modified 'outer gap' models[11] do allow an extension of the spectrum up to 10 GeV, the detection of pulsed, very high-energy (VHE) γ-ray emission demands a different radiation component. The extrapolation of the fluxes reported by Fermi to the VHE domain as a power law with photon index $\alpha \approx 3.8$, and the claim that such a formal fit is evidence that γ-rays of gigaelectronvolt (GeV) energies have the same magnetospheric origin as those of teraelectronvolt (TeV) energies[8,9,12], in fact requires a drastic revision of basic concepts used at present in magnetospheric models. Moreover, the assumption of a magnetospheric origin for radiation over the entire γ-ray domain contradicts the essentially different light curves reported at GeV (ref. 10) and TeV (refs 7, 9) energies (unless the production sites of these two components are well separated), as well as the apparent tendency of spectral flattening above 100 GeV (Fig. 1).

A natural and more plausible site of production of pulsed VHE γ-rays is the ultrarelativistic wind illuminated by photons originating in the pulsar's magnetosphere and/or the surface of the neutron star[13]. In the case of the Crab pulsar, the phase-averaged flux of the pulsed (magnetospheric) component exceeds the flux of the thermal emission of the neutron star by two orders of magnitude. The combination of the hard spectral energy distribution of the pulsed emission and the

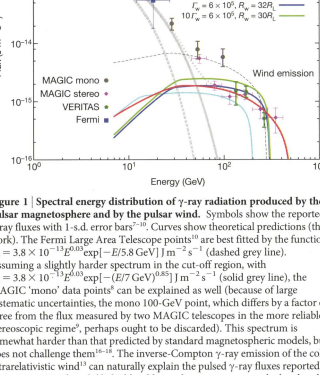

Figure 1 | Spectral energy distribution of γ-ray radiation produced by the pulsar magnetosphere and by the pulsar wind. Symbols show the reported γ-ray fluxes with 1-s.d. error bars[7–10]. Curves show theoretical predictions (this work). The Fermi Large Area Telescope points[10] are best fitted by the function $F_E = 3.8 \times 10^{-13} E^{0.03} \exp[-E/5.8\ \mathrm{GeV}]\ \mathrm{J\ m^{-2}\ s^{-1}}$ (dashed grey line). Assuming a slightly harder spectrum in the cut-off region, with $F_E = 3.8 \times 10^{-13} E^{0.03} \exp[-(E/7\ \mathrm{GeV})^{0.85}]\ \mathrm{J\ m^{-2}\ s^{-1}}$ (solid grey line), the MAGIC 'mono' data points[8] can be explained as well (because of large systematic uncertainties, the mono 100-GeV point, which differs by a factor of three from the flux measured by two MAGIC telescopes in the more reliable stereoscopic regime[9], perhaps ought to be discarded). This spectrum is somewhat harder than that predicted by standard magnetospheric models, but does not challenge them[14–18]. The inverse-Compton γ-ray emission of the cold ultrarelativistic wind[13] can naturally explain the pulsed γ-ray fluxes reported[7–9] above 100 GeV. The solid light-blue, blue and green curves are calculated under the assumption of 'instant' acceleration of the wind at the fixed radius R_w. In principle, the acceleration can start earlier, but closer to the light cylinder the acceleration rate should be modest; otherwise it would lead to overproduction of inverse-Compton γ-rays. Earlier acceleration is demonstrated by the dashed black curve, which is calculated under the assumption that acceleration starts at the light cylinder with a rate that increases in proportion with R^3 up to $R_w = 30R_L$, where the Lorenz factor equals 5.5×10^5 (Supplementary Information). The solid red curve corresponds to the case in which the Poynting flux transformation takes place within the $20R_L$–$50R_L$ zone, assuming the wind's acceleration rate to be independent of distance; the maximum Lorentz factor, achieved at $50R$, is set to 10^6. (The dotted grey line corresponds to the superposition of the red and solid grey lines and shows the transition between the two radiation components.) Because of the decrease in the density of target photons with distance, the main fraction of VHE radiation is produced at around $30R_L$ with a Lorentz factor close to 5×10^5. This explains the general similarity of the red curve to the instant-acceleration curves, apart from in the highest-energy region, where the sharp cut-off of the red curve is shifted to ~500 GeV.

[1]Dublin Institute for Advanced Studies, School of Cosmic Physics, 31 Fitzwilliam Place, Dublin 2, Ireland. [2]Max Planck Institute for Nuclear Physics, Saupferchreckweg 1, 69117 Heidelberg, Germany. [3]National Research Nuclear University (MEPhI), Kashirskoe shosse 31, Moscow, 115409, Russia. [4]Institute of Space and Astronautical Science/JAXA, 3-1-1 Yoshinodai, Chuo-ku, Sagamihara, Kanagawa 252-5210, Japan.

reduction of the Compton cross-section due to the Klein–Nishina effect means that the X-ray band is the main contributor to the Comptonization of the wind. The X-ray flux is well measured up to 100 keV (ref. 14) and therefore the calculations of the inverse-Compton radiation depend basically on the site and the dynamics (speed) of transformation of the Poynting flux to kinetic energy of bulk motion.

We assume that at a distance R_w from the pulsar, the wind is accelerated to the Lorentz factor Γ_w (Fig. 2). Particles of the accelerated wind cannot move purely radially, because the wind should carry both the energy and the angular momentum lost by the pulsar. From the relation between the rotation energy (E_{rot}) and angular momentum (M_{rot}) losses, $\dot{E}_{rot} = \Omega \dot{M}_{rot}$, where Ω is the angular velocity of the rotating sphere and a dot denotes a time derivative, we can define the trajectory of the wind particles. Indeed, each particle of the wind carries energy $\Gamma_w mc^2$ and angular momentum $\Gamma_w m r_\perp v$, where m, $r_\perp$ and v are the particle's mass, lever arm and speed, respectively, and c is the speed of light. Because $\Gamma_w m r_\perp v\Omega = \Gamma_w mc^2$, particles in the accelerated wind move along straight lines, tangent to the light cylinder. Therefore, all photons emitted by the magnetosphere will collide with electrons of the wind at a non-zero angle, θ, resulting in inverse-Compton γ-rays. The γ-ray production efficiency depends on the electron Lorentz factor, the density of the target photons and the interaction angle. Because the cold wind carries almost the entire spin-down luminosity, even a tiny efficiency of about $\kappa \approx 10^{-6}$ should be sufficient to produce detectable γ-rays at an energy flux level of $F_E = \kappa \dot{E}_{rot}/4\pi d^2 \approx 10^{-15}$ J m^{-2} s^{-1}, where $d \approx 6 \times 10^{19}$ m is the distance to the Crab.

Generally, the light curve of the target photons should be reflected in the time structure of the inverse-Compton γ-ray signal; however, they cannot be identical, owing, for example, to the effects related to the specifics of the anisotropic inverse-Compton scattering. More importantly, the geometrical effects may lead to non-negligible differences between the arrival times of the target photon and the secondary γ-ray pulses (Fig. 3). For wind located close to the light cylinder, the γ-ray signal seems shifted in time relative to the reported γ-ray data, by $\Delta t \approx 0.1T$. By contrast, for wind acceleration at $R_w = 30R_L$, the widths and the positions of the predicted and observed γ-ray peaks (P1 and P2, respectively) are in very good agreement. However, whereas in the case of the isotropic wind the predicted P1/P2 flux ratio of the γ-ray signal mimics the X-ray light curve[15] (Fig. 3, black crosses), the reported γ-ray data[7,9] seem to correspond to a smaller ratio, P1/P2 < 1. This can be explained by there being a non-negligible wind anisotropy, which would introduce noticeable corrections to the shape of the γ-ray light curve in general and to the P1/P2 ratio in particular (Fig. 3). The large uncertainties in the present γ-ray data prevent us from a reaching a strong conclusion in this regard, but the improvement of the quality of VHE γ-ray light curves should in future allow the strength and the character of the wind anisotropy to be decisively probed.

GeV γ-rays have a light curve[10] that is essentially different from the reported VHE light curves[7,9]. This can be interpreted as a result of the production of GeV and TeV γ-rays in regions well separated from each other. This conclusion is supported by the spectral energy distribution of the time-averaged GeV and TeV signals. As demonstrated in Fig. 1, the entire γ-ray region can be considered a superposition of two separate components. Indeed, by introducing a new, flat-spectrum VHE component of the Comptonized wind, in addition to the nominal (magnetospheric) GeV component, the reported data in the GeV-to-TeV energy intervals can be smoothly matched.

Although inverse-Compton γ-rays are produced by mono-energetic electrons, the spectral energy distribution of γ-rays in the range of tens to hundreds of GeV is quite flat. This is caused by the combination of effects related to the broad power-law distribution of seed photons and the transition of the Compton cross-section from the Thomson regime to the Klein–Nishina regime. On the other hand, the spectrum is expected to have a very sharp cut-off at $E = \Gamma_w mc^2$. This not only can serve as a distinct feature for the identification of the wind origin of γ-rays, but also should allow us to determine the Lorentz factor of the wind. In fact, the measurements available at present do not allow strong deviation of the Lorentz factor from 5×10^5. We note that the calculations do not depend on the 'magnetization parameter' σ (the ratio of the electromagnetic energy flux to the kinetic energy flux) as long as $R_w \gg R_L$. However, formally we can explain the pulsed VHE emission even for $\sigma \geq 1$. In this case, the acceleration should occur closer to the pulsar ($R_w \propto 1/\sigma^{1/2}$) to compensate for the reduction in the wind's kinetic energy. But in this case, the inverse-Compton γ-ray radiation is expected to have quite different spectral and temporal features.

The above estimates of the location of wind's acceleration site and its Lorentz factor are quite robust, but they are obtained under the assumption that the transformation of the Poynting flux proceeds very quickly, at a specific radius between R_w and $R_w \pm \delta R_w$ with $\delta R_w/R_w \leq 1$. This is not an obvious assumption, but is instead a working hypothesis that the wind acceleration takes place in a narrow zone at the radius $R_w \approx 30R_L$. We cannot a priori exclude the possibility

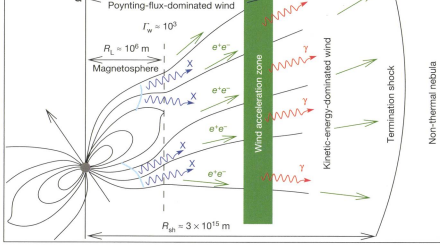

Figure 2 | Complex comprising the pulsar magnetosphere, the ultrarelativistic wind and the pulsar wind nebula. Dense electron (e^-)–positron (e^+) plasma produced in the pulsar magnetosphere by pair creation processes[19] initiates an electron–positron wind at the light cylinder, which has radius $R_L \approx 10^6$ m. Initially, the rotational energy lost by the pulsar, $\dot{E}_{rot} = 5 \times 10^{31}$ J s^{-1}, is released mainly in the form of electromagnetic energy (Poynting flux) and the wind's Lorentz factor therefore cannot be very large. At a distance R_w, the Poynting flux is converted to the kinetic energy of bulk motion (green zone), leading to an increase in the bulk-motion Lorentz factor to at least[20] $\Gamma_w \approx 10^4$. The termination of the wind by a standing reverse shock at $R_{sh} \approx 3 \times 10^{15}$ m boosts the energy of the electrons to 10^{15} eV and randomizes their pitch angles[2]. The radiative cooling of these electrons through the synchrotron and inverse-Compton processes results in an extended non-thermal source[21–23], the Crab nebula.

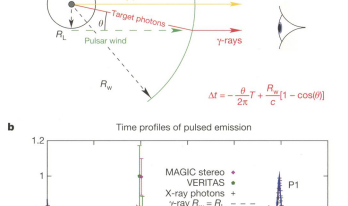

Figure 3 | Formation of the pulsed VHE inverse-Compton γ-ray signal in the wind of the Crab pulsar. a, Geometry of the inverse Compton scattering of magnetospheric X-rays by the electron–positron wind. **b**, Theoretical γ-ray light curves of the wind presented together with the reported VHE data[7,9]. The velocity of the accelerated wind is tangential to the light cylinder (the direction of motion of electrons towards the observer is shown by the dashed green arrow). The interaction of electrons with the magnospheric X-rays occurs predominantly at a distance $R \approx R_w$, where the wind is accelerated. Owing to the decrease in the target photon density with distance, the production of inverse-Compton γ-rays is suppressed at larger distances. The target X-ray photon converted to a VHE γ-ray photon reaches the observer earlier than an 'identical' photon emitted directly towards the observer. Two factors contribute to the time shift, Δt: the up-scattered X-ray photon is emitted by the pulsar earlier, by a time $(\theta/2\pi)T$, where T is the pulsar period; and it travels an additional path length of $R_w[1-\cos(\theta)]$. For $R_w \gg R_L$, the time shift is negligibly small: $\Delta t \approx -(T/4\pi)R_L/R_w$. For acceleration of the isotropic pulsar wind at $R_w = 30R_L$, the γ-ray light curve (solid blue line) closely resembles the shape of the measured X-ray light curve[10] (black crosses). For wind accelerated close to the light cylinder, the γ-ray light curve is shifted and somewhat broadened by comparison with wind accelerated at $R_w \gg R_L$. The anisotropy of the wind can also strongly deform the γ-ray light curve; in particular, it can change the ratio of the fluxes corresponding to peaks P1 and P2. The solid red line is calculated for an anisotropy factor proportional to the square of the sine of the angle between the line of sight and the direction of the magnetic momentum. This light curve seems to be in better agreement with the VERITAS[7] and MAGIC[9] points than the light curve corresponding to the fully isotropic wind, although the statistical and systematic uncertainties of observations (only Poisson error bars corresponding to the total count rates are shown on the plot) do not allow a definite conclusion in this regard.

that the wind is gradually accelerated starting from the edge of the magnetosphere, but our numerical calculations show that this cannot be the case (Fig. 1 and Supplementary Information). This is because the gradual acceleration would lead to a large number of high-energy electrons being accelerated close to the light cylinder and, consequently, to the prolific production of inverse-Compton γ-rays, in contradiction with the reported fluxes. Thus, the effective acceleration of the wind should start not much before the radius of $30R_L$ and not much beyond it. Such a case, assuming a linear acceleration rate of $\Gamma(R) = \Gamma_0 + a(R/R_L - 1)$ within the $20R_L$–$50R_L$ radial interval and a maximum Lorenz factor of 10^6 achieved at $50R_L$, is shown in Fig. 1. The corresponding γ-ray spectrum is smoother than the energy spectra predicted in the case of an instant acceleration, and better fits the VHE spectral points (Fig. 1) with the position of the sharp cut-off in the γ-ray spectrum shifted to 500 GeV. Although the wind acceleration within the $20R_L$–$50R_L$ interval seems to be a physically more realistic scenario than an instant acceleration, this is still quite a narrow zone and the acceleration of the wind up to the Lorentz factor of 10^6 is therefore quite abrupt. This conclusion does not agree with those of alternative models, for example the so-called reconnection models of pulsar wind nebulae[3,4] based on the assumption that the transformation of the Poynting flux to kinetic energy of bulk motion is a slow process that takes place over the entire region of the unshocked wind.

Received 5 September; accepted 15 December 2011.
Published online 15 February 2012.

1. Rees, M. J. & Gunn, J. E. The origin of the magnetic field and relativistic particles in the Crab Nebula. *Mon. Not. R. Astron. Soc.* **167,** 1–12 (1974).
2. Kennel, C. F. & Coroniti, F. V. Magnetohydrodynamic model of Crab nebula radiation. *Astrophys. J.* **283,** 710–730 (1984).
3. Coroniti, F. V. Magnetically striped relativistic magnetohydrodynamic winds: the Crab Nebula revisited. *Astrophys. J.* **349,** 538–545 (1990).
4. Lyubarsky, Y. & Kirk, J. G. Reconnection in the striped pulsar wind. *Astrophys. J.* **547,** 437–448 (2001).
5. Vlahakis, N. Ideal magnetohydrodynamic solution to the σ problem in Crab-like pulsar winds and general asymptotic analysis of magnetized outflows. *Astrophys. J.* **600,** 324–337 (2004).
6. Beskin, V. S. & Nokhrina, E. E. The effective acceleration of plasma outflow in the paraboloidal magnetic field. *Mon. Not. R. Astron. Soc.* **367,** 375–386 (2006).
7. Aliu, E. *et al.* Detection of pulsed gamma rays above 100 GeV from the Crab pulsar. *Science* **334,** 69–72 (2011).
8. Aleksić, J. *et al.* Observations of the Crab pulsar between 25 and 100 GeV with the MAGIC I telescope. *Astrophys. J.* **742,** 43 (2011).
9. Aleksić, J. *et al.* Phase-resolved energy spectra of the Crab Pulsar in the range of 50-400 GeV measured with the MAGIC Telescopes. *Astron. Astrophys.* (submitted); preprint at (http://arxiv.org/abs/1109.6124) (2011).
10. Abdo, A. A. *et al. Fermi* Large Area Telescope observations of the Crab pulsar and nebula. *Astrophys. J.* **708,** 1254–1267 (2010).
11. Tang, A. P. S., Takata, J., Jia, J. J. & Cheng, K. S. A revisit of the phase-resolved X-ray and γ-ray spectra of the Crab pulsar. *Astrophys. J.* **676,** 562–572 (2008).
12. Lyutikov, M., Otte, N. & McCann, A. The very-high energy emission from pulsars: a case for inverse Compton scattering. *Astrophys. J.* (submitted); preprint at (http://arxiv.org/abs/1108.3824) (2011).
13. Bogovalov, S. V. & Aharonian, F. A. Very-high-energy γ radiation associated with the unshocked wind of the Crab pulsar. *Mon. Not. R. Astron. Soc.* **313,** 504–514 (2000).
14. Kuiper, L. *et al.* The Crab pulsar in the 0.75–30 MeV range as seen by the CGRO COMPTEL. A coherent high-energy picture from soft X-rays to high-energy γ-rays. *Astron. Astrophys.* **378,** 918–935 (2001).
15. Rots, A. H. *et al.* Absolute timing of the Crab pulsar with the Rossi X-Ray Timing Explorer. *Astrophys. J.* **605,** L129–L132 (2004).
16. Hirotani, K. Outer-gap versus slot-gap models for pulsar high-energy emissions: the case of the Crab pulsar. *Astrophys. J.* **688,** 1254–1267 (2010).
17. Osmanov, Z. & Rieger, F. M. On particle acceleration and very high energy γ-ray emission in Crab-like pulsars. *Astron. Astrophys.* **502,** L25–L28 (2008).
18. Chkheidze, N., Machabeli, G. & Osmanov, Z. On the very high energy spectrum of the Crab pulsar. *Astrophys. J.* **730,** 62 (2011).
19. Sturrock, P. A. A model of pulsars. *Astrophys. J.* **164,** 529–556 (1971).
20. Wilson, D. B. & Rees, M. J. Induced Compton scattering in pulsar winds. *Mon. Not. R. Astron. Soc.* **185,** 297–304 (1978).
21. Gould, R. J. High-energy photons from the Compton-synchrotron process in the Crab nebula. *Phys. Rev. Lett.* **15,** 577–579 (1965).
22. de Jager, O. C. & Harding, A. K. The expected high-energy to ultra-high-energy γ-ray spectrum of the Crab nebula. *Astrophys. J.* **283,** 710–730 (1992).
23. Atoyan, A. M. & Aharonian, F. A. On the mechanisms of γ radiation in the Crab nebula. *Mon. Not. R. Astron. Soc.* **278,** 161–172 (1992).

Supplementary Information is linked to the online version of the paper at www.nature.com/nature.

Acknowledgements We would like to thank J. Cortina, E. de Ona Wilhemi, S. Klepser and N. Otte for information about high-energy γ-ray observations. We also appreciate discussions with F. Rieger, D. Jones and P. Gandhi.

Author Contributions F.A.A., S.V.B. and D.K. jointly contributed in comparable proportions to all aspects of the work, including the calculations and preparation of the manuscript.

Author Information Reprints and permissions information is available at www.nature.com/reprints. The authors declare no competing financial interests. Readers are welcome to comment on the online version of this article at www.nature.com/nature. Correspondence and requests for materials should be addressed to F.A.A. (felix.aharonian@dias.ie).

LETTER

doi:10.1038/nature10779

Wetting of flexible fibre arrays

C. Duprat[1], S. Protière[2,3], A. Y. Beebe[1] & H. A. Stone[1]

Fibrous media are functional and versatile materials, as demonstrated by their ubiquity both in natural systems such as feathers[1–4] and adhesive pads[5] and in engineered systems from nanotextured surfaces[6] to textile products[7], where they offer benefits in filtration, insulation, wetting and colouring. The elasticity and high aspect ratios of the fibres allow deformation under capillary forces, which cause mechanical damage[8], matting[5,9] self-assembly[10,11] or colour changes[12], with many industrial and ecological consequences. Attempts to understand these systems have mostly focused on the wetting of rigid fibres[13–17] or on elastocapillary effects in planar geometries[18] and on a fibre brush withdrawn from an infinite bath[19]. Here we consider the frequently encountered case of a liquid drop deposited on a flexible fibre array and show that flexibility, fibre geometry and drop volume are the crucial parameters that are necessary to understand the various observations referred to above. We identify the conditions required for a drop to remain compact with minimal spreading or to cause a pair of elastic fibres to coalesce. We find that there is a critical volume of liquid, and, hence, a critical drop size, above which this coalescence does not occur. We also identify a drop size that maximizes liquid capture. For both wetting and deformation of the substrates, we present rules that are deduced from the geometric and material properties of the fibres and the volume of the drop. These ideas are applicable to a wide range of fibrous materials, as we illustrate with examples for feathers, beetle tarsi, sprays and microfabricated systems.

Owing to the numerous environmental and industrial applications of fibrous media, their wetting has been studied extensively. Most research focuses on drops or flow on individual rigid fibres, often in an array. However, in most applications, the elasticity of the fibres is important, as evidenced from the matting of feather barbules[9], the shrinkage of porous fibre membranes[8], strengthening of paper after drying[20], the clumping of the setae of beetle tarsi after release of tarsal oil[5], or the collapse of micro- or nanopillar arrays[10–12]. Therefore, we are motivated by the interaction of a mist of drops with a deformable, or flexible, array of fibres. The basic elastocapillary response is observed in the behaviour of a liquid drop on a pair of fibres, which is where we begin.

For a perfectly wetting drop (that is, a drop that connects with the fibre with a zero contact angle) deposited on two parallel, rigid fibres, the minimization of surface energy yields three distinct drop shapes depending on the ratio of the distance between the fibres, $2d_0$ (measured from their outer surfaces), and their diameter, $2r$ (Fig. 1b). As d_0/r is decreased, the drop evolves from a bridge to a barrel shape and then spreads out into a liquid column[13–17]: a drop forms for $d_0/r > \sqrt{2}$, a column forms for $d_0/r < 0.57$ and there is non-uniqueness of the shape for $0.57 < d_0/r < \sqrt{2}$.

In this Letter, we investigate the behaviour of a perfectly wetting drop deposited onto two horizontal, flexible fibres that at one end are clamped, parallel to each other, a distance $2d_0 > 2\sqrt{2}r$ apart and at the other end are free to move (Methods and Fig. 1a). Our results can be extended to the case of partial wetting by adding as an additional parameter the effective contact angle, $\theta < \pi/2$ (Supplementary Fig. 4). We neglect gravitational effects because the fibres do not bend under their own weight and the drop sizes are smaller than the capillary length, l_c, above which gravitational effects become important. By $2d$ we denote the distance between the fibres at the drop location. When the drop is placed on the fibres close to the clamped ends, the fibres deflect inwards and the drop moves spontaneously towards the free ends, which are closer together (Fig. 1c and Supplementary Movie 2), as observed for a drop in a wedge[21]. As the drop advances, the deflection increases, that is, d/r continuously decreases. The drop accelerates, elongates and then spreads spontaneously between the fibres, drawing them together finally to form a liquid column between coalesced fibres.

We performed a large set of experiments to characterize the final state as a function of the drop volume, V; the fibre length, L; and the ratio d_0/r (Methods). For every value of d_0/r, we find three different final states as L and V are varied (Fig. 2a–c). Whereas the final state (drop or column) of a finite volume of liquid deposited on two rigid fibres depends on only one parameter, that is, d_0/r, and is hence independent of the drop volume and fibre length, we find that the final equilibrium state for a drop on two flexible fibres depends on six

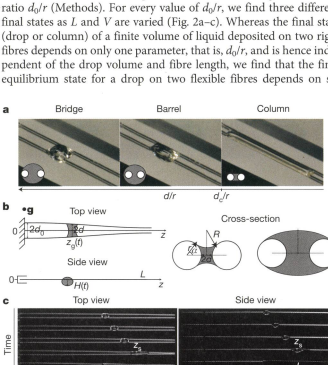

Figure 1 | Shape transitions of a drop sitting on two parallel fibres. a, A drop of perfectly wetting liquid (silicone oil) of volume 2 µl deposited on two parallel, rigid glass fibres (radius, $r = 0.145$ mm) adopts three different shapes depending on the distance between the fibres: a 'bridge' ($d_0/r = 2.5$), a 'barrel' ($d_0/r = 1.5$) and a column ($d_0/r = 1$). d_c, critical distance at which the drop-to-column transition occurs. **b**, Experimental set-up used to investigate the behaviour of a drop deposited on two flexible fibres, which are clamped at one end and free to move at the other. Left: top and side views, recorded simultaneously using a mirror. Right: expected cross-sections for a concave liquid column and a convex drop. The direction of gravity is indicated by **g**. **c**, Typical experiment with $d_0/r = 2.7$, $V = 1.5$ µl and $L = 4$ cm. The time between successive images is 25 s. When the drop is deposited on flexible fibres, the fibres deflect inward. The drop spontaneously moves towards the free ends of the fibres. At a given location, z_s, the drop starts spreading and the fibres are drawn together. The final wet length is denoted L_s.

[1]Department of Mechanical and Aerospace Engineering, Princeton University, Princeton, New Jersey 08544, USA. [2]CNRS, UMR 7190, Institut Jean le Rond d'Alembert, F-75005 Paris, France. [3]UPMC Université Paris 06, UMR 7190, Institut Jean le Rond d'Alembert, F-75005 Paris, France.

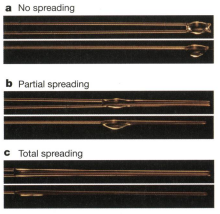

Figure 2 | The three different final states of a drop between two flexible fibres. a–c, Top and side views of the final state obtained for $d_0/r = 2.6$; a fixed volume, $V = 2$ µl; and increasing length, $L = 3$, 3.5 and 4 cm. The final state changes from one of no spreading to one of partial spreading to one of total spreading as L increases. **d**, Phase diagram of the different regimes for $d_0/r = 2.1$. Depending on L and V, three different regimes are observed: the drop either moves towards the ends without spreading (diamonds; **a**), spreads until partial depletion of the drop (circles; **b**) or spreads completely into a liquid column (squares; **c**). The solid and dashed curves correspond to equations (2) and (3), respectively. The vertical dashed line corresponds to $L = L_{dry}$.

parameters: r; d_0; L; the bending stiffness, B, of the fibre; the surface tension, γ; and V. For short fibres ($L \ll 2$ cm in the system presented in Fig. 2) and almost all drop volumes, the fibres deflect slightly inwards and the drop moves towards the free ends, but there is no spreading (Fig. 2a and Supplementary Movie 1). For longer fibres, there is a range of drop volumes such that when we increase L, the deflection increases and the whole drop spreads into a column ('total spreading'; Fig. 2c and Supplementary Movie 2). Alternatively, for sufficiently large volumes, we observe a state of 'partial spreading', where there is a liquid column with a smaller drop remaining at the edge (Fig. 2b and Supplementary Movie 3). We summarize in Fig. 2d our results in a phase diagram of V versus L, which suggests that a critical size of drops in a spray can trigger coalescence of a fibrous material.

To understand the transitions between the different regimes in Fig. 2d, we first consider the case of long fibres, for which either partial or total spreading occurs for all volumes investigated. We fix the fibre length and measure the length, L_s, along which the liquid spreads for various drop volumes (Fig. 3a). For small V, the whole drop spreads into a liquid column. As V increases, the column length increases until, above a critical volume, V_c, a drop remains at the wider end of the column and the length L_s actually decreases (Fig. 3a). The existence of a maximum spreading length here is a consequence of elasticity.

We can understand the maximum spreading length, $L_{s,max}$, reached at V_c as a balance between elasticity and capillarity. There is a minimal distance, L_{dry}, along which the dry portions of the fibres can be bent by capillary forces. This is determined by minimizing the total energy of the system[22], yielding

$$L_{dry} = \left(\frac{9Bd_0^2}{2\gamma r S(\alpha)}\right)^{1/4} \quad (1)$$

where $S(\alpha)$ is a geometric factor evaluated approximately for a flat liquid column as $S(\alpha = \pi/2) = \pi - 2$. This length is the minimum length of the fibres beyond which collapse, or significant deformation, can occur. For a given d_0/r ratio, L_{dry} is constant and the maximum wet length, $L_{s,max}$, increases linearly with L, that is, $L_{s,max} = L - L_{dry}$, in agreement with our experiments (Supplementary Fig. 1). This elastocapillary balance results in an optimal, or critical, drop volume for which the spreading length is maximal: $V_c = A(\alpha)L_{s,max}$, where $A(\alpha)$ is the column cross-section ($A(\pi/2) \approx \pi r^2$ for a flat column). The boundary between total and partial spreading is then predicted to be

$$V = V_c = \pi r^2 (L - L_{dry}) \quad (2)$$

which is also in agreement with the experimental transition (Fig. 2d). When liquid is added to this maximum column (Supplementary Fig. 2), the configuration is unstable: the liquid forms a drop at the wider end of the column. Minimization of the surface energy causes the liquid to retract to form this spherical drop, decreasing the length of the column.

To understand the critical drop size beyond which no spreading (Fig. 2a) and, hence, no fibre coalescence occurs, we measured the spacing, d_s, at which the drop starts spreading. We find that the ratio

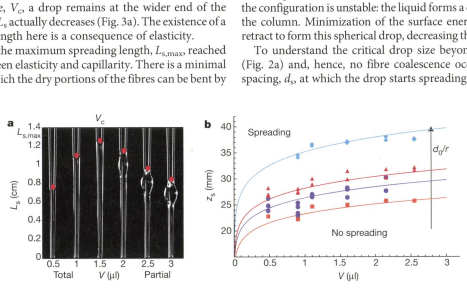

Figure 3 | Influence of the initial drop volume on the final state. **a**, Transition between total and partial spreading: evolution of the spreading length, L_s, with the volume, V, of the drop for $d_0/r = 2.6$ and $L = 3.5$ cm. We observe an optimum (maximum L_s) at a critical volume of $V_c = 1.5$ µl. **b**, Transition between spreading and no spreading: evolution of the position of the drop at spreading, z_s, with V for $d_0/r = 1.9$ (orange), 2.4 (purple), 2.7 (red) and 4.2 (blue). The position of the drop at spreading is independent of the fibre length and increases with increasing volume, spacing and fibre rigidity (that is, the bending modulus, which is proportional to r^4). The solid lines correspond to the theoretical prediction (Supplementary Information, equation (2)).

$d_0/r = 1.11 \pm 0.07$ is constant, independent of V, L and d_0/r. We conclude that spreading occurs when locally the spacing between the fibres is such that a liquid column is energetically favourable relative to a drop. This criterion for spreading is similar to that obtained theoretically for rigid fibres[15] and similar to that found in our experiments on rigid glass fibres: $d_0/r = 1.04 \pm 0.07$.

Next we estimated the critical drop volume responsible for this spreading, where liquid is captured in a column. The drop is in a barrel shape (Fig. 1a) and thus is pierced by the two fibres. The capillary force applied by the drop, $F \approx 2\gamma l^*$, where l^* is the typical length of the contact line, brings the fibres together. Coalescence of fibres will therefore occur if F is great enough to achieve a deflection of $d_0 - d_s$ along the fibres, that is, if the capillary torque, Fz_s, where z_s is the position of the drop, equals the elastic resisting torque, $B(d_0 - d_s)/z_s^2$. For a given value of V and, hence, F, this estimate leads to a critical drop position, $z_s^3 \propto B(d_0 - d_s)/F$, below which no spreading will occur, which is also verified experimentally (Fig. 3b). For a fixed value of d_0, z_s increases with increasing volume and, hence, the capillary force decreases. Therefore, for a given fibre length, there is a minimal force, that is, a maximal drop volume, for spreading to occur, set by $z_s = L$. The force $F \approx 2\gamma l^*$ depends on the complex shape of the contact line, which has a typical length $l^* \propto 2\pi r d_0 V^{-1/3}$ (Supplementary Information). Combining these results yields the critical volume for spreading

$$V_s \approx \left(\beta \frac{\gamma d_0 r L^3}{B(d_0 - d_s)}\right)^3 \tag{3}$$

where the constant β depends only on the complex shape of the drop (Supplementary Fig. 3); this result involves all of the geometric and material properties. The boundary between the regimes of spreading and no spreading, $V = V_s$, is in agreement with the experiments (Fig. 2d).

Because the final state of the drop placed on the fibre array depends on the six parameters r, d_0, L, B, γ and V, we conclude by dimensional analysis that the system is characterized by three parameters, $L/L_{s,max}$, V/V_c and d_0/r where $L_{s,max} = L - L_{dry}$ (from equation (1)) and $V_c = \pi r^2 L_{s,max}$ (from equation (2)). We define a phase diagram of the three possible final states in the space of the two parameters $L/L_{s,max}$ and V/V_c (Fig. 4a). First we identify a threshold, $V/V_c = 1$, below which a drop will always totally spread, which maximizes the wetted length and the amount of trapped liquid. Second, for $V/V_c > 1$, the spreading is partial: the remaining edge drop can be shed by any perturbation such as shaking, which results in a smaller amount of liquid being captured by the fibre array. The transition from spreading to no spreading ($V > V_s$) is identified by equation (3) and depends on the parameter d_0/r as reflected by the successive hyperbolic curves in Fig. 4a. For partial wetting, θ, the effective contact angle, should be included in equations (1), (2) and (3) (Supplementary Information and Supplementary Figs 4–7). All of the experimental data (symbols in Fig. 4a) obtained by varying all of the parameters are well within each regime defined by the model.

This map allows us to predict the interaction of natural or engineered fibrous materials with a mist of drops. An example of a natural fibre array is a bird feather, which consists of well-ordered hair-like structures (barbs and barbules) that produce hydrophobicity and thermal insulation[1,3]. Small amounts of oil disrupt this arrangement by clumping adjacent barbules, affecting their water repellency and insulating properties and thus reducing the survival rate of oiled birds[9,23]. We sprayed a polydisperse aerosol of oil on goose feathers and observed all three possible final states (Fig. 4b). Using our model system, we find that a volume of oil less than V_c (here a drop radius less than 20 μm) spreads, thus clumping adjacent barbules and making the cleaning process difficult. Drops larger than V_s (drop radius, 140 μm) do not spread and may be dislodged from the bird's plumage. These results are in agreement with our map (Fig. 4a). Despite complex initial conditions (multiple fibres and/or drops, different wettabilities or surface roughnesses) the final states can thus be captured by our model and we can predict the main effects arising when a mist of drops interacts with a dilute fibre array.

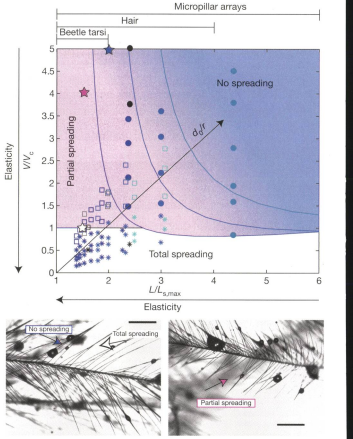

Figure 4 | Aerosol size and fibre matrix properties needed to collect, trap or displace a known volume of liquid. a, Map of the three spreading regimes as a function of the two dimensionless parameters $L/L_{s,max}$ and V/V_c. The solid curves show three limits for $d_0/r = 2.4$, 2.7 and 4.2 and the points show data for total spreading (asterisks), partial spreading (squares) and no spreading (circles) of silicone oil (total wetting, $d_0/r = 2.1$; blue and purple points) and water (partial wetting, $d_0/r = 3$; black and grey points). Stars correspond to the three situations observed in **b**. **b**, Microscope pictures of goose feathers sprayed with oil (smaller drops have volumes of order 10^{-14}–10^{-13} m^3), showing no spreading ($d_0/r = 4.8$, $L/L_{s,max} = 2$, $V/V_c \approx 5$; blue star in **a**), total spreading ($d_0/r = 3.4$, $L/L_{s,max} = 1.5$ and $L_s = L_{s,max} = 0.8$ mm; white star in **a**) and partial spreading ($d_0/r = 3.5$, $L/L_{s,max} = 1.5$, $V/V_c \approx 4$; pink star in **a**) in agreement with our predictions. Scale bars, 500 μm.

In addition, aerosol-removal filters, hairsprays, adhesive pads for insects and some applications in microstructure design require total spreading, that is, optimal coating of the fibres or maximal liquid capture. Conversely, fibres in living systems may have evolved a certain length or material properties to adapt to their environmental conditions. For example, we can now use our model to make quantitative estimates for various fibrous media and liquids (Supplementary Table 1) as reported in the universal map (Fig. 4a). For beetles, we predict that drops of optimal diameter 5 μm released from ventral pores travel along the setae and spread totally (that is, without liquid loss) where the tarsi contact a substrate; we predict that the collapse of pillars in microfabrication, observed during solvent evaporation[10–12], could be controlled by depositing an optimum volume of liquid (drops of diameter 0.9–5.4 μm); and we predict that microstructures could be designed to respond (by changing colour) to aerosols of different drop sizes because light scattering is influenced by clustering of the microelements. These examples illustrate the wide range of flexible systems that could be controlled using elastocapillarity and an optimally chosen drop volume.

METHODS SUMMARY

The glass fibres (radius, $r = 0.145$ mm; bending stiffnesses, $B = 1 \times 10^{-6}$ N m^2 and $B = 7 \times 10^{-7}$ N m^2; length, 2 cm $< L <$ 5.5 cm) are clamped at one end, separated by a distance $2d_0$ ($d_0/r = 1.9, 2.1, 2.6$ and 4.3). A drop of silicone oil (viscosity, $\eta = 97$ mPa s; density, $\rho = 970$ kg m^{-3}; surface tension, $\gamma = 0.021$ N m^{-1}) of controlled volume V (0.48 µl $< V <$ 2.55 µl) precise to 5% for large volumes and to 10% for smaller volumes, is deposited onto the fibres with a micropipette, close to the clamped edge. The positions of the front, $z_f(t)$, and the rear, $z_r(t)$, of the drop (relative to the clamped end at $z = 0$), as well as the distance between the fibres, d, are recorded from the top with a digital camera. A mirror placed at 45° allows us to capture a simultaneous side view of the drop and measure its size, $H(z, t)$. We define the average position of the drop as $z_g = (z_f + z_r)/2$, and its length is $l = z_f - z_r$. The capillary length, $l_c = (\gamma/\rho g)^{1/2}$, is the length beyond which gravitational effects become more important than capillary effects. Here $l_c = 1.5$ mm.

Received 8 August; accepted 6 December 2011.

1. Rijke, A. M. & Jesser, W. A. The feather structure of dippers: water repellency and resistance to water penetration. *Wilson J. Ornithol.* **122,** 563–568 (2010).
2. Rijke, B. Y. A. M. The water repellency and feather structure of cormorants, Phalacrocoracidae. *J. Exp. Biol.* **48,** 185–189 (1968).
3. Dawson, C., Vincent, J., Jeronimidis, G., Rice, G. & Forshaw, P. Heat transfer through penguin feathers. *J. Theor. Biol.* **199,** 291–295 (1999).
4. Zi, J. *et al.* Coloration strategies in peacock feathers. *Proc. Natl Acad. Sci. USA* **100,** 12576–12578 (2003).
5. Eisner, T. & Aneshansley, D. J. Defense by foot adhesion in a beetle (Hemisphaerota cyanea). *Proc. Natl Acad. Sci. USA* **97,** 6568–6573 (2000).
6. Liu, K. & Jiang, L. Bio-inspired design of multiscale structures for function integration. *Nano Today* **6,** 155–175 (2011).
7. Eadie, L. & Ghosh, T. K. Biomimicry in textiles: past, present and potential. An overview. *J. R. Soc. Interface* **6,** 761–775 (2011).
8. Kamo, J., Hiram, T. & Kamada, K. Solvent-induced morphological change of microporous hollow fiber membranes. *J. Membr. Sci.* **70,** 217–224 (1992).
9. O'Hara, P. D. & Morandin, L. A. Effects of sheens associated with offshore oil and gas development on the feather microstructure of pelagic seabirds. *Mar. Pollut. Bull.* **60,** 672–678 (2010).
10. Pokroy, B., Kang, S. H., Mahadevan, L. & Aizenberg, J. Self-organization of a mesoscale bristle into ordered, hierarchical helical assemblies. *Science* **323,** 237–240 (2009).
11. Chandra, D. & Yang, S. Stability of high-aspect-ratio micropillar arrays against adhesive and capillary forces. *Acc. Chem. Res.* **43,** 1080–1091 (2010).
12. Chandra, D., Yang, S., Soshinsky, A., a. & Gambogi, R. J. Biomimetic ultrathin whitening by capillary-force-induced random clustering of hydrogel micropillar arrays. *ACS Appl. Mater. Interfaces* **1,** 1698–1704 (2009).
13. Princen, H. Capillary phenomena in assemblies of parallel cylinders III. Liquid columns between horizontal parallel cylinders. *J. Colloid Interface Sci.* **34,** 171–184 (1970).
14. Wu, X.-F., Bedarkar, A. & Vaynberg, K. A. Droplets wetting on filament rails: surface energy and morphology transition. *J. Colloid Interface Sci.* **341,** 326–332 (2010).
15. Bedarkar, A., Wu, X.-f. & Vaynberg, A. Wetting of liquid droplets on two parallel filaments. *Appl. Surf. Sci.* **256,** 7260–7264 (2010).
16. Minor, F. W., Schwartz, M., Wulkow, E., a. & Buckles, L. C. Part III: The behavior of liquids on single textile fibers. *Text. Res. J.* **29,** 940–949 (1959).
17. Keis, K., Kornev, K. G., Kamath, Y. K. & Neimark, A. V. in *Nanoengineered Nanofibrous Materials* (eds Guceri, S., Gogotsi, Y. G & Kuznetsov, V.) 173–180 (Kluwer, 2004).
18. Kwon, H.-M., Kim, H.-Y., Pulli, J. R. M. & Mahadevan, L. Equilibrium of an elastically confined liquid drop. *J. Appl. Phys.* **103,** 093519 (2008).
19. Roman, B. & Bico, J. Elasto-capillarity: deforming an elastic structure with a liquid droplet. *J. Phys. Condens. Matter* **22,** 493101 (2010).
20. Hubbe, M. A. Bonding between cellulosic fibers in the absence and presence of dry-strength agents - a review. *BioResources* **1,** 281–318 (2006).
21. Prakash, M., Quéré, D. & Bush, J. W. M. Surface tension transport of prey by feeding shorebirds: the capillary ratchet. *Science* **320,** 931–934 (2008).
22. Py, C., Bastien, R., Bico, J., Roman, B. & Boudaoud, A. 3D aggregation of wet fibers. *Europhys. Lett.* **77,** 44005 (2007).
23. Hartung, R. Energy metabolism in oil-covered ducks. *J. Wildl. Mgmt* **31,** 798–804 (1967).

Supplementary Information is linked to the online version of the paper at www.nature.com/nature.

Acknowledgements C.D. and H.A.S. acknowledge Unilever and the NFS for financial support. S.P. acknowledges financial support from the Emergence(s) Program of the City of Paris and CNRS and thanks Princeton University for its hospitality. We thank A. Lips and P. Warren for comments.

Author Contributions C.D. and S.P. designed the experiments; A.Y.B., C.D. and S.P. carried out the experiments; C.D., S.P. and H.A.S. discussed and interpreted the results; C.D. and H.A.S. developed the models; and C.D., S.P. and H.A.S. wrote the manuscript.

Author Information Reprints and permissions information is available at www.nature.com/reprints. The authors declare no competing financial interests. Readers are welcome to comment on the online version of this article at www.nature.com/nature. Correspondence and requests for materials should be addressed to H.A.S. (hastone@princeton.edu).

LETTER

doi:10.1038/nature10847

Recent contributions of glaciers and ice caps to sea level rise

Thomas Jacob[1]†, John Wahr[1], W. Tad Pfeffer[2,3] & Sean Swenson[4]

Glaciers and ice caps (GICs) are important contributors to present-day global mean sea level rise[1–4]. Most previous global mass balance estimates for GICs rely on extrapolation of sparse mass balance measurements[1,2,4] representing only a small fraction of the GIC area, leaving their overall contribution to sea level rise unclear. Here we show that GICs, excluding the Greenland and Antarctic peripheral GICs, lost mass at a rate of 148 ± 30 Gt yr^{-1} from January 2003 to December 2010, contributing 0.41 ± 0.08 mm yr^{-1} to sea level rise. Our results are based on a global, simultaneous inversion of monthly GRACE-derived satellite gravity fields, from which we calculate the mass change over all ice-covered regions greater in area than 100 km^2. The GIC rate for 2003–2010 is about 30 per cent smaller than the previous mass balance estimate that most closely matches our study period[2]. The high mountains of Asia, in particular, show a mass loss of only 4 ± 20 Gt yr^{-1} for 2003–2010, compared with 47–55 Gt yr^{-1} in previously published estimates[2,5]. For completeness, we also estimate that the Greenland and Antarctic ice sheets, including their peripheral GICs, contributed 1.06 ± 0.19 mm yr^{-1} to sea level rise over the same time period. The total contribution to sea level rise from all ice-covered regions is thus 1.48 ± 0.26 mm yr^{-1}, which agrees well with independent estimates of sea level rise originating from land ice loss and other terrestrial sources[6].

Interpolation of sparse mass balance measurements on selected glaciers is usually used to estimate global GIC mass balance[1,2,4]. Models are also used[3,7], but these depend on the quality of input climate data and include simplified glacial processes. Excluding Greenland and Antarctic peripheral GICs (PGICs), GICs have variously been reported to have contributed 0.43–0.51 mm yr^{-1} to sea level rise (SLR) during 1961–2004[3,7,8], 0.77 mm yr^{-1} during 2001–2004[8], 1.12 mm yr^{-1} during 2001–2005[1] and 0.95 mm yr^{-1} during 2002–2006[2].

The Gravity Recovery and Climate Experiment (GRACE) satellite mission[9] has provided monthly, global gravity field solutions since 2002, allowing users to calculate mass variations at the Earth's surface[10]. GRACE has been used to monitor the mass balance of selected GIC regions[11–14] that show large ice mass loss, as well as of Antarctica and Greenland[15].

Here we present a GRACE solution that details individual mass balance results for every region of Earth with large ice-covered areas. The main focus of this paper is on GICs, excluding Antarctic and Greenland PGICs. For completeness, however, we also include results for the Antarctic and Greenland ice sheets with their PGICs. GRACE does not have the resolution to separate the Greenland and Antarctic ice sheets from their PGICs. All results are computed for the same 8-yr time period (2003–2010).

To determine losses of individual GIC regions, we cover each region with one or more 'mascons' (small, arbitrarily defined regions of Earth) and fit mass values for each mascon (ref. 16 and Supplementary Information) to the GRACE gravity fields, after correcting for hydrology and for glacial isostatic adjustment (GIA) computed using the ICE-5G deglaciation model. We use 94 monthly GRACE solutions from the University of Texas Center for Space Research, spanning January 2003 to December 2010. The GIA corrections do not include the effects of post-Little Ice Age (LIA) isostatic rebound, which we separately evaluate and remove. All above contributions and their effects on the GRACE solutions are discussed in Supplementary Information.

Figure 1 shows mascons for all ice-covered regions, constructed from the Digital Chart of the World[17] and the Circum-Arctic Map of Permafrost and Ground-Ice Conditions[18]. Each ice-covered region is chosen as a single mascon, or as the union of several non-overlapping mascons. We group 175 mascons into 20 regions. Geographically isolated regions with glacierized areas less than 100 km^2 in area are excluded. Because GRACE detects total mass change, its results for an ice-covered region are independent of the glacierized surface area (Supplementary Information).

Mass balance rates for each region are shown in Table 1 (see Supplementary Information for details on the computation of the rates and uncertainties). We note that Table 1 includes a few positive rates, but none are significantly different from zero. We also performed an inversion with GRACE fields from the GFZ German Research Centre for Geosciences and obtained results that agreed with those from the Center for Space Research (Table 1) to within 5% for each region.

The results in Table 1 are in general agreement with previous GRACE studies for the large mass loss regions of the Canadian Arctic[12] and Patagonia[13], as well as for the Greenland and Antarctic ice sheets with

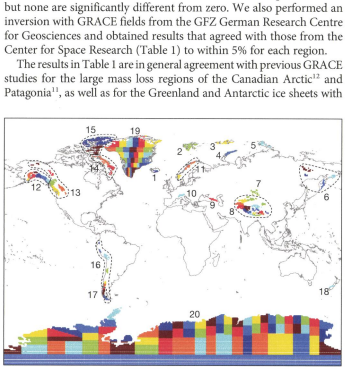

Figure 1 | Mascons for the ice-covered regions considered here. Each coloured region represents a single mascon. Numbers correspond to regions shown in Table 1. Regions containing more than one mascon are outlined with a dashed line.

[1]Department of Physics and Cooperative Institute for Environmental Studies, University of Colorado at Boulder, Boulder, Colorado 80309, USA. [2]Institute of Arctic and Alpine Research, University of Colorado at Boulder, Boulder, Colorado 80309, USA. [3]Department of Civil, Environmental, and Architectural Engineering, University of Colorado at Boulder, Boulder, Colorado 80309, USA. [4]National Center for Atmospheric Research, Boulder, Colorado 80305, USA. †Present address: Bureau de Recherches Géologiques et Minières, Orléans 45060, France.

Table 1 | Inverted 2003–2010 mass balance rates

Region	Rate (Gt yr^{-1})
1. Iceland	−11 ± 2
2. Svalbard	−3 ± 2
3. Franz Josef Land	0 ± 2
4. Novaya Zemlya	−4 ± 2
5. Severnaya Zemlya	−1 ± 2
6. Siberia and Kamchatka	2 ± 10
7. Altai	3 ± 6
8. High Mountain Asia	−4 ± 20
8a. Tianshan	−5 ± 6
8b. Pamirs and Kunlun Shan	−1 ± 5
8c. Himalaya and Karakoram	−5 ± 6
8d. Tibet and Qilian Shan	7 ± 7
9. Caucasus	1 ± 3
10. Alps	−2 ± 3
11. Scandinavia	3 ± 5
12. Alaska	−46 ± 7
13. Northwest America excl. Alaska	5 ± 8
14. Baffin Island	−33 ± 5
15. Ellesmere, Axel Heiberg and Devon Islands	−34 ± 6
16. South America excl. Patagonia	−6 ± 12
17. Patagonia	−23 ± 9
18. New Zealand	2 ± 3
19. Greenland ice sheet + PGICs	−222 ± 9
20. Antarctica ice sheet + PGICs	−165 ± 72
Total	−536 ± 93
GICs excl. Greenland and Antarctica PGICs	−148 ± 30
Antarctica + Greenland ice sheet and PGICs	−384 ± 71
Total contribution to SLR	1.48 ± 0.26 mm yr^{-1}
SLR due to GICs excl. Greenland and Antarctica PGICs	0.41 ± 0.08 mm yr^{-1}
SLR due to Antarctica + Greenland ice sheet and PGICs	1.06 ± 0.19 mm yr^{-1}

Uncertainties are given at the 95% (2σ) confidence level.

their PGICs[19]. Our results for Alaska also show considerable mass loss, although our mass loss rate is smaller than some previously published GRACE-derived rates that used shorter and earlier GRACE data spans (Supplementary Information). The global GIC mass balance, excluding Greenland and Antarctic PGICs, is -148 ± 30 Gt yr^{-1}, contributing 0.41 ± 0.08 mm yr^{-1} to SLR.

Mass balance time series for all GIC regions are shown in Fig. 2. The seasonal and interannual variabilities evident in these time series have contributions from ice and snow variability on the glaciers, as well as from imperfectly modelled hydrological signals in adjacent regions and from random GRACE observational errors. Interannual variability can affect rates determined over short time intervals. Figure 2 and Supplementary Table 2 show that there was considerable interannual variability during 2003–2010 for some of the regions, especially High Mountain Asia (HMA). The HMA results in Supplementary Table 2 show that this variability induces large swings in the trend solutions when it is fitted to subsets of the entire time period. These results suggest that care should be taken in extending the 2003–2010 results presented in this paper to longer time periods.

For comparison with studies in which PGICs are included with GICs, we upscale our GIC-alone rate to obtain a GIC rate that includes PGIC, based on ref. 3 (Supplementary Information). The result is that GICs including PGICs lost mass at a rate of 229 ± 82 Gt yr^{-1} (0.63 ± 0.23 mm yr^{-1} SLR), and that the combined ice sheets without their PGICs lost mass at 303 ± 100 Gt yr^{-1} (0.84 ± 0.28 mm yr^{-1} SLR). Although no other study encompasses the same time span, published non-GRACE estimates for GICs plus PGICs are larger: 0.98 ± 0.19 mm yr^{-1} over 2001–2004[8], 1.41 ± 0.20 mm yr^{-1} over 2001–2005[1] and 0.765 mm yr^{-1} (no uncertainty given) over 2006–2010[20]. These differences could be due to the small number of mass balance measurements those estimates must rely on, combined with uncertain regional glacier extents. In addition, there are indications from more recent non-GRACE measurements that the GIC mass loss rate decreased markedly beginning in 2005[20].

Our results for HMA disagree significantly with previous studies. A recent GRACE-based study[5] over 2002–2009 yields significantly

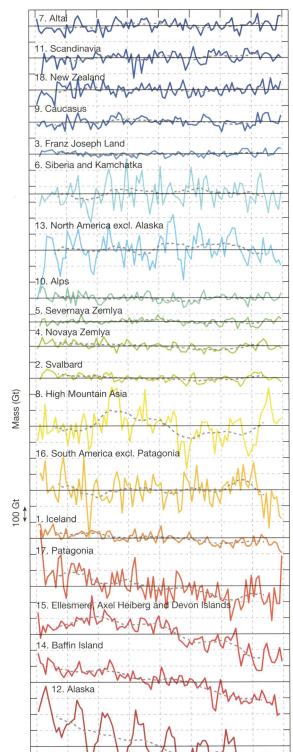

Figure 2 | Mass change during 2003–2010 for all GIC regions shown in Fig. 1 and Table 1. The black horizontal lines run through the averages of the time series. The grey lines represent 13-month-window, low-pass-filtered versions of the data. Time series are shifted for legibility. Modelled contributions from GIA, LIA and hydrology have been removed.

larger mass loss for HMA than does ours; we explain why the result of ref. 5 may be flawed in Supplementary Information. Conventional mass balance methods have been used to estimate a 2002–2006 rate of $-55\,\mathrm{Gt\,yr^{-1}}$ for this entire region[2], with $-29\,\mathrm{Gt\,yr^{-1}}$ over the eastern Himalayas alone, by contrast with our HMA estimate, of $-4 \pm 20\,\mathrm{Gt\,yr^{-1}}$ (Table 1). We show results for the four subregions of HMA (Fig. 3) in Table 1.

This difference prompts us to examine this region in more detail. GRACE mass trends show considerable mass loss across the plains of northern India, Pakistan and Bangladesh, centred south of the glaciers and at low elevations (Fig. 3a, b). Some of the edges of this mass loss region seem to extend over adjacent mountainous areas to the north, but much of that, particularly above north-central India, is leakage of the plains signal caused by the 350-km Gaussian smoothing function used to generate the figure. The plains signal has previously been identified as groundwater loss[16,21]. To minimize leakage in the HMA GIC estimates, additional mascons are chosen to cover the plains (Fig. 3a), the sum of which gives an average 2003–2010 water loss rate of $35\,\mathrm{Gt\,yr^{-1}}$. Our plains results are consistent with the results of refs 16 and 21, which span shorter time periods.

The lack of notable mass loss over glacierized regions is consistent with our HMA mascon solutions that indicate relatively modest losses (Table 1). We simulate what the ice loss rates predicted by ref. 2 would look like in the GRACE results. We use those rates to construct synthetic gravity fields and process them using the same methods applied to the GRACE data, to generate the trend map shown in Fig. 3c. It is apparent that an ice loss of this order would appear in the GRACE map as a large mass loss signal centred over the eastern Himalayas, far larger in amplitude and extent than the GRACE results in that region (compare Fig. 3b with Fig. 3c).

It is reasonable to wonder whether a tectonic process could be causing a positive signal in the glacierized region that offsets a large negative glacier signal in HMA. To see what this positive rate would have to look like, we remove the simulated gravity field (based on ref. 2) from the GRACE data and show the resulting difference map in Fig. 3d. If the ice loss estimate were correct, the tectonic process would be causing an anomalous mass increase over the Himalayas of $\sim 3\,\mathrm{cm\,yr^{-1}}$ equivalent water thickness, equivalent to $\sim 1\,\mathrm{cm\,yr^{-1}}$ of uncompensated crustal uplift. Although we cannot categorically rule out such a possibility, it seems unlikely. Global Positioning System and levelling observations in this region indicate long-term uplift rates as large as 0.5–0.7 cm $\mathrm{yr^{-1}}$ in some places[22,23]. But it is highly probable that any broad-scale tectonic uplift would be isostatically compensated by an increasing mass deficiency at depth, with little net effect on gravity[24] and, consequently, no significant contribution to the GRACE results. The effects of compensation are evident in the static gravity field. Supplementary Fig. 4

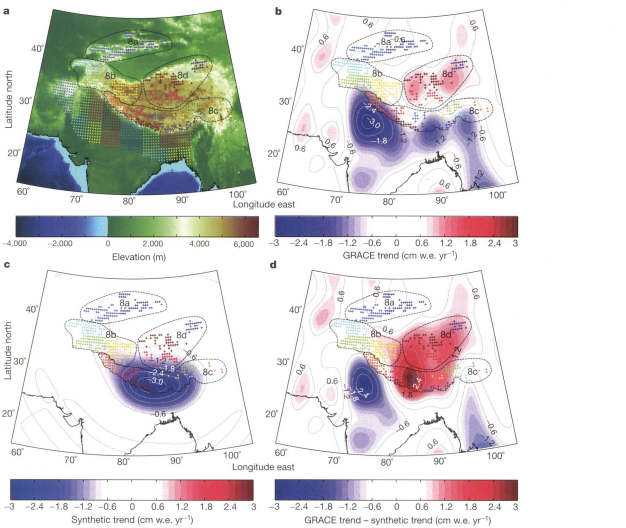

Figure 3 | HMA mass balance determination. a, Topographic map overlaid with the HMA mascons (crosses) and India plain mascons (dots); the dashed lines delimit the four HMA subregions (labelled as in Table 1). **b**, GRACE mass rate corrected for hydrology and GIA and smoothed with a 350-km Gaussian smoothing function, overlaid with the HMA mascons. w.e., water equivalent. **c**, Synthetic GRACE rates that would be caused by a total mass loss of $55\,\mathrm{Gt\,yr^{-1}}$ over HMA mascons, with $29\,\mathrm{Gt\,yr^{-1}}$ over the eastern Himalayas, after ref. 2. **d**, The difference between **b** and **c**.

shows the free-air gravity field, computed using a 350-km Gaussian smoothing function (used to generate Fig. 3) applied to the EGM96 mean global gravity field[25]. The topography leaves no apparent signature on the static gravity field at these scales, indicating near-perfect compensation.

For a solid-Earth process to affect GRACE significantly, it must be largely isostatically uncompensated, which for these broad spatial scales would require characteristic timescales of the same order or less than the mantle's viscoelastic relaxation times (several hundred to a few thousand years). One possible such process might be the ongoing viscoelastic response of the Earth to past glacial unloading. We have investigated this effect, as well as possible contributions from erosion, and find that neither is likely to be important (Supplementary Information).

Another possible explanation for the lack of a large GRACE HMA signal is that most of the glacier melt water might be sinking into the ground before it has a chance to leave the glaciated region, thus causing GRACE to show little net mass change. Some groundwater recharge undoubtedly does occur, but it seems unlikely that such cancellation would be this complete. Much of HMA, for example, is permafrost, so local storage capacity is small (see the Circum-Arctic Map of Permafrost and Ground-Ice Conditions; http://nsidc.org/fgdc/maps/ipa_browse.html). Therefore, although there would be surface melt, the frozen ground would inhibit local recharge and there would be little ability to store the melt water locally. How far the water might have to travel before finding recharge pathways, we do not know. It is true that some rivers originating in portions of HMA do not reach the sea. Most notable are the Amu Darya and Syr Darya, which historically feed the Aral Sea but have been diverted for irrigation. Any fraction of that diverted water that ends up recharging aquifers will not directly contribute to SLR. However, the irrigation areas lie well outside our HMA mascons, and so even if there is notable recharge it is unlikely to affect the HMA mascon solutions significantly.

Our emphasis here is on GICs; the Greenland and Antarctic ice sheets have previously been well studied with GRACE[15]. But for comparison with non-GRACE global estimates, we combine our GIC results with our estimates for Greenland plus Antarctica to obtain a total SLR contribution from all ice-covered regions of $1.48 \pm 0.26\ \mathrm{mm\ yr^{-1}}$ during 2003–2010. Within the uncertainties, this value compares favourably with the estimate of $1.8 \pm 0.5\ \mathrm{mm\ yr^{-1}}$ for 2006 from ref 4. However, there are regional differences between these and prior results, which need further study and reconciliation.

SLR from the addition of new water can be determined from GRACE alone as well as by subtracting Argo steric heights from altimetric SLR measurements[6]. The most recent new-water SLR estimate, comparing the two methods, is $1.3 \pm 0.6\ \mathrm{mm\ yr^{-1}}$ for 2005–2010[6], which agrees with our total ice-covered SLR value to within the uncertainties. The difference, $0.2 \pm 0.6\ \mathrm{mm\ yr^{-1}}$, could represent an increase in land water storage outside ice-covered regions, but we note that it is not significantly different from zero.

METHODS SUMMARY

GRACE solutions consist of spherical harmonic (Stokes) coefficients and are used to determine month-to-month variations in Earth's mass distribution[9,10]. We use monthly values of C_{20} (the zonal, degree-2 spherical harmonic coefficient of the geopotential) from satellite laser ranging[26], and include degree-one terms[27].

To determine mass variability for each mascon, we find the set of Stokes coefficients produced by a unit mass distributed uniformly across that mascon. We fit these sets of Stokes coefficients, simultaneously, to the GRACE Stokes coefficients, to obtain monthly mass values for each mascon. This method is similar to previously published mascon methods[28], though here we fit to Stokes coefficients rather than to raw satellite measurements and we do not impose smoothness constraints. To determine the optimal shape and number of mascons in a region, we construct a sensitivity kernel for several possible configurations, and choose the configuration that optimizes that kernel and minimizes the GRACE trend residuals (Supplementary Fig. 1c).

The average of two land surface models is used to correct for hydrology, and the model differences are used to estimate uncertainties (Supplementary Information).

LIA loading corrections have been previously derived for Alaska[13] and Patagonia[29], and equal 7 and 9 Gt yr^{-1}, respectively. These numbers are subtracted from our Alaska and Patagonia inversions. For other GIC regions, where LIA characteristics are not well known, we estimate an upper bound for the correction by constructing a GIA model that tends to maximize the positive LIA gravity trend. Of all the additional GIC regions, only HMA has a predicted LIA correction that reaches 1 Gt yr^{-1}. There, the model suggests we remove 5 Gt yr^{-1} from our inverted result. But because the LIA correction in this region is likely to be an overestimate (Supplementary Information), our preferred result splits the difference (Supplementary Table 1), and we use that difference to augment the total HMA uncertainty.

Received 28 July 2011; accepted 9 January 2012.
Published online 8 February 2012.

1. Cogley, J. G. Geodetic and direct mass-balance measurements: comparison and joint analysis. *Ann. Glaciol.* **50**, 96–100 (2009).
2. Dyurgerov, M. B. Reanalysis of glacier changes: from the IGY to the IPY, 1960–2008. *Data Glaciol. Stud.* **108,** 1–116 (2010).
3. Hock, R., de Woul, M., Radic, V. & Dyurgerov, M. Mountain glaciers and ice caps around Antarctica make a large sea-level rise contribution. *Geophys. Res. Lett.* **36,** L07501 (2009).
4. Meier, M. F. *et al.* Glaciers dominate eustatic sea-level rise in the 21st century. *Science* **317,** 1064–1067 (2007).
5. Matsuo, K. & Heki, K. Time-variable ice loss in Asian high mountains from satellite gravimetry. *Earth Planet. Sci. Lett.* **290,** 30–36 (2010).
6. Willis, J. K., Chambers, D. P., Kuo, C. Y. & Shum, C. K. Global sea level rise, recent progress and challenges for the decade to come. *Oceanography (Wash. DC)* **23,** 26–35 (2010).
7. Hirabayashi, Y., Doll, P. & Kanae, S. Global-scale modeling of glacier mass balances for water resources assessments: glacier mass changes between 1948 and 2006. *J. Hydrol. (Amst.)* **390,** 245–256 (2010).
8. Kaser, G., Cogley, J. G., Dyurgerov, M. B., Meier, M. F. & Ohmura, A. Mass balance of glaciers and ice caps: consensus estimates for 1961–2004. *Geophys. Res. Lett.* **33,** L19501 (2006).
9. Tapley, B. D., Bettadpur, S., Watkins, M. & Reigber, C. The gravity recovery and climate experiment: mission overview and early results. *Geophys. Res. Lett.* **31,** L09607 (2004).
10. Wahr, J., Swenson, S., Zlotnicki, V. & Velicogna, I. Time-variable gravity from GRACE: first results. *Geophys. Res. Lett.* **31,** L11501 (2004).
11. Chen, J. L., Wilson, C. R., Tapley, B. D., Blankenship, D. D. & Ivins, E. R. Patagonia icefield melting observed by gravity recovery and climate experiment (GRACE). *Geophys. Res. Lett.* **34,** L22501 (2007).
12. Gardner, A. S. *et al.* Sharply increased mass loss from glaciers and ice caps in the Canadian Arctic Archipelago. *Nature* **473,** 357–360 (2011).
13. Luthcke, S. B., Arendt, A. A., Rowlands, D. D., McCarthy, J. J. & Larsen, C. F. Recent glacier mass changes in the Gulf of Alaska region from GRACE mascon solutions. *J. Glaciol.* **54,** 767–777 (2008).
14. Riva, R. E. M., Bamber, J. L., Lavallee, D. A. & Wouters, B. Sea-level fingerprint of continental water and ice mass change from GRACE. *Geophys. Res. Lett.* **37,** L19605 (2010).
15. Rignot, E., Velicogna, I., van den Broeke, M. R., Monaghan, A. & Lenaerts, J. Acceleration of the contribution of the Greenland and Antarctic ice sheets to sea level rise. *Geophys. Res. Lett.* **38,** L05503 (2011).
16. Tiwari, V. M., Wahr, J. & Swenson, S. Dwindling groundwater resources in northern India, from satellite gravity observations. *Geophys. Res. Lett.* **36,** L18401 (2009).
17. Raup, B. H., Kieffer, H. H., Hare, J. M. & Kargel, J. S. Generation of data acquisition requests for the ASTER satellite instrument for monitoring a globally distributed target: glaciers. *IEEE Trans. Geosci. Remote Sens.* **38,** 1105–1112 (2000).
18. Brown, J., Ferrians, O. J., Heginbottom, J. A. & Melnikov, E. S. *Circum-Arctic Map of Permafrost and Ground-Ice Conditions.* National Snow and Ice Data Center/World Data Center for Glaciology (1998, revised, February 2001).
19. Velicogna, I. Increasing rates of ice mass loss from the Greenland and Antarctic ice sheets revealed by GRACE. *Geophys. Res. Lett.* **36,** L19503 (2009).
20. Cogley, J. G. in *Future Climates of the World* (eds Henderson-Sellers, A. & McGuffie, K.) 189–214 (Elsevier, 2012).
21. Rodell, M., Velicogna, I. & Famiglietti, J. S. Satellite-based estimates of groundwater depletion in India. *Nature* **460,** 999–1002 (2009).
22. Bettinelli, P. *et al.* Plate motion of India and interseismic strain in the Nepal Himalaya from GPS and DORIS measurements. *J. Geod.* **80,** 567–589 (2006).
23. Jackson, M. & Bilham, R. Constraints on Himalayan deformation inferred from vertical velocity-fields in Nepal and Tibet. *J. Geophys. Res. Solid Earth* **99,** 13897–13912 (1994).
24. Zhong, S. J. & Zuber, M. T. Crustal compensation during mountain-building. *Geophys. Res. Lett.* **27,** 3009–3012 (2000).
25. Lemoine, F. *et al. The Development of the Joint NASA GSFC and NIMA Geopotential Model EGM96.* NASA Goddard Space Flight Center (1998).
26. Cheng, M. K. & Tapley, B. D. Variations in the Earth's oblateness during the past 28 years. *J. Geophys. Res.* **109,** B04402 (2004).
27. Swenson, S., Chambers, D. & Wahr, J. Estimating geocenter variations from a combination of GRACE and ocean model output. *J. Geophys. Res. Solid Earth* **113,** B08410 (2008).

28. Rowlands, D. D. *et al.* Resolving mass flux at high spatial and temporal resolution using GRACE intersatellite measurements. *Geophys. Res. Lett.* **32,** L04310 (2005).
29. Ivins, E. R. & James, T. S. Bedrock response to Llanquihue Holocene and present-day glaciation in southernmost South America. *Geophys. Res. Lett.* **31,** L24613 (2004).

Supplementary Information is linked to the online version of the paper at www.nature.com/nature.

Acknowledgements We thank Geruo A for providing the glacial isostatic adjustment model, and G. Cogley, G. Kaser, I. Velicogna, T. Perron and M. Tamisiea for comments. This work was partially supported by NASA grants NNX08AF02G and NNXI0AR66G, and by NASA's 'Making Earth Science Data Records for Use in Research Environments (MEaSUREs) Program'.

Author Contributions T.J. and J.W. developed the study and wrote the paper. W.T.P. and S.S. discussed, commented on and improved the manuscript. S.S. provided the CLM4 hydrology model output.

Author Information Reprints and permissions information is available at www.nature.com/reprints. The authors declare no competing financial interests. Readers are welcome to comment on the online version of this article at www.nature.com/nature. Correspondence and requests for materials should be addressed to J.W. (john.wahr@gmail.com).

LETTER

doi:10.1038/nature10810

The microRNA miR-34 modulates ageing and neurodegeneration in *Drosophila*

Nan Liu[1]†, Michael Landreh[1]†, Kajia Cao[2,3], Masashi Abe[1], Gert-Jan Hendriks[1], Jason R. Kennerdell[1], Yongqing Zhu[1], Li-San Wang[2,4,5] & Nancy M. Bonini[1,6]

Human neurodegenerative diseases have the temporal hallmark of afflicting the elderly population. Ageing is one of the most prominent factors to influence disease onset and progression[1], yet little is known about the molecular pathways that connect these processes. To understand this connection it is necessary to identify the pathways that functionally integrate ageing, chronic maintenance of the brain and modulation of neurodegenerative disease. MicroRNAs (miRNA) are emerging as critical factors in gene regulation during development; however, their role in adult-onset, age-associated processes is only beginning to be revealed. Here we report that the conserved miRNA miR-34 regulates age-associated events and long-term brain integrity in *Drosophila*, providing a molecular link between ageing and neurodegeneration. Fly *mir-34* expression exhibits adult-onset, brain-enriched and age-modulated characteristics. Whereas *mir-34* loss triggers a gene profile of accelerated brain ageing, late-onset brain degeneration and a catastrophic decline in survival, *mir-34* upregulation extends median lifespan and mitigates neurodegeneration induced by human pathogenic polyglutamine disease protein. Some of the age-associated effects of miR-34 require adult-onset translational repression of *Eip74EF*, an essential ETS domain transcription factor involved in steroid hormone pathways. Our studies indicate that miRNA-dependent pathways may have an impact on adult-onset, age-associated events by silencing developmental genes that later have a deleterious influence on adult life cycle and disease, and highlight fly miR-34 as a key miRNA with a role in this process.

Recent evidence reveals that miRNA pathways are important in the adult nervous system, notably in the maintenance of neurons and in the regulation of genes and pathways associated with neurodegenerative disease[2,3]. Given these findings, we considered that there may be a fundamental role for select miRNAs in ageing. We examined flies carrying a hypomorphic mutation in *loquacious* (*loqs*), a key gene in fly miRNA processing[4] (Supplementary Fig. 1a). Flies bearing the $loqs^{f00791}$ mutation were viable, but detailed examination indicated a significantly shortened lifespan (Supplementary Fig. 1b). Further analysis indicated that $loqs^{f00791}$ flies showed late-onset brain morphological deterioration: although normal as young adults, by 25 days $loqs^{f00791}$ flies developed large vacuoles in the retina and lamina of the brain (Supplementary Fig. 1c). Although developmental processes may contribute to shortened lifespan, the adult-onset brain degeneration of $loqs^{f00791}$ mutants indicated that one or more specific miRNAs may be critically involved in age-associated events impacting on long-term brain integrity.

To explore this question, we determined whether specific miRNAs displayed age-modulated expression in the brain. RNA was isolated from dissected brains of adult flies of young (3 days), mid (30 days) and old time points (60 days). Using an array for *Drosophila* miRNAs, 29 were expressed in the adult brain (Fig. 1a). Whereas most miRNAs maintained a steady level or decreased with age, one miRNA, *mir-34*, increased (Fig. 1a). Small RNA northern blot analysis confirmed that *mir-34* expression was barely detectable during development, but became high in the adult and was further upregulated with age (Supplementary Fig. 2a, b). Expression of *mir-34* was affected in $loqs^{f00791}$ flies (Supplementary Fig. 1d). miR-34 falls into a category of *Drosophila* miRNAs whose processing requires the exoribonuclease *nibbler* (*nbr*)[5,6]. In the adult, mature miR-34 displayed three major differentially sized forms (24 nucleotides, 22 nucleotides and 21 nucleotides) with a uniform 5′ end, descending by single nucleotides at the 3′ end which result from *nbr*-mediated trimming; only isoform c became upregulated with age (Supplementary Fig. 2c and Fig. 1b, c; see also refs 5–7).

miR-34 is a markedly conserved miRNA, with orthologues in fly, *Caenorhabditis elegans*, mouse and human showing identical seed sequence (Supplementary Fig. 2d). To define miR-34 function, flies deleted for the gene were generated (Supplementary Fig. 3a). The resulting *mir-34* mutant flies retained normal wild-type expression of neighbouring genes, but selectively lacked *mir-34* (Supplementary

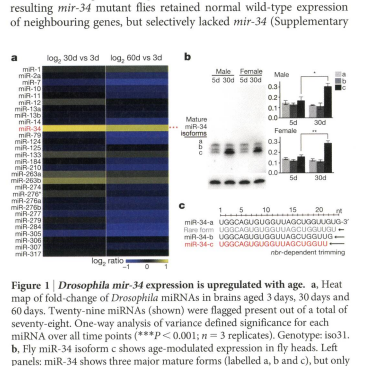

Figure 1 | *Drosophila mir-34* expression is upregulated with age. a, Heat map of fold-change of *Drosophila* miRNAs in brains aged 3 days, 30 days and 60 days. Twenty-nine miRNAs (shown) were flagged present out of a total of seventy-eight. One-way analysis of variance defined significance for each miRNA over all time points ($^{***}P < 0.001$; $n = 3$ replicates). Genotype: iso31. **b**, Fly miR-34 isoform c shows age-modulated expression in fly heads. Left panels: miR-34 shows three major mature forms (labelled a, b and c), but only isoform c increases with age. Right panels: quantification of miR-34 isoforms with age. $n = 3$ independent experiments; signal density of all isoforms normalized at the same time point to 2S rRNA loading control. $^{*}P < 0.01$; $^{**}P < 0.001$; one-way analysis of variance, with post test: Tukey's multiple comparison test. Genotype: 5905. **c**, Sequences of miR-34 isoforms are generated through *nbr*-dependent 3′-end trimming.

[1]Department of Biology, University of Pennsylvania, Philadelphia, Pennsylvania 19104, USA. [2]Department of Pathology and Laboratory Medicine, University of Pennsylvania, Philadelphia, Pennsylvania 19104, USA. [3]Cell and Developmental Biology, University of Pennsylvania, Philadelphia, Pennsylvania 19104, USA. [4]Institute on Aging, University of Pennsylvania, Philadelphia, Pennsylvania 19104, USA. [5]Penn Center for Bioinformatics, University of Pennsylvania, Philadelphia, Pennsylvania 19104, USA. [6]Howard Hughes Medical Institute, University of Pennsylvania, Philadelphia, Pennsylvania 19104, USA. †Present addresses: Division of Biological Sciences, Section of Neurobiology, Howard Hughes Medical Institute, University of California, San Diego, California 92093, USA (N.L.); Division of Physiological Chemistry I, Department of Medical Biochemistry and Biophysics, Karolinska Institutet, SE-17177 Stockholm, Sweden (M.L.).

Fig. 3b, c). To interrogate age-associated phenotypes carefully, we generated *mir-34* null flies in the same uniform homogeneous genetic background (see Methods). *mir-34* mutants displayed no obvious developmental defects, consistent with its adult-onset expression. However, detailed examination of adult animals indicated that *mir-34* mutants, although showing normal adult appearance and early survival, displayed a catastrophic decline in viability just after 30 days (Fig. 2a and Supplementary Table 4). Analysis of age-associated functions revealed that young mutants (3 days) had normal locomotion and stress resistance, but by 20 days the mutants had dramatic climbing deficits and were markedly stress-sensitive compared to age-matched controls (Fig. 2b). Because *mir-34* expression was brain-enriched, we also examined the brain. Typically, older flies show sporadic, age-correlated vacuoles in the brain—a morphological hallmark of neural deterioration[8]. *mir-34* mutants were born with normal brain morphology, but showed dramatic vacuolization with age, indicative of loss of brain integrity (Fig. 2c). Rescue with a 9-kb genomic DNA fragment containing *mir-34* and its endogenous *cis*-regulatory elements (Supplementary Fig. 3a, b) partially restored the age-associated expression of *mir-34* to *mir-34* null flies in the same homogeneous genetic background (Supplementary Fig. 3d). Although rescue was not complete, indicative of a complexity in genomic elements that regulate *mir-34*, rescue was sufficient to mitigate the mutant effects, indicating that miR-34 function normally underlies these age-associated aspects (Supplementary Table 1).

These data indicated that *mir-34* mutants were normal as young adults, but with age developed deficits reflective of much older animals, including loss of locomotion, stress sensitivity and brain deterioration,

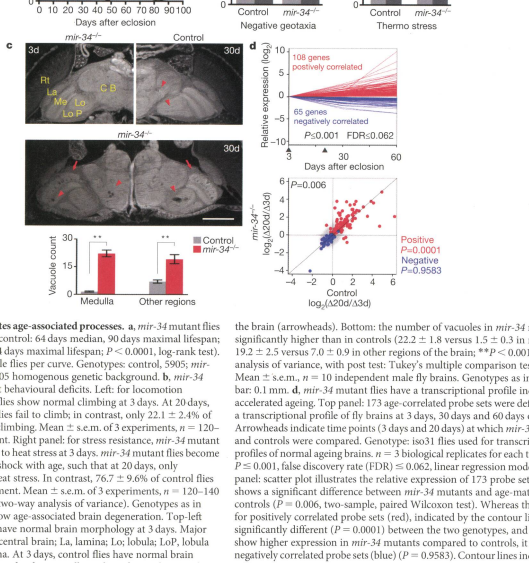

Figure 2 | miR-34 modulates age-associated processes. a, *mir-34* mutant flies have a shortened lifespan (control: 64 days median, 90 days maximal lifespan; *mir-34*: 40 days medium, 64 days maximal lifespan; $P < 0.0001$, log-rank test). Mean ± s.e.m., $n \geq 240$ male flies per curve. Genotypes: control, 5905; *mir-34*$^{-/-}$, *miR-34* null-1 in 5905 homogenous genetic background. **b**, *mir-34* mutant flies have late-onset behavioural deficits. Left: for locomotion behaviour, *mir-34* mutant flies show normal climbing at 3 days. At 20 days, 50 ± 3.4% *mir-34* mutant flies fail to climb; in contrast, only 22.1 ± 2.4% of control flies have defective climbing. Mean ± s.e.m. of 3 experiments, $n = 120$–140 male flies per experiment. Right panel: for stress resistance, *mir-34* mutant flies have normal resistance to heat stress at 3 days. *mir-34* mutant flies become markedly sensitive to heat shock with age, such that at 20 days, only 27.5 ± 3.8% survive after heat stress. In contrast, 76.7 ± 9.6% of control flies survive after the same treatment. Mean ± s.e.m. of 3 experiments, $n = 120$–140 male flies. ***$P < 0.0001$ (two-way analysis of variance). Genotypes as in **a**. **c**, *mir-34* mutant flies show age-associated brain degeneration. Top-left panel: *mir-34* mutant flies have normal brain morphology at 3 days. Major anatomical structures: CB, central brain; La, lamina; Lo; lobula; LoP, lobula plate; Me, medulla; Rt, retina. At 3 days, control flies have normal brain morphology (not shown), but develop a small number of sporadic vacuoles at 30 days (top-right panel, arrowheads). Middle panel: aged *mir-34* mutants (30 days) show striking vacuoles in the medulla (arrows) and other regions of the brain (arrowheads). Bottom: the number of vacuoles in *mir-34* mutants is significantly higher than in controls (22.2 ± 1.8 versus 1.5 ± 0.3 in medulla; 19.2 ± 2.5 versus 7.0 ± 0.9 in other regions of the brain; **$P < 0.001$, one-way analysis of variance, with post test: Tukey's multiple comparison test). Mean ± s.e.m., $n = 10$ independent male fly brains. Genotypes as in **a**. Scale bar: 0.1 mm. **d**, *mir-34* mutant flies have a transcriptional profile indicative of accelerated ageing. Top panel: 173 age-correlated probe sets were defined from a transcriptional profile of fly brains at 3 days, 30 days and 60 days of age. Arrowheads indicate time points (3 days and 20 days) at which *mir-34* mutants and controls were compared. Genotype: iso31 flies used for transcriptional profiles of normal ageing brains. $n = 3$ biological replicates for each time point. $P \leq 0.001$, false discovery rate (FDR) ≤ 0.062, linear regression model. Bottom panel: scatter plot illustrates the relative expression of 173 probe sets, which shows a significant difference between *mir-34* mutants and age-matched controls ($P = 0.006$, two-sample, paired Wilcoxon test). Whereas the pattern for positively correlated probe sets (red), indicated by the contour lines, is significantly different ($P = 0.0001$) between the two genotypes, and tends to show higher expression in *mir-34* mutants compared to controls, it is not for negatively correlated probe sets (blue) ($P = 0.9583$). Contour lines indicate that positively correlated probe sets tend to show higher expression in *mir-34* mutants compared to controls. Genotypes as in **a**. $n = 5$ biological replicates for each time point.

coupled with shortened lifespan. We therefore hypothesized that loss of *mir-34* accelerated brain ageing. To address this, we transcriptionally profiled the fly brain (3 days, 30 days and 60 days) from wild-type animals. On the basis of a linear regression model[9], we extracted 173 probe sets from this profile the expression of which was tightly correlated with the progression of normal ageing (Fig. 2d and Supplementary Tables 2 and 3). We next made another set of brain transcriptional profiles for *mir-34* mutants and controls of matched chronological age (3 days and 20 days). We measured relative changes of these probe sets between 3 days and 20 days within each genotype, and compared the extent of such changes between *mir-34* mutants and controls. This indicated that the overall pattern of these probe sets was significantly different between the two genotypes ($P = 0.006$, two-sample, paired Wilcoxon test; Fig. 2d). In particular, most positively correlated probe sets displayed a faster pace of increase in *mir-34* mutants compared to controls—thus showing accelerated age-associated expression changes in *mir-34* mutants (Fig. 2d). This result, combined with the physiological and histological evidence of more rapid loss of age-associated functions, suggested that *mir-34* mutants were undergoing accelerated brain ageing.

miRNAs function by binding to the 3′ UTRs of target mRNAs and often result in downregulation of protein translation. We therefore reasoned that age-associated activities of miR-34 might be mediated through silencing of critical targets that have a negative impact on the adult animal. miRNA-target prediction algorithms indicated miR-34 binding sites within the 3′ UTR of the *Eip74EF* gene; notably, these binding sites were conserved in the orthologous *Eip74EF* genes from different *Drosophila* species (Supplementary Fig. 4a). We confirmed the miR-34 interaction through mutations in the seed sequences of the predicted miR-34 binding sites in the 3′ UTR of the *Eip74EF* mRNA (Supplementary Fig. 4b). The *Eip74EF* gene is a component of steroid hormone signalling pathways. Although such pathways have generally been studied for effects during development, data have implicated these pathways in lifespan regulation[10].

The *Eip74EF* gene encodes two major protein isoforms, E74A and E74B (referred to as the *E74A* and *E74B* genes, respectively[11]); the isoforms share the same 3′ UTR (Supplementary Fig. 4a). Northern blots indicated that transcription of *E74A*, but not *E74B*, persisted in adults, overlapping the time period when *mir-34* is expressed (Supplementary Fig. 4c). Given this, we focused on *E74A* as a regulated target of miR-34 in the adult. Despite robust expression of the mRNA transcript, the E74A protein was expressed at low levels in adult heads throughout lifespan (Fig. 3a, b and Supplementary Fig. 4d). In flies lacking miR-34, E74A protein was markedly increased (Fig. 3b); E74A was also de-regulated in the $loqs^{f00791}$ mutant flies (Supplementary Fig. 1e). Genomic rescue of *mir-34* mitigated this de-regulation of the E74A protein (Fig. 3c). Fine temporal analysis indicated that the E74A protein was highly expressed in young flies, but underwent a marked decrease within a 24-h time window (Supplementary Fig. 5). This temporal pattern seemed to be mutually exclusive to that of miR-34 (see Supplementary Fig. 2a). Moreover, in flies lacking miR-34, the downregulation of E74A protein during this critical period was dampened (Supplementary Fig. 5). This evidence indicates that adult-onset expression of *mir-34* functions, at least in part, to attenuate E74A protein expression in the young adult, and maintain that repression through adulthood (Supplementary Fig. 4d).

We next determined whether deregulated expression of E74A protein contributed to the age-associated defects in *mir-34* mutants. Because E74A function is essential during development, with strong mutations leading to pre-adult lethality[11], we used the mild, but viable, $E74A^{BG01805}$ hypomorphic mutation (Supplementary Fig. 4a). When the $E74A^{BG01805}$ mutation was combined with *mir-34* mutant flies in the same homogenous genetic background, proper regulation of E74A protein was partially restored (Fig. 3d), and age-associated defects due to loss of *mir-34*, including shortened lifespan and brain vacuolization, were mitigated (Fig. 3e, f; $E74A^{BG01805}$ mutants alone have a normal lifespan (Supplementary Fig. 6a)). To assess further the adult activity of E74A, we upregulated E74A in the adult with an *E74A* transgene that lacks miR-34 binding sites driven by a temperature-sensitive promoter[12]. At 29 °C, these flies demonstrated increased levels of E74A expression in the adult (Supplementary Fig. 6b). Notably, these animals also showed late-onset brain degeneration (Supplementary Fig. 6c) and a significantly shortened lifespan (Supplementary Fig. 6d). These data indicate that deregulated expression of E74A has a negative impact on normal ageing, and that one function of miR-34 is to silence E74A in the adult to prevent the adult-stage deleterious activity of E74A on brain integrity and viability.

Notably, during the course of these studies, we noted that *mir-34* mutants also displayed a defect in protein misfolding—a molecular process implicated in ageing and common to many human neurodegenerative diseases[13]. Whereas normally with age, the fly brain accumulates a low level of inclusions that immunostain for stress chaperones like Hsp70/Hsc70, *mir-34* mutants showed a marked increase compared to control flies of matched age (30 days) (Supplementary Fig. 7). Given that *mir-34* expression increases with age, and *mir-34* loss shows altered chaperone accumulation, we tested whether *mir-34* expression itself is upregulated by stresses like heat shock or oxidative toxins, but found no evidence to support this (data not shown). However, given that loss of *mir-34* caused an increase in protein misfolding, this raised the possibility that upregulation of *mir-34* expression might mitigate disease-associated protein misfolding. In *Drosophila*, expression of a pathogenic ataxin-3 polyglutamine (polyQ) disease protein (SCA3trQ78) leads to inclusion formation, a decrease in polyQ protein solubility and progressive neural loss[14] (Supplementary Fig. 8a). Upregulation of *mir-34* markedly mitigated polyQ degeneration, such that inclusion formation was slowed, the protein retained greater solubility, and neural degeneration was suppressed (Fig. 3g, h and Supplementary Fig. 8b–d). Lowering *E74A* expression by heterozygous reduction in flies expressing pathogenic polyQ protein revealed a minimal effect (data not shown), indicating that E74A may not be a target of miR-34 activity in this process. However, our studies with E74A were of necessity limited to hypomorphic alleles that may not uncover the full extent of E74A function mediated by miR-34. Furthermore, additional targets of miR-34 may be involved in different aspects of miR-34-directed pathways, including disease.

Given this effect to mitigate disease-associated neural toxicity with upregulation of *mir-34*, and that *mir-34* expression naturally increases with age, we investigated whether enhanced expression of *mir-34* in wild-type flies could modulate the ageing process. We increased miR-34 dosage in wild-type flies with genomic rescue transgenes, which express *mir-34* under its endogenous regulatory elements (see Supplementary Fig. 2a). Analysis of multiple independent transgenics in the same genetic background with that of control indicated that upregulation of miR-34 levels with genomic constructs (~20%, Supplementary Fig. 3d) promoted median survival rate by ~10% compared to wild type (Fig. 3i; other traits, such as the occurrence of brain vacuolization, despite being an age-associated phenomenon, are sporadic and low in normal flies, thus were difficult to assess). Thus, upregulation of *mir-34* expression can protect from neurodegenerative disease and extend median lifespan.

Our findings indicate that miR-34 in *Drosophila* presents a key miRNA that couples long-term maintenance of the brain with healthy ageing of the organism. miR-34 activity, enhanced by its age-modulated expression and processing, is critically involved in silencing of the *E74A* transcript through adulthood and in modulation of protein homeostasis with age, as well as in polyQ disease. Select neural cell types may be especially vulnerable in ageing and disease[15]; miR-34 function may have an impact on the integrity or activity of these systems. Intriguingly, E74A seems to confer sharply opposing function on animal fitness at different life stages, being essential during pre-adult development[11], but harmful to the adult during ageing (this study). This biological property—of a gene being beneficial at one

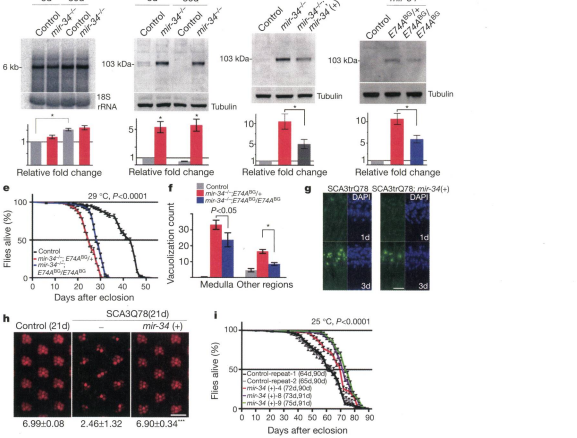

Figure 3 | The *Drosophila Eip74EF* gene is a target of miR-34 in modulation of the ageing process. a, *E74A* mRNA is robustly expressed in the adult and unchanged between age-matched controls and *mir-34* mutants. In control flies, *E74A* mRNA is significantly upregulated in 30 day compared to 3 day animals. RNA was from male heads. Mean ± s.e.m., $n = 3$ independent experiments; signal density of *E74A* mRNA normalized to 18S rRNA loading control (*$P < 0.01$, one-way analysis of variance, with post test: Tukey's multiple comparison test). Genotypes: control, 5905; *mir-34*$^{-/-}$, *mir-34* null-1 in 5905 homogenous genetic background. **b**, E74A protein is deregulated in *mir-34* mutants. Protein was from male heads. Mean ± s.e.m., $n = 3$ independent experiments; signal density normalized to tubulin loading control (*$P < 0.05$, one-way analysis of variance, with post test: Tukey's multiple comparison test). Genotypes: control, 5905; *mir-34*$^{-/-}$, *mir-34* null-1 in 5905 homogenous genetic background; *mir-34*$^{-/-}$; *mir-34*(+), *mir-34* genomic rescue in *mir-34* null-1 in 5905 homogenous genetic background. **d**, *mir-34* mutants homozygous for the *E74A*^{BG01805} allele have lower levels of E74A protein. Protein was from male heads of 20 day flies raised at 29 °C. Mean ± s.e.m., $n = 3$ independent experiments; signal density normalized to tubulin loading control (*$P < 0.01$, one-way analysis of variance, with post test: Tukey's multiple comparison test). Genotypes: control, 5905; *mir-34*$^{-/-}$ *E74A*^{BG}/+, *E74A*^{BG01805}/+, *miR-34* null-1 in 5905 homogenous genetic background; *mir-34*$^{-/-}$ *E74A*^{BG}/*E74A*^{BG}, *E74A*^{BG01805}/*E74A*^{BG01805}, *miR-34* null-1 in 5905 homogenous genetic background. **e**, **f**, Reducing E74A protein levels in the adult mitigates age-related defects of *mir-34* mutants. *mir-34* mutants also homozygous for *E74A*^{BG01805} show rescued lifespan (**e**) and brain morphology (**f**), compared to *mir-34* mutants heterozygous for *E74A*^{BG01805} (these flies have a lifespan that is the same as *mir-34* mutants alone; see Supplementary Table 4). Flies raised at 29 °C. Lifespan: $P < 0.0001$ (log-rank test). Mean ± s.e.m., $n \geq 150$ male flies. Brain vacuoles: *$P < 0.01$ (one-way analysis of variance, with post test: Tukey's multiple comparison test). Mean ± s.e.m., $n = 10$ independent male animals. Genotypes as in **d**. **g**, Upregulation of *mir-34* reduces accumulation of pathogenic polyQ protein inclusions. Left panels: in the retina of flies expressing SCA3trQ78 alone, pathogenic polyQ protein is initially diffuse (1 day, top), but gradually accumulates into nuclear inclusions (3 day, bottom). Right panels: upregulation of *mir-34* reduces inclusion formation. DAPI staining highlights nuclei. 3 day controls show 53.75 ± 12.55 inclusions in a retinal section versus 23.67 ± 7.57 with *mir-34* upregulation; mean ± s.d., $n \geq 3$ cryosections from independent male animals; $P < 0.01$ (*t*-test). Genotypes: SCA3trQ78 is *w*$^{+}$; *rh1-GAL4, UAS-SCA3trQ78/+*. SCA3trQ78; *mir-34* (+) is *w*$^{+}$; *rh1-GAL4, SCA3trQ78/+; UAS-mir-34/+*. Scale bar, 0.05 mm. **h**, Upregulation of *mir-34* prevents neural degeneration. At 21 days, male flies expressing SCA3trQ78 show a marked loss of photoreceptor neuronal integrity (middle panel), with an average of only 2.46 ± 1.32 photoreceptors per ommatidium remaining by pseudopupil analysis. Flies with upregulated *mir-34* (right panel) retain 6.90 ± 0.34 photoreceptors per ommatidium. Control (left panel) and upregulation of *mir-34* alone (not shown) have normal photoreceptor numbers per ommatidium. Mean ± s.d., $n = 619$, 722 and 700 ommatidia, for SCA3trQ78, SCA3trQ78; *mir-34* (+) and control, respectively; ***$P < 0.0001$ (one-way analysis of variance, with Bonferroni's multiple comparison test). Genotypes as in **b**; control: *w*$^{+}$; *rh1-GAL4/+*. Scale bar, 0.05 mm. **i**, Flies with upregulated *mir-34* (colour) have an extended median lifespan compared to control flies (black and grey curves for repeats 1 and 2, respectively) (log-rank test). Lifespan result for each genotype is indicated in median and maximal days. Mean ± s.e.m., $n \geq 150$ male flies per genotype, 25 °C. Three independent *mir-34* genomic transgenic lines (4, 8, 9) were analysed. Genotypes: control, 5905; *mir-34* (+), *mir-34* genomic rescue in 5905 homogenous genetic background.

life stage, but damaging at another—is referred to as antagonistic pleiotropy[16]. Genes associated with antagonistic pleiotropy are likely to be evolutionarily retained due to their earlier beneficial function[17]. Their adult-onset activities, however, antagonize the ageing process if they are not properly regulated. miRNA pathways provide a tantalizing mechanism by which to suppress potentially deleterious age-related activities of such genes; a number of miRNAs have been noted to show age-modulated expression and activity[18,19]. Roles of

select miRNAs normally expressed in the adult may be of evolutionary advantage to tune-down events that promote age-associated decline and potentially disease, in order to prolong healthy lifespan and longevity. Upregulation of *lin-4*, a *C. elegans* miRNA with a known developmental role, extends nematode lifespan[18], raising the possibility that this upregulation, like the natural increase of *mir-34* expression in *Drosophila*, functions to silence genes that have a negative impact on ageing and potentially promote disease. Notably, *mir-34* expression is elevated with age in *C. elegans*[19,20], and mammalian *mir-34* orthologues are highly expressed in the adult brain[21] and have also been noted to increase with age and be misregulated in degenerative disease in humans[22–26]. Current data regarding miR-34 function indicate that it is neutral or adverse in *C. elegans*[19,27], and can be either protective or contributory to age-associated events in vertebrates[22–26]. Thus, miR-34 seems to be a key miRNA poised to integrate age-associated physiology; the precise function will reflect the diverse spatiotemporal expression and activity of distinct orthologues, the mRNA target spectrum, as well as the complexity of the adult brain and life cycle. The conservation of miR-34, coupled with in-depth comparative analysis of *mir-34* expression, 3′ end processing, targets and pathways in the ageing process of nematodes, flies and mammals, make it a tempting subject for understanding features of ageing and disease susceptibility.

METHODS SUMMARY

Flies were grown in standard media at 25 °C unless otherwise specified. Stock lines and *GAL4* driver lines were obtained from the *Drosophila* Stock centre at Bloomington, or are described[14]. Deletion of the *mir-34* region was made by site-specific recombination. Fly transgenics were generated by standard procedures. Flies were generated or backcrossed a minimum of five generations into a controlled uniform homogeneous genetic background (line 5905 (FlyBase ID FBst0005905, w^{1118})), to assure that all phenotypes were robust and not associated with variation in genetic background. In this uniform homogeneous genetic background, the lifespan of control flies is highly uniform with repetition when 150 or more individuals are used for lifespan analysis. Negative geotaxis and thermo stress were used to examine fly locomotion and stress resistance, respectively. Adult male heads were processed for paraffin sections as described[14]. To determine lifespan, newly eclosed males were collected and maintained at 15 flies per vial, transferred to fresh vials every 2 days while scored for survival. A total of 150–200 flies were used per genotype per lifespan; all experiments were repeated multiple times (see Supplementary Table 4). Lifespans were analysed in Excel (Microsoft) and by Prism software (GraphPad) for survival curves and statistics. Techniques of molecular biology, western immunoblots and histology were standard. Fly brain mRNA was prepared using Trizol reagent for array and mRNA analysis, miRNA arrays were miRCURY LNA arrays version 8.1 (Exiqon), and mRNA expression was profiled using Affymetrix *Drosophila* 2.0 chips (Affymetrix). The microarray data can be found in the Gene Expression Omnibus (GEO) of NCBI through accession number GSE25009.

Full Methods and any associated references are available in the online version of the paper at www.nature.com/nature.

Received 11 June; accepted 22 December 2011.
Published online 15 February 2012.

1. Amaducci, L. & Tesco, G. Aging as a major risk for degenerative diseases of the central nervous system. *Curr. Opin. Neurol.* **7,** 283–286 (1994).
2. Eacker, S. M., Dawson, T. M. & Dawson, V. L. Understanding microRNAs in neurodegeneration. *Nature Rev. Neurosci.* **10,** 837–841 (2009).
3. Bilen, J., Liu, N., Burnett, B. G., Pittman, R. N. & Bonini, N. M. MicroRNA pathways modulate polyglutamine-induced neurodegeneration. *Mol. Cell* **24,** 157–163 (2006).
4. Jiang, F. *et al.* Dicer-1 and R3D1-L catalyze microRNA maturation in *Drosophila*. *Genes Dev.* **19,** 1674–1679 (2005).
5. Liu, N. *et al.* The exoribonuclease Nibbler controls 3′ end processing of microRNAs in *Drosophila*. *Curr. Biol.* **21,** 1888–1893 (2011).
6. Han, B. W. H., u. n. g. J. H., Weng, Z., Zamore, P. D. & Ameres, S. L. The 3′-to-5′ exoribonuclease Nibbler shapes the 3′ ends of microRNAs bound to *Drosophila* Argonaute1. *Curr. Biol.* **21,** 1878–1887 (2011).
7. Chung, W. J., Okamura, K., Martin, R. & Lai, E. C. Endogenous RNA interference provides a somatic defense against *Drosophila* transposons. *Curr. Biol.* **18,** 795–802 (2008).
8. Kretzschmar, D., Hasan, G., Sharma, S., Heisenberg, M. & Benzer, S. The *swiss cheese* mutant causes glial hyperwrapping and brain degeneration in *Drosophila*. *J. Neurosci.* **17,** 7425–7432 (1997).
9. Cao, K., Chen-Plotkin, A. S., Plotkin, J. B. & Wang, L. S. Age-correlated gene expression in normal and neurodegenerative human brain tissues. *PLoS ONE* **5** (2010).
10. Simon, A. F., Shih, C., Mack, A. & Benzer, S. Steroid control of longevity in *Drosophila melanogaster*. *Science* **299,** 1407–1410 (2003).
11. Fletcher, J. C. & Thummel, C. S. The *Drosophila* E74 gene is required for the proper stage- and tissue-specific transcription of ecdysone-regulated genes at the onset of metamorphosis. *Development* **121,** 1411–1421 (1995).
12. Fletcher, J. C., D'Avino, P. P. & Thummel, C. S. A steroid-triggered switch in E74 transcription factor isoforms regulates the timing of secondary-response gene expression. *Proc. Natl Acad. Sci. USA* **94,** 4582–4586 (1997).
13. Morimoto, R. I. Proteotoxic stress and inducible chaperone networks in neurodegenerative disease and aging. *Genes Dev.* **22,** 1427–1438 (2008).
14. Warrick, J. M. *et al.* Expanded polyglutamine protein forms nuclear inclusions and causes neural degeneration in *Drosophila*. *Cell* **93,** 939–949 (1998).
15. Hirth, F. *Drosophila melanogaster* in the study of human neurodegeneration. *CNS Neurol. Disord. Drug Targets* **9,** 504–523 (2010).
16. Williams, G. C. Pleitropy, natural selection and the evolution of senescence. *Evolution* **11,** 398–411 (1957).
17. Kirkwood, T. B. Understanding the odd science of aging. *Cell* **120,** 437–447 (2005).
18. Boehm, M. & Slack, F. A developmental timing microRNA and its target regulate life span in *C. elegans*. *Science* **310,** 1954–1957 (2005).
19. de Lencastre, A. *et al.* MicroRNAs both promote and antagonize longevity in *C. elegans*. *Curr. Biol.* **20,** 2159–2168 (2010).
20. Ibanez-Ventoso, C. *et al.* Modulated microRNA expression during adult lifespan in *Caenorhabditis elegans*. *Aging Cell* **5,** 235–246 (2006).
21. Bak, M. *et al.* MicroRNA expression in the adult mouse central nervous system. *RNA* **14,** 432–444 (2008).
22. Zovoilis, A. *et al.* microRNA-34c is a novel target to treat dementias. *EMBO J.* **30,** 4299–4308 (2011).
23. Minones-Moyano, E. *et al.* MicroRNA profiling of Parkinson's disease brains identifies early downregulation of miR-34b/c which modulate mitochondrial function. *Hum. Mol. Genet.* **20,** 3067–3078 (2011).
24. Li, X., Khanna, A., Li, N. & Wang, E. Circulatory miR34a as an RNA based, noninvasive biomarker for brain aging. *Aging* **3,** 985–1002 (2011).
25. Khanna, A., Muthusamy, S., Liang, R., Sarojini, H. & Wang, E. Gain of survival signaling by down-regulation of three key miRNAs in brain of calorie-restricted mice. *Aging* **3,** 223–236 (2011).
26. Gaughwin, P. M. *et al.* Hsa-miR-34b is a plasma-stable microRNA that is elevated in pre-manifest Huntington's disease. *Hum. Mol. Genet.* **20,** 2225–2237 (2011).
27. Yang, J. *et al.* MiR-34 modulates *Caenorhabditis elegans* lifespan via repressing the autophagy gene *atg9*. Age. doi:10.1007/s11357-011-9324-3 (2011).

Supplementary Information is linked to the online version of the paper at www.nature.com/nature.

Acknowledgements We thank C. Thummel, T. Jongens and A. Bashirullah for reagents. We are grateful to A. Cashmore, A. Burguete, J. Kim, S. Cherry, B. Gregory, A. Gitler and the Bonini laboratory for discussion and critical reading of the manuscript. We thank X. Teng for assistance with fly paraffin section. This work was funded by the NINDS (R01-NS043578) and the Ellison Foundation (to N.M.B.). L.-S.W. and K.C. are supported by a pilot grant from Penn Genome Frontiers Institute. L.-S.W. is supported by NIA (U01-AG-032984-02 and RC2-AG036528-01) and a Penn Institute on Aging pilot grant (AG010124). N.M.B. is an Investigator of the Howard Hughes Medical Institute. J.R.K. received support from NIH T32 AG00255.

Author Contributions N.L. and N.M.B. conceived and designed the project. N.L., M.L., M.A., G.-J.H., J.R.K. and Y.Z. planned, executed and analysed experiments. K.C. and L.S.-W. performed aging computational modelling. N.L. and N.M.B. wrote the manuscript with input from all authors.

Author Information The microarray data can be found in the Gene Expression Omnibus (GEO) of NCBI through accession number GSE25009. Reprints and permissions information is available at www.nature.com/reprints. The authors declare no competing financial interests. Readers are welcome to comment on the online version of this article at www.nature.com/nature. Correspondence and requests for materials should be addressed to N.M.B. (nbonini@sas.upenn.edu).

LETTER

doi:10.1038/nature10834

Maintenance of muscle stem-cell quiescence by microRNA-489

Tom H. Cheung[1,2], Navaline L. Quach[1,2], Gregory W. Charville[1,2,3], Ling Liu[1,2], Lidia Park[1,2], Abdolhossein Edalati[1,2], Bryan Yoo[1,2], Phuong Hoang[1,2] & Thomas A. Rando[1,2,4,5]

Among the key properties that distinguish adult mammalian stem cells from their more differentiated progeny is the ability of stem cells to remain in a quiescent state for prolonged periods of time[1,2]. However, the molecular pathways for the maintenance of stem-cell quiescence remain elusive. Here we use adult mouse muscle stem cells (satellite cells) as a model system and show that the microRNA (miRNA) pathway is essential for the maintenance of the quiescent state. Satellite cells that lack a functional miRNA pathway spontaneously exit quiescence and enter the cell cycle. We identified quiescence-specific miRNAs in the satellite-cell lineage by microarray analysis. Among these, miRNA-489 (miR-489) is highly expressed in quiescent satellite cells and is quickly downregulated during satellite-cell activation. Further analysis revealed that miR-489 functions as a regulator of satellite-cell quiescence, as it post-transcriptionally suppresses the oncogene *Dek*, the protein product of which localizes to the more differentiated daughter cell during asymmetric division of satellite cells and promotes the transient proliferative expansion of myogenic progenitors. Our results provide evidence of the miRNA pathway in general, and of a specific miRNA, miR-489, in actively maintaining the quiescent state of an adult stem-cell population.

The miRNA pathway has been shown to be essential for stem-cell pluripotency, proliferation and differentiation[3,4]. To understand whether adult quiescent stem cells are under active post-transcriptional control by miRNAs, we conditionally ablated the miRNA processing enzyme Dicer in adult muscle stem cells, or satellite cells, using a mouse strain that expresses a satellite-cell-specific, tamoxifen-inducible *Cre/loxP* system[5] (Supplementary Fig. 1) and is homozygous for a floxed Dicer allele[6] and a Cre-dependent yellow fluorescent protein (YFP) reporter[7]. Six days after the first tamoxifen injection to this conditional knockout strain, Dicer protein and miRNA levels were significantly downregulated in YFP-positive satellite cells ($P < 0.001$; Supplementary Figs 2 and 3). Notably, in conditional knockout mice we detected YFP-positive satellite cells that had spontaneously exited quiescence and entered the cell cycle (Fig. 1a, b). In control mice, less than 1% of YFP-positive satellite cells were Ki67-positive at this time. These observations suggest that an intact miRNA pathway is essential for the maintenance of satellite-cell quiescence. Deletion of Dicer also led to apoptosis of proliferating satellite-cell progeny (Fig. 1c, d and Supplementary Fig. 4). Together, these experiments demonstrate the essential role of miRNAs in the maintenance of satellite-cell quiescence and in the survival of proliferating myogenic progenitors.

To assess the impact of miRNA pathway disruption on satellite-cell homeostasis, we quantified the number of satellite cells using single-fibre explants and mononuclear cells that were isolated from uninjured muscles of conditional knockout mice 2 weeks after tamoxifen injections. We observed a marked reduction in satellite-cell number in the absence of Dicer (Fig. 1e, f). To confirm the functional loss of satellite cells, hindlimb muscles of tamoxifen-injected conditional knockout mice were injured to induce satellite-cell-mediated regeneration. Seven days after injury, very few regenerated fibres were observed in the conditional knockout mice, indicating severely impaired regeneration (Fig. 1g). Further analysis 6 months after injury revealed a marked reduction in the mass of injured muscles compared to the contralateral, uninjured muscles. By comparison, control mice exhibited a hypertrophic response after muscle injury (Fig. 1h). Consistent with the finding that adult muscle satellite cells have a low turnover rate[8], uninjured muscle appeared in general to be normal 6 months after disruption of the Dicer gene (Supplementary Fig. 5a). However, the loss of satellite cells resulted in mild muscle-fibre atrophy in conditional knockout animals over time (Supplementary Fig. 5b).

As the disruption of Dicer caused satellite cells to break quiescence and enter the cell cycle, we were interested in defining the role of specific miRNAs in maintaining the quiescent state. Quantitative real-time polymerase-chain-reaction (qRT–PCR)-based miRNA microarray analysis of highly purified quiescent satellite cells (QSCs) and activated satellite cells (ASCs) (Supplementary Fig. 6) revealed that 351 miRNAs were differentially regulated during satellite-cell activation (Supplementary Table 1). Of these, 22 were highly expressed in the quiescent state and markedly downregulated after satellite-cell activation (Fig. 2a). Among the 22 quiescence-specific miRNAs, we focused on miR-489 because it is evolutionarily conserved among species[9] and because it resides in intron 4 of the gene encoding calcitonin receptor (the *Ctr* gene; also known as *Calcr*) (Supplementary Fig. 7a), which is highly expressed in QSCs (Supplementary Fig. 7b, c) and has previously been shown to regulate satellite-cell quiescence[10]. Previous reports have suggested that intronic miRNAs co-express with host genes to co-regulate similar pathways[11]. The quiescence-specific expression of miR-489 and CTR was verified by qRT–PCR analysis (Fig. 2b, c). To determine whether miR-489 is specifically expressed in QSCs, we performed qRT–PCR analysis of isolated satellite cells and other mononuclear cell populations from uninjured muscle. As expected from the expression pattern of CTR (Supplementary Fig. 7c), miR-489 was highly enriched in QSCs relative to multinucleate muscle fibres or other mononuclear cells in the muscle (Fig. 2d, e).

To test whether a sustained expression of miR-489 could lead to an impairment of muscle regeneration by suppressing satellite-cell activation, an miR-489 expression plasmid was electroporated into hindlimb muscles *in vivo*. qRT–PCR analysis revealed a high level of miR-489 expression in tibialis anterior muscles electroporated with miR-489 plasmid compared with the level in controls (Supplementary Fig. 8b). Six days after electroporation, control muscles exhibited normal regeneration, whereas muscles expressing miR-489 exhibited a severe defect in regeneration (Fig. 3a and Supplementary Fig. 8a).

To test the hypothesis that overexpression of miR-489 suppresses muscle regeneration by maintaining satellite-cell quiescence and

[1]Paul F. Glenn Laboratories for the Biology of Aging, Stanford University School of Medicine, Stanford, California 94305, USA. [2]Department of Neurology and Neurological Sciences, Stanford University School of Medicine, Stanford, California 94305, USA. [3]Department of Developmental Biology, Stanford University School of Medicine, Stanford, California 94305, USA. [4]Neurology Service, Veterans Affairs Palo Alto Health Care System, Palo Alto, California 94304, USA. [5]Rehabilitation Research and Development Center of Excellence, Veterans Affairs Palo Alto Health Care System, Palo Alto, California 94304, USA.

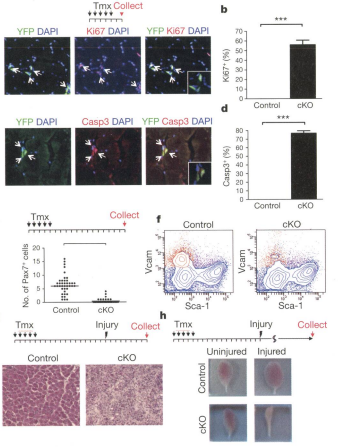

Figure 1 | The miRNA pathway is essential for the maintenance of satellite-cell quiescence and survival of activated satellite cells. **a**, The tamoxifen (Tmx) injection scheme (black arrows) for conditional Dicer gene inactivation is shown (top). Each tick represents 1 day. Six days after the first injection, Ki67 YFP double-positive satellite cells were found (white arrows). Nuclei were stained with DAPI. **b**, Quantification of the percentage of YFP-positive cells that were Ki67-positive (Ki67$^+$) in control and conditional knockout strain (cKO) mice (***$P < 0.001$). **c**, Six days after the first tamoxifen injection, muscles from control or cKO mice were analysed for apoptosis by staining for cleaved caspase 3. Nuclei were stained with DAPI. Inset in **a** and **c**, magnified view of the satellite cells in the full-size images. **d**, Quantification of the percentage of YFP-positive cells that were caspase-3-positive (Casp3$^+$) in control and cKO animals (***$P < 0.001$). **e**, Satellite-cell numbers were quantified on freshly isolated single fibres from control and cKO mice 2 weeks after tamoxifen injections (*$P < 0.001$). **f**, Satellite-cell numbers were quantified by FACS analyses of mononuclear cells from hindlimb muscles of control and cKO mice. Satellite cells are shown in orange in these representative FACS plots (See Supplementary Fig. 4). In four replicates, the percentage of satellite cells in total mononuclear cells in cKO muscles was markedly reduced (0.7%) compared to that in control muscles (3.0%). Blue, all other mononuclear cells. **g**, Tibialis anterior muscles from control or cKO mice were injured 2 weeks after tamoxifen injection and cryosections were stained with haematoxylin and eosin 7 days after injury. **h**, Tibialis anterior muscles from control or cKO mice were injured 2 weeks after tamoxifen injection and collected 6 months after injury. Severe muscle loss was observed in injured muscles from cKO mice only (shown next to the contralateral, uninjured muscle for comparison). Error bars in **b** and **d** indicate s.e.m.

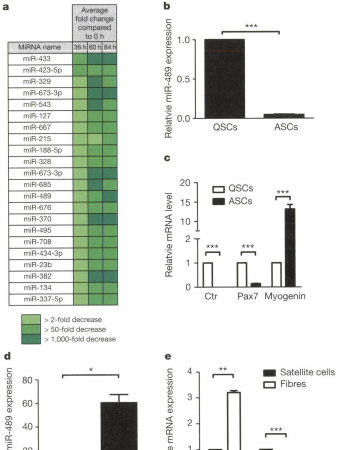

Figure 2 | miRNA expression in purified QSCs and ASCs. **a**, miRNA expression profiling during satellite-cell activation using qRT–PCR-based miRNA arrays. QSCs from uninjured muscles and ASCs from injured muscles at indicated time points were isolated by FACS (Supplementary Fig. 6). QSC-specific mouse miRNAs are shown. The complete data set is shown in Supplementary Table 1. **b**, qRT–PCR analysis of miR-489 transcript in QSCs and ASCs. Expression levels were normalized to snoRNA420. ***$P < 0.001$. **c**, qRT–PCR analysis of CTR, Pax7 and myogenin mRNA. Expression levels were normalized to glyceraldehyde-3-phosphate dehydrogenase (GAPDH). ***$P < 0.001$; **$P < 0.01$. **d**, qRT–PCR analysis of miR-489 transcript in QSCs and all other mononuclear cells in hindlimb muscles. Expression levels were normalized to snoRNA420. *$P < 0.05$. **e**, qRT–PCR analysis of miR-206 and miR-489 transcript in QSCs and single-fibre explants. Expression levels were normalized to snoRNA420. ***$P < 0.001$; **$P < 0.01$. All error bars indicate s.e.m.

suppressing activation, we overexpressed miR-489 or anti-miR-489 in fibre-associated QSCs *ex vivo*. Using syndecan 4 as a satellite-cell marker on fibre explants[12,13], we quantified the number of satellite cells on fibres 3 days after transfection. Satellite cells treated with anti-miR-489 exhibited similar proliferative activity as control satellite cells, whereas satellite cells treated with miR-489 exhibited markedly reduced proliferation (and no evidence of apoptosis) (Fig. 3b). Furthermore, fewer than 50% of the cells treated with miR-489 progressed through a single round of cell division over the course of the experiment as determined by 5-ethynyl-2′-deoxyuridine (EdU) labelling (Fig. 3c). To test whether miR-489 regulates satellite-cell quiescence in a cell-autonomous manner, we used myogenic differentiation 1 (Myod; also known as Myod1) expression as an indicator of satellite-cell activation[14] and quantified the percentage of satellite cells expressing Myod 48 h after miR-489 transfection. Consistent with the fibre-explant experiment, miR-489 suppressed satellite-cell activation (Fig. 3d). Together, these experiments demonstrate that miR-489 regulates satellite-cell quiescence in a cell-autonomous manner and that over-expression of a single miRNA is sufficient to prolong the quiescent state and delay QSC activation, resulting in an impairment of regeneration *in vivo*.

Next, we tested whether inhibition of miR-489 could result in the spontaneous activation of QSCs, which rarely divide in the absence of any activating stimuli[8]. Cholesterol-conjugated 'antagomirs' (ref. 15) that specifically target miR-489, or control scrambled antagomirs,

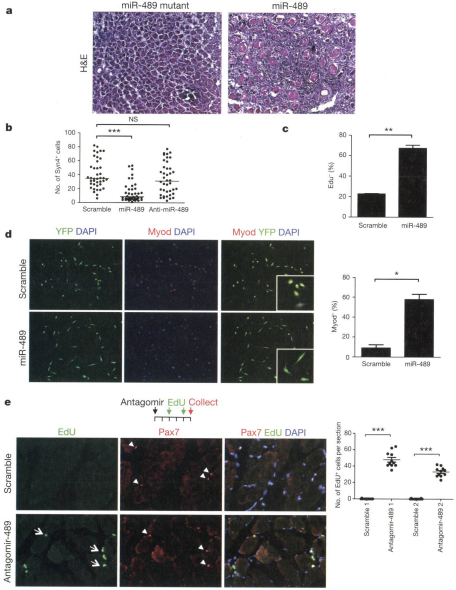

Figure 3 | miRNA-489 regulates satellite-cell quiescence. **a**, Hindlimb muscles were electroporated with either miR-489 expression plasmid (right) or a control miR-489 mutant plasmid (left). Muscles were collected 6 days later and haematoxylin and eosin staining was performed on cryosections. A representative image of three independent replicates is shown. **b**, miR-489 or anti-miR-489 was overexpressed in fibre-associated satellite cells. Three days after transfection, the number of syndecan-4-positive ($Syn4^+$) satellite-cell progeny was quantified. $^{***}P < 0.001$; NS, not significant. **c**, In studies such as those in **b**, EdU was added to the medium at the time of miR-489 (or control) transfection and the percentage of $Syn4^+$ cells that were EdU-negative (EdU^-) was determined after 3 days. $^{**}P < 0.01$. **d**, Left, FACS-sorted QSCs from $Pax7^{CreER/+}$; $ROSA^{eYFP/+}$ mice were plated and transfected with miR-489 and analysed for Myod expression 48 h later. Right, quantification of the percentage of YFP-positive cells that were Myod-negative ($Myod^-$). Nuclei were stained with DAPI. $^{*}P < 0.05$. **e**, Left, satellite-cell activation *in vivo*, as determined by EdU incorporation, was assessed in muscles in which miR-489 was inhibited by the systemic injection of a cholesterol-conjugated anti-miR-489 oligonucleotide (antagomir-489) or a scrambled antagomir (scramble). Pax7 EdU double-positive (arrows) and Pax7-positive cells (arrowheads) are highlighted. Right, quantitation of the number of EdU-positive (EdU^+) cells on cryosections. Two representative replicates of four independent experiments are shown (nuclei were stained with DAPI). $^{***}P < 0.001$. All error bars indicate s.e.m.

were delivered systemically to adult mice. Four days after a single antagomir injection, miR-489 transcript levels decreased precipitously (Supplementary Fig. 9). In contrast to the control mice, which were injected with scrambled antagomirs, mice injected with anti-miR-489 antagomirs exhibited spontaneous activation of QSCs that incorporated EdU (Fig. 3e). Notably, inhibition of one quiescence-specific miRNA, miR-489, was sufficient to induce QSCs to break quiescence and progress through the cell cycle in uninjured muscle.

The observation that inhibition of miR-489 induced satellite-cell activation and proliferation prompted us to test whether miR-489 functions to suppress one or more key regulators of proliferation, thereby maintaining the quiescent state. We used the bioinformatics tool TargetScan to search for miR-489 target genes that contain putative miR-489 target sites in their 3′ untranslated regions (3′ UTRs)[9]. Among the 86 targets predicted by TargetScan, the transcript with the highest context score[16] was the oncogene *Dek* (Supplementary Fig. 10), which has been shown to be induced in tumour cells and to regulate cell proliferation and messenger RNA splicing[17,18]. We analysed the temporal expression of *Dek* mRNA and protein during satellite-cell activation. Using paired box protein 7 (Pax7) as a marker of QSCs and Myod as a marker of ASCs[19,20], we found that Dek protein was not expressed in QSCs but was strongly upregulated after satellite-cell activation both in fibre-explant studies *ex vivo* and in regeneration studies *in vivo* (Fig. 4a and Supplementary Fig. 11a–c). Likewise, *Dek* mRNA levels were higher in ASCs compared to QSCs (Supplementary Fig. 11d).

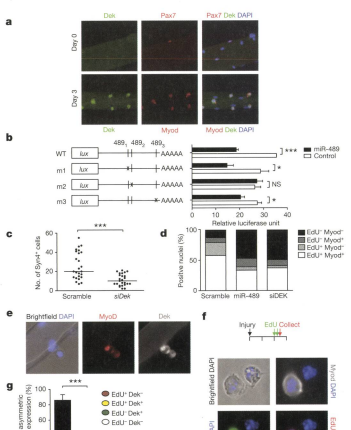

Figure 4 | Targeting of *Dek* mRNA by miR-489 and regulation of cell-fate decision of satellite-cell progeny by Dek. **a**, Co-localization of Dek and myogenic markers in fibre-associated satellite cells. Fibre explants were fixed immediately after isolation (Day 0) or cultured for 3 days in suspension and stained for expression of Pax7 and Dek, or Myod and Dek, as indicated. Nuclei were stained with DAPI. **b**, CMV-miR-489 was co-transfected into 293T cells with wild-type (WT) or mutant *Dek* 3′ UTR constructs inserted after the stop codon of a luciferase gene. The Dek 3′ UTR carries three putative miR-489 target sites (489$_1$, 489$_2$ and 489$_3$) (putative pairing as shown in Supplementary Fig. 10). Schematics of wild-type and mutant constructs (m1, m2 and m3) are shown with the relative luciferase activities associated with each construct. $^{***}P < 0.001$; $^{*}P < 0.05$; NS: not significant. **c**, Satellite cells in fibre explants were transfected with *Dek* short interfering RNA (siRNA) (*siDek*) and cultured for 3 days, and the satellite-cell progeny were quantified by syndecan 4 staining ($n = 3$). $^{***}P < 0.001$. **d**, FACS-purified QSCs were plated and transfected with miR-489 or *siDek* for 48 h. EdU was added to the medium at the same time as transfection. Cells were stained for EdU incorporation and Myod expression. Bar graphs show the proportion of cells expressing each marker under each condition. **e**, Dek asymmetrically localizes to one daughter after cell division. Fibre-associated satellite cells were cultured for 48 h and stained for expression of Myod and Dek. Nuclei were stained with DAPI. **f**, The timeline for injury, EdU injections and collection of cells is shown (top). Cells were stained for EdU incorporation to reveal nonrandom template-strand segregation and for Myod expression to reveal divergent cell fates. Dek co-segregates almost exclusively with the newly synthesized template strands. Images show a representative example of a cell pair exhibiting divergent cell fates with asymmetric segregation of template strands. Nuclei were stained with DAPI. **g**, Quantitative analysis of concordant and discordant asymmetries of Dek and EdU in asymmetric satellite-cell divisions in studies such as those in **f**. $^{**}P < 0.001$. All error bars indicate s.e.m.

Dek protein was downregulated when QSCs or myoblasts were transfected with miR-489 (Supplementary Fig. 12), suggesting that Dek is a direct target of miR-489. To test this directly, wild-type and mutant versions of the 3′ UTR of Dek were cloned downstream of a luciferase reporter, and these reporter constructs were co-transfected with an miR-489 expression construct into 293T cells. The wild-type *Dek* 3′ UTR was effectively downregulated by miR-489 (Fig. 4b). Although TargetScan analysis revealed three potential target sites for miR-489, a single site (m2) was sufficient to account for the suppression of reporter expression by miR-489 (Fig. 4b).

We next examined the role of Dek in satellite-cell quiescence and activation using a loss-of-function approach. Dek knockdown reduced satellite-cell proliferation (Fig. 4c) and prevented satellite-cell activation to the same degree as did miR-489 overexpression (Fig. 4d). The ability of Dek knockdown to phenocopy the effect of miR-489 overexpression suggests a central role of Dek in regulating satellite-cell exit from quiescence. To understand whether miR-489 overexpression suppresses proliferation by regulating Dek expression, we overexpressed miR-489 or miR-489 mutant with a Dek complementary DNA construct that lacks its 3′ UTR in proliferating myoblasts. Overexpression of miR-489 alone reduced cell proliferation, whereas overexpression of Dek substantially increased cell proliferation independent of the expression of miR-489 or miR-489 mutant (Supplementary Fig. 13). Together, these experiments suggest that Dek is an important target of miR-489 that is involved in the regulation of satellite-cell quiescence and activation.

Although Dek expression was highly induced after satellite-cell activation, consistent with its role in proliferative expansion of the transit-amplifying myogenic progenitors, it was absent in self-renewed satellite cells after muscle injury *in vivo* (Supplementary Fig. 11c). We therefore studied satellite-cell self-renewal in fibre explants *ex vivo*, in which the asymmetric expression of Myod by daughter cells heralds a divergent cell fate whereby the Myod-positive daughter progresses along the myogenic lineage and the Myod-negative daughter renews the satellite-cell population[19]. Intriguingly, in such pairs, we observed asymmetric Dek expression, in which Dek expression coincided with Myod expression in the same daughter cell (Fig. 4e). This co-localization suggests that the Dek-positive daughter is destined for proliferative amplification as a progenitor and that the Dek-negative daughter is destined for self-renewal. To test whether the process of self-renewal is associated with the absence of Dek, we examined cells undergoing asymmetric division by analysing nonrandom chromosome segregation, a process that we and others have previously shown to distinguish the differentiating progenitor from the self-renewing stem cell[21,22]. Consistent with the Myod asymmetry, we found that Dek was absent in the daughter cell inheriting chromosomes bearing older template DNA strands, an inheritance pattern that is characteristic of the self-renewing cell, whereas Dek was expressed in the daughter cell that is destined for proliferative amplification and differentiation (Fig. 4f, g and Supplementary Fig. 14).

The finding that Dek is a key target of miR-489 in maintaining quiescence provides insight into the molecular pathways that regulate the quiescent state. These data demonstrate that the molecular regulation of quiescence is dependent on the expression of specific miRNAs and is integrated in the signalling network that regulates divergent fates of stem-cell progeny during asymmetric cell division.

METHODS SUMMARY

Single-fibre explants. Extensor digitorum longus (EDL) muscles were excised and digested in Collagenase II (500 units per ml in Ham's F10 medium) as previously described[23]. Fibres were then washed extensively and cultured in medium containing Ham's F10, 10% horse serum and 0.05% chick embryo extract. Every 24 h, 50% of the medium was replaced with Ham's F10 medium with 20% FBS. Extensor digitorum longus (EDL) fibres were cultured in suspension. Fixed fibres were stained and the number of satellite cells was quantified per fibre.

Satellite-cell isolation and fluorescence-activated cell sorting. Hindlimb muscles were dissected and dissociated to yield a muscle suspension and digested with Collagenase II (500 units per ml; Invitrogen) in Ham's F10 medium with 10% horse serum (Invitrogen) for 90 min. Digested fibre suspensions were washed and digested further with Collagenase II (100 units per ml) and Dispase (2 units per ml;

invitrogen) for 30 min. Digested fibre suspensions were triturated and washed further to yield a mononuclear-cell suspension for cell-surface staining for fluorescence-activated cell sorting (FACS). Mononuclear cells were stained with Vcam-biotin (clone 429; BD Bioscience), CD31-APC (clone MEC 13.3; BD Bioscience), CD45-APC (clone 30-F11; BD Bioscience) and Sca-1-Pacific-Blue (clone D7; Biolegend) at 1:75. Streptavidin-PE-cy7 was used to amplify the Vcam signal (BD Biosciences, 1:75). Cell sorting was performed using a BD FACSAria II or BD FACSAria III cell sorter equipped with 488-nm, 633-nm and 405-nm lasers. The machine was optimized for purity and viability, and sorted cells were subjected to FACS analysis directly after sorting to ensure purity. A small fraction of sorted cells was plated and stained for Pax7 and Myod to assess the purity of the sorted population purity.

Full Methods and any associated references are available in the online version of the paper at www.nature.com/nature.

Received 16 January 2011; accepted 5 January 2012.

1. Li, L. & Clevers, H. Coexistence of quiescent and active adult stem cells in mammals. *Science* **327,** 542–545 (2010).
2. Fuchs, E. The tortoise and the hair: slow-cycling cells in the stem cell race. *Cell* **137,** 811–819 (2009).
3. Yi, R., Poy, M. N., Stoffel, M. & Fuchs, E. A skin microRNA promotes differentiation by repressing 'stemness'. *Nature* **452,** 225–229 (2008).
4. Tiscornia, G. & Izpisua Belmonte, J. C. MicroRNAs in embryonic stem cell function and fate. *Genes Dev.* **24,** 2732–2741 (2010).
5. Nishijo, K. *et al.* Biomarker system for studying muscle, stem cells, and cancer *in vivo*. *FASEB J.* **23,** 2681–2690 (2009).
6. Harfe, B. D., McManus, M. T., Mansfield, J. H., Hornstein, E. & Tabin, C. J. The RNaseIII enzyme Dicer is required for morphogenesis but not patterning of the vertebrate limb. *Proc. Natl Acad. Sci. USA* **102,** 10898–10903 (2005).
7. Srinivas, S. *et al.* Cre reporter strains produced by targeted insertion of EYFP and ECFP into the ROSA26 locus. *BMC Dev. Biol.* 1, 4 (2001).f.
8. Morgan, J. E. & Partridge, T. A. Muscle satellite cells. *Int. J. Biochem. Cell Biol.* **35,** 1151–1156 (2003).
9. Friedman, R. C., Farh, K. K., Burge, C. B. & Bartel, D. P. Most mammalian mRNAs are conserved targets of microRNAs. *Genome Res.* **19,** 92–105 (2009).
10. Fukada, S. *et al.* Molecular signature of quiescent satellite cells in adult skeletal muscle. *Stem Cells* **25,** 2448–2459 (2007).
11. van Rooij, E. *et al.* Control of stress-dependent cardiac growth and gene expression by a microRNA. *Science* **316,** 575–579 (2007).
12. Olguin, H. C. & Olwin, B. B. Pax-7 up-regulation inhibits myogenesis and cell cycle progression in satellite cells: a potential mechanism for self-renewal. *Dev. Biol.* **275,** 375–388 (2004).
13. Tanaka, K. K. *et al.* Syndecan-4-expressing muscle progenitor cells in the SP engraft as satellite cells during muscle regeneration. *Cell Stem Cell* **4,** 217–225 (2009).
14. Zammit, P. S., Partridge, T. A. & Yablonka-Reuveni, Z. The skeletal muscle satellite cell: the stem cell that came in from the cold. *J. Histochem. Cytochem.* **54,** 1177–1191 (2006).
15. Krutzfeldt, J. *et al.* Silencing of microRNAs in vivo with 'antagomirs'. *Nature* **438,** 685–689 (2005).
16. Grimson, A. *et al.* MicroRNA targeting specificity in mammals: determinants beyond seed pairing. *Mol. Cell* **27,** 91–105 (2007).
17. Khodadoust, M. S. *et al.* Melanoma proliferation and chemoresistance controlled by the DEK oncogene. *Cancer Res.* **69,** 6405–6413 (2009).
18. Soares, L. M., Zanier, K., Mackereth, C., Sattler, M. & Valcarcel, J. Intron removal requires proofreading of U2AF/3′ splice site recognition by DEK. *Science* **312,** 1961–1965 (2006).
19. Zammit, P. S. *et al.* Muscle satellite cells adopt divergent fates: a mechanism for self-renewal? *J. Cell Biol.* **166,** 347–357 (2004).
20. Zammit, P. S. *et al.* Pax7 and myogenic progression in skeletal muscle satellite cells. *J. Cell Sci.* **119,** 1824–1832 (2006).
21. Conboy, M. J., Karasov, A. O. & Rando, T. A. High incidence of non-random template strand segregation and asymmetric fate determination in dividing stem cells and their progeny. *PLoS Biol.* **5,** e102 (2007).
22. Shinin, V., Gayraud-Morel, B., Gomes, D. & Tajbakhsh, S. Asymmetric division and cosegregation of template DNA strands in adult muscle satellite cells. *Nature Cell Biol.* **8,** 677–687 (2006).
23. Rosenblatt, J. D., Lunt, A. I., Parry, D. J. & Partridge, T. A. Culturing satellite cells from living single muscle fibre explants. *In vitro Cell Dev. Biol. Anim.* **31,** 773–779 (1995).

Supplementary Information is linked to the online version of the paper at www.nature.com/nature.

Acknowledgements We thank the members of the Rando laboratory for comments and discussions. We thank B. Olwin for providing the syndecan 4 antibody. This work was supported by the Glenn Foundation for Medical Research and by grants from the National Institutes of Health (NIH) (P01 AG036695, R01 AG23806 (R37 MERIT Award), R01 AR062185 and DP1 OD000392 (an NIH Director's Pioneer Award)) and the Department of Veterans Affairs (Merit Review) to T.A.R.

Author Contributions T.H.C. and T.A.R. conceived the study. T.H.C., N.L.Q., G.W.C., L.L. and T.A.R. designed the experiments. T.H.C., B.Y. and L.L. performed all FACS analyses. T.H.C., N.L.Q., G.W.C., L.P., A.E., B.Y. and P.H. performed the experiments and analysed the experimental data. T.H.C. and T.A.R. wrote the manuscript.

Author Information Reprints and permissions information is available at www.nature.com/reprints. The authors declare no competing financial interests. Readers are welcome to comment on the online version of this article at www.nature.com/nature. Correspondence and requests for materials should be addressed to T.A.R. (rando@stanford.edu).

LETTER

doi:10.1038/nature10825

Clonal selection drives genetic divergence of metastatic medulloblastoma

Xiaochong Wu[1], Paul A. Northcott[1], Adrian Dubuc[1], Adam J. Dupuy[2], David J. H. Shih[1], Hendrik Witt[3], Sidney Croul[4], Eric Bouffet[5], Daniel W. Fults[6], Charles G. Eberhart[7], Livia Garzia[1], Timothy Van Meter[8], David Zagzag[9], Nada Jabado[10], Jeremy Schwartzentruber[11], Jacek Majewski[10], Todd E. Scheetz[2], Stefan M. Pfister[3], Andrey Korshunov[12], Xiao-Nan Li[13], Stephen W. Scherer[14], Yoon-Jae Cho[15], Keiko Akagi[16], Tobey J. MacDonald[17], Jan Koster[18], Martin G. McCabe[19], Aaron L. Sarver[20], V. Peter Collins[21], William A. Weiss[22], David A. Largaespada[20], Lara S. Collier[23] & Michael D. Taylor[24]

Medulloblastoma, the most common malignant paediatric brain tumour, arises in the cerebellum and disseminates through the cerebrospinal fluid in the leptomeningeal space to coat the brain and spinal cord[1]. Dissemination, a marker of poor prognosis, is found in up to 40% of children at diagnosis and in most children at the time of recurrence. Affected children therefore are treated with radiation to the entire developing brain and spinal cord, followed by high-dose chemotherapy, with the ensuing deleterious effects on the developing nervous system[2]. The mechanisms of dissemination through the cerebrospinal fluid are poorly studied, and medulloblastoma metastases have been assumed to be biologically similar to the primary tumour[3,4]. Here we show that in both mouse and human medulloblastoma, the metastases from an individual are extremely similar to each other but are divergent from the matched primary tumour. Clonal genetic events in the metastases can be demonstrated in a restricted subclone of the primary tumour, suggesting that only rare cells within the primary tumour have the ability to metastasize. Failure to account for the bicompartmental nature of metastatic medulloblastoma could be a major barrier to the development of effective targeted therapies.

Thirty percent of patched-1-heterozygous ($Ptch^{+/-}$) mice develop non-disseminated medulloblastoma by 8 months of age[5]. Recently, the *Sleeping Beauty* (SB) transposon system was shown to be an effective tool for functional genomics studies of solid tumour initiation and progression[6,7]. We expressed the SB11 transposase in cerebellar progenitor cells in transgenic mice under the *Math1* (also known as *Atoh1*) enhancer/promoter, but we did not observe any tumours when these mice were bred with mice transgenic for a concatemer of the T2/Onc transposon[8] (Fig. 1a–j and Supplementary Figs 1 and 2). However, on a $Ptch^{+/-}$ background, these *Math1-SB11*/T2Onc mice showed increased penetrance of medulloblastoma (~97%; 271 of 279 mice) compared with controls (~39%; 54 of 139 mice), as well as decreased latency (2.5 months compared with 8 months) (Fig. 1 and Supplementary Fig. 2). Although $Ptch^{+/-}$ medulloblastomas are usually localized, the addition of SB transposition results in metastatic dissemination through the cerebrospinal fluid pathways, identical to the pattern that is seen in human children (Fisher's exact test, $P = 1.8 \times 10^{-7}$, odds ratio = 5.2; Supplementary Table 1) (Fig. 1c, d and Supplementary Fig. 2). As neither transposon nor transposase alone had an effect on tumour incidence, latency or dissemination, we conclude that SB-induced insertional mutagenesis drives medulloblastoma progression on the $Ptch^{+/-}$ background (Fig. 1i and Supplementary Fig. 2).

Humans with germline mutations in the tumour-suppressor gene *TP53* have Li–Fraumeni syndrome and have an increased risk of developing medulloblastoma. Although no medulloblastomas were found in mice with mutant *Tp53* (also known as *Trp53*) (denoted $Tp53^{mut}$ mice, which includes $Tp53^{+/-}$ and $Tp53^{-/-}$), 40% of $Tp53^{mut}$/*Math1-SB11*/T2Onc mice developed disseminated medulloblastoma[9] (Fig. 1e–h, j and Supplementary Fig. 2). Human medulloblastomas with *TP53* mutations frequently have large cell/anaplastic histology. $Tp53^{mut}$/*Math1-SB11*/T2Onc medulloblastomas have large cells, nuclear atypia and nuclear moulding that is typical of large cell/anaplastic histology (Fig. 1f). We conclude that SB transposition can drive the initiation and progression of metastatic medulloblastoma on a $Tp53^{mut}$ background.

We used linker-mediated PCR and 454 sequencing to identify the site of T2/Onc insertions in $Ptch^{+/-}$/*Math1-SB11*/T2Onc and $Tp53^{mut}$/*Math1-SB11*/T2Onc primary medulloblastomas and their matched metastases. Genes that contained insertions statistically more frequently than the background rate were identified as gene-centric common insertion sites (gCISs)[10]. We identified 359 gCISs in 139 primary tumours on the $Ptch^{+/-}$ background and 26 gCISs in 36 primary medulloblastomas on the $Tp53^{mut}$ background (Supplementary Tables 2–7 and Supplementary Figs 3–5). A large number of gCISs were candidate medulloblastoma oncogenes or tumour-suppressor genes[11] (Supplementary Table 8). Insertions in candidate tumour-suppressor genes, including *Ehmt1*, *Crebbp* and *Mxi1*, are predicted to cause a loss of function (Fig. 1k–m), whereas insertions in putative medulloblastoma oncogenes are largely gain of function, as exemplified by *Myst3* (Fig. 1n).

Many gCISs mapped to regions of amplification, focal hemizygous deletion and homozygous deletion (Supplementary Table 8) that we

[1]Arthur and Sonia Labatt Brain Tumour Research Center, and Program in Developmental and Stem Cell Biology, The Hospital for Sick Children, Toronto, Ontario M5G 1X8, Canada. [2]Molecular & Cellular Biology Program, The University of Iowa, Iowa City, Iowa 52242, USA. [3]German Cancer Research Center (DKFZ), and Department of Pediatric Oncology, Hematology and Immunology, University Hospital Heidelberg, Im Neuenheimer Feld 280, 69120 Heidelberg, Germany. [4]University Health Network Pathology, Arthur and Sonia Labatt Brain Tumour Research Centre, Department of Laboratory Medicine and Pathobiology, University of Toronto, Toronto, Ontario M5S 1A1, Canada. [5]Brain Tumour Program, Haematology and Oncology, The Hospital for Sick Children, Toronto, Ontario M5G 1X8, Canada. [6]Department of Neurosurgery, University of Utah School of Medicine, Salt Lake City, Utah 84132, USA. [7]Johns Hopkins University, Baltimore, Maryland 21210, USA. [8]Virginia Commonwealth University, Richmond, Virginia 23284, USA. [9]Department of Pathology and Neurosurgery, Division of Neuropathology, New York University School of Medicine, New York, New York 10016, USA. [10]Departments of Human Genetics and Experimental Medicine, McGill University, Montreal H3Z 2Z3, Quebec, Canada. [11]McGill University and Genome Quebec Innovation Centre, Montreal, Quebec H3A 0G1, Canada. [12]German Cancer Research Institute (DKFZ) and Department of Neuropathology, University of Heidelberg, Im Neuenheimer Feld 220/221, 69120 Heidelberg, Germany. [13]Brain Tumor Program, Texas Children's Cancer Center, and Department of Pediatrics, Baylor College of Medicine, Houston, Texas 77030, USA. [14]Program in Genetics and Genomic Biology and The Centre for Applied Genomics, The Hospital for Sick Children, and McLaughlin Centre and Department of Molecular Genetics, University of Toronto, Toronto, Ontario M5S 1A1, Canada. [15]Departments of Neurology and Neurosurgery, Stanford University School of Medicine, Stanford, California 94305, USA. [16]Department of Molecular Virology, Immunology and Medical Genetics, The Ohio State University Comprehensive Cancer Center, Columbus, Ohio 43210, USA. [17]Pediatric Neuro-Oncology Program, Emory University School of Medicine, Atlanta, Georgia 30307, USA. [18]Department of Human Genetics, Academic Medical Center, University of Amsterdam, 1100 DE Amsterdam, The Netherlands. [19]School of Cancer and Enabling Sciences, University of Manchester, Manchester M20 4BX, UK. [20]Masonic Cancer Center, University of Minnesota, Minneapolis, Minnesota 55455, USA. [21]Department of Pathology, University of Cambridge, Cambridge CB2 1QP, UK. [22]Departments of Neurology, Pediatrics and Neurological Surgery, University of California, San Francisco, California 94143, USA. [23]School of Pharmacology, University of Wisconsin, Madison, Wisconsin 53715, USA. [24]Division of Neurosurgery, Arthur and Sonia Labatt Brain Tumour Research Center, and Program in Developmental and Stem Cell Biology, The Hospital for Sick Children, University of Toronto, Toronto, Ontario M5G 1X8, Canada.

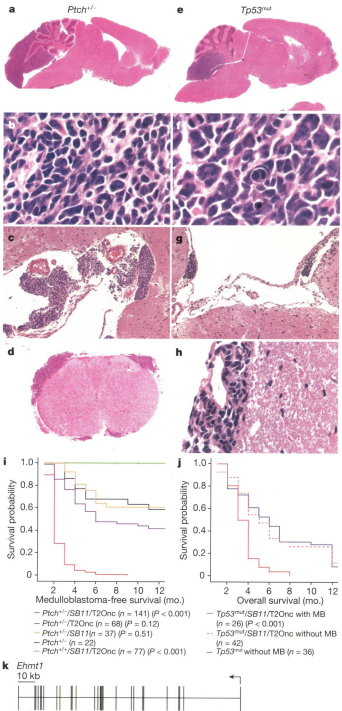

recently reported in the genome of a large cohort of human medulloblastomas[11]. There is a high level of overlap between gCISs and known cancer genes (in the Catalogue of Somatic Mutations in Cancer (COSMIC) database) (Supplementary Tables 9 and 10), suggesting that many gCISs are bona fide driver genes in medulloblastoma (Fisher's exact test, $P = 0.0012$)[12]. Similarly, many of the mouse gCISs and the genes amplified in human medulloblastomas are overexpressed in human *SHH*-driven medulloblastomas (Supplementary Fig. 6). Conversely, mouse gCISs hemizygously deleted in human medulloblastomas were frequently expressed at a lower level in human medulloblastomas (Supplementary Fig. 6). The expression of six out of seven gCISs that had been studied by immunohistochemistry on a human medulloblastoma tissue microarray was associated with significantly worse overall and progression-free survival in human medulloblastoma[13] (Supplementary Table 11 and Supplementary Figs 7 and 8). We conclude that our SB-driven leptomeningeal-disseminated medulloblastoma model resembles the human disease anatomically, pathologically and genetically and thus is an accurate model of the human disease that can be used to identify candidate driver events and understand the pathogenesis of human medulloblastoma.

We compared the gCISs identified from $Ptch^{+/-}$/*Math1-SB11*/T2Onc and $Tp53^{mut}$/*Math1-SB11*/T2Onc primary medulloblastomas and matched metastases (Supplementary Table 2). Strikingly, the overlap between primary tumour gCISs (pri-gCISs) from $Ptch^{+/-}$/*Math1-SB11*/T2Onc tumours and those from metastases (met-gCISs) from the same animals was only 9.3% of all gCISs (Fig. 2a). Similarly, the overlap between pri-gCISs from $Tp53^{mut}$/*Math1-SB11*/T2Onc mice and the matching met-gCISs was only 8.9% (Fig. 2b). The leptomeningeal metastases and the matched primary tumour have identical, highly clonal insertion sites on both genetic backgrounds (Fig. 2c). The probability of two (or three) unrelated tumours having SB insertions in exactly the same TA dinucleotide is extremely low. We conclude that the leptomeningeal metastases and the matched primary tumour arise from a common transformed progenitor cell and have subsequently undergone genetic divergence.

Sequencing also identified insertions that are highly clonal in the metastases but are not observed in the matched primary tumour (data not shown). End-point PCR for these insertions in the matched primary and metastatic tumours shows that the insertion is highly clonal in the metastasis (or metastases) and is present in a very small subclone of the primary tumour (Fig. 2d and Supplementary Fig. 9). These data are consistent with a model in which metastatic disease arises from a minor restricted subclone of the primary tumour. Dissemination could occur repeatedly from the same subclone of the primary tumour, which seeds the rest of the central nervous system, or it could occur once, followed by reseeding of the rest of the leptomeningeal space by the initial metastasis. Insertions that are restricted to a minor subclone of the

Figure 1 | Transposon mutagenesis models of disseminated human medulloblastoma. a–**d**, The histology of transposon-driven medulloblastoma on the $Ptch^{+/-}$ background resembles human medulloblastoma, with leptomeningeal metastases on the surface of the brain (**c**) and spinal cord (**d**). Images show haematoxylin and eosin staining (**a**, entire brain; **b**, upper spinal cord). **e**–**h**, The histology of transposon-driven medulloblastoma on the $Tp53^{mut}$ background shows histological features of large cell/anaplastic medulloblastoma, including nuclear pleomorphism and nuclear wrapping (**f**). Dissemination to the leptomeningeal spaces of the brain (**g**) and spinal cord (**h**) also occurs on this background. **i**, $Ptch^{+/-}$ mice with SB transposition develop more frequent medulloblastomas with a shorter latency than $Ptch^{+/-}$ mice without transposition. *P* values are from *t*-tests of survival comparing individual genotypes to $Ptch^{+/-}$ mice; *n*, number of mice per genotype. mo., months. **j**, Medulloblastoma (MB) was not observed in $Tp53^{mut}$ mice without transposition but was observed in 42% of $Tp53^{mut}$ mice with transposition. *P* values are from *t*-tests comparing survival between $Tp53^{mut}$ mice and $Tp53^{mut}$/*SB11*/T2Onc mice with MB; *n*, number of mice. **k**–**n**, Insertion maps of notable gCISs. Insertions in the direction of transcription are denoted by green arrows, and those against the direction of transcription are denoted by red arrows. Transcription start sites are denoted by black arrows.

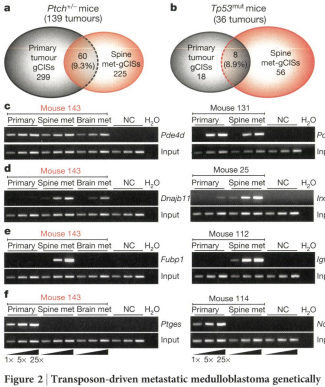

Figure 2 | Transposon-driven metastatic medulloblastoma genetically differs from the primary tumour. **a**, **b**, Venn diagrams depicting the degree of overlap and discordance in the gCISs in primary tumours and metastases, on the *Ptch*$^{+/-}$ and *Tp53*^{mut} backgrounds. **c**–**f**, Insertion-site end-point PCR was used to demonstrate the relative clonality of insertions between samples. Data for medulloblastoma in five mice are shown (mouse 143, left; and four mice, right). Three levels of input DNA were used for each sample (1×, 5× and 25×, with the increase depicted by a wedge). Shown are clonal events found in both the primary tumour and matching metastases (met) (*c*), insertions that are highly clonal in the metastases but very subclonal in the matching primary tumour (**d**), insertions that are highly clonal in the metastases but undetectable in the matching primary tumour (**e**), and insertions that are highly clonal in the primary tumour but undetectable in the matching metastases (**f**). NC, negative control; genomic DNA from a *Math1-SB11*/T2Onc double-transgenic mouse cerebellum.

primary tumour but that are clonal in the metastases could correspond to the previously described 'metastasis virulence' genes[14], which offer a genetic advantage during dissemination but not to the primary tumour. Another explanation for our data could be that the primary tumour was reseeded by a metastatic clone that had acquired additional genetic events in the periphery. This hypothesis is mitigated by the presence of highly clonal insertions in the metastasis that are completely absent from the primary tumour in the same animal[15] (Fig. 2e). As reseeding should be accompanied by contamination of the primary tumour with events found in the metastases, the absence of these events in the matched primary tumour makes reseeding much less likely (Fig. 2e). We propose that events found in only one metastasis represent progression events that are acquired post metastasis and that could lead to localized progression of metastatic disease, as is sometimes observed in human children.

We observed highly clonal insertions in the primary tumour, including in known medulloblastoma oncogenes such as *Notch2* and *Tert*, that were not found in the matching metastases (Fig. 2f). This pattern could be explained through remobilization of the SB transposon in the metastatic tumour; however, no signs of the DNA footprint remaining after SB remobilization at these loci were observed[16] (Supplementary Fig. 10). We suggest that these events, which may constitute driver events in the primary tumour, have arisen in the primary tumour after the metastases have disseminated (post-dispersion events). Although these known oncogenes are attractive targets for therapy, their utility as targets may be limited if the targets are not also found in the leptomeningeal compartment of the disease. Our data from two separate mouse lines support a model in which medulloblastoma disseminates early from a restricted subclone of the primary tumour and in which the primary tumour and the matched metastases then undergo differential clonal selection and evolution. Failure to account for the differences between the primary and leptomeningeal compartments could lead to the failure of targeted therapies. Failure to study the leptomeningeal disease (Fig. 2d, e) could result in systematically overlooking crucial targets for therapy in this compartment.

Examining the met-gCISs using Gene Set Enrichment Analysis (GSEA) demonstrated differences between the primary and metastatic disease, including enrichment for genes involved in the cytoskeleton in metastases (Supplementary Table 12). Targets that are present in both compartments and are maintenance genes, as exemplified by *Pdgfra*, will be optimal targets for treating both the primary tumour and the metastases (Fig. 2c and Supplementary Tables 7 and 9).

Pten, *Akt2*, *Igf2* and *Pik3r1* are all met-gCISs, implicating the phosphatidylinositol-3-OH kinase (PI(3)K) pathway in medulloblastoma progression. We injected the cerebellum of Nestin-TVA mice[17] with either an *Shh*-overexpressing retroviral vector (denoted *Shh* virus) or an *Shh*- and *Akt*-overexpressing retroviral vector (denoted *Shh* + *Akt* virus). Cerebellar injection of *Shh* virus alone resulted in medulloblastomas in 6 of 41 animals, compared with 20 of 42 animals injected with *Shh* + *Akt* virus ($P = 0.0018$). Although metastases were not observed with *Shh* virus alone (0 of 41), medulloblastoma metastases were observed in 9 of 42 animals injected with *Shh* + *Akt* virus ($P = 0.0024$) (Supplementary Fig. 11). *In vivo* modelling validates PI(3)K signalling as a putative contributor to leptomeningeal dissemination of medulloblastoma.

Previous publications and clinical approaches to human medulloblastoma have largely assumed that the primary tumour and its matched metastases are highly similar[3,4]. To test this assertion, we formally reviewed all cases of medulloblastoma from the past decade at The Hospital for Sick Children, in Ontario, Canada, and we identified 19 patients who had bulk residual primary tumour after surgery and metastases visible by magnetic resonance imaging, both of which could be followed for response to treatment (Supplementary Fig. 12 and Supplementary Table 13). Although it is possible that the metastases received less radiotherapy than the primary tumour in a subset of patients, in 58% of all cases (11 of 19) we observed a disparate response to therapy between the primary tumour and the matched metastases (binomial test, $P < 2.2 \times 10^{-16}$). Identification of definitive differences in the clinical response to standard therapy between the primary and the metastatic compartment awaits the completion of large, well-controlled, prospective clinical trials.

We examined seven matched primary and metastatic medulloblastomas for copy number aberrations (Fig. 3, Supplementary Figs 13 and 14, and Supplementary Tables 14 and 15). In each case, the primary tumour and the matched metastases shared complicated genetic events that provide strong support for their descent from a common transformed progenitor cell. Similar to our mouse data, in each case we observed clonal genetic events in the metastatic tumour(s) that were not present in the matched primary tumour (Fig. 3 and Supplementary Fig. 14). We also observed genetic events in the primary tumour that were absent from the matched metastases, consistent with a post-dispersion event (Fig. 3 and Supplementary Fig. 14). One patient with multiple leptomeningeal metastases had a deletion of chromosome 1p in only one of three examined metastases (Fig. 3a). This pattern of genetic events being present in only a subset of metastases could be a mechanism for the emergence of therapy-resistant metastatic clones.

We performed interphase fluorescence *in situ* hybridization (FISH) for the known medulloblastoma oncogenes *MYCN* and *MYC* on a collection of 17 paraffin-embedded primary and metastatic pairs of human medulloblastomas[18–20]. *MYCN* was amplified in three primary medulloblastomas but not in the matching metastases (Fig. 3b and

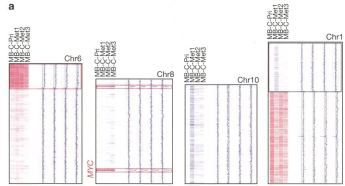

Figure 3 | Human medulloblastoma metastases are biologically distinct from their matched primary tumour. **a**, Copy number data from a primary medulloblastoma (MB-C-Pri) and three patient-matched metastases (MB-C-Met1, MB-C-Met2 and MB-C-Met3), with chromosomal regions in red representing genetic gain (amplification) and in blue denoting genetic loss (deletion). Examples of shared clonal events (red boxes) and events limited to one but not all metastases (black box) are shown. Chr, chromosome. **b**, Interphase FISH shows amplification of *MYCN* in a primary tumour but not the matched metastasis. Nuclei appear blue owing to 4′,6-diamidino-2-phenylindole (DAPI) staining. **c**, Interphase FISH for *MYC* demonstrates amplification in both the primary tumour and its matched metastases. **d**, Venn diagrams depicting the degree of overlap and discordance in promoter CpG methylation events and CNAs in primary medulloblastomas and their matched metastases, with MB-C, MB-D and MB-F and MB-H denoting different patients.

Supplementary Fig. 15). Conversely, *MYC* was amplified in two primary tumours and their matching metastases (Fig. 3c). These data are consistent with *MYCN* amplification being a post-dispersion event, similar to examples in SB-driven mouse medulloblastoma, and strongly indicate that anti-MYCN therapeutics may lack efficacy in the metastatic compartment of human medulloblastoma. The possibility that *MYCN* amplicons in the metastases have been 'lost' over time cannot be excluded.

We subsequently analysed promoter CpG methylation in these matched pairs and found much discordance between the primary tumour and matched metastases (Fig. 3d, Supplementary Figs 13 and 16, and Supplementary Tables 16 and 17). Finally, we performed whole-exome sequencing on a limited set of matched primary and metastatic medulloblastomas and found many single nucleotide variants (SNVs) that were restricted to a single compartment (Supplementary Fig. 13 and Supplementary Table 18). The discordance of CNAs, promoter CpG methylation events and SNVs between the primary tumour and its matched metastases supports a bicompartmental model for metastatic medulloblastoma. The mutational load in the human tumours (the combination of CNAs, CpG methylation and SNVs) compares favourably with the mutational load in our transposon-driven mouse models (in which the median number of gCISs is 25 per tumour; Supplementary Table 19). Validation of the individual CNAs that were restricted to the metastases showed that these CNAs can be detected in a very minor subclone of the primary tumour, in keeping with the relationship identified in the mouse model (Supplementary Fig. 17 and Supplementary Tables 20 and 21). Pathway analysis using the Database for Annotation, Visualization and Integrated Discovery (DAVID) to compare mouse gCISs with the genes that were affected in the human metastases identified only one statistically significant shared signalling pathway: insulin signalling ($P = 0.027$) (Supplementary Table 22). The known role of insulin receptor signalling in primary medulloblastoma[21], together with the data presented here on the role of AKT in metastatic medulloblastoma, suggests that insulin signalling should be prioritized as a therapeutic target to be tested in clinical trials.

We performed unsupervised hierarchical clustering on the CpG methylation data, and we found that normal cerebellar controls cluster away from the medulloblastomas, whereas metastases cluster with their matching primary tumour (Fig. 4a). However, metastases cluster

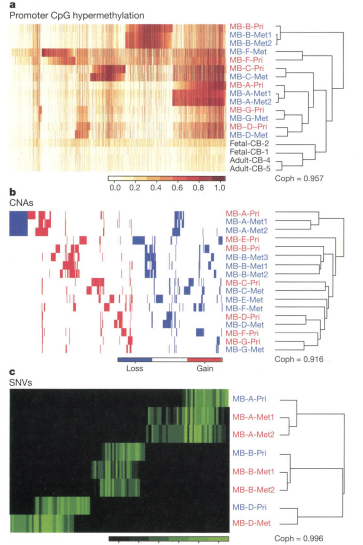

Figure 4 | Human medulloblastoma metastases are genetically distinct from their matched primary tumour. **a**, Profiling the methylation status of 27,578 CpG dinucleotide sites in the human genome in a collection of human matched primary and metastatic medulloblastomas; the top 2,000 genes are shown. Unsupervised hierarchical clustering by CpG methylation pattern demonstrates that patient-matched metastases are more similar to each other than to the matched primary tumour. **b**, Unsupervised clustering of regions of copy number gain and loss demonstrates that patient-matched metastases are more similar to each other than to the matched primary tumour. **c**, Unsupervised hierarchical clustering of SNV data from whole-exome sequencing demonstrates that patient-matched metastases are more similar to each other than to the matched primary tumour. SNVs that are found only in the primary compartment or only in both examined tumours in the metastatic compartment are evident. Coph, cophenetic correlation coefficient.

closer to each other than they do to the matched primary tumour (z-test, $P = 0.0014$) (Supplementary Fig. 18). Unsupervised hierarchical clustering of CNA and exome SNV data uncovered the same relationships (Fig. 4b, c). Evident within the exome data are many events that are shared only by patient-matched metastases (that is, metastases from a single patient), as well as events that are restricted to the primary tumour, both of which are similar to the genetic patterns observed in mice. These three data sets support a model in which patient-matched human medulloblastoma metastases are epigenetically and genetically very similar to each other but have substantially diverged from the primary tumour, resulting in two different disease compartments: the primary and metastatic compartments.

Our data from two mouse models, with support from initial data from human medulloblastoma, suggest that leptomeningeal metastases of medulloblastoma from a single human or mouse are genetically similar to each other but are highly divergent from the matched primary tumour, consistent with a biocompartmental model of disease. Our results are consistent with a model in which metastases arise from a restricted subclone of the primary tumour through a process of clonal selection in both humans and mice. That metastases might arise from a pre-existing minor subclone of the primary tumour through clonal selection was suggested more than three decades ago, but it remains a controversial hypothesis that might not be true of all cancers[22–25]. Failure to account for the divergent molecular pathology of the metastatic compartment may result in selection of therapeutic targets present in the primary tumour, which is more amenable to surgical control, but not the metastases, which are the more frequent cause of death.

METHODS SUMMARY

Generation of *Math1-SB11* construct. *SB11* cDNA was excised from the vector pCMV-*SB11* and ligated into the vector J2Q-*Math1* (refs 8, 26).

Linker-mediated PCR and 454 deep sequencing. Bar-coded, linker-mediated PCR was performed as previously described[6]. Sample preparation for the 454 sequencing and the subsequent procedures was performed as previously described[27].

Determination of gCISs. A chi-squared analysis was performed to determine whether the number of observed integration events within each transcription unit in the SB-driven medulloblastomas was significantly greater than expected given the following: the number of TA dinucleotide sites within the gene relative to the number of TA sites in the genome, the number of integration sites within each tumour, and the total number of tumours in each cohort. This gCIS analysis produced a P value for each of the ~19,000 mouse RefSeq genes, and Bonferroni correction was therefore used to adjust for multiple hypothesis testing.

Full Methods and any associated references are available in the online version of the paper at www.nature.com/nature.

Received 10 October 2010; accepted 3 January 2012.
Published online 15 February 2012.

1. Gajjar, A. *et al.* Risk-adapted craniospinal radiotherapy followed by high-dose chemotherapy and stem-cell rescue in children with newly diagnosed medulloblastoma (St Jude Medulloblastoma-96): long-term results from a prospective, multicentre trial. *Lancet Oncol.* **7,** 813–820 (2006).
2. Mabbott, D. J. *et al.* Serial evaluation of academic and behavioral outcome after treatment with cranial radiation in childhood. *J. Clin. Oncol.* **23,** 2256–2263 (2005).
3. MacDonald, T. J. *et al.* Expression profiling of medulloblastoma: PDGFRA and the RAS/MAPK pathway as therapeutic targets for metastatic disease. *Nature Genet.* **29,** 143–152 (2001).
4. Ramaswamy, S., Ross, K. N., Lander, E. S. & Golub, T. R. A molecular signature of metastasis in primary solid tumors. *Nature Genet.* **33,** 49–54 (2003).
5. Goodrich, L. V., Milenkovic, L., Higgins, K. M. & Scott, M. P. Altered neural cell fates and medulloblastoma in mouse patched mutants. *Science* **277,** 1109–1113 (1997).
6. Collier, L. S., Carlson, C. M., Ravimohan, S., Dupuy, A. J. & Largaespada, D. A. Cancer gene discovery in solid tumours using transposon-based somatic mutagenesis in the mouse. *Nature* **436,** 272–276 (2005).
7. Dupuy, A. J., Akagi, K., Largaespada, D. A., Copeland, N. G. & Jenkins, N. A. Mammalian mutagenesis using a highly mobile somatic *Sleeping Beauty* transposon system. *Nature* **436,** 221–226 (2005).
8. Helms, A. W., Abney, A. L., Ben-Arie, N., Zoghbi, H. Y. & Johnson, J. E. Autoregulation and multiple enhancers control *Math1* expression in the developing nervous system. *Development* **127,** 1185–1196 (2000).
9. Wetmore, C., Eberhart, D. E. & Curran, T. Loss of *p53* but not *ARF* accelerates medulloblastoma in mice heterozygous for *patched*. *Cancer Res.* **61,** 513–516 (2001).
10. Brett, B. T. *et al.* Novel molecular and computational methods improve the accuracy of insertion site analysis in *Sleeping Beauty*-induced tumors. *PLoS ONE* **6,** e24668 (2011).
11. Northcott, P. A. *et al.* Multiple recurrent genetic events converge on control of histone lysine methylation in medulloblastoma. *Nature Genet.* **41,** 465–472 (2009).
12. Forbes, S. A. *et al.* in *Current Protocols in Human Genetics* Ch. 10.11 doi:10.1002/0471142905.hg1011s57 (2008).
13. Northcott, P. A. *et al.* Medulloblastoma comprises four distinct molecular variants. *J. Clin. Oncol.* **29,** 1408–1414 (2011).
14. Nguyen, D. X. & Massagué, J. Genetic determinants of cancer metastasis. *Nature Rev. Genet.* **8,** 341–352 (2007).
15. Norton, L. & Massague, J. Is cancer a disease of self-seeding? *Nature Med.* **12,** 875–878 (2006).
16. Luo, G., Ivics, Z., Izsvák, Z. & Bradley, A. Chromosomal transposition of a Tc1/mariner-like element in mouse embryonic stem cells. *Proc. Natl Acad. Sci. USA* **95,** 10769–10773 (1998).
17. Rao, G., Pedone, C. A., Coffin, C. M., Holland, E. C. & Fults, D. W. c-Myc enhances sonic hedgehog-induced medulloblastoma formation from nestin-expressing neural progenitors in mice. *Neoplasia* **5,** 198–204 (2003).
18. Swartling, F. J. *et al.* Pleiotropic role for *MYCN* in medulloblastoma. *Genes Dev.* **24,** 1059–1072 (2010).
19. Pfister, S. *et al.* Outcome prediction in pediatric medulloblastoma based on DNA copy-number aberrations of chromosomes 6q and 17q and the *MYC* and *MYCN* loci. *J. Clin. Oncol.* **27,** 1627–1636 (2009).
20. Korshunov, A. *et al.* Accumulation of genomic aberrations during clinical progression of medulloblastoma. *Acta Neuropathol.* **116,** 383–390 (2008).
21. Hahn, H. *et al. Patched* target *Igf2* is indispensable for the formation of medulloblastoma and rhabdomyosarcoma. *J. Biol. Chem.* **275,** 28341–28344 (2000).
22. Fidler, I. J. & Kripke, M. L. Metastasis results from preexisting variant cells within a malignant tumor. *Science* **197,** 893–895 (1977).
23. Scheel, C., Onder, T., Karnoub, A. & Weinberg, R. A. Adaptation versus selection: the origins of metastatic behavior. *Cancer Res.* **67,** 11476–11480 (2007).
24. Talmadge, J. E. Clonal selection of metastasis within the life history of a tumor. *Cancer Res.* **67,** 11471–11475 (2007).
25. Talmadge, J. E. & Fidler, I. J. The biology of cancer metastasis: historical perspective. *Cancer Res.* **70,** 5649–5669 (2010).
26. Geurts, A. M. *et al.* Gene transfer into genomes of human cells by the *Sleeping Beauty* transposon system. *Mol. Ther.* **8,** 108–117 (2003).
27. Starr, T. K. *et al.* A transposon-based genetic screen in mice identifies genes altered in colorectal cancer. *Science* **323,** 1747–1750 (2009).

Supplementary Information is linked to the online version of the paper at www.nature.com/nature.

Acknowledgements M.D.T. holds a Canadian Institutes of Health Research Clinician-Scientist Phase II Award, was a Sontag Foundation Distinguished Scholar, and is supported by grants from the National Institutes of Health (R01CA148699), the Pediatric Brain Tumor Foundation, the Canadian Cancer Society, and Brainchild. X.W. was supported by a fellowship from the American Brain Tumor Association in tribute to Tracy Greenwood. L.G. was supported by a fellowship from the Davis M. Ferguson Fund from the American Brain Tumor Association. A.D. was supported by a Vanier Doctoral Fellowship from the Canadian Institutes of Health Research. L.S.C. was supported by a grant (K01CA122183) and a Kimmel Scholar award from the Kimmel Foundation. C.E. was supported by a grant from the National Institutes of Health (NS055089). We thank S. Archer for technical writing assistance.

Author Contributions M.D.T., X.W., P.A.N., L.S.C., A.D. and D.L. conceived the research and planned the experiments. X.W., P.A.N., A.D., L.G. and D.J.H.S. carried out the vast majority of the experiments under M.D.T.'s guidance. C.E., T.V.M., D.Z., Y.-J.C., T.M., X.-N.L., V.P.C., M.G.M. and W.A.W. provided human tumour materials. All authors contributed experimental expertise and participated in the writing of the manuscript. A.J.D., D.J.H.S., T.E.S., S.W.S., K.A., J.K., A.L.S., D.L. and L.S.C. provided biostatistical and bioinformatic expertise. E.B. provided the clinical data and analysis. D.W.F. carried out the *Akt* experiments. N.J., J.S. and J.M. carried out the exome sequencing. H.W., S.M.P. and A.K. carried out the immunostaining of human medulloblastoma tissue microarrays and FISH for *MYCN* and *MYC*. S.C. carried out the pathological analysis of mouse brain tumours.

Author Information CpG methylation data have been deposited in the Gene Expression Omnibus under accession number GSE34356. Reprints and permissions information is available at www.nature.com/reprints. The authors declare no competing financial interests. Readers are welcome to comment on the online version of this article at www.nature.com/nature. Correspondence and requests for materials should be addressed to M.D.T. (mdtaylor@sickkids.ca).

LETTER

doi:10.1038/nature10708

DCC constrains tumour progression via its dependence receptor activity

Marie Castets[1]*, Laura Broutier[1]*, Yann Molin[1], Marie Brevet[2], Guillaume Chazot[1], Nicolas Gadot[2], Armelle Paquet[2], Laetitia Mazelin[1], Loraine Jarrosson-Wuilleme[1], Jean-Yves Scoazec[2], Agnès Bernet[1] & Patrick Mehlen[1]

The role of deleted in colorectal carcinoma (DCC) as a tumour suppressor has been a matter of debate for the past 15 years. *DCC* gene expression is lost or markedly reduced in the majority of advanced colorectal cancers[1] and, by functioning as a dependence receptor, DCC has been shown to induce apoptosis unless engaged by its ligand, netrin-1 (ref. 2). However, so far no animal model has supported the view that the DCC loss-of-function is causally implicated as predisposing to aggressive cancer development[3]. To investigate the role of DCC-induced apoptosis in the control of tumour progression, here we created a mouse model in which the pro-apoptotic activity of DCC is genetically silenced. Although the loss of DCC-induced apoptosis in this mouse model is not associated with a major disorganization of the intestines, it leads to spontaneous intestinal neoplasia at a relatively low frequency. Loss of DCC-induced apoptosis is also associated with an increase in the number and aggressiveness of intestinal tumours in a predisposing APC mutant context, resulting in the development of highly invasive adenocarcinomas. These results demonstrate that DCC functions as a tumour suppressor via its ability to trigger tumour cell apoptosis.

The development of colonic carcinoma from normal colonic epithelium has been shown to be associated with the mutation of a specific set of genes[4]. Loss of heterozygosity on chromosome 18q in more than 70% of primary colorectal tumours prompted the search for a tumour suppressor gene at that locus. This search led to the cloning of a putative cell-surface receptor, DCC[1]. *DCC* expression is markedly reduced in more than 50% of colorectal tumours, as well as in many other neoplasms (for a review, see ref. 5). Moreover, loss of *DCC* is associated with poor prognosis and potentially decreased response to adjuvant chemotherapy in colorectal cancer patients. Lastly, restoration of *DCC* expression can suppress tumorigenic growth properties *in vitro* and in nude mice[5]. Altogether, these data led to the proposal that *DCC* expression is a constraint for tumour progression, and thus that *DCC* functions as a tumour suppressor gene. However, a major controversy resulted from this proposal, because the localization of the *DCC* gene close to well-established tumour suppressors such as *Smad4* (ref. 6) and the absence of increased tumour susceptibility in a mouse model in which *Dcc* was mutated[3] created scepticism about its potential role as a tumour suppressor gene[7].

It has been shown that DCC belongs to the family of dependence receptors[2]. Such receptors induce apoptosis when their trophic ligands are absent, thus conferring a state of cellular dependence on ligand availability for survival[8]. On the basis of this classification, DCC may represent not a classical tumour suppressor but rather a conditional tumour suppressor, inducing the death of tumour cells in settings of ligand limitation, thus preventing invasion and metastasis, but failing to suppress tumour formation (and potentially supporting tumour progression) in settings of high ligand concentration. In support of this view, overexpression of the DCC ligand netrin-1 in the digestive tract has been shown to result in the inhibition of epithelial cell death and the promotion of tumour progression[9].

The pro-apoptotic signalling induced by unbound DCC requires its intracellular domain cleavage by caspase after aspartic acid 1290 (refs 2, 10; Fig. 1a). Point mutation of the aspartic acid residue (D1290N) did not affect the positive signalling mediated by netrin-1 treatment (Fig. 1b). However, compared to wild-type DCC, DCC(D1290N) failed to trigger apoptosis in cell culture (Fig. 1c–g). To address formally the role of DCC as a tumour suppressor and to determine the relative importance of DCC pro-apoptotic activity in its putative tumour suppressor activity, we generated a mouse model with the D1290N point mutation in the DCC coding sequence (Fig. 1h–j). Contrary to DCC homozygous null mutants, which die at birth with many nervous system defects[3], mice bearing one ($DCC^{+/mut}$) or two mutated alleles ($DCC^{mut/mut}$) were viable. The fact that these mice do not show obvious defects in the brain further supports the view that the D1290N mutation does not inhibit or enhance DCC 'positive' signalling, which has been shown to be required for adequate neuronal guidance[11,12]. We thus investigated whether this mouse model showed a loss of DCC-induced apoptosis. Murine embryonic fibroblasts (MEFs) were cultured from $DCC^{+/+}$ or $DCC^{mut/mut}$ embryos (Fig. 2a). As predicted by the dependence receptor paradigm, MEF cells expressing a wild-type DCC underwent apoptosis in response to serum and netrin-1 deprivation, whereas the addition of netrin-1 delayed MEF cell death (Fig. 2b). In the same settings, MEF homozygous for the DCC mutation were less sensitive to serum withdrawal, and netrin-1 addition failed to augment survival (Fig. 2b). Thus, in this mouse model, cells expressing DCC should not undergo apoptosis in settings of netrin-1 limitation.

In the intestine, because of the restricted expression of netrin-1 at the bases of the intestinal villi[9] (Fig. 2c, d and Supplementary Fig. 1a), in contrast to the uniform expression of DCC along the villi[9] (Fig. 2e, f and Supplementary Fig. 1a), we hypothesized that epithelial cell death, which is generally observed at the tips of the villi, could result at least in part from unbound DCC-induced apoptosis. As shown in Fig. 2h–j and Supplementary Fig. 1b, apoptosis in the intestinal epithelium of $DCC^{mut/mut}$ mice was significantly decreased compared to $DCC^{+/+}$ mice, although no change was observed in cell proliferation (Fig. 2g) or differentiation (data not shown). These findings, coupled with the previous demonstration that, in mice, ectopic expression of netrin-1 reduces intestinal cell death, whereas netrin-1 hypomorphic mutant newborn mice show increased cell death[9], suggest that DCC and netrin-1 may be homeostatic regulators of intestinal epithelial turnover via a dependence receptor mechanism (Supplementary Fig. 1 and Supplementary Fig. 1c). It is noteworthy that, even though DCC mutation was shown to decrease intestinal cell death at the tips of the villi, global disorganization of the intestinal epithelium of these animals was not observed, probably because intestinal cell apoptosis levels

[1]Apoptosis, Cancer and Development Laboratory - Equipe labellisée 'La Ligue', LabEx DEVweCAN, Centre de Cancérologie de Lyon, INSERM U1052-CNRS UMR5286, Université de Lyon, Centre Léon Bérard, 69008 Lyon, France. [2]Endocrine Differentiation Laboratory, Centre de Cancérologie de Lyon, INSERM U1052-CNRS UMR5286, Université de Lyon, Hospices Civils de Lyon, Hôpital Edouard Herriot, Anatomie Pathologique, 69437 Lyon, France.
*These authors contributed equally to this work.

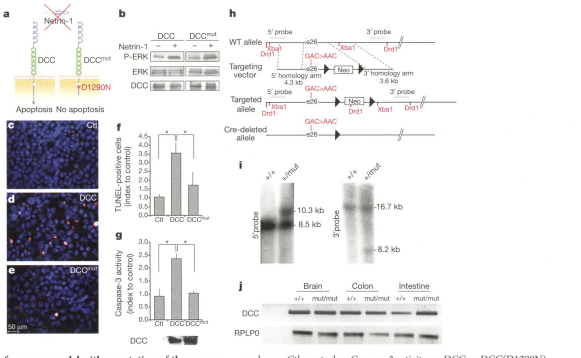

Figure 1 | Establishment of a mouse model with a mutation of the caspase cleavage site in DCC. **a**, Without netrin-1, DCC induces apoptosis unless mutated in D1290. **b**, In HEK293T cells, netrin-1-induced DCC-mediated ERK1/2 phosphorylation is not affected by D1290N point mutation. **c**–**f**, TdT-mediated dUTP nick end labelling (TUNEL) assay on DCC or DCC(D1290N) transfected HEK293T cells (mean + s.e.m., $n = 3$). *$P < 0.005$, U-test. Representative images are shown. Ctl, control. **g**, Caspase-3 activity on DCC or DCC(D1290N) transfected HEK293T cells (mean + s.e.m., $n = 3$). *$P < 0.005$, U-test. Inset: DCC immunoblot. **h**, Mutant mouse model generated by introduction of the D1290N point mutation in exon 26 (e26) of *Dcc*. Arrows indicate Cre recombination sites. **i**, Southern blots after restriction by Xba1 (5′ probe) or Drd1 (3′ probe). **j**, DCC expression (qRT–PCR) in $DCC^{+/+}$ and $DCC^{mut/mut}$ mice.

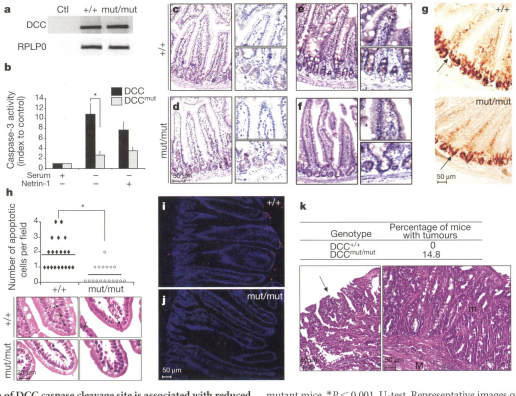

Figure 2 | Mutation of DCC caspase cleavage site is associated with reduced apoptosis in mice. **a**, DCC expression (qRT–PCR) in $DCC^{+/+}$ and $DCC^{mut/mut}$ MEFs from embryonic day (E)13.5 embryos. **b**, Caspase-3 activity in $DCC^{+/+}$ and $DCC^{mut/mut}$ MEFs after serum deprivation and netrin-1 treatment (mean + s.e.m., $n = 3$). *$P < 0.02$, U-test. **c**–**f**, Immunohistochemistry of netrin-1 (**c**, **d**) or DCC (**e**, **f**) in proximal intestine of $DCC^{+/+}$ (**c**, **e**) and $DCC^{mut/mut}$ (**d**, **f**) mice. Right panels, enlargement of villi and crypt staining. **g**, Cell proliferation in intestinal crypt analysed by anti-Ki67 staining. **h**, Intestinal cell death in wild-type or DCC mutant mice. *$P < 0.001$, U-test. Representative images of pyknotic cells from haematoxylin–eosin–saffron staining of $DCC^{+/+}$ and $DCC^{mut/mut}$ mice are shown. **i**, **j**, TUNEL staining of intestinal villi. No difference in apoptosis rate was observed between control and mutant animals in intestinal crypt (data not shown). **k**, Incidence of spontaneous tumour formation in intestines of $DCC^{mut/mut}$ ($n = 28$) compared to $DCC^{+/+}$ ($n = 18$) mice. Haematoxylin–eosin–saffron staining of an adenoma (left panel; arrow) and of an adenocarcinoma (right panel) observed in $DCC^{mut/mut}$ mice. m, mucosa; M, muscularis.

throughout the villi remain quite low under physiological conditions[13,14]. Thus, netrin-1 regulation of DCC-induced cell death is unlikely to be solely responsible for a general homeostatic regulatory process that would balance intestinal epithelial cell proliferation and differentiation; rather, it is more likely to limit the lifespan of cells arriving at the tips of the villi and, as such, to serve as a mechanism that limits the occurrence of genetic alterations. In support of this possibility, reduction of apoptosis in $DCC^{mut/mut}$ mice was accompanied by spontaneous, albeit limited, intestinal tumour formation: whereas no tumours were detected in wild-type control littermates, 14.8% of mutant mice showed spontaneous neoplastic transformation, including both adenomas and adenocarcinomas (Fig. 2k; $P < 0.05$). Because intestinal cells are known to undergo multiple proliferative steps within the crypt, and repeated mechanical and chemical insults originate from the intestinal lumen, we propose that DCC-mediated cell death may represent a factor for limiting the initiation of malignant transformation.

In human pathological samples, loss of DCC is observed with especially high frequency in late-stage tumours. Together with the fact that spontaneous neoplastic transformation was observed only at low frequency in these DCC mutant mice, this suggested that the putative tumour suppressive role of DCC may modulate a predominantly late event in tumorigenesis. We investigated the possibility that DCC pro-apoptotic activity may affect tumour progression by analysing the effect of the DCC(D1290N) mutation on adenocarcinoma formation in an $APC^{+/1638N}$ genetic background. APC is a well-known tumour suppressor gene in human colorectal cancer, and APC mutations in mice are associated with neoplasm formation. We chose the $APC^{+/1638N}$ mutant mice, which were shown to develop tumours in the intestinal tract at a moderate level[15]. Consistent with a previous report, the number of adenocarcinomatous lesions per $DCC^{+/+}$ $APC^{+/1638N}$ control mice was 0.79 ± 0.77 (Fig. 3a)[15]. The incidence of adenocarcinomas was increased by more than 2.5-fold in $DCC^{mut/mut}$ $APC^{+/1638N}$ mice, (Fig. 3a; $P = 0.0002$). Moreover, whereas 21.4% of $DCC^{+/+}$ $APC^{+/1638N}$ control mice were tumour free (Fig. 3b), all $DCC^{mut/mut}$ $APC^{+/1638N}$ mice had at least one neoplasm. Lastly, whereas adenocarcinomas were detected in 50% of the $DCC^{+/+}$ $APC^{+/1638N}$ control mice, consistent with previous reports[15], the frequency of $DCC^{mut/mut}$ $APC^{+/1638N}$ mice with adenocarcinomas was markedly increased to 100% (Fig. 3a; $P = 0.003$). Mice heterozygous for the DCC mutation in the $APC^{+/1638N}$ background showed an intermediate phenotype, with a significantly increased number of adenocarcinomas compared to $APC^{+/1638N}$ mice (Supplementary Fig. 2).

Of interest, 45.5% of $DCC^{mut/mut}$ $APC^{+/1638N}$ mice showed aggressive adenocarcinomas with serosal invasion, compared to 8% in controls (Fig. 3c, d; $P < 0.04$). Because serosal invasion in $DCC^{mut/mut}$ $APC^{+/1638N}$ mice supports the view of tumour cells spreading in these mutant mice, we analysed distant organs for metastasis. None of the mice showed macrometastatic lesions in the peritoneum, liver or lung. However, highly proliferative micrometastases were observed in the livers of $DCC^{mut/mut}$ $APC^{+/1638N}$ mice with adenocarcinoma with serosal invasion, but not in controls (Supplementary Fig. 3).

Together with the finding that, in human tumours, DCC is typically deleted in late-stage tumours, this markedly increased aggressivness suggests that the loss of DCC may enhance tumour cell survival at the transition from adenoma to adenocarcinoma. We therefore assessed whether, in accordance with this hypothesis, apoptosis is quantitatively different in low-grade tumours of $DCC^{mut/mut}$ $APC^{+/1638N}$ versus $DCC^{+/+}$ $APC^{+/1638N}$ control mice. As shown in Fig. 3e and f, we observed a marked decrease in apoptosis rate in adenomas from $DCC^{mut/mut}$ $APC^{+/1638N}$ mice compared to that in size-matched $DCC^{+/+}$ $APC^{+/1638N}$ controls, while both tumours persistently

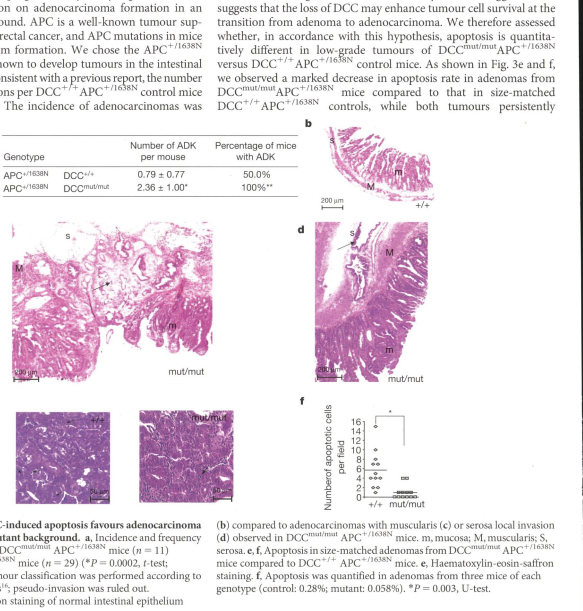

Figure 3 | Inactivation of DCC-induced apoptosis favours adenocarcinoma formation in an $APC^{+/1638}$ mutant background. **a**, Incidence and frequency of adenocarcinomas (ADK) in $DCC^{mut/mut}$ $APC^{+/1638N}$ mice ($n = 11$) compared to $DCC^{+/+}$ $APC^{+/1638N}$ mice ($n = 29$) (*$P = 0.0002$, *t*-test; **$P = 0.003$, Fisher's test). Tumour classification was performed according to international recommendations[16]; pseudo-invasion was ruled out. **b**–**e**, Haematoxylin-eosin-saffron staining of normal intestinal epithelium (**b**) compared to adenocarcinomas with muscularis (**c**) or serosa local invasion (**d**) observed in $DCC^{mut/mut}$ $APC^{+/1638N}$ mice. m, mucosa; M, muscularis; S, serosa. **e**, **f**, Apoptosis in size-matched adenomas from $DCC^{mut/mut}$ $APC^{+/1638N}$ mice compared to $DCC^{+/+}$ $APC^{+/1638N}$ mice. **e**, Haematoxylin-eosin-saffron staining. **f**, Apoptosis was quantified in adenomas from three mice of each genotype (control: 0.28%; mutant: 0.058%). *$P = 0.003$, U-test.

showed DCC expression (data not shown). Thus, the inhibition of DCC-induced apoptosis may modulate, in low-grade tumours, the balance between proliferation and death, favouring proliferation. Consequently, this may increase the likelihood of occurrence of additional genetic or epigenetic alterations, thus enhancing tumour progression.

The current results provide a definitive demonstration that DCC is a bona fide tumour suppressor in the intestinal tract. Our results demonstrate the importance of DCC as a late gatekeeper, which limits tumour progression. Moreover, because the D1290N mutation inhibits DCC-induced apoptosis but not netrin-1-dependent signalling, this DCC tumour suppressive activity probably occurs via the ability of DCC to trigger apoptosis of neoplastic or pre-neoplastic cells in settings of netrin-1 limitation. DCC expression is not only decreased or lost in colorectal cancer but in a large variety of cancers such as prostate, breast, endometrial, ovarian, oesophageal, testicular, glial, neuroblastoma and hematological malignancies[5]. It will therefore be of interest to analyse, using transgenic mouse models, the tumour suppressor role of DCC in these malignancies. In light of our data, the function of DCC as a dependence receptor and a conditional tumour suppressor seems to represent an important safeguard mechanism, limiting tumour progression by engaging the apoptotic process.

METHODS SUMMARY

Further details about materials and methods are provided in Methods. Briefly, the DCC(D1290N) targeting vector was constructed using a fragment of *Dcc* gene encompassing 7.9 kb around exon 26. Embryonic stem cell electroporation, selection and culture, as well as generation of chimaeric mice and Southern blot analysis were performed in the Institut de la Clinique de la Souris (ICS) according to classical procedures. Germline transmission and genotyping were detected by Southern blot and PCR analysis of tail genomic DNA. $APC^{+/1638N}$ mice were obtained from R. Fodde. Tumour analysis was performed in blind from haematoxylin-eosin-saffron stained sections. Apoptosis was quantified in blind on haematoxylin-eosin-saffron stained intestine and adenoma sections of controls and mutant DCC mice or after TUNEL staining. Quantitative polymerase chain reaction with reverse transcription (qRT–PCR), immunohistochemistry, immunoblots, MEF culture and cell death assays were performed as described in Methods.

Full Methods and any associated references are available in the online version of the paper at www.nature.com/nature.

Received 27 May; accepted 9 November 2011.
Published online 11 December 2011.

1. Fearon, E. R. *et al.* Identification of a chromosome 18q gene that is altered in colorectal cancers. *Science* **247,** 49–56 (1990).
2. Mehlen, P. *et al.* The DCC gene product induces apoptosis by a mechanism requiring receptor proteolysis. *Nature* **395,** 801–804 (1998).
3. Fazeli, A. *et al.* Phenotype of mice lacking functional deleted in colorectal cancer (*Dcc*) gene. *Nature* **386,** 796–804 (1997).
4. Fearon, E. R. & Vogelstein, B. A genetic model for colorectal tumorigenesis. *Cell* **61,** 759–767 (1990).
5. Mehlen, P. & Fearon, E. R. Role of the dependence receptor DCC in colorectal cancer pathogenesis. *J. Clin. Oncol.* **22,** 3420–3428 (2004).
6. Takaku, K. *et al.* Intestinal tumorigenesis in compound mutant mice of both *Dpc4* (*Smad4*) and *Apc* genes. *Cell* **92,** 645–656 (1998).
7. Roush, W. Putative cancer gene shows up in development instead. *Science* **276,** 534–535 (1997).
8. Goldschneider, D. & Mehlen, P. Dependence receptors: a new paradigm in cell signaling and cancer therapy. *Oncogene* **29,** 1865–1882 (2010).
9. Mazelin, L. *et al.* Netrin-1 controls colorectal tumorigenesis by regulating apoptosis. *Nature* **431,** 80–84 (2004).
10. Forcet, C. *et al.* The dependence receptor DCC (deleted in colorectal cancer) defines an alternative mechanism for caspase activation. *Proc. Natl Acad. Sci. USA* **98,** 3416–3421 (2001).
11. Li, W. *et al.* Activation of FAK and Src are receptor-proximal events required for netrin signaling. *Nature Neurosci.* **7,** 1213–1221 (2004).
12. Forcet, C. *et al.* Netrin-1-mediated axon outgrowth requires deleted in colorectal cancer-dependent MAPK activation. *Nature* **417,** 443–447 (2002).
13. Watson, A. J. *et al.* Epithelial barrier function *in vivo* is sustained despite gaps in epithelial layers. *Gastroenterology* **129,** 902–912 (2005).
14. Kiesslich, R. *et al.* Identification of epithelial gaps in human small and large intestine by confocal endomicroscopy. *Gastroenterology* **133,** 1769–1778 (2007).
15. Fodde, R. *et al.* A targeted chain-termination mutation in the mouse *Apc* gene results in multiple intestinal tumors. *Proc. Natl Acad. Sci. USA* **91,** 8969–8973 (1994).
16. Boivin, G. P. *et al.* Pathology of mouse models of intestinal cancer: consensus report and recommendations. *Gastroenterology* **124,** 762–777 (2003).

Supplementary Information is linked to the online version of the paper at www.nature.com/nature.

Acknowledgements We wish to thank D. E. Bredesen and J.-G. Delcros for critical reading of the manuscript. We thank C. H. Herbreteau and C. Bonod-Bidaud for their initial involvement in this work and the animal facility staff for animal care. We thank the ICS for the generation of the DCC mutant mice. We thank the LMT (Laboratoire des Modèles Tumoraux) and AniPath for the analysis of animal models. This work was supported by institutional grants from the Ligue Contre le Cancer, INCA, ANR, IP ApoSys and the LabEX DEVweCAN (ANR-10-LABX-61).

Author Contributions M.C., L.B., Y.M., G.C., L.M., L.J.-W., A.B. and P.M. designed the experiments, the mice models and performed data analysis. M.C., L.B. and Y.M. performed most of the experiments. J.-Y.S., M.B., N.G. and A.P. performed pathological analysis of tumour grade and *in vivo* quantification of apoptosis. M.C. and P.M. wrote the manuscript. P.M. and A.B. are co-senior authors.

Author Information Reprints and permissions information is available at www.nature.com/reprints. The authors declare no competing financial interests. Readers are welcome to comment on the online version of this article at www.nature.com/nature. Correspondence and requests for materials should be addressed to P.M. (patrick.mehlen@lyon.unicancer.fr).

LETTER

doi:10.1038/nature10790

Deleted in colorectal carcinoma suppresses metastasis in p53-deficient mammary tumours

Paul Krimpenfort[1], Ji-Ying Song[2], Natalie Proost[1], John Zevenhoven[1], Jos Jonkers[2] & Anton Berns[1,4]

Since its discovery in the early 1990s the deleted in colorectal cancer (*DCC*) gene, located on chromosome 18q21, has been proposed as a tumour suppressor gene as its loss is implicated in the majority of advanced colorectal and many other cancers[1]. DCC belongs to the family of netrin 1 receptors, which function as dependence receptors as they control survival or apoptosis depending on ligand binding. However, the role of DCC as a tumour suppressor remains controversial because of the rarity of DCC-specific mutations and the presence of other tumour suppressor genes in the same chromosomal region. Here we show that in a mouse model of mammary carcinoma based on somatic inactivation of p53, additional loss of DCC promotes metastasis formation without affecting the primary tumour phenotype. Furthermore, we demonstrate that in cell cultures derived from p53-deficient mouse mammary tumours DCC expression controls netrin-1-dependent cell survival, providing a mechanistic basis for the enhanced metastatic capacity of tumour cells lacking DCC. Consistent with this idea, *in vivo* tumour-cell survival is enhanced by DCC loss. Together, our data support the function of DCC as a context-dependent tumour suppressor that limits survival of disseminated tumour cells.

In the developing nervous system, netrin 1 receptors, DCC and UNC5H, regulate axon guidance by mediating chemo-repulsion and attraction as a result of ligand interaction[2–4]. These receptors also act as dependence receptors inducing cell survival in the presence of their ligand netrin 1 or cell death in the absence of netrin 1 (refs 5, 6). Consequently, netrin 1 overexpression or loss of expression of its receptors confers a selective advantage to (tumour) cells. Overexpression of netrin 1 has been implicated in lung cancers[7] and in metastatic breast cancer[8], and enforced netrin 1 expression in the mouse gastrointestinal tract contributes to adenocarcinoma formation[9]. Downregulation of netrin 1 receptors has been reported in the progression of multiple cancers including colorectal, breast, ovary, stomach, lung and kidney cancers[10], and is associated with loss of heterozygosity or epigenetic silencing[11]. However, although specific tumour-related misssense mutations in coding exons have been reported for *UNC5H* (ref. 12), inactivating mutations were not found in *DCC* (refs 13, 14). The lack of definitive support, the possible impact of loss of heterozygosity or epigenetic silencing on expression of other tumour suppressor genes in the same chromosomal region and the absence of a cancer phenotype of *Dcc*-deficient mice[15] have raised doubts about whether DCC has a tumour suppressor function[16].

To directly address the role of DCC loss in tumour progression we introduced a Cre/*loxP*-technology-based conditional mutant *Dcc* allele into a well-defined mouse model for mammary carcinoma. In this model cytokeratin 14 (K14) promoter-driven Cre expression ablates both *p53* alleles in mammary epithelial cells, resulting in mammary tumours[17,18]. We have chosen this model to study the effect of DCC loss for two reasons. First, the expression of *Unc5h* genes is positively regulated by p53 (refs 19, 20, 21) and consequently, under p53-deficient conditions any effect of DCC loss could no longer be masked by *Unc5* expression. Second, mammary tumours arising in the K14-*cre p53*$^{F/F}$ model are well-encapsulated and only rarely metastasize[17,18], allowing *in vivo* assessment of the effects of additional mutations on tumour invasion and metastasis[22].

Dcc is a large gene stretching over 1.2 Mb and is located on human and mouse chromosome 18 (ref. 14). To generate a conditional knockout for *Dcc* (*Dcc*^{F}) we inserted *loxP* sites in introns 22 and 23 by homologous recombination in embryonic stem cells, enabling the Cre-mediated excision of exon 23 encoding the transmembrane (Supplementary Fig. 1a). Details of the *Dcc*^{F} allele are shown in Supplementary Fig. 2 and in the Methods. Homozygous *Dcc*$^{F/F}$ mice are born in normal Mendelian ratios and do not show any aberrancies. Previously generated *Dcc*-deficient mice showed defects in axonal projections in the central nervous system and died shortly after birth[15]. To confirm that Cre-mediated deletion of exon 23 results in a non-functional *Dcc* allele we analysed the phenotype of mice carrying the recombined *Dcc* allele (*Dcc*^{D23}) obtained from crosses of *Dcc*^{F} mice with germline-expressing Cre mice. All homozygous *Dcc*$^{D23/D23}$ mice died within 1 day of birth and we noticed defects in the central nervous system that were very similar to those that have been described for the *Dcc* knockout mice[15], for example, all *Dcc*$^{D23/D23}$ pups showed complete absence of the corpus callosum (Supplementary Fig. 1b) and immunostaining showed the loss of *Dcc* expression in the cerebral cortex (Supplementary Fig. 1c). We then generated cohorts of female K14-*cre Dcc*$^{F/+}$ *p53*$^{F/F}$ and K14-*cre Dcc*$^{F/F}$ *p53*$^{F/F}$ mice and compared mammary tumour development with respect to latency, histopathology and progression in these mice to a cohort of female K14-*cre p53*$^{F/F}$ mice. In all three cohorts a high incidence of mammary neoplasias was observed (80%), with similar latency as proved by the complete overlapping of Kaplan–Meier curves of mammary-tumour-free survival (Fig. 1a). The lesions were found in all the mammary glands, either as a single tumour or as multiple independent tumours. Macroscopically, they were solid with clear demarcations. Microscopically, a comparable diversity of tumour cell properties was observed in the three cohorts. Tumours were classified as moderately differentiated adenocarcinomas and/or carcinosarcomas. Ductal and/or solid nests and trabecular structures could be seen in the carcinomatous compartment, whereas sarcomatoid lesions were mainly composed of spindle cells that were arranged in bundles and interlacing structures (Fig. 2 and Supplementary Fig. 3). Immunohistochemical characterization of the tumours from the three cohorts did not show significant differences in marker profile using antibodies against epithelial (CK8, CK14, E-cadherin) and mesenchymal markers (vimentin, smooth muscle actin) or in apoptotic or proliferative activity (Supplementary Fig. 4). An overview of the mammary tumours that were observed in the three cohorts is presented in Table 1.

However, whereas the primary mammary tumour phenotypes were similar in all three groups, metastases in K14-*cre Dcc*$^{F/}$ *p53*$^{F/F}$ mice were much more frequent (6 out of 14) than in K14-*cre Dcc*$^{F/+}$ *p53*$^{F/F}$ and K14-*cre p53*$^{F/F}$ cohorts (in total, 1 out of 21 ($P < 0.01$; Table 1)). These

[1]Division of Molecular Genetics, The Netherlands Cancer Institute, 1066 CX Amsterdam, The Netherlands. [2]Division of Molecular Biology and Centre for Biomedical Genetics, The Netherlands Cancer Institute, 1066 CX Amsterdam, The Netherlands. [3]Department of Experimental Animal Pathology, The Netherlands Cancer Institute, 1066 CX Amsterdam, The Netherlands. [4]The Amsterdam Medical Center (AMC), The Netherlands Cancer Institute, 1066 CX Amsterdam, The Netherlands.

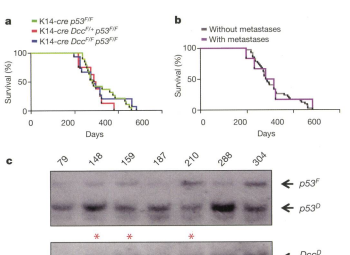

Figure 1 | DCC loss does not affect latency of p53-deficient mammary tumour development. a, Tumour-free survival curves of K14-*cre* $p53^{F/F}$, K14-*cre* $Dcc^{F/+}$ $p53^{F/F}$ and K14-*cre* $Dcc^{F/F}$ $p53^{F/F}$ mice. **b**, Tumour-free survival of mice with and without metastases. **c**, Southern blot analysis of tumours from K14-*cre* $Dcc^{F/F}$ $p53^{F/F}$ mice showing Cre-mediated recombination of $p53^{F}$ and Dcc^{F} alleles. Red asterisk, lanes with metastatic tumours. Numbers indicate different mice.

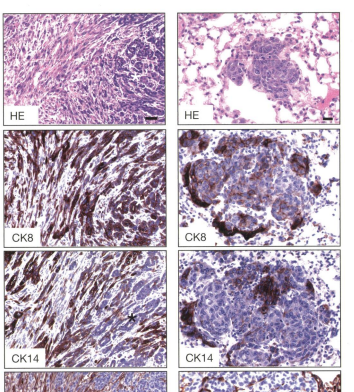

Figure 2 | Microphotographs of primary mammary carcinosarcoma (left) and metastasis in the lung (right) in serial sections. HE staining of the primary carcinosarcoma together with immunohistochemical stains of CK8, CK14 and vimentin reveals epithelial as well as mesenchymal differentiations. However, the metastasis in the lung mainly shows epithelial properties. Scale bars; left column, 50 μm; right column, 20 μm. Asterisk, indication of carcinomatoid differentiation of the tumour.

metastases were found in draining lymph nodes and/or lung. They showed a similar immunohistochemical staining pattern to their corresponding primary tumours (Fig. 2 and Supplementary Fig. 5). The latency of metastasizing tumours did not differ from that of the non-metastasizing tumours (Fig. 1b) and both primary carcinoma and carcinosarcoma could give rise to metastasis formation (Supplementary Table 1). From four metastatic and six non-metastatic tumours from K14-*cre* $Dcc^{F/F}$ $p53^{F/F}$ mice we could isolate sufficient DNA for Southern blot analysis to estimate Cre-recombination-mediated exon 23 deletion. We found that the Dcc^{F} allele is not a very efficient Cre recombinase substrate and the extent of exon 23 deletion varied considerably (see Fig. 1c). Out of the ten tumours that we were able to analyse only six showed widespread deletion of exon 23, and out of these six there were four that showed metastasis formation, whereas none of the four tumours with only partial exon 23 deletion showed metastatic spread (Supplementary Table 1). These data indicate that the loss of DCC function per se is not selected for in primary tumour development but that its loss facilitates metastasis.

Dcc is expressed at high levels in distinct regions of the brain[23,24] and at much lower levels in various other tissues. Polymerase chain reaction with reverse transcription (RT–PCR) analysis showed that DCC is expressed in mammary tumours from K14-*cre* $p53^{F/F}$ mice and its expression is lost in many of the primary tumours of K14-*cre* $Dcc^{F/F}$ $p53^{F/F}$ mice. None of these tumours showed features that are associated with metastasis, such as loss of E-cadherin expression[22]. We speculated that the increased metastasis formation in the K14-*cre* $Dcc^{F/F}$ $p53^{F/F}$ mice might relate to the ability of DCC to trigger apoptosis when netrin 1 availability is limited, for example, in specific conditions when cells have disseminated from the primary tumour mass. To address this issue in an accessible system we used p53-deficient ($p53^{D/D}$) cell cultures derived from K14-*cre* $p53^{F/F}$ tumours and assayed whether cell survival under apoptosis-inducing conditions is dependent on the netrin 1–DCC interaction. RT–PCR showed that *Dcc* expression varied between the $p53^{D/D}$ tumour cell lines. To study the effect of netrin 1 on apoptosis we used three tumour cell lines expressing DCC and two with no, or hardly detectable, Dcc expression (Fig. 3a). We tested the consequences of serum deprivation, the absence of cell–matrix interaction (on non-coated polystyrene dishes) or both. Apoptosis induction in these cultures was quantified by cell-surface phosphatidylserine expression using fluorescein (FITC)-conjugated annexin 5. The effect of adding netrin 1 was calculated as a percentage reduction in the apoptosis induced by serum deprivation. Under adherent culture conditions, with or without serum, apoptotic cells were hardly detectable in the cell cultures tested and thus a netrin 1 effect on cell survival could not be measured. Apoptosis can be induced in $p53^{D/D}$ tumour cells grown in the absence of cell–matrix interaction[25], although the extent of apoptosis induction varied between the tumour cell lines tested (Fig. 3b and c). In tumour cell lines with no—or hardly detectable—DCC expression, serum deprivation resulted in a mild increase of apoptosis on which netrin 1 addition had

Table 1 | Frequent metastasis formation of mammary tumours in the K14-*cre* $Dcc^{F/F}$ $p53^{F}$ cohort

	Carcinoma	Carcinosarcoma	Metastasis
K14-*cre* $p53^{F/F}$	8/16 (50%)	13/16 (81%)	1/16 (6%)
K14-*cre* $Dcc^{F/+}$ $p53^{F/F}$	4/7 (57%)	5/7 (71%)	0/7
Total*	12/23 (52%)	18/23 (78%)	1/23 (4%)
K14-*cre* $Dcc^{F/F}$ $p53^{F/F}$	6/14 (43%)	10/14 (71%)	6/14 (43%)†

* Total refers to the sum of the values for K14-*cre* $p53^{F/F}$ mice and K14-*cre* $Dcc^{F/+}$ $p53^{F/F}$ mice.
† $P < 0.05$ between the proportion of metastases in K14-*cre* $p53^{F/F}$ and that in K14-*cre* $Dcc^{F/F}$ $p53^{F/F}$ mice; $P < 0.01$ between the proportion of metastases in the sum of K14-*cre* $p53^{F/F}$ and K14-*cre* $Dcc^{F/+}$ $p53^{F/F}$ mice and that in K14-*cre* $Dcc^{F/F}$ $p53^{F/F}$ mice.

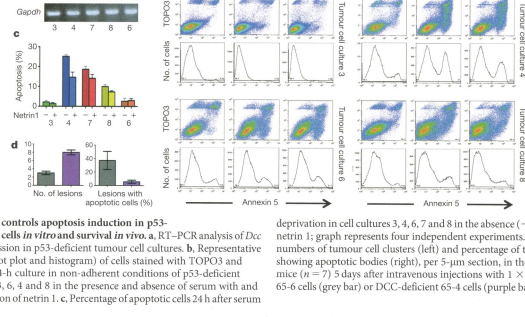

Figure 3 | DCC controls apoptosis induction in p53-deficient tumour cells *in vitro* and survival *in vivo*. **a**, RT–PCR analysis of *Dcc* and *Gapdh* expression in p53-deficient tumour cell cultures. **b**, Representative FACS analysis (dot plot and histogram) of cells stained with TOPO3 and annexin 5 after 24 h culture in non-adherent conditions of p53-deficient tumour cultures 3, 6, 4 and 8 in the presence and absence of serum with and without the addition of netrin 1. **c**, Percentage of apoptotic cells 24 h after serum deprivation in cell cultures 3, 4, 6, 7 and 8 in the absence (−) or presence (+) of netrin 1; graph represents four independent experiments. **d**, Quantification of numbers of tumour cell clusters (left) and percentage of tumour cell clusters showing apoptotic bodies (right), per 5-μm section, in the lungs of Balb/c nu mice ($n = 7$) 5 days after intravenous injections with 1×10^6 DCC-proficient 65-6 cells (grey bar) or DCC-deficient 65-4 cells (purple bar). Error bars, s.e.m.

virtually no effect. By contrast, serum withdrawal from cultures of DCC-expressing $p53^{DD}$ tumour cells led to a substantial increase in apoptotic cells. This apoptosis could be partly rescued by the addition of netrin 1. Depending on the tumour cell culture the rescuing effect of netrin 1 varied from 20% to 40% (Fig. 3b and c). These data indicate that the netrin 1–DCC interaction is functional in apoptosis regulation in mammary tumour cells. Moreover, these observations support our premise that the response of p53-deficient cells to netrin 1 relies on DCC, as the absence of p53 results in abrogation of expression of other netrin 1 receptors. In p53-proficient cells DCC loss would not provide substantial protection from apoptosis as the other netrin 1 receptors would still convey an apoptotic signal in the absence of netrin 1. To test whether DCC loss also confers increased apoptosis resistance or survival *in vivo* we performed intravenous transplantation experiments using two cell lines derived from the same primary tumour, one proficient in DCC (65-6) and the other deficient in DCC (65-4). We confirmed that 65-6 cells are much more sensitive than 65-4 cells to apoptosis induction after serum withdrawal. Consistent with the *in vitro* data we found that 5 days after intravenous injection there were significantly more tumour cell clusters ($P < 0.03$) (for a representative image see Supplementary Fig. 6) in the lungs of mice transplanted with DCC-deficient cells than in the lungs of mice that received DCC-proficient cells (Fig. 3d). Moreover, in mice that were injected with DCC-proficient cells the lesions showed many more apoptotic bodies. It has been shown previously that DCC does not play an important part in tumour development[15]. However, apart from using a different tumour setting they addressed the effect of DCC loss in an Apc^{min}-sensitized but p53-proficient background. Our observations do not contradict their observation. Consistent with their results, we show that DCC loss is irrelevant for primary tumour development. *Dcc* loss does not affect tumour latency or tumour phenotype and it is not selected for in primary tumour development. However, we observe a significantly enhanced metastatic capacity of p53-deficient tumours cells after loss of DCC ($P < 0.01$). In human tumours loss of DCC results from genetic and epigenetic events affecting a large region on chromosome 18q21, which harbours multiple genes with tumour suppressor activity, such as *SMAD4* and *SMAD2* (also known as *Jv18*). Notably, in mice the loss of *Smad2* (ref. 25) or *Smad4* (ref. 26) leads to progression of Apc^{-}-driven intestinal tumours, but without additional metastasis formation. Many trivial reasons can underlie the contradiction between our idea that the effect of DCC loss is p53-dependent and the classical multistep 'Vogelgram' model for colorectal carcinogenesis in which DCC is lost before p53 inactivation[27]. We favour the scenario in which 18q21 deletions, including *DCC*, occur before p53 loss owing to the selective advantage that is conveyed by the loss of the other tumour suppressors in this chromosomal region. *DCC* loss would then serve as a passenger mutation that is initially harmless but becomes critical after subsequent p53 inactivation as it then promotes the survival of cells released from the primary tumour, thereby facilitating their colonization of other tissues. In contrast to the small metastases we observe in our mouse model, DCC-deficient metastases in patients are life threatening. They are composed of cells that have been selected for higher malignancy during primary tumour growth. Indeed, loss of DCC in breast cancer cells has been associated with worse prognosis with a higher risk of recurrent disease[28].

METHODS SUMMARY

Animal experiments comply with international regulations and ethical guidelines, and have been authorized by the experimental animal committee at The Netherlands Cancer Institute.

The Dcc^{F} strain was obtained through embryonic-stem-cell targeting. K14-*cre* and $p53^{F}$ strains have been described[17].

For histopathological studies, mice were killed when seriously ill or when tumours reached a diameter of 1.5 cm. Tissues were fixed in EAF (ethanol–acetic acid–formol; acidified 4% formalin; ethanol/acetic acid/formol/saline at 40:5:10:45 v/v). Haematoxylin and eosin (HE) stains were performed according to standard procedures. A list of all the antibodies used can be found in the Methods section. RNA expression analysis was performed using TaqMan quantitative PCR methods. Apotosis in cell cultures was assayed by measuring annexin 5-positive cells by fluorescence-activated cell sorting (FACS) as described[22].

Full Methods and any associated references are available in the online version of the paper at www.nature.com/nature.

Received 25 November; accepted 14 December 2011.

1. Fearon, E. R. *et al.* Identification of a chromosome 18q gene that is altered in colorectal cancers. *Science* **247,** 49–56 (1990).
2. Keino-Masu, K. *et al. Deleted in colorectal cancer (DCC)* encodes a netrin receptor. *Cell* **87,** 175–185 (1996).
3. Serafini, T. *et al.* Netrin-1 is required for commissural axon guidance in the developing vertebrate nervous system. *Cell* **87,** 1001–1014 (1996).
4. Hong, K. *et al.* A ligand-gated association between cytoplasmic domains of UNC5 and DCC family receptors converts netrin-induced growth cone attraction to repulsion. *Cell* **97,** 927–941 (1999).
5. Mehlen, P. *et al.* The DCC gene product induces apoptosis by a mechanism requiring receptor proteolysis. *Nature* **395,** 801–804 (1998).

6. Thiebault, K. *et al.* The netrin-1 receptors UNC5H are putative tumor suppressors controlling cell death commitment. *Proc. Natl Acad. Sci. USA* **100,** 4173–4178 (2003).
7. Delloye-Bourgeois, C. *et al.* Interference with netrin-1 and tumor cell death in non-small cell lung cancer. *J. Natl Cancer Inst.* **101,** 237–247 (2009).
8. Fitamant, J. *et al.* Netrin-1 expression confers a selective advantage for tumor cell survival in metastatic breast cancer. *Proc. Natl Acad. Sci. USA* **105,** 4850–4855 (2008).
9. Mazelin, L. *et al.* Netrin-1 controls colorectal tumorigenesis by regulating apoptosis. *Nature* **431,** 80–84 (2004).
10. Mehlen, P. & Fearon, E. R. Role of the dependence receptor DCC in colorectal cancer pathogenesis. *J. Clin. Oncol.* **22,** 3420–3428 (2004).
11. Hibi, K. *et al.* Aberrant methylation of the *UNC5C* gene is frequently detected in advanced colorectal cancer. *Anticancer Res.* **29,** 271–273 (2009).
12. Shin, S. K. *et al.* Epigenetic and genetic alterations in netrin-1 receptors *UNC5C* and *DCC* in human colon cancer. *Gastroenterology* **133,** 1849–1857 (2007).
13. Peltomäki, P. *et al.* Evidence supporting exclusion of the *DCC* gene and a portion of chromosome 18q as the locus for susceptibility to hereditary nonpolyposis colorectal carcinoma in five kindreds. *Cancer Res.* **51,** 4135–4140 (1991).
14. Cho, K. R. *et al.* The DCC gene: structural analysis and mutations in colorectal carcinomas. *Genomics* **19,** 525–531 (1994).
15. Fazeli, A. *et al.* Phenotype of mice lacking functional *Deleted in colorectal cancer (Dcc)* gene. *Nature* **386,** 796–804 (1997).
16. Roush, W. Putative cancer gene shows up in development instead. *Science* **276,** 534–535 (1997).
17. Jonkers, J. *et al.* Synergistic tumor suppressor activity of BRCA2 and p53 in a conditional mouse model for breast cancer. *Nature Genet.* **29,** 418–425 (2001).
18. Liu, X. *et al.* Somatic loss of BRCA1 and p53 in mice induces mammary tumors with features of human *BRCA1*-mutated basal-like breast cancer. *Proc. Natl Acad. Sci. USA* **104,** 12111–12116 (2007).
19. Tanikawa, C., Matsuda, K., Fukuda, S., Nakamura, Y. & Arakawa, H. p53RDL1 regulates p53-dependent apoptosis. *Nature Cell Biol.* **5,** 216–223 (2003).
20. Wang, H. *et al.* A newly identified dependence receptor UNC5H4 is induced during DNA damage-mediated apoptosis and transcriptional target of tumor suppressor p53. *Biochem. Biophys. Res. Commun.* **370,** 594–598 (2008).
21. Miyamoto, Y. *et al.* Identification of UNC5A as a novel transcriptional target of tumor suppressor p53 and a regulator of apoptosis. *Int. J. Oncol.* **36,** 1253–1260 (2010).
22. Derksen, P. W. *et al.* Somatic inactivation of E-cadherin and p53 in mice leads to metastatic lobular mammary carcinoma through induction of anoikis resistance and angiogenesis. *Cancer Cell* **10,** 437–449 (2006).
23. Volenec, A., Bhogal, R. K., Moorman, J. M., Leslie, R. A. & Flanigan, T. P. Differential expression of DCC mRNA in adult rat foretrain. *Neuroreport* **8,** 2913–2917 (1997).
24. Livesey, F. J. & Hunt, S. P. Netrin and netrin receptor expression in the embryonic mammalian nervous system suggests roles in retinal, striatal, nigral, and cerebellar development. *Mol. Cell. Neurosci.* **8,** 417–429 (1997).
25. Hamamoto, T. *et al.* Compound disruption of *Smad2* accelerates malignant progression of intestinal tumors in *Apc* knockout mice. *Cancer Res.* **62,** 5955–5961 (2002).
26. Alberici, P. *et al. Smad4* haploinsufficiency in mouse models for intestinal cancer. *Oncogene* **25,** 1841–1851 (2006).
27. Kinzler, K. W. & Vogelstein, B. Lessons from hereditary colorectal cancer. *Cell* **87,** 159–170 (1996).
28. Austrup, F. *et al.* Prognostic value of genomic alterations in minimal residual cancer cells purified from the blood of breast cancer patients. *Br. J. Cancer* **83,** 1664–1673 (2000).

Supplementary Information is linked to the online version of the paper at www.nature.com/nature.

Acknowledgements We thank R. B. Ali for assistance in generating the mice, J. Blitz and the staff of the NKI animal facility for providing animal care, the staff of the histology department for the processing of tissues, I. Huijbers and H. van Zeeburg for help with apoptosis and FACS analysis, A. Kraft, S. Klarenbeek, S. Rottenberg and G. Doumont for discussions, and T. Braumuller and A. Kersbergen for technical support. We also thank the laboratory of P. Mehlen for the gift of netrin 1.

Author Contributions J.Y.S. carried out the histopathological analysis, N.P. was involved in animal experiments and J.Z. performed the confocal microscopy. J.J. and A.B. participated in discussions and interpretations of the experiments. P.K. was responsible for the design and execution of the experiments, and P.K. and A.B. wrote the paper.

Author Information Reprints and permissions information is available at www.nature.com/reprints. The authors declare no competing financial interests. Readers are welcome to comment on the online version of this article at www.nature.com/nature. Correspondence and requests for materials should be addressed to A.B. (a.berns@nki.nl).

LETTER

doi:10.1038/nature10806

The same pocket in menin binds both MLL and JUND but has opposite effects on transcription

Jing Huang[1,2], Buddha Gurung[3]*, Bingbing Wan[1,2]*, Smita Matkar[3], Natalia A. Veniaminova[4], Ke Wan[1,2], Juanita L. Merchant[4,5], Xianxin Hua[3] & Ming Lei[1,2]

Menin is a tumour suppressor protein whose loss or inactivation causes multiple endocrine neoplasia 1 (MEN1), a hereditary autosomal dominant tumour syndrome that is characterized by tumorigenesis in multiple endocrine organs[1]. Menin interacts with many proteins and is involved in a variety of cellular processes[2–8]. Menin binds the JUN family transcription factor JUND and inhibits its transcriptional activity[2,9]. Several *MEN1* missense mutations disrupt the menin–JUND interaction, suggesting a correlation between the tumour-suppressor function of menin and its suppression of JUND-activated transcription[2,10]. Menin also interacts with mixed lineage leukaemia protein 1 (MLL1), a histone H3 lysine 4 methyltransferase, and functions as an oncogenic cofactor to upregulate gene transcription and promote MLL1-fusion-protein-induced leukaemogenesis[3,7,11,12]. A recent report on the tethering of MLL1 to chromatin binding factor lens epithelium-derived growth factor (LEDGF) by menin indicates that menin is a molecular adaptor coordinating the functions of multiple proteins[13]. Despite its importance, how menin interacts with many distinct partners and regulates their functions remains poorly understood. Here we present the crystal structures of human menin in its free form and in complexes with MLL1 or with JUND, or with an MLL1–LEDGF heterodimer. These structures show that menin contains a deep pocket that binds short peptides of MLL1 or JUND in the same manner, but that it can have opposite effects on transcription. The menin–JUND interaction blocks JUN N-terminal kinase (JNK)-mediated JUND phosphorylation and suppresses JUND-induced transcription. In contrast, menin promotes gene transcription by binding the transcription activator MLL1 through the peptide pocket while still interacting with the chromatin-anchoring protein LEDGF at a distinct surface formed by both menin and MLL1.

The amino-terminal region of MLL1 interacts with menin[12,14,15]. Isothermal titration calorimetry measurements showed that the menin-binding motif (residues 6–25) of MLL1 ($MLL1_{MBM}$) is necessary and sufficient for menin binding (Fig. 1a and Supplementary Fig. 1a–c).

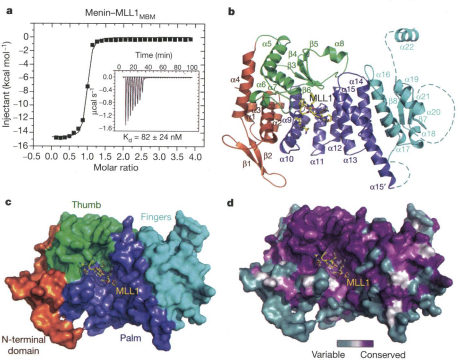

Figure 1 | Overview of the human menin–$MLL1_{MBM}$ complex structure. **a**, Isothermal titration calorimetry measurement of the menin–$MLL1_{MBM}$ interaction. The inset shows the isothermal titration data. **b**, Overall structure of the menin–$MLL1_{MBM}$ complex. The N-terminal domain is shown in orange, the thumb domain in green, the palm domain in blue, the fingers domain in cyan, and loop regions that are disordered or not included in the crystal structure are shown as dashed lines. $MLL1_{MBM}$ is shown as a stick model in yellow. **c**, The surface representation of menin indicates that menin adopts a curved left-hand-shaped conformation. **d**, Front view of the menin–$MLL1_{MBM}$ complex, coloured according to the degree of amino acid conservation among menin homologues.

[1]Howard Hughes Medical Institute, University of Michigan Medical School, 1150 West. Medical Center Drive, Ann Arbor, Michigan 48109, USA. [2]Department of Biological Chemistry, University of Michigan Medical School, 1150 West. Medical Center Drive, Ann Arbor, Michigan 48109, USA. [3]Abramson Family Cancer Research Institute, Department of Cancer Biology, University of Pennsylvania Perelman School of Medicine, Philadelphia, Pennsylvania 19104, USA. [4]Department of Internal Medicine, University of Michigan, 109 Zina Pitcher Place, Ann Arbor, Michigan 48109, USA. [5]Department of Molecular and Integrative Physiology, Division of Gastroenterology, University of Michigan, 109 Zina Pitcher Place, Ann Arbor, Michigan 48109, USA.
*These authors contributed equally to this work.

MLL2, the closest relative of MLL1, contains a sequence that is almost identical to $MLL1_{MBM}$ at its N terminus (Supplementary Fig. 1b); $MLL2_{16–35}$ ($MLL2_{MBM}$) binds to menin with an affinity that is comparable to that of $MLL1_{MBM}$ (Supplementary Fig. 1d). To understand how MLL1 and MLL2 (collectively referred to as MLL) are recognized by menin, we determined the crystal structures of human menin alone or in complex with $MLL1_{MBM}$ (Supplementary Fig. 2, Supplementary Table 1 and Supplementary Information). The structure of human menin closely resembles a recently published menin homologue structure from *Nematostella*[16].

The conformation of menin resembles a curved left 'hand' with a deep pocket formed by its 'thumb' and 'palm' (Fig. 1b, c). Menin consists

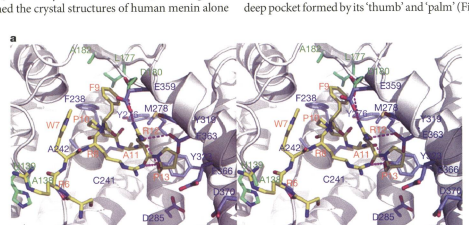

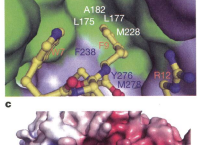

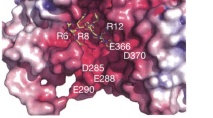

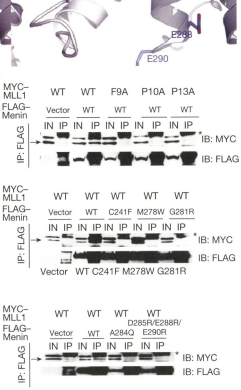

Figure 2 | Structural and mutational analyses of the menin–$MLL1_{MBM}$ interaction. **a**, Stereo view of the menin–$MLL1_{MBM}$ interface. The intermolecular hydrogen bonds are shown as dashed magenta lines. **b**, Phe 9^{MLL1} (yellow) is nested in a hydrophobic pocket of menin formed by the thumb (green) and the palm (blue). **c**, Electrostatic surface potential of the $MLL1_{MBM}$-binding cavity of menin (positive potential, blue; negative potential, red). **d**, Co-immunoprecipitation of wild-type (WT) or mutant menin and MLL1 proteins from 293T cells. Arrows and asterisks indicate the positions of MYC–MLL1 and immunoglobulin *G* (IgG), respectively. IB, immunoblot; IN, input; IP, immunoprecipitation. **e**, **f**, Expression of *Hoxc8* (**e**) and distributions of menin, MLL1 and H3K4me3 at the *Hoxc8* promoter (**f**) in $Men1^{-/-}$ mouse embryonic fibroblasts (MEFs) complemented with control vector, WT or mutant menin ($n = 6$; error bar, standard deviation).

of four associated domains: an N-terminal domain characterized by a long β-hairpin, a transglutaminase-like domain that forms the thumb, a helical palm domain that contains three TPR motifs[17] and a carboxy-terminal fingers domain (Fig. 1b, c, Supplementary Fig. 3 and Supplementary Information). Menin is highly conserved across species, and the conserved residues are either buried in the hydrophobic core or clustered together on a surface patch that covers the thumb and palm (Fig. 1d). MEN1 disease-derived missense and in-frame deletion mutations are evenly distributed throughout the protein (Supplementary Fig. 4), indicating that all four domains are important for the *in vivo* function of menin (Supplementary Fig. 4 and Supplementary Table 2).

The $MLL1_{MBM}$ peptide adopts a compact conformation and plugs into the deep pocket of menin (Fig. 2a and Supplementary Fig. 5). Mutagenesis data indicates that $MLL1_{MBM}$ residues Arg 6-Trp 7-Arg 8-Phe 9-Pro 10-Ala 11-Arg 12-Pro 13 and their interacting residues in menin contribute the most towards the interaction (Supplementary Figs 6 and 7, and Supplementary Tables 3 and 4). The side-chain of Phe 9^{MLL1} fits into a hydrophobic cavity formed by the thumb and palm of menin (Fig. 2b). A menin Met278Trp substitution altered the cavity shape and led to complete loss of binding (Supplementary Table 4). The $MLL1_{MBM}$-binding pocket is highly acidic (Fig. 2c). The two C-terminal arginine residues (Arg 24 and Arg 25) in $MLL1_{MBM}$ are disordered, but they seem to be important for interaction, given that glutamate substitution resulted in a 21-fold decrease in binding affinity (Supplementary Table 3). Consistent with this, mutation of the acidic residues of menin also led to decreased binding (Supplementary Table 4).

Next, we examined the $MLL1_{MBM}$-binding activity of several MEN1 disease-derived mutations (His139Asp, Cys241Phe, Ala242Val, Gly281Arg, Ala284Gln, and Thr344Arg). Except for Ala284Gln and Thr344Arg, which yielded insoluble proteins, the remaining mutants impaired the menin–$MLL1_{MBM}$ interaction (Supplementary Table 4). To further examine the menin–MLL1 interaction *in vivo*, we studied the interactions of mutant proteins that are transiently expressed in human embryonic kidney 293T cells. Consistent with the isothermal titration calorimetry analysis, co-immunoprecipitation data showed that mutations of the key residues at the interface completely abolished the menin–MLL1 interaction in cells (Fig. 2d).

Menin upregulates the expression of homeobox genes *Hoxc8* and *Hoxc6* (ref. 5). To test the effect of the menin–MLL interaction on the expression levels of *Hoxc8* and *Hoxc6*, wild-type and MLL-binding deficient mutants of menin were individually used to complement menin-null mouse embryonic fibroblasts. Western blot analyses indicated comparable expression of wild-type and mutant proteins in cells (Supplementary Fig. 8a). When $Men1^{-/-}$ cells were complemented with wild-type menin, expression of *Hoxc8* and *Hoxc6* dramatically increased compared to vector-expressing cells (Fig. 2e and Supplementary Fig. 8b). In contrast, overexpression of the menin mutants in $Men1^{-/-}$ cells failed to upregulate the messenger RNA levels of *Hoxc8* or *Hoxc6* (Fig. 2e and Supplementary Fig. 8b), suggesting that the menin–MLL interaction is essential for *Hoxc8* and *Hoxc6* expression.

Next we performed chromatin immunoprecipitation (ChIP) assays to determine the binding of mutant menin at the *Hoxc8* promoter. Except for Ala284Gln (a mutant that leads to insoluble proteins), all other mutants bound to the *Hoxc8* promoter as effectively as wild-type menin (Fig. 2f). Expression of wild-type or mutant menin did not greatly affect H3 distribution at the *Hoxc8* promoter (Supplementary Fig. 8c). Notably, $Men1^{-/-}$ cells complemented with wild-type menin exhibited a substantial increase in MLL1 binding and histone H3K4me3 trimethylation at the *Hoxc8* promoter compared with vector-expressing or mutant-menin-expressing cells (Fig. 2f). Therefore, although menin mutants were able to bind to the *Hoxc8* promoter, their ability to recruit MLL1 and thus establish H3K4me3 at the *Hoxc8* promoter was compromised, resulting in reduced *Hoxc8* expression.

LEDGF, a chromatin-associated protein[18], is required for MLL1-dependent transcription and leukaemic transformation[13]. Isothermal titration calorimetry measurement showed that a complex composed of menin and an N-terminal fragment of MLL1, called $MLL1_{MBM\text{-}LBM}$ (comprising residues 6–153 and including both menin-binding and LEDGF-binding motifs) binds to the integrase binding domain of LEDGF ($LEDGF_{IBD}$) with an affinity of 470 nM (Fig. 3a and Supplementary Fig. 9a). In contrast, neither menin nor $MLL1_{MBM\text{-}LBM}$ alone could interact with $LEDGF_{IBD}$ (Supplementary Fig. 9b)[13]. We determined the menin–$MLL1_{MBM\text{-}LBM}$–$LEDGF_{IBD}$ complex structure at a resolution of 3.0 Å (Supplementary Fig. 9c and Supplementary Table 1). $MLL1_{MBM\text{-}LBM}$ exhibits an extended conformation and binds to menin through two major sites (Fig. 3b); the N-terminal $MLL1_{MBM}$ coil folds into the high-affinity pocket of menin in the same manner as in the menin–$MLL1_{MBM}$ structure (Supplementary Figs 9d, e), whereas the C-terminal helix α2 packs on the surface of the N-terminal domain of menin to form a V-shaped groove for $LEDGF_{IBD}$ binding (Fig. 3b and Supplementary Fig. 9f). The middle loop of $MLL1_{MBM\text{-}LBM}$ spans a large distance on menin without many specific interactions except for two leucine residues (Leu 106 and Leu 116) with side-chains that point to

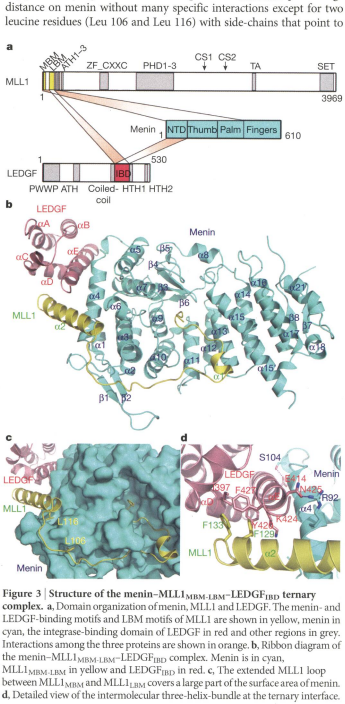

Figure 3 | Structure of the menin–$MLL1_{MBM\text{-}LBM}$–$LEDGF_{IBD}$ ternary complex. a, Domain organization of menin, MLL1 and LEDGF. The menin- and LEDGF-binding motifs and LBM motifs of MLL1 are shown in yellow, menin in cyan, the integrase-binding domain of LEDGF in red and other regions in grey. Interactions among the three proteins are shown in orange. **b**, Ribbon diagram of the menin–$MLL1_{MBM\text{-}LBM}$–$LEDGF_{IBD}$ complex. Menin is in cyan, $MLL1_{MBM\text{-}LBM}$ in yellow and $LEDGF_{IBD}$ in red. **c**, The extended MLL1 loop between $MLL1_{MBM}$ and $MLL1_{LBM}$ covers a large part of the surface area of menin. **d**, Detailed view of the intermolecular three-helix-bundle at the ternary interface.

two shallow pockets on the menin surface, defining the path of the loop (Fig. 3c and Supplementary Fig. 9g). Helix αE of $LEDGF_{IBD}$ is sandwiched between helices α2 of MLL1 and α4 of menin through both hydrophobic and electrostatic interactions (Fig. 3d). In support of the crystal structure, mutations of residues on the α4 helix of the N-terminal domain of menin (Ala95Arg and Ser104Tyr) specifically disrupted the interaction with LEDGF (Supplementary Table 5 and Supplementary Fig. 10). Notably, *Men1*$^{-/-}$ cells that were complemented with these two mutants failed to stimulate *Hoxc8* expression (Supplementary Fig. 11), suggesting that a functional menin–MLL1–LEDGF complex is required for upregulation of *Hoxc8* expression. Together, our data show that menin functions as an adaptor molecule to modulate gene expression by binding MLL1 at one site while also interacting with LEDGF at a distinct surface.

Although MLL1 and MLL2 share many functional motifs, including the menin-binding motif (Supplementary Fig. 12), MLL2 does not contain a LEDGF-binding motif sequence and thus would not form a ternary complex with menin and LEDGF. Given that the PWWP domain of LEDGF, which contains a relatively well conserved Pro-Trp-Trp-Pro signature, is required for MLL1-mediated leukaemic transformation[13,18], the inability of MLL2 to form a menin–MLL2–LEDGF complex explains why only *MLL1*, and not *MLL2*, has so far been described as a proto-oncogene that can be activated by chromosomal translocations.

Menin also interacts directly with transcription factor JUND[2,9]. We defined JUND residues 27–47 as the menin-binding motif ($JUND_{MBM}$) with an affinity of 1.6 μM (Fig. 4a and Supplementary Fig. 13). Sequence comparison of $JUND_{MBM}$ and $MLL1_{MBM}$ revealed a striking similarity (Fig. 4a), suggesting that $JUND_{MBM}$ might interact with menin through the same binding pocket as does $MLL1_{MBM}$. Consistent with this idea, both isothermal titration calorimetry and glutathione *S*-transferase (GST) pull-down assays showed that MLL1 could efficiently compete with JUND for menin binding (Supplementary Fig. 14).

We determined the menin–$JUND_{MBM}$ complex structure, which shows many similarities to the menin–$MLL1_{MBM}$ structure (Fig. 4b and Supplementary Table 1). First, the Phe-Pro-(Ala or Gly)-(Arg or Ala)-Pro motifs in both menin-binding motifs are almost identical in overall conformation (Supplementary Fig. 15a). Second, Phe32, Pro33 and Pro36 of JUND interact with menin in the same way as their counterparts in $MLL1_{MBM}$ (Supplementary Fig. 15b, c). Notably, two lysine residues (Lys 46 and Lys 47) in $JUND_{MBM}$, equivalent to the disordered Arg 24 and Arg 25 in $MLL1_{MBM}$, are visible in the electron density map and point to an acidic surface on menin (Supplementary Fig. 15c). Mutation of these lysine residues and other key binding residues at the interface abolished or weakened the interaction both *in vitro* and *in vivo* (Fig. 4c, Supplementary Fig. 16 and Supplementary Table 6).

Menin uncouples JUND phosphorylation from JNK activation, but the mechanism is poorly understood[19]. The consensus JNK-docking domain (D-domain) contains a cluster of basic amino acids preceding two leucine residues[20] (Fig. 4d). $JUND_{MBM}$ is partially overlapped with a putative D-domain of JUND ($JUND_D$)[21] (Fig. 4d). Both the basic residues and the leucine residues in $JUND_D$ are indispensable for JNK docking on JUND as well as JNK-mediated JUND phosphorylation (Fig. 4e, f and Supplementary Fig. 17a, b). Thus, Lys 46 and Lys 47 are both required for menin binding and JUND phosphorylation by sites are labelled. **e**, *In vitro* GST-pull-down analysis of the interactions between FLAG-tagged JNK and the indicated JUN proteins. **f**, *In vitro* phosphorylation of WT or mutant JUND by JNK. **g**, *In vitro* phosphorylation of WT or menin-binding-deficient JUND by JNK in the presence or absence of menin. **h**, Menin suppresses JUND phosphorylation in response to anisomycin activation of JNK in 293T cells. **i**, WT or mutant JUND plasmids were transfected into 293T cells with AP1 and Renilla reporter plasmids, and with or without menin. Luciferase assays were performed 2 days after transfection ($n = 4$; error bar, standard deviation).

Figure 4 | Structural and functional studies of the menin–JUND interaction. **a**, Sequence alignment of the menin-binding motif sequences of JUND, MLL1 and MLL2. Conserved residues are highlighted in yellow. **b**, Crystal structure of the menin–$JUND_{MBM}$ complex. Menin is coloured as in Fig. 1c and $JUND_{MBM}$ is shown as a purple stick model. **c**, Co-immunoprecipitation of WT or mutant menin and JUND from 293T cells. **d**, Sequence comparison of the N termini of JUND and c-JUN. The menin-binding motif sequence of JUND is highlighted in purple. Key residues in the JNK-docking domain are denoted with blue dots and three phosphorylation

JNK. This led us to test whether menin inhibits JUND phosphorylation through sequestering JUND from JNK. In GST-pull-down assay, GST–JUND can only pull down JNK in the absence of menin, indicating that menin has a higher affinity to JUND (Fig. 4e and Supplementary Fig. 17a). Furthermore, when menin was added, phosphorylation of JUND was clearly inhibited (Fig. 4g and Supplementary Fig. 17c). In contrast, phosphorylation of menin-binding-deficient mutants of JUND was not affected by menin (Fig. 4g and Supplementary Fig. 17c). Next, we examined whether menin could inhibit JUND phosphorylation in response to anisomycin activation of JNK in 293T cells[19]. Although wild-type JUND phosphorylation was suppressed by menin, menin-binding deficient mutants remained robustly phosphorylated in the presence of menin (Fig. 4h). Notably, menin had no effects on JNK binding and JNK-mediated phosphorylation of c-JUN, a close homologue of JUND that lacks a menin-binding motif (Fig. 4d, e, g and Supplementary Fig. 17a, c, d). Together, our findings reveal that the menin–JUND interaction blocks JNK docking on JUND and inhibits the JNK-mediated phosphorylation.

Menin represses JUND-mediated transcriptional activation[2,9]. To examine whether this repression depends on the menin–JUND interaction, wild-type or menin-binding-deficient mutants of JUND were co-transfected into 293T cells with an AP1 luciferase reporter plasmid in the presence or absence of menin (Supplementary Fig. 17e). Consistent with previous studies, transactivation by JUND was effectively repressed by menin[2,9] (Fig. 4i). In contrast, menin exhibited a marginal effect on mutant JUND-mediated transcriptional activation (Fig. 4i). We recently demonstrated that JUND induces gastrin gene expression in human AGS gastric cells and that this induction can be suppressed by menin[22]. Consistent with the luciferase assay, menin failed to suppress the gastrin upregulation that was induced by mutant JUND, suggesting that the menin–JUND interaction is important in gastrin expression regulation (Supplementary Fig. 18). Thus, we conclude that the menin–JUND interaction plays a key part in suppressing JUND-mediated transcriptional activation.

In summary, our structural and functional studies provide a mechanistic explanation of how menin could both positively and negatively regulate gene transcription. Our findings also provide evidence that menin acts as a scaffold protein to assemble a menin–MLL1–LEDGF ternary complex to coordinate gene transcription and promote MLL1-fusion-protein-induced leukaemogenesis.

METHODS SUMMARY

Human menin, $LEDGF_{IBD}$ and the MLL and JUND peptides were expressed in *Escherichia coli* BL21(DE3) and purified by sequential affinity and gel-filtration chromatography purification. Menin crystals were obtained in sitting drops over 100 mM sodium cacodylate (pH 6.5) and 1.4 M sodium acetate. Crystallization of menin with the $MLL1_{MBM}$ or $JUND_{MBM}$ peptides was achieved by sitting-drop diffusion with a well solution containing 100 mM Tris-HCl (pH 7.0), 200 mM $MgCl_2$ and 2.3 M NaCl. The menin–$MLL1_{MBM\text{-}LBM}$–$LEDGF_{IBD}$ complex was crystallized by hanging-drop vapour diffusion against a well solution of 50 mM HEPES (pH 7.0), 1.6 M $(NH_4)_2SO_4$, 10 mM $MgCl_2$, 0.016% L-canavanine, 0.016% O-phospho-L-serine, 0.016% taurine, 0.016% quinine, 0.016% sodium glyoxylate monohydrate and 0.016% cholic acid, and were dehydrated with the solution containing 50 mM HEPES (pH 7.0), 2.3 M $(NH_4)_2SO_4$ and 10 mM $MgCl_2$. The menin–$MLL1_{MBM}$ complex structure was determined by multi-wavelength anomalous dispersion to a resolution of 3.0 Å. The structures of menin alone, the menin–$MLL1_{MBM\text{-}LBM}$–$LEDGF_{IBD}$ ternary complex, and the menin–$JUND_{MBM}$ complex were solved by molecular replacement and refined to resolutions of 2.5 Å, 3.0 Å and 2.85 Å, respectively.

Full Methods and any associated references are available in the online version of the paper at www.nature.com/nature.

Received 17 July; accepted 19 December 2011.
Published online 12 February 2012.

1. Chandrasekharappa, S. C. *et al.* Positional cloning of the gene for multiple endocrine neoplasia-type 1. *Science* **276,** 404–407 (1997).
2. Agarwal, S. K. *et al.* Menin interacts with the AP1 transcription factor JunD and represses JunD-activated transcription. *Cell* **96,** 143–152 (1999).
3. Busygina, V., Kottemann, M. C., Scott, K. L., Plon, S. E. & Bale, A. E. Multiple endocrine neoplasia type 1 interacts with forkhead transcription factor CHES1 in DNA damage response. *Cancer Res.* **66,** 8397–8403 (2006).
4. Chen, G. *et al.* Menin promotes the Wnt signaling pathway in pancreatic endocrine cells. *Mol. Cancer Res.* **6,** 1894–1907 (2008).
5. Hughes, C. M. *et al.* Menin associates with a trithorax family histone methyltransferase complex and with the *Hoxc8* locus. *Mol. Cell* **13,** 587–597 (2004).
6. Jin, S. *et al.* Menin associates with FANCD2, a protein involved in repair of DNA damage. *Cancer Res.* **63,** 4204–4210 (2003).
7. Yokoyama, A. *et al.* Leukemia proto-oncoprotein MLL forms a SET1-like histone methyltransferase complex with menin to regulate *Hox* gene expression. *Mol. Cell. Biol.* **24,** 5639–5649 (2004).
8. Yang, Y. & Hua, X. In search of tumor suppressing functions of menin. *Mol. Cell. Endocrinol.* **265–266,** 34–41 (2007).
9. Knapp, J. I. *et al.* Identification and characterization of JunD missense mutants that lack menin binding. *Oncogene* **19,** 4706–4712 (2000).
10. Groussin, L. & Bertherat, J. Mechanisms of multiple endocrine neoplasia type 1: evidence for regulation of the AP-1 family of transcription factors by menin. *Eur. J. Endocrinol.* **141,** 15–16 (1999).
11. Knrivtsov, A. V. & Armstrong, S. A. MLL translocations, histone modifications and leukaemia stem-cell development. *Nature Rev. Cancer* **7,** 823–833 (2007).
12. Yokoyama, A. *et al.* The menin tumor suppressor protein is an essential oncogenic cofactor for MLL-associated leukemogenesis. *Cell* **123,** 207–218 (2005).
13. Yokoyama, A. & Cleary, M. L. Menin critically links MLL proteins with LEDGF on cancer-associated target genes. *Cancer Cell* **14,** 36–46 (2008).
14. Caslini, C. *et al.* Interaction of MLL amino terminal sequences with menin is required for transformation. *Cancer Res.* **67,** 7275–7283 (2007).
15. Grembecka, J., Belcher, A. M., Hartley, T. & Cierpicki, T. Molecular basis of the mixed lineage leukemia-menin interaction: implications for targeting mixed lineage leukemias. *J. Biol. Chem.* **285,** 40690–40698 (2010).
16. Murai, M. J., Chruszcz, M., Reddy, G., Grembecka, J. & Cierpicki, T. Crystal structure of menin reveals binding site for mixed lineage leukemia (MLL) protein. *J. Biol. Chem.* **286,** 31742–31748 (2011).
17. Lamb, J. R., Tugendreich, S. & Hieter, P. Tetratrico peptide repeat interactions: to TPR or not to TPR? *Trends Biochem. Sci.* **20,** 257–259 (1995).
18. Llano, M., Morrison, J. & Poeschla, E. M. Virological and cellular roles of the transcriptional coactivator LEDGF/p75. *Curr. Top. Microbiol. Immunol.* **339,** 125–146 (2009).
19. Gallo, A. *et al.* Menin uncouples Elk-1, JunD and c-Jun phosphorylation from MAP kinase activation. *Oncogene* **21,** 6434–6445 (2002).
20. Yang, S. H., Whitmarsh, A. J., Davis, R. J. & Sharrocks, A. D. Differential targeting of MAP kinases to the ETS-domain transcription factor Elk-1. *EMBO J.* **17,** 1740–1749 (1998).
21. Yazgan, O. & Pfarr, C. M. Regulation of two JunD isoforms by Jun N-terminal kinases. *J. Biol. Chem.* **277,** 29710–29718 (2002).
22. Mensah-Osman, E. J., Veniaminova, N. A. & Merchant, J. L. Menin and JunD regulate gastrin gene expression through proximal DNA elements. *Am. J. Physiol. Gastrointest. Liver Physiol.* **301,** G783–G790 (2011).

Supplementary Information is linked to the online version of the paper at www.nature.com/nature.

Acknowledgements We thank G. Wilding for the human JUND complementary DNA and P. Cherepanov for the human LEDGF cDNA. We thank Y. Chen and W. Deng for help at various stages of the project. M.L. is a Howard Hughes Medical Institute Early Career Scientist. Work was supported by National Institutes of Health grants (GM 083015-01 to M.L., R01-DK085121 to X.H. and R37-DK45729 to J.L.M.), an American Cancer Society Research Scholar grant (to M.L.) and an American Association for Cancer Research Caring for Carcinoid Foundation Grant (to X.H.). The General Medicine and Cancer Institutes Collaborative Access Team has been funded in whole or in part with federal funds from the National Cancer Institute (grant Y1-CO-1020) and the National Institute of General Medical Science (grant Y1-GM-1104). Use of the Advanced Photon Source was supported by the US Department of Energy, Office of Science, Office of Basic Energy Sciences, under contract number DE-AC02-06CH11357.

Author Contributions J.H. is responsible for the bulk of the experiments, B.G. for the qRT-PCR and ChIP assays; B.W. for the co-immunoprecipitation and *in vivo* phosphorylation analyses, S.M. for the luciferase assay, N.A.V. and J.L.M. for the analysis of gastrin expression, and K.W. for some of the protein purification. M.L. and X.H. supervised the project and wrote the paper.

Author Information The atomic coordinates and structure factors of menin, menin–$MLL1_{MBM}$, menin–$JUND_{MBM}$ and menin–$MLL1_{MBM\text{-}LBM}$–$LEDGF_{IBD}$ have been deposited in the RCSB Protein Data Bank under accession codes 3U84, 3U85, 3U86 and 3U88, respectively. Reprints and permissions information is available at www.nature.com/reprints. The authors declare no competing financial interests. Readers are welcome to comment on the online version of this article at www.nature.com/nature. Correspondence and requests for materials should be addressed to M.L. (leim@umich.edu) or X.H. (huax@mail.med.upenn.edu).

LETTER

doi:10.1038/nature10753

Structure of the human M2 muscarinic acetylcholine receptor bound to an antagonist

Kazuko Haga[1]*, Andrew C. Kruse[2]*, Hidetsugu Asada[3,4]*, Takami Yurugi-Kobayashi[3,4], Mitsunori Shiroishi[4,5], Cheng Zhang[2], William I. Weis[2,6], Tetsuji Okada[1], Brian K. Kobilka[2], Tatsuya Haga[1] & Takuya Kobayashi[3,4,7]

The parasympathetic branch of the autonomic nervous system regulates the activity of multiple organ systems. Muscarinic receptors are G-protein-coupled receptors that mediate the response to acetylcholine released from parasympathetic nerves[1–3]. Their role in the unconscious regulation of organ and central nervous system function makes them potential therapeutic targets for a broad spectrum of diseases. The M2 muscarinic acetylcholine receptor (M2 receptor) is essential for the physiological control of cardiovascular function through activation of G-protein-coupled inwardly rectifying potassium channels, and is of particular interest because of its extensive pharmacological characterization with both orthosteric and allosteric ligands. Here we report the structure of the antagonist-bound human M2 receptor, the first human acetylcholine receptor to be characterized structurally, to our knowledge. The antagonist 3-quinuclidinyl-benzilate binds in the middle of a long aqueous channel extending approximately two-thirds through the membrane. The orthosteric binding pocket is formed by amino acids that are identical in all five muscarinic receptor subtypes, and shares structural homology with other functionally unrelated acetylcholine binding proteins from different species. A layer of tyrosine residues forms an aromatic cap restricting dissociation of the bound ligand. A binding site for allosteric ligands has been mapped to residues at the entrance to the binding pocket near this aromatic cap. The structure of the M2 receptor provides insights into the challenges of developing subtype-selective ligands for muscarinic receptors and their propensity for allosteric regulation.

Muscarinic receptors constitute a family with five subtypes, M1–M5 (ref. 1). M1, M3 and M5 subtypes couple with the G_q family of G proteins, and M2 and M4 subtypes with the G_i/G_o family of G proteins. Previous work showing that the muscarinic action by a series of choline esters and other substances in various tissues could be differentiated from their nicotinic action[2] led to muscarinic acetylcholine receptors being defined as a functional concept. Muscarinic receptors are now known to be G-protein-coupled receptors (GPCRs)[3] and the nicotinic receptor a ligand-gated ion channel. Muscarinic receptors were initially defined biochemically as proteins that specifically bound 3-quinuclidinyl-benzilate (QNB) and N-methylscopolamine (NMS). They were among the first GPCRs to be purified from cerebral membranes[4], and to be functionally reconstituted with purified G protein in lipid vesicles[3]. The M1 receptor[5] together with the β_2 adrenergic receptor[6] were the first neurotransmitter-activated GPCRs to be cloned, revealing the seven transmembrane (TM) segment topology initially observed for rhodopsin[7], and subsequently found to be common to all members of the GPCR family.

As a consequence of their roles in both the central and parasympathetic nervous systems, muscarinic receptors are targets for the treatment of a spectrum of disorders including Alzheimer's disease, schizophrenia and Parkinson's disease, and chronic obstructive pulmonary disease[8]. However, developing highly subtype-selective orthosteric drugs for muscarinic receptors has been challenging and thus far largely unsuccessful. Recent drug discovery efforts have therefore shifted to the development of small molecule allosteric modulators. Muscarinic receptors have long been a model system for studying allosteric regulation of GPCR signalling because of their exceptional propensity to bind allosteric ligands[9]. To understand better the structural basis for challenges in developing orthosteric drugs and the susceptibility for allosteric regulation, we obtained a crystal structure of the M2 receptor.

In our initial efforts to obtain the structure of the M2 receptor we expressed and purified M2 receptor lacking most of the third intracellular loop (IL3) and the native glycosylation sites. The central part of IL3 of the M2 receptor can be removed without impairing its ability to bind to agonists or activate G proteins[10], and IL3 was shown to have a flexible structure[11]. Using this modified M2 receptor bound to the high-affinity inverse agonist *R*-(−)-3-QNB, we performed crystallization by hanging-drop vapour diffusion and obtained crystals that diffracted to around 9 Å, but were not able to improve the quality of these crystals. We subsequently replaced IL3 of the M2 receptor with T4 lysozyme (T4L) as initially described for the β_2 adrenergic receptor[12] (Supplementary Fig. 1a). This method has been used to obtain crystal structures of four other GPCRs: the adenosine A_{2A} receptor[13], the CXCR4 receptor[14], the dopamine receptor D3 (ref. 15) and most recently the histamine H_1 receptor[16]. The binding properties of M2-T4L with muscarinic ligands were essentially the same as for the wild-type M2 receptor (Supplementary Fig. 1b, c), indicating that the overall TM architecture of M2-T4L was minimally affected by introduction of T4L. The M2-T4L receptor was subsequently crystallized in lipidic cubic phase. A 3.0 Å structure was solved by molecular replacement from a data set obtained by merging diffraction data from 23 crystals.

As is typical for proteins crystallized by the lipidic cubic phase method, the lattice for the M2 receptor shows alternating aqueous and lipidic layers with M2 receptor molecules embedded in the latter while T4L is confined to aqueous regions (Supplementary Fig. 2). Within the membrane plane, receptor molecules are packed closely against one another, alternating orientations within the bilayer. There are abundant hydrophobic contacts between receptor molecules within the membrane, whereas polar interactions primarily involve contacts between T4L molecules as well as receptor–T4L interactions.

The overall structure of the M2 receptor (Fig. 1a) is similar to that of rhodopsin and other recently crystallized inactive GPCR structures (compared in Supplementary Fig. 3). The cytoplasmic surface of the M2 receptor is in an inactive conformation, but as with most other GPCR structures, there is no interaction involving Arg $121^{3.50}$ (superscripts indicate Ballesteros–Weinstein numbers) in the conserved

[1]Department of Life Science, Faculty of Science, Gakushuin University, Mejiro 1-5-1, Tokyo 171-8588, Japan. [2]Department of Molecular and Cellular Physiology, Stanford University School of Medicine, 279 Campus Drive, Stanford, California 94305, USA. [3]Department of Medical Chemistry and Cell Biology, Kyoto University Faculty of Medicine, Konoe-cho, Yoshdida, Sakyo-Ku, Kyoto 606-8501, Japan. [4]Human Receptor Crystallography Project, ERATO, Japan Science and Technology Agency, Konoe-cho, Yoshida, Sakyo-Ku, Kyoto 606-8501, Japan. [5]Graduate School of Pharmaceutical Sciences, Kyushu University, 3-1-1 Maidashi, Higashi-ku, Fukuoka 812-8582, Japan. [6]Department of Structural Biology, Stanford University School of Medicine, 299 Campus Drive, Stanford, California 94305, USA. [7]Japan Science and Technology Agency, Core Research for Evolutional Science and Technology (CREST), Kyoto University Faculty of Medicine, Kyoto 606-8501, Japan.
*These authors contributed equally to this work.

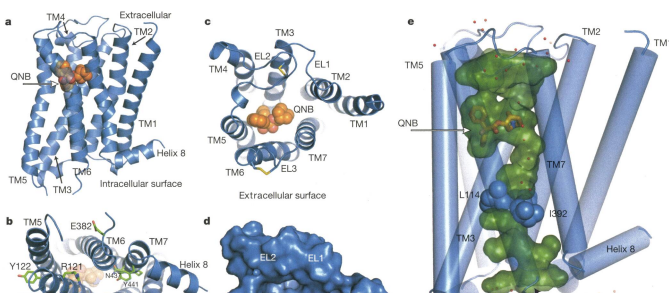

Figure 1 | The M2 receptor with bound QNB. a–**e**, The M2 receptor is shown as a blue ribbon and QNB as orange spheres. **a**, M2 receptor in profile. **b**, Cytoplasmic surface showing conserved DRY residues in TM3. **c**, Extracellular view into QNB binding pocket. **d**, Extracellular view with solvent-accessible-surface rendering shows a funnel-shaped vestibule and a nearly buried QNB binding pocket. **e**, Aqueous channel (green) extending from the extracellular surface into the transmembrane core is interrupted by a layer of three hydrophobic residues (blue spheres). Well-ordered water molecules are shown as red dots.

E/DRY sequence in TM3 and Glu $382^{6.30}$ in TM6 (Fig. 1b). Instead, the Arg $121^{3.50}$ side chain forms a salt bridge only with Asp $120^{3.49}$. In rhodopsin, the homologous residues form part of a charge–charge interaction that stabilizes the cytoplasmic ends of TM3 and TM6 in an inactive state[17]. The second intracellular loop shows a helical conformation similar to that first seen for the turkey β_1 adrenergic receptor[18].

GPCR crystal structures show the greatest differences in the extracellular surface (Supplementary Fig. 3). The M2 receptor has a relatively simple and open extracellular surface (Fig. 1c, d) with the longer extracellular loop (ECL)2 stabilized by a conserved disulphide with Cys $96^{3.25}$ at the N terminus of TM3 and Cys 176 in the middle of ECL2. In addition, the second disulphide bond was detected between C413 and C416 in the ECL3. The extracellular surface of the M2 receptor most resembles that of the dopamine D3 receptor (Supplementary Fig. 3).

Crystal structures of GPCRs reveal a network of hydrogen bonding interactions that extend from the binding pocket to the cytoplasmic surface. However, a distinctive feature of the M2 receptor is that this network is part of a long, continuous aqueous channel extending from the extracellular surface to a depth of approximately 33 Å when measured from ECL2 (Fig. 1e). This channel contains the ligand binding pocket, but extends beyond the ligand and is separated from the cytoplasmic surface by a hydrophobic layer formed by three amino acids: Leu $65^{2.46}$ in TM2, Leu $114^{4.43}$ in TM4 and Ile $392^{6.40}$ in TM6. Each of these is absolutely conserved among all five muscarinic subtypes. The dimensions of the channel below the QNB binding site are large enough to accommodate a long, extended orthosteric ligand. Supplementary Fig. 4 compares the aqueous channels of other GPCRs.

The ligand QNB binds within a deeply buried pocket defined by the side chains of TM3, 4, 5, 6 and 7 (Fig. 2a–c and Supplementary Fig. 5 and Supplementary Table 3). An aromatic cage encloses the amine and forms a lid over the ligand, separating the orthosteric site from the extracellular vestibule. Asp $103^{3.32}$ and Asn $404^{6.52}$ serve to orient the ligand in the largely hydrophobic binding cavity, with Asn $404^{6.52}$ forming paired hydrogen bonds with the hydroxyl and carbonyl groups in QNB while Asp $103^{3.32}$ engages in a charge–charge interaction with the amine moiety of the ligand (Fig. 2). The TM amino acids that form the QNB binding pocket are identical in all five muscarinic receptor subtypes (Supplementary Table 1), consistent with results of QNB binding experiments on M1–M4 receptors, and with site-directed mutagenesis experiments on M1 (ref. 19), M2 (ref. 20) and M3 (ref. 21) receptors. Only Phe 181, which extends downward from ECL2 and interacts with one of the two phenyl rings on QNB (Fig. 2), differs from all other muscarinic receptor subtypes, which have leucine in the homologous position. The importance of Asp $^{3.32}$ for both agonist and antagonist binding has been demonstrated in mutagenesis and covalent-labelling experiments and modelling studies[19–22]. In contrast, mutation of Asn $404^{6.52}$ to Ala on M1 (ref. 23) and M3 (ref. 24) receptors was shown to greatly affect binding of QNB but have little effect on binding of or activation by acetylcholine. It is possible that Asn $404^{6.52}$ is hydrogen bonded with the ester group of QNB but not that of acetylcholine.

The M2 and other muscarinic receptors represent one of four families of acetylcholine binding proteins to be structurally characterized thus far. Figure 3a shows the orthosteric binding site of the M2 receptor with acetylcholine docked with the *gauche* form of the O–C2–C1–N dihedral angle, which places the choline group in the aromatic cage interacting with Asp $103^{3.32}$, while the carbonyl oxygen is tentatively bound to Asn $404^{6.52}$ (Fig. 3a). The natural agonist acetylcholine is much smaller than the bulky antagonist QNB. As described in the agonist-bound structure of the β_2 adrenergic receptor, the contraction of the ligand binding pocket is expected as a result of an inward shift of TM5 (ref. 25). This result is consistent with the previous mutation studies showing that Thr $187^{5.39}$ and Thr $190^{5.42}$ in TM5 (Fig. 2) alter binding of most agonists but not of antagonists[20]. Bulky compounds capable of blocking activation-related contraction of the pocket would be very efficient in locking the M2 receptor in an inactive conformation, as is exemplified here by the antagonist QNB. It has been proposed that the conformational change of the M2 receptor upon activation might be

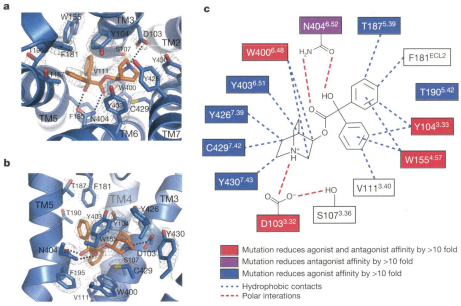

Figure 2 | Binding interactions between the M2 receptor and QNB. **a**, **b**, Two views of the QNB binding pocket. Amino acids within 4 Å of the ligand are shown as light blue sticks, with QNB in orange. Nitrogen and oxygen atoms are coloured dark blue and red, respectively. Polar interactions are indicated by dashed lines. A $2F_o - F_c$ map is shown in wire at 1.5σ contour. **c**, A schematic representation of QNB binding interactions is shown. Mutations of amino acids in the red boxes have been shown to reduce both antagonist and agonist binding by more than tenfold. Mutations of the amino acid in the purple boxes reduce antagonist binding affinity by more than tenfold. Mutations of amino acids in the blue boxes reduce agonist binding by more than tenfold. Blue dotted lines indicate potential hydrophobic interactions and red lines indicate potential polar interactions.

accompanied by a conformational change of acetylcholine from the *gauche* to the *trans* form of the O–C2–C1–N dihedral angle[26]. It remains to be determined in which pose acetylcholine binds to the M2 receptor or to the M2-receptor–G-protein complex, and whether acetylcholine hydrogen bonds with Asn $404^{6.52}$ or other residues.

In a striking example of convergent evolution, the orthosteric site of the M2 receptor exhibits many features noted previously as common structural elements in unrelated acetylcholine binding proteins[27]. Like the M2 receptor, a nicotinic acetylcholine receptor homologue bound to acetylcholine (Fig. 3b) shows an aromatic cage comprised of three tyrosines and a tryptophan, although it notably lacks a counterion to the choline group[28], whereas in the M2 receptor this role is filled by Asp $103^{3.32}$. A bacterial acetylcholine binding protein, ChoX, from *Sinorhizobium meliloti* (Fig. 3c) also possesses an aromatic cage, and

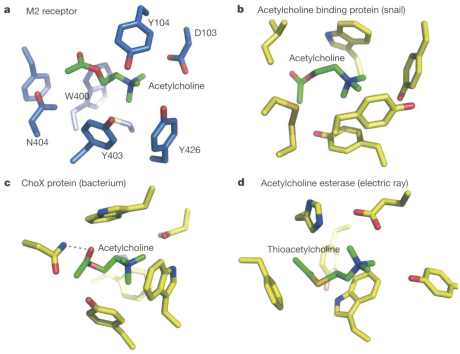

Figure 3 | Convergent evolution of acetylcholine binding sites. **a**, Acetylcholine is modelled into the crystal structure of the M2 receptor. **b**, Acetylcholine binding pocket in the crystal structure of the acetylcholine binding protein from the snail *Aplysia californica* (PDB accession 2XZ5). **c**, Acetylcholine binding pocket in the acetylcholine binding protein ChoX from the Gram negative bacterium *Sinorhizobium meliloti* (PDB accession 2RIN). **d**, Binding site for thio-acetylcholine in the enzyme acetylcholine esterase from the electric ray *Torpedo californica* (PDB accession 2C4H).

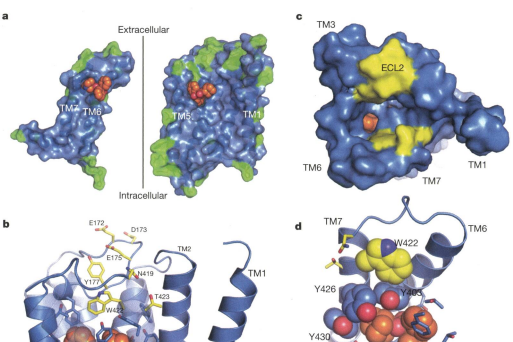

Figure 4 | Allosteric binding in the M2 receptor. a, Differences between the M2 and M4 receptors are shown as green residues mapped onto the inner surface of the M2 receptor (blue), with QNB in orange spheres. The sequence conservation within the orthosteric site is apparent, while residues outside show more variability. **b**–**d**, Mutations that alter allosteric binding are shown with yellow carbons, and amino acids involved in QNB binding are shown with blue carbons as sticks or spheres. **b**, **c**, Different views of possible allosteric binding sites in the M2 receptor. The surface view in **c** shows the positions of possible allosteric binding sites (yellow) lining the path to the QNB binding pocket. **d**, Trp 422 (yellow spheres), implicated in binding of allosteric ligands, forms an edge-to-face aromatic interaction with Tyr 403, part of the aromatic cage (blue spheres) of the orthosteric site.

like the M2 receptor has an aspartate in close proximity to the amine engaging in a charge–charge interaction[29]. Also like the M2 receptor, ChoX has an asparagine hydrogen bonding to the ligand carbonyl. Like these proteins, the enzyme acetylcholine esterase (Fig. 3d) uses an aromatic cage and a carboxylate to bind the choline group, while the (thio)acetyl group interacts with a phenylalanine, probably through π–π interactions[30]. Taken together, these structures suggest that an aromatic cage and buried carboxylate are likely to be critical elements for acetylcholine recognition and binding in general.

There is a growing interest in the development of allosteric ligands for GPCR targets. This is motivated by the ability to develop more subtype-selective drugs targeted at less conserved regions of the receptor. Moreover, allosteric ligands modulate the effects of natural hormones and neurotransmitters, and may therefore regulate receptor activity in a more physiological manner. As noted above, the orthosteric binding pocket is highly conserved among all muscarinic receptor subtypes. Allosteric regulation of GPCRs was first observed for the M2 receptor and this receptor has been one of the most extensively characterized allosteric model systems[9]. Figure 4a shows the inner surface of the M2 receptor, highlighting residues that are not conserved with its closest relative, the M4 receptor. It can be seen that the orthosteric binding pocket and transmembrane core are highly conserved. The greatest diversity is observed in the extracellular loops and the extracellular end of TM segments that form the entrance to the orthosteric binding pocket. These amino acids represent structural diversity that could be exploited for the development of more subtype-selective ligands[9]. Of interest, site-directed mutagenesis and chimaeric receptor studies have implicated several of these amino acids in the binding of several well-characterized allosteric modulators[9]. As shown in Fig. 4b–d, these residues are located in ECL2 and the amino-terminus of TM7 at the entrance to the binding pocket. Trp $422^{7.35}$, a residue implicated in the binding of several allosteric modulators, appears to form an edge-to-face π–π interaction with Tyr $403^{6.51}$, part of the aromatic cage surrounding the charged amine of the orthosteric ligand (Fig. 4d). Binding of allosteric ligands to this site would be expected to influence the association and disassociation rates of orthosteric ligands.

The structure of the M2 receptor provides insights into both orthosteric and allosteric regulation of muscarinic receptors. The development of more selective drugs for muscarinic receptors will probably require exploitation of the more diverse allosteric surface, either as exclusively allosteric ligands or as ligands that occupy both orthosteric and allosteric sites.

METHODS SUMMARY

Untagged human M2 muscarinic acetylcholine receptor was expressed in Sf9 cells with the IL3 replaced with T4 lysozyme, then extracted with digitonin and sodium cholate and purified by ligand affinity chromatography, then exchanged into decyl maltoside buffer. Purified receptor was crystallized by the lipidic cubic phase technique following addition of a stabilizing neopentyl glycol detergent. Data collection was performed at Advanced Photon Source beamlines 23ID-B and 23ID-D, and the structure solved by molecular replacement. Refinement statistics are given in Supplementary Table 2.

Full Methods and any associated references are available in the online version of the paper at www.nature.com/nature.

Received 10 August; accepted 1 December 2011.
Published online 25 January 2012.

1. Hulme, E. C., Birdsall, N. J. & Buckley, N. J. Muscarinic receptor subtypes. *Annu. Rev. Pharmacol. Toxicol.* **30,** 633–673 (1990).
2. Dale, H. H. The action of certain esters and ethers of choline, and their relation to muscarine. *J. Pharmacol. Exp. Ther.* **6,** 147–190 (1914).
3. Haga, K. *et al.* Functional reconstitution of purified muscarinic receptors and inhibitory guanine nucleotide regulatory protein. *Nature* **316,** 731–733 (1985).

4. Haga, K. & Haga, T. Purification of the muscarinic acetylcholine receptor from porcine brain. *J. Biol. Chem.* **260,** 7927–7935 (1985).
5. Kubo, T. *et al.* Cloning, sequencing and expression of complementary DNA encoding the muscarinic acetylcholine receptor. *Nature* **323,** 411–416 (1986).
6. Dixon, R. A. *et al.* Cloning of the gene and cDNA for mammalian β-adrenergic receptor and homology with rhodopsin. *Nature* **321,** 75–79 (1986).
7. Ovchinnikov, Y. A. Rhodopsin and bacteriorhodopsin: structure–function relationships. *FEBS Lett.* **148,** 179–191 (1982).
8. Wess, J., Eglen, R. M. & Gautam, D. Muscarinic acetylcholine receptors: mutant mice provide new insights for drug development. *Nature Rev. Drug Discov.* **6,** 721–733 (2007).
9. Gregory, K. J., Sexton, P. M. & Christopoulos, A. Allosteric modulation of muscarinic acetylcholine receptors. *Curr. Neuropharmacol.* **5,** 157–167 (2007).
10. Kameyama, K., Haga, K., Haga, T., Moro, O. & Sadée, W. Activation of a GTP-binding protein and a GTP-binding-protein-coupled receptor kinase (β-adrenergic-receptor kinase-1) by a muscarinic receptor M2 mutant lacking phosphorylation sites. *Eur. J. Biochem. FEBS* **226,** 267–276 (1994).
11. Ichiyama, S. *et al.* The structure of the third intracellular loop of the muscarinic acetylcholine receptor M_2 subtype. *FEBS Lett.* **580,** 23–26 (2006).
12. Rosenbaum, D. M. *et al.* GPCR engineering yields high-resolution structural insights into β_2-adrenergic receptor function. *Science* **318,** 1266–1273 (2007).
13. Jaakola, V. P. *et al.* The 2.6 Ångstrom crystal structure of a human A_{2A} adenosine receptor bound to an antagonist. *Science* **322,** 1211–1217 (2008).
14. Wu, B. *et al.* Structures of the CXCR4 chemokine GPCR with small-molecule and cyclic peptide antagonists. *Science* **330,** 1066–1071 (2010).
15. Chien, E. Y. *et al.* Structure of the human dopamine D3 receptor in complex with a D2/D3 selective antagonist. *Science* **330,** 1091–1095 (2010).
16. Shimamura, T. *et al.* Structure of the human histamine H_1 receptor complex with doxepin. *Nature* **475,** 65–70 (2011).
17. Palczewski, K. *et al.* Crystal structure of rhodopsin: A G protein-coupled receptor. *Science* **289,** 739–745 (2000).
18. Warne, T. *et al.* Structure of a β_1-adrenergic G-protein-coupled receptor. *Nature* **454,** 486–491 (2008).
19. Hulme, E. C., Lu, Z. L. & Bee, M. S. Scanning mutagenesis studies of the M_1 muscarinic acetylcholine receptor. *Receptors Channels* **9,** 215–228 (2003).
20. Heitz, F. *et al.* Site-directed mutagenesis of the putative human muscarinic M_2 receptor binding site. *Eur. J. Pharmacol.* **380,** 183–195 (1999).
21. Wess, J. Mutational analysis of muscarinic acetylcholine receptors: structural basis of ligand/receptor/G protein interactions. *Life Sci.* **53,** 1447–1463 (1993).
22. Goodwin, J. A., Hulme, E. C., Langmead, C. J. & Tehan, B. G. Roof and floor of the muscarinic binding pocket: variations in the binding modes of orthosteric ligands. *Mol. Pharmacol.* **72,** 1484–1496 (2007).
23. Ward, S. D., Curtis, C. A. & Hulme, E. C. Alanine-scanning mutagenesis of transmembrane domain 6 of the M_1 muscarinic acetylcholine receptor suggests that Tyr381 plays key roles in receptor function. *Mol. Pharmacol.* **56,** 1031–1041 (1999).
24. Bluml, K., Mutschler, E. & Wess, J. Functional role in ligand binding and receptor activation of an asparagine residue present in the sixth transmembrane domain of all muscarinic acetylcholine receptors. *J. Biol. Chem.* **269,** 18870–18876 (1994).
25. Rasmussen, S. G. *et al.* Structure of a nanobody-stabilized active state of the β_2 adrenoceptor. *Nature* **469,** 175–180 (2011).
26. Furukawa, H. *et al.* Conformation of ligands bound to the muscarinic acetylcholine receptor. *Mol. Pharmacol.* **62,** 778–787 (2002).
27. Zacharias, N. & Dougherty, D. A. Cation-π interactions in ligand recognition and catalysis. *Trends Pharmacol. Sci.* **23,** 281–287 (2002).
28. Brams, M. *et al.* Crystal structures of a cysteine-modified mutant in loop D of acetylcholine-binding protein. *J. Biol. Chem.* **286,** 4420–4428 (2011).
29. Oswald, C. *et al.* Crystal structures of the choline/acetylcholine substrate-binding protein ChoX from *Sinorhizobium meliloti* in the liganded and unliganded-closed states. *J. Biol. Chem.* **283,** 32848–32859 (2008).
30. Colletier, J. P. *et al.* Structural insights into substrate traffic and inhibition in acetylcholinesterase. *EMBO J.* **25,** 2746–2756 (2006).

Supplementary Information is linked to the online version of the paper at www.nature.com/nature.

Acknowledgements We thank S. Iwata at Kyoto University for supporting the production of M2 receptor, and we acknowledge support from the Japan Society for the Promotion of Science (Research for Future Program) (T.H.), from the Japan Science and Technology Corporation (CREST) (T.H.), from the Ministry of Education, Culture, Sports, Science and Technology of Japan (Grants-in-Aid for Scientific Research on Priority Area 15083201 (T.H.), from the Japan Science and Technology Corporation (ERATO) (T.K.), from Toray Science Foundation (T.K.), from Takeda Science Foundation (T.K.), from Ichiro Kanehara Foundation (T.K.), from The Sumitomo Foundation (T.K.), from the National Institutes of Health Grants NS028471 and GM083118 (B.K.K.), from the Mathers Foundation (B.K.K. and W.I.W.), and from the National Science Foundation (A.C.K.). We thank T. S. Kobilka for organizing the GPCR Workshop 2010 that brought together the research groups, and for facilitating this collaboration

Author Contributions K.H. purified M2 and M2-T4L receptors, characterized their ligand binding activity, and performed attempts to crystallize them with hanging drop and other methods for more than ten years. A.C.K. crystallized the M2-T4L receptors in lipidic cubic phase, collected and processed diffraction data, solved and refined the structure, and assisted with manuscript preparation. H.A. set up the expression system and expressed M2-T4L in large amounts using the insect cell/baculovirus expression system. T.Y.-K. expressed M2 and M2-T4L receptors using a yeast expression system, and purified and crystallized M2 and M2-T4L receptors for five years. M.S. constructed several mutants of M2-T4L, and evaluated their stabilities. C.Z. assisted with data collection and processing. W.I.W. oversaw data processing and refinement. T.O. gave advice to K.H. and T.H. on crystallization of the M2 receptor and interpretation of its structure. B.K.K. oversaw lipidic cubic phase crystallization, assisted with data collection, and wrote the manuscript together with T.H. and T.K. T.H., together with K.H., has engaged in biochemical studies of muscarinic receptors for more than thirty years, prepared M2 and M2-T4L receptors, and wrote part of the manuscript. T.K. has been collaborating with T.H. for five years, designed the receptor production strategy with T.H., and wrote part of the manuscript.

Author Information Coordinates and structure factors for M2-T4L are deposited in the Protein Data Bank under accession code 3UON. Reprints and permissions information is available at www.nature.com/reprints. The authors declare no competing financial interests. Readers are welcome to comment on the online version of this article at www.nature.com/nature. Correspondence and requests for materials should be addressed to B.K.K. (kobilka@stanford.edu), T.H. (tatsuya.haga@gakushuin.ac.jp) or T.K. (t-coba@mfour.med.kyoto-u.ac.jp).

LETTER

doi:10.1038/nature10867

Structure and dynamics of the M3 muscarinic acetylcholine receptor

Andrew C. Kruse[1], Jianxin Hu[2], Albert C. Pan[3], Daniel H. Arlow[3], Daniel M. Rosenbaum[4], Erica Rosemond[2], Hillary F. Green[3], Tong Liu[2], Pil Seok Chae[5], Ron O. Dror[3], David E. Shaw[3], William I. Weis[1,6], Jürgen Wess[2] & Brian K. Kobilka[1]

Acetylcholine, the first neurotransmitter to be identified[1], exerts many of its physiological actions via activation of a family of G-protein-coupled receptors (GPCRs) known as muscarinic acetylcholine receptors (mAChRs). Although the five mAChR subtypes (M1–M5) share a high degree of sequence homology, they show pronounced differences in G-protein coupling preference and the physiological responses they mediate[2–4]. Unfortunately, despite decades of effort, no therapeutic agents endowed with clear mAChR subtype selectivity have been developed to exploit these differences[5,6]. We describe here the structure of the $G_{q/11}$-coupled M3 mAChR ('M3 receptor', from rat) bound to the bronchodilator drug tiotropium and identify the binding mode for this clinically important drug. This structure, together with that of the $G_{i/o}$-coupled M2 receptor[7], offers possibilities for the design of mAChR subtype-selective ligands. Importantly, the M3 receptor structure allows a structural comparison between two members of a mammalian GPCR subfamily displaying different G-protein coupling selectivities. Furthermore, molecular dynamics simulations suggest that tiotropium binds transiently to an allosteric site *en route* to the binding pocket of both receptors. These simulations offer a structural view of an allosteric binding mode for an orthosteric GPCR ligand and provide additional opportunities for the design of ligands with different affinities or binding kinetics for different mAChR subtypes. Our findings not only offer insights into the structure and function of one of the most important GPCR families, but may also facilitate the design of improved therapeutics targeting these critical receptors.

The mAChR family consists of five subtypes, M1–M5, which can be subdivided into two major classes (Fig. 1a). The M1, M3 and M5 receptors show selectivity for G proteins of the $G_{q/11}$ family (that is, G_q and G_{11}), whereas the M2 and M4 receptors preferentially couple to $G_{i/o}$-type G proteins (G_i and G_o)[2–4]. The development of small molecule ligands that can selectively act on specific mAChR subtypes has proven extremely challenging, primarily owing to the high degree of sequence similarity in the transmembrane (TM) core of these receptors[2–4]. More recently, considerable progress has been made in targeting drugs to non-classical (allosteric) binding sites of certain mAChR subtypes[5].

Within the mAChR family, the M3 subtype mediates many important physiological functions, including smooth muscle contraction and glandular secretion[3,4,6,8–10]. Central M3 receptors have also been implicated in the regulation of food intake[8], learning and memory[9], and the proper development of the anterior pituitary gland[10]. Selective drugs targeted at this receptor subtype may prove clinically useful[4,6,8–10], and non-selective muscarinic ligands are already widely used in current practice.

Owing to the profound physiological importance of the M3 receptor and its long-standing role as a model system for understanding GPCR function[3,11], we used the T4 lysozyme (T4L) fusion protein strategy[12] to obtain crystals of *Rattus norvegicus* M3 receptor–T4L fusion protein (Supplementary Fig. 1) by lipidic cubic phase crystallization. Diffraction data from more than 70 crystals were merged to create a data set to 3.4 Å resolution and to solve the structure by molecular replacement. The M3 receptor structure, together with that of the M2 receptor[7], affords an opportunity to compare two closely related mammalian receptors with divergent G-protein coupling selectivities.

The overall structure of the M3 receptor is similar to that of M2 (Fig. 1b–d). Surprisingly, structural conservation includes intracellular loops (ICLs) 1 and 2, and extracellular loops (ECLs) 1–3, which share highly similar overall folds despite low sequence conservation (Fig. 1f). Like the M2 receptor, the M3 receptor exhibits unique mAChR features, including a large extracellular vestibule as part of an extended hydrophilic channel containing the orthosteric binding site (Fig. 1e). Also like M2, the M3 receptor features a pronounced outward bend at the extracellular end of TM4 (Fig. 1d; Supplementary Fig. 2b). This bend, not seen in any other GPCR family crystallized so far, is stabilized by a hydrogen bond from the Q207 (Q163 in M2) side chain to the L204 backbone peptide carbonyl (Supplementary Fig. 2b). This bond is part of a polar interaction network involving four residues absolutely conserved within the mAChR family, suggesting that this unusual feature is important to mAChRs in general. Indeed, mutagenesis of Q207 in M3 impaired both ligand binding and receptor activation[13].

The M3 receptor was crystallized in complex with tiotropium (Spiriva), a potent muscarinic inverse agonist[14,15] used clinically for the treatment of chronic obstructive pulmonary disease (COPD). The M2 receptor was crystallized in complex with *R*-(−)-3-quinuclidinyl benzilate (QNB) which, like tiotropium, is a non-subtype-selective mAChR blocker[14,16]. The two ligands bind in remarkably similar poses (Fig. 2b), and it is likely that this pose represents a conserved binding mode for structurally similar anticholinergics. In the M3 receptor, as in M2, the ligand is deeply buried within the TM receptor core (Fig. 2a, d) and is covered by a lid comprising three conserved tyrosines—Y148$^{3.33}$, Y506$^{6.51}$ and Y529$^{7.39}$ (Fig. 2a; superscripts indicate Ballesteros-Weinstein numbers[17]). The ligand is almost completely occluded from solvent and engages in extensive hydrophobic contacts with the receptor. A pair of hydrogen bonds are formed from N507$^{6.52}$ to the ligand carbonyl and hydroxyl, while D147$^{3.32}$ interacts with the ligand amine.

Reflecting the difficulty in developing subtype-selective orthosteric ligands, the residues forming the orthosteric binding pocket are absolutely conserved among the five mAChR subtypes (Fig. 1f). However, this conservation at the amino acid level does not preclude the existence of differences in the three-dimensional architecture of the orthosteric site between the different mAChR subtypes. In fact, comparison of the structures of the M3 and M2 receptor ligand binding sites reveals structural divergences that might be exploited in the development of subtype-selective ligands.

[1]Department of Molecular and Cellular Physiology, Stanford University School of Medicine, 279 Campus Drive, Stanford, California 94305, USA. [2]Molecular Signaling Section, Laboratory of Bioorganic Chemistry, National Institute of Diabetes and Digestive and Kidney Diseases, Bethesda, Maryland 20892, USA. [3]D. E. Shaw Research, New York, New York 10036, USA. [4]Department of Biochemistry, University of Texas Southwestern Medical Center, Dallas, Texas 75390, USA. [5]Department of Bionano Engineering, Hanyang University, Ansan 426-791, Korea. [6]Department of Structural Biology, Stanford University School of Medicine, 299 Campus Drive, Stanford, California 94305, USA.

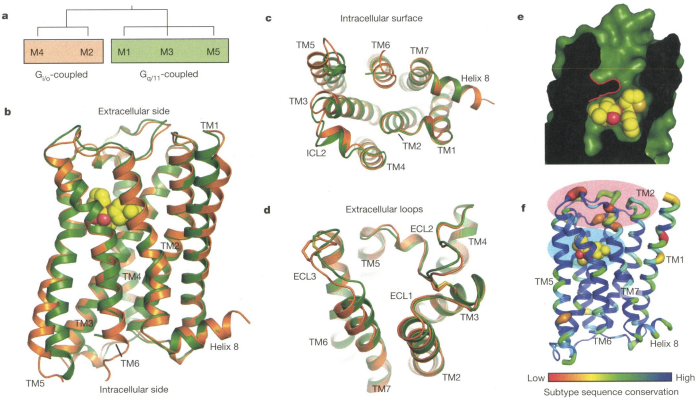

Figure 1 | Major structural features of the M3 receptor. a, Analysis of muscarinic receptor sequences divides them into two classes. **b**, The overall structure of the M3 receptor (green) is similar to that of the M2 receptor (orange). The M3-bound ligand, tiotropium, is shown as spheres coloured according to element, with carbon in yellow and oxygen in red. **c**, Comparison of the intracellular surfaces shows divergence in the cytoplasmic end of TM5. **d**, Comparison of the extracellular surfaces shows less deviation, with near perfect conservation of backbone fold of extracellular loops (ECLs). **e**, A solvent accessible surface for the M3 receptor bound to tiotropium (spheres) shows the receptor covering the ligand with a tyrosine lid (outlined in red). The surface of the receptor is shown in green and its interior in black. **f**, M3 receptor structure coloured by sequence conservation among the five mAChR subtypes. Poorly conserved regions are shown with larger backbone diameter. The orthosteric and allosteric sites are indicated in blue and red elliptical shaded areas, respectively, and the ligand tiotropium is shown as spheres.

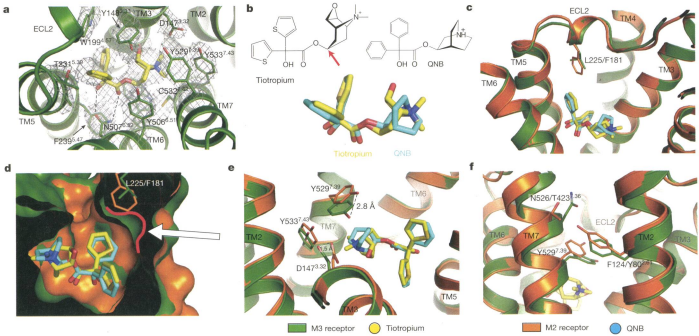

Figure 2 | Orthosteric binding sites of the M2 and M3 receptors. In all panels, the M3 receptor is shown green with its ligand tiotropium in yellow, while the M2 receptor and its ligand QNB are shown in orange and cyan, respectively. **a**, Tiotropium binding site in the M3 receptor. A $2F_o - F_c$ map contoured at 2σ is shown as mesh. **b**, Chemical structures of ligands. A red arrow indicates the tropane C3 atom used as a tracking landmark in Fig. 3. Superimposing the receptor structures reveals that the two ligands adopt highly similar poses (bottom). **c**, There is a Phe (M2)/Leu (M3) sequence difference between the M2 and M3 receptors near the binding site. **d**, This produces an enlarged binding pocket in the M3 receptor, outlined in red and indicated with an arrow. **e**, Displacements of M3 $Y529^{7.39}$ and $D147^{3.32}$ are seen (black dashed lines). **f**, The displacement of $Y529^{7.39}$ may arise from a sequence difference at position 2.61 (Tyr 80 in M2 and Phe 124 in M3).

One such difference derives from the replacement of Phe 181 in ECL2 of M2 with Leu 225 in M3 (this residue is leucine in all mAChRs except M2). This creates a pocket in M3 not found in M2 (Fig. 2c, d). A second difference is a 2.8 Å shift of $Tyr529^{7.39}$ relative to the position of the corresponding M2 residue (Tyr 426; Fig. 2e). This feature may derive from a difference in the identity of the residue in position 2.61 (Phe 124 in M3 and Tyr 80 in M2; Fig. 2f). This residue interacts directly with TM7, influencing the position of this helix and the residues within it, including $Tyr529^{7.39}$. Notably, the residue at position 2.61 is not a part of the orthosteric binding pocket, but is positioned near a probable allosteric binding site[7]. Because tiotropium and QNB are structurally similar but not identical, the observed binding site differences must be interpreted with some degree of caution. However, site-directed mutagenesis studies with M1 and M3 receptors support the concept that the residue at position 2.61 plays a role in receptor activation[18,19] and ligand binding selectivity[20]. This site does not appear to play a role in determining antagonist dissociation rates, because mutation of M3 $F^{2.61}$ to tyrosine or of M2 $Y^{2.61}$ to phenylalanine had no effect on dissociation rates for [^{3}H]N-methyl scopolamine ([^{3}H]NMS) or [^{3}H]QNB.

We used molecular dynamics simulations to characterize the pathway by which tiotropium binds to and dissociates from the M2 and M3 receptors. Similar techniques have previously been shown to correctly predict crystallographic ligand binding poses and kinetics in studies of β-adrenergic receptors[21]. In both the M2 and M3 receptors, our simulations indicate that as tiotropium binds to or dissociates from the receptor, it pauses at an alternative binding site in the extracellular vestibule (Fig. 3, Supplementary Fig. 3). Intriguingly, this site corresponds to an allosteric site that has been previously identified by mutagenesis[7], a finding consistent with pharmacological studies showing that orthosteric ligands can act as allosteric modulators at the M2 receptor[22]. Tiotropium adopts different preferred allosteric binding poses in M2 and M3 (Fig. 3d, Supplementary Fig. 4). These metastable binding poses, which appear independently in both binding and dissociation simulations, may represent the first structural view of a clinically used 'orthosteric' GPCR ligand binding to an experimentally validated allosteric site. Conceivably, therapeutic molecules could be rationally engineered to act independently as both allosteric and orthosteric ligands (in contrast to previously described bitopic ligands that bind at both orthosteric and allosteric sites simultaneously[23]).

Tiotropium dissociates from M3 receptors more slowly than from M2 receptors, a phenomenon thought to provide clinically important 'kinetic selectivity' of this drug for M3 receptors despite similar equilibrium binding affinities for both subtypes[14]. In simulations with tiotropium bound, the portion of ECL2 nearest the binding pocket proved more mobile in M2 than in M3 (Supplementary Fig. 5), probably

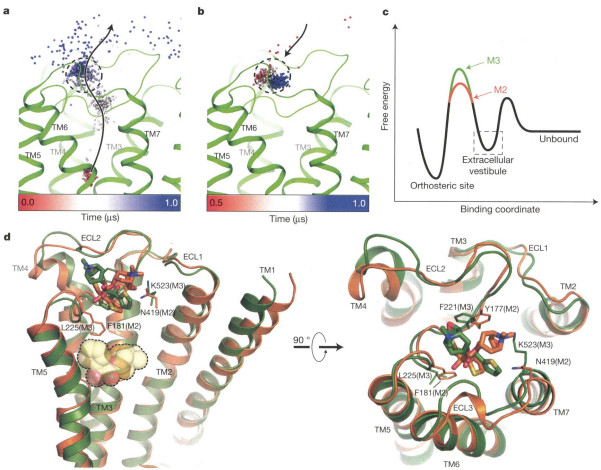

Figure 3 | Molecular dynamics of ligand binding. Simulations suggest that the tiotropium binding/dissociation pathway for both receptors involves a metastable state in the extracellular vestibule. **a**, When tiotropium is pushed out of the binding pocket of M3, it pauses in the extracellular vestibule in the region outlined with a dashed circle. Spheres represent positions of the ligand's C3 tropane atom at successive points in time. The direction of motion is indicated by an arrow. **b**, When tiotropium is placed in solvent, it binds to the same site in the extracellular vestibule. Our simulations are insufficiently long for it to proceed into the orthosteric binding pocket; the agonist acetylcholine (ACh), a much smaller molecule, bound spontaneously to the orthosteric site in similar simulations (Supplementary Methods). **c**, Schematic free-energy landscape for binding/dissociation. Differences between M2 and M3 are shown in orange and green, respectively, with the rest of the curve in black. **d**, Common binding poses for tiotropium in the extracellular vestibule of M2 (orange) and of M3 (green). Non-conserved residues that contact the ligand are shown as thin sticks. The location of the orthosteric site is indicated by tiotropium (as spheres).

owing to multiple sequence differences between the two receptor subtypes. This increased mobility disrupts a hydrophobic cluster involving a thiophene ring of tiotropium, the ECL2 residue Phe181(M2)/Leu225(M3), and $Tyr^{3.33}$, facilitating movement of Phe181/Leu225 away from the orthosteric site and rotation of $Tyr^{3.33}$ towards TM4. In simulations of ligand dissociation, such motions clear a path for tiotropium's egress from the orthosteric site to the extracellular vestibule. The increased mobility of ECL2 in M2 thus appears to facilitate tiotropium's traversal of the largest energetic barrier on the binding/dissociation pathway (Fig. 3c). Experimental measurements with wild-type and mutant receptors (M3 L225F and M2 F181L) suggest that the Leu225/Phe181 sequence difference alone is insufficient to explain the difference in off-rates (for practical reasons these measurements were performed with QNB rather than tiotropium; see Methods).

One of the most interesting features of the M2 and M3 receptors is the fact that the two highly similar receptors display pronounced differences in G-protein coupling specificity. For this reason, the M2/M3 receptor pair has long served as an excellent model system to identify features contributing to the selectivity of coupling between GPCRs and G proteins[3]. As no simple sequence elements have been identified as general determinants of coupling specificity across GPCR families[24], it is likely that recognition depends on features such as overall conformation in addition to specific inter-residue contacts.

The M2 and M3 receptor structures show a significant difference in the position of the cytoplasmic end of TM5 and of ICL2 (Fig. 4a, b). The highly conserved tyrosine residue at position 5.58 (M3 $Tyr250^{5.58}$, M2 $Tyr206^{5.58}$) shows a clear deviation between the two receptors, pointing towards the core of the protein in M2, and away from the receptor towards the surrounding lipid bilayer in M3. Interestingly, mutagenesis studies have identified a tetrad of residues ('AALS' in M3, 'VTIL' in M2) located on the cytoplasmic end of TM6 that are critical in determining G-protein coupling selectivity[25,26]. In both structures, these residues interact directly with TM5 (Fig. 4a), and in the β_2 adrenergic receptor–G_s complex[27] two of the four corresponding residues make contact with the carboxy-terminal helix of $G\alpha_s$. M3 $Tyr254^{5.62}$ at the bottom of TM5 also plays a role in activation of $G_{q/11}$ (ref. 28). In the M2 receptor structure, the corresponding residue ($Ser210^{5.62}$) is displaced by approximately 4 Å relative to $Tyr254^{5.62}$ in M3 (Fig. 4a).

When we compared the position of TM5 in the M2 and M3 receptors to that in other GPCR structures, we found that it is M2-like in all $G_{i/o}$-coupled receptors, whereas the two mammalian $G_{q/11}$-coupled receptors solved to date exhibit another conformation (Fig. 4c, d). An important caveat here is that these structures have been solved using the T4L fusion strategy, and we cannot completely exclude the possibility that this approach perturbs the conformation of TM5 and TM6. However, in

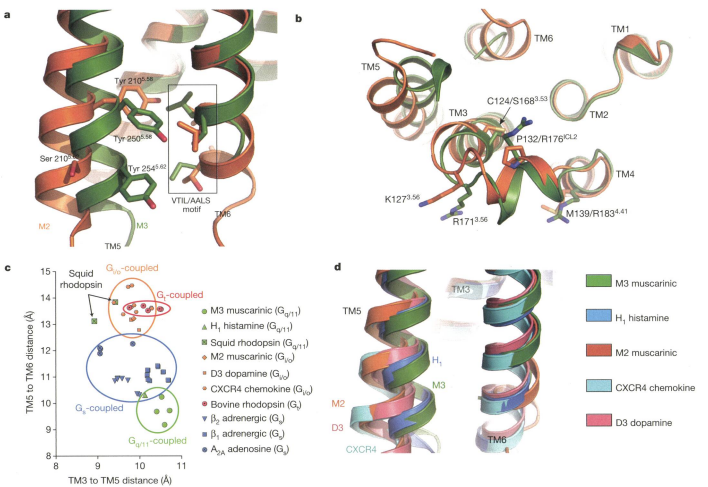

Figure 4 | G-protein coupling specificity determinants. a, The M3 receptor shows displacement of TM5 relative to its position in M2, and a conserved tyrosine (M3 Tyr $250^{5.58}$) adopts different positions in the two receptors. Four TM6 residues near TM5 (AALS in M3, VTIL in M2; boxed) have been shown to be important coupling specificity determinants. **b**, ICL2 is also divergent between the two structures. Four residues previously implicated as specificity determinants[25] are shown, with residue numbers for M2 followed by M3. **c**, Plot of interhelical distances for crystallographically unique inactive GPCR structures published to date. Distances were measured between C_α atoms of TM5 residue 5.62 and TM3 residue 3.54 (*x*-axis), and TM5 residue 5.62 and TM6 residue 6.37 (*y*-axis). GPCRs cluster by coupling specificity, although squid rhodopsin is an exception. GPCRs coupling preferentially to $G_{i/o}$ and those coupling to the homologous G protein G_t cluster together. **d**, Structural alignment of mammalian $G_{i/o}$-coupled and $G_{q/11}$-coupled receptor structures.

molecular dynamics simulations of M2 and M3 receptors without T4L, each of the receptors adopts a set of conformations that includes its own crystallographically observed conformation (Supplementary Fig. 6, 7). These simulations suggest that the observed conformations are unlikely to be artefacts of the crystallization methodology, though the crystal structures probably represent only one conformation among many adopted by the receptors in a biological context.

The structure of the M3 receptor, together with that of the M2 receptor[7], offers a unique opportunity to directly compare the structural properties of two members of a mammalian GPCR subfamily endowed with different G-protein coupling selectivities. Examination of the M3 structure has provided structural evidence of differences between ligand binding sites of mAChR subtypes that could be exploited for the design of more selective therapeutics. Moreover, computational studies have identified a pathway by which the COPD drug tiotropium may bind to and dissociate from the M3 receptor, offering a structural view of an orthosteric GPCR ligand binding to an experimentally validated allosteric site. This information should facilitate the rational design of new muscarinic drugs exhibiting increased receptor subtype selectivity, potentially improving treatment for a wide variety of important clinical disorders.

METHODS SUMMARY

The M3 muscarinic receptor–T4 lysozyme fusion protein was expressed in Sf9 insect cells and purified by nickel affinity chromatography followed by Flag antibody affinity chromatography and then size exclusion chromatography. It was crystallized using the lipidic cubic phase technique, and diffraction data were collected at the GM/CA-CAT beamline at the Advanced Photon Source at Argonne National Laboratory. The structure was solved by molecular replacement using merged data from 76 crystals. All-atom classical molecular dynamics (MD) simulations with explicitly represented lipids and water were performed using the CHARMM force field[29] on Anton[30]. Ligand-binding simulations included no artificial forces. Dissociation studies included a time-varying biasing term that gradually forces the ligand away from its crystallographic position, but not along any prespecified pathway or direction. Full details are provided in Methods.

Full Methods and any associated references are available in the online version of the paper at www.nature.com/nature.

Received 23 October 2011; accepted 18 January 2012.

1. Loewi, O. Über humorale übertragbarkeit der Herznervenwirkung. *Pflugers Arch.* **189,** 239–242 (1921).
2. Hulme, E. C., Birdsall, N. J. M. & Buckley, N. J. Muscarinic receptor subtypes. *Annu. Rev. Pharmacol. Toxicol.* **30,** 633–673 (1990).
3. Wess, J. Molecular biology of muscarinic acetylcholine receptors. *Crit. Rev. Neurobiol.* **10,** 69–99 (1996).
4. Caulfield, M. P. & Birdsall, N. J. M. International Union of Pharmacology. XVII. Classification of muscarinic acetylcholine receptors. *Pharmacol. Rev.* **50,** 279–290 (1998).
5. Conn, P. J., Jones, C. K. & Lindsley, C. W. Subtype-selective allosteric modulators of muscarinic receptors for the treatment of CNS disorders. *Trends Pharmacol. Sci.* **30,** 148–155 (2009).
6. Wess, J., Eglen, R. M. & Gautam, D. Muscarinic acetylcholine receptors: mutant mice provide new insights for drug development. *Nature Rev. Drug Discov.* **6,** 721–733 (2007).
7. Haga, K. *et al.* Structure of the human M2 muscarinic acetylcholine receptor bound to an antagonist. *Nature* http://dx.doi.org/10.1038/nature10753 (this issue); published online 25 January 2012.
8. Yamada, M. *et al.* Mice lacking the M3 muscarinic acetylcholine receptor are hypophagic and lean. *Nature* **410,** 207–212 (2001).
9. Poulin, B. *et al.* The M_3-muscarinic receptor regulates learning and memory in a receptor phosphorylation/arrestin-dependent manner. *Proc. Natl Acad. Sci. USA* **107,** 9440–9445 (2010).
10. Gautam, D. *et al.* Neuronal M_3 muscarinic acetylcholine receptors are essential for somatotroph proliferation and normal somatic growth. *Proc. Natl Acad. Sci. USA* **106,** 6398–6403 (2009).
11. Wess, J., Han, S.-J., Kim, S.-K., Jacobson, K. A. & Li, J. H. Conformational changes involved in G-protein-coupled-receptor activation. *Trends Pharmacol. Sci.* **29,** 616–625 (2008).
12. Rosenbaum, D. M. *et al.* GPCR engineering yields high-resolution structural insights into β_2-adrenergic receptor function. *Science* **318,** 1266–1273 (2007).
13. Scarselli, M., Li, B., Kim, S.-K. & Wess, J. Multiple residues in the second extracellular loop are critical for M_3 muscarinic acetylcholine receptor activation. *J. Biol. Chem.* **282,** 7385–7396 (2007).
14. Barnes, P. J. The pharmacological properties of tiotropium. *Chest* **117,** 63S–66S (2000).
15. Casarosa, P., Kiechle, T., Sieger, P., Pieper, M. & Gantner, F. The constitutive activity of the human muscarinic M_3 receptor unmasks differences in the pharmacology of anticholinergics. *J. Pharmacol. Exp. Ther.* **333,** 201–209 (2010).
16. Bolden, C., Cusack, B. & Richelson, E. Antagonism by antimuscarinic and neuroleptic compounds at the five cloned human muscarinic cholinergic receptors expressed in Chinese hamster ovary cells. *J. Pharmacol. Exp. Ther.* **260,** 576–580 (1992).
17. Ballesteros, J. A. & Weinstein, H. Integrated methods for the construction of three-dimensional models and computational probing of structure-function relations in G protein coupled receptors. *Methods Neurosci.* **25,** 366–428 (1995).
18. Li, B. *et al.* Rapid identification of functionally critical amino acids in a G protein-coupled receptor. *Nature Methods* **4,** 169–174 (2007).
19. Lebon, G., Langmead, C. J., Tehan, B. G. & Hulme, E. C. Mutagenic mapping suggests a novel binding mode for selective agonists of M_1 muscarinic acetylcholine receptors. *Mol. Pharmacol.* **75,** 331–341 (2009).
20. Drübbisch, V., Lameh, J., Philip, M., Sharma, Y. K. & Sadee, W. Mapping the ligand binding pocket of the human muscarinic cholinergic receptor Hm1: contribution of tyrosine-82. *Pharm. Res.* **9,** 1644–1647 (1992).
21. Dror, R. O. *et al.* Pathway and mechanism of drug binding to G-protein-coupled receptors. *Proc. Natl Acad. Sci. USA* **108,** 13118–13123 (2011).
22. Redka, D. S., Pisterzi, L. F. & Wells, J. W. Binding of orthosteric ligands to the allosteric site of the M_2 muscarinic cholinergic receptor. *Mol. Pharmacol.* **74,** 834–843 (2008).
23. Valant, C. *et al.* A novel mechanism of G protein-coupled receptor functional selectivity. *J. Biol. Chem.* **283,** 29312–29321 (2008).
24. Wong, S. K. F. G protein selectivity is regulated by multiple intracellular regions of GPCRs. *Neurosignals* **12,** 1–12 (2003).
25. Blin, N., Yun, J. & Wess, J. Mapping of single amino acid residues required for selective activation of G_q by the M_3 muscarinic acetylcholine receptor. *J. Biol. Chem.* **270,** 17741–17748 (1995).
26. Liu, J., Conklin, B. R., Blin, N., Yun, J. & Wess, J. Identification of a receptor/G-protein contact site critical for signaling specificity and G-protein activation. *Proc. Natl Acad. Sci. USA* **92,** 11642–11646 (1995).
27. Rasmussen, S. G. F. *et al.* Crystal structure of the β_2 adrenergic receptor-Gs protein complex. *Nature* **477,** 549–555 (2011).
28. Blüml, K., Mutschler, E. & Wess, J. Functional role of a cytoplasmic aromatic amino acid in muscarinic receptor-mediated activation of phospholipase C. *J. Biol. Chem.* **269,** 11537–11541 (1994).
29. MacKerell, A. D. *et al.* All-atom empirical potential for molecular modeling and dynamics studies of proteins. *J. Phys. Chem. B* **102,** 3586–3616 (1998).
30. Shaw, D. E. *et al.* Millisecond-scale molecular dynamics simulations on Anton. In *Proceedings of the Conference on High Performance Computing, Networking, Storage and Analysis* (ACM Press, 2009); available at http://dl.acm.org/citation.cfm?doid=1654059.1654099 (2009).

Supplementary Information is linked to the online version of the paper at www.nature.com/nature.

Acknowledgements We acknowledge support from National Institutes of Health grants NS028471 (B.K.K.) and GM56169 (W.I.W.), from the Mathers Foundation (B.K.K. and W.I.W.), and from the National Science Foundation (A.C.K.). This work was supported in part by the Intramural Research Program, NIDDK, NIH, US Department of Health and Human Services. We thank R. Grisshammer and S. Costanzi for advice and discussions during various stages of the project, Y. Zhou for carrying out radioligand binding assays with several M3 receptor–T4 fusion constructs, D. Scarpazza for developing software that enabled forced dissociation simulations, and A. Taube, K. Palmo and D. Borhani for advice related to simulations.

Author Contributions A.C.K cloned, expressed, and purified several M3 receptor crystallization constructs; developed the purification procedure; performed crystallization trials, collected diffraction data, solved and refined the structure. J.H. prepared, expressed and characterized various M3 receptor constructs in ligand binding and functional assays. A.C.P. and D.H.A. designed, performed and analysed MD simulations and assisted with manuscript preparation. D.M.R. assisted in design and characterization of initial M3–T4L fusion constructs. E.R. prepared, expressed and tested the pharmacology and stability of several M3 receptor–T4 fusion constructs in insect cells. H.F.G. analysed MD simulations and crystallographic data and assisted with manuscript preparation. T.L. performed binding assays and functional experiments together with J.H. P.S.C. developed and prepared neopentyl glycol detergents used for purifying the M3 receptor. R.O.D. oversaw, designed and analysed MD simulations. D.E.S. oversaw MD simulations and analysis. W.I.W. oversaw refinement of the M3 receptor structure, and assisted in analysis of diffraction data. J.W. provided advice regarding construct design, protein expression and project strategy; and oversaw initial insect cell expression and pharmacological and functional characterization of M3 receptor constructs. B.K.K. was responsible for overall project strategy; guided design of crystallization constructs; and assisted with crystal harvesting and data collection. A.C.K., R.O.D., J.W. and B.K.K. wrote the manuscript.

Author Information Coordinates and structure factors for M3–T4L are deposited in the Protein Data Bank (accession code 4DAJ). Reprints and permissions information is available at www.nature.com/reprints. The authors declare no competing financial interests. Readers are welcome to comment on the online version of this article at www.nature.com/nature. Correspondence and requests for materials should be addressed to B.K.K. (kobilka@stanford.edu) or J.W. (jwess@helix.nih.gov).

Product Focus: Chromatography

Keep 'Em Separated

Advances in Chromatography

In December of 2011, Pfizer reported that its top selling prescription drug of all time, Lipitor®, would lose its patent. A record number of blockbuster drugs will also see their patents expire this year, opening the door for new generics—discounted at 90 percent to list—for market entry this June. Biosimilar production is also expected to increase due to the imminent arrival of a US approval pathway. While pharmaceutical companies have been scrambling to adjust to this changing landscape, manufacturers are anticipating a surge in demand for their services.

In preparation, these manufacturers are seeking new ways to generate higher productivity at lower cost. Higher titer feeds resulting from improvements in upstream processing have allowed process engineers to produce larger volumes of biomolecules. Now the bottleneck is in the separation and purification phases. Read on to learn more about the latest innovative chromatography systems and tools that aim to reduce these inefficiencies.

Improving Downstream Process Efficiencies

Bio-Rad Laboratories, Inc. launched its Nuvia™ Q ultra–high capacity anion exchange media specifically designed to deliver the robustness, productivity, and selectivity demanded by today's downstream processes. Nuvia Q targets the purification of monoclonal antibodies, recombinant proteins, and vaccines. Developed to meet the demanding pressure-flow requirements of commercial scale bioprocesses, Nuvia Q exhibits a dynamic binding capacity of greater than 170 mg/mL at a flow rate of 300 cm/hr, approximately tripling the binding capacity of first generation Sepharose Fast Flow media. Furthermore, Nuvia Q demonstrates strong selectivity for common feed stream contaminants. By maintaining high binding capacity and selectivity even at fast flow rates, Nuvia Q can significantly improve productivity, while reducing cycle time for downstream biotherapeutics purification. Moreover, the high binding capacity reduces media use, capital costs, and space requirements.

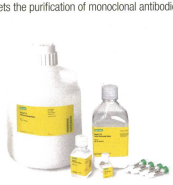

Bio-Rad Laboratories' Nuvia Q ultra–high capacity anion exchange media is specifically designed to deliver the robustness, productivity, and selectivity demanded by today's downstream processes

"With downstream processing representing a significant amount of all manufacturing costs, the introduction of Nuvia Q addresses the need for robust, high-capacity process chromatography media that can consistently purify large volumes of drugs used in therapeutics," said Randy Jacinto, senior product manager in Bio-Rad's Process Chromatography Division.

DSM's RHOBUST® Technology is a downstream process technology for direct capture of product of interest from different sources such as cell culture, microbial fermentation, and plant or animal materials. It replaces multiple process steps such as centrifugation, depth-filtration, and packed bed chromatography with one unit operation. Operating in the expanded bed mode, RHOBUST® allows crude cell-containing harvest to be directly loaded onto the column.

RHOBUST® Technology utilizes a new generation of agarose beads that are prepared with tungsten carbide and consequently have a high density (3 g/mL). This allows processing to occur at higher flow rates compared to packed bed chromatography. Labor-intensive procedures such as column packing and qualification under high-pressure conditions are no longer necessary.

In the **Rhobust® Flex System**, processes are scalable from 1-2 cm diameter columns to 60 cm columns and beyond. Use of the RHOBUST® system can result in less preparation and process time, lower cost of goods, and reduced investment costs.

The **PLC 2020 Personal Purification System** from **Gilson** was developed for quick, easy purification and is ideally suited for low throughput, high- and low-pressure purification to support individual chemists or groups. The PLC 2020 is a personal liquid chromatography system for reverse and normal-phase HPLC with FLASH purification capabilities. Its easy-to-use, self-contained design is intended to meet purification needs on a more personal level.

The PLC 2020 is a compact and independent purification platform capable of performing manual injection purification runs from 1mL/min to 100mL/min with pressures up to 4,060psi. The system can hold up to four 1L solvent reservoirs and select between four different elution solvents. Its integrated variable, dual wavelength UV/VIS detection and fraction collection capabilities are controlled by touch-screen for compact

Material compiled by the Chempetitive Group

chempetitive group®
www.chempetitive.com

Product Focus: Chromatography

The PLC 2020 Personal Purification System from Gilson was developed for quick, easy purification

DSM's RHOBUST® Technology replaces multiple process steps with one unit operation

and convenient operation. This 'HPLC in a box' offers the diversity that chemists need with fully functioning facilities and an intuitive software interface.

Bonna-Agela Technologies has developed a new, fully automated multi-dimensional preparative LC system, the **Flexa MD**. This liquid chromatography system was designed to isolate single organic compounds from complex natural products and single bio-molecules from complex bio-samples. Due to the complexity of natural products and biological samples, it is extremely difficult to obtain pure single molecules in a single chromatographic run. Instead, chromatographers have to run multiple separations, which rely on lengthy and difficult manual operations. Solvent incompatibility between normal phases and reverse phases add even more complexities. The Flexa MD, however, allows chromatographers to switch automatically from one column to another, without evaporating solvents. It also offers multi-stationary phases for a complete chromatography solution.

New Tools and Accessories

Many scientists are considering moving their current HPLC methods to new column geometries and particle sizes to improve speed, resolution and/or sensitivity. **Thermo Fisher Scientific Inc.** now offers the **HPLC Method Development Calculator** to help optimize methods with those column technologies. Their range of online tools is hosted on the Thermo Scientific Chromatography Resource Center and helps calculate initial conditions for gradient and isocratic methods. In addition, there's a tool to help choose the appropriate column for any application.

The HPLC Method Development Calculator provides users with quick and easy access to the technical expertise of chromatographers at Thermo Fisher Scientific to significantly reduce the time spent in experimentally defining optimal analysis conditions.

J.G. Finneran Associates, Inc's redesigned chromatography vials uniquely combine glass and plastic to make laboratory tasks easier and safer. **The Vista Vial™ Series'** patented two-part design takes glass vials and pairs them up with pre-crimped plastic vial toppers. The wide opening of the vial body allows for direct pipetting and is ideal for viscous fluids such as detergents and oils. When filled, the pre-crimped vial topper is easily snapped into place, making the sample prep easier, faster, and more precise. Pre-crimping the vial toppers not only saves time, it eliminates the need for expensive crimping tools in the lab. It also means there is no need for a decapper. Because users can remove the vial topper from the glass base, they avoid the usual risks caused by decapping aluminum seals, such as broken vial necks and cuts from sharp aluminum. Clear and amber Vista Vials are available in a variety of combinations, including crimp and screw-thread vial toppers. They can be purchased separately or in kits.

To better visualize separated chemicals after thin layer chromatography (TLC), **UVP, LLC** designed the **ChromaDoc-it™ Imaging System**. Connect it to your computer for acquisition and documentation of TLC images using the DigiCam 120 digital color camera with 15.1 megapixel resolution. Its functions, including live preview and image enhancement, are controlled by UVP's exclusive capture software. The lightweight cabinet features a built-in overhead shortwave and longwave UV light positioned on two sides of the cabinet for uniform UV illumination in fluorescence studies.

Companies mentioned in this Product Focus

Bio-Rad Laboratories, Inc.	www.bio-rad.com/nuvia
DSM Biologics	www.dsmbiologics.com
Gilson UK	www.gilsonuk.com
Bonna-Agela Technologies	www.agela.com
Thermo Fisher Scientific, Inc.	www.thermoscientific.com/crc
J.G. Finneran Associates, Inc.	www.jgfinneran.com
UVP, LLC	www.uvp.com

"This article was compiled by Chemputitive Group and submitted to Nature. It has not been written by or reviewed by the Nature editorial team and Nature takes no responsibility for the accuracy or otherwise of the information provided. Submit press releases for consideration to productfocus@nature.com with the topic in the subject line."

nature REVIEWS GENETICS

ARKITEK STUDIOS

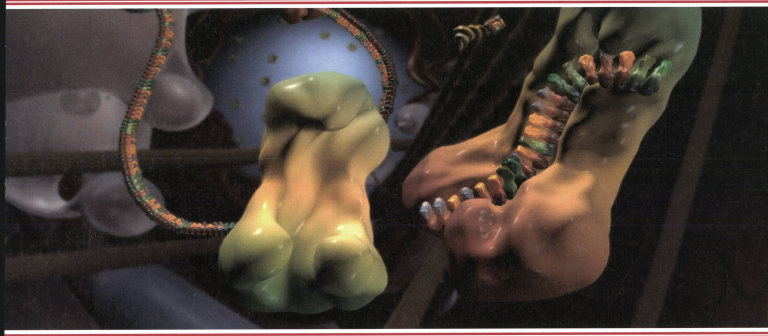

Animation on RNA interference

RNA interference (RNAi) has enormous scientific implications, from shaping our understanding of how gene expression is regulated to providing new tools for basic and clinical research. Now you can learn about the principles RNAi through an up-to-date animation that introduces you to gene regulation by small interfering RNAs (siRNAs) and microRNAs (miRNAs).

Nature Reviews Genetics, in association with Arkitek Studios, has brought RNAi to life in this vivid, audio-visual journey into the cell.

See RNAi in action by viewing the animation for FREE at:
www.nature.com/nrg/multimedia/rnai

Also, download a **FREE** poster on tools for studying and using small RNAs at:
www.nature.com/nrg/posters/small-rna

The Animation and Poster are freely available thanks to support from:

Thermo SCIENTIFIC
Part of Thermo Fisher Scientific

nature publishing group npg

nature REVIEWS CANCER

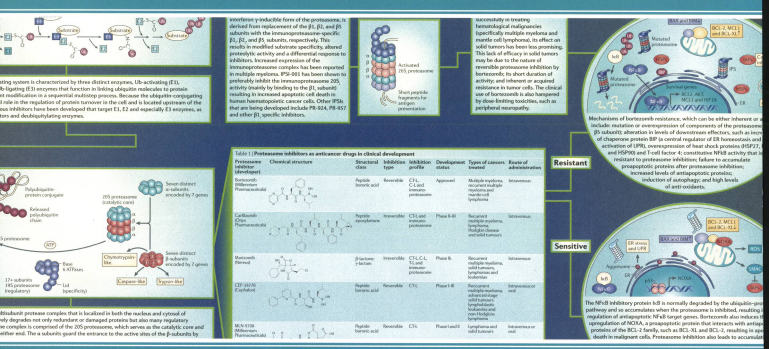

Poster – Proteasome inhibition and cancer therapy

Author: Q. Ping Dou

In recent years the ubiquitin-proteasome system has been identified as essential for maintaining a crucial balance between cell growth and death, the progression of human malignancies, and the development of drug resistance in cancer cells. Emerging evidence shows that targeting the ubiquitin-proteasome degradation pathway is a useful anticancer strategy. The approval of bortezomib by the US Food and Drug Administration (FDA) as the first proteasome inhibitor to be implemented in the treatment of malignant disease, either alone or in combination with other therapies, represents a substantial milestone in this field. Other novel proteasome inhibitors, such as marizomib and carfilzomib, have recently been developed and are being tested in clinical trials. These recent achievements and the development of new drugs that target the ubiquitin–proteasome pathway are highlighted in this poster.

Access the poster **FREE** online!
www.nature.com/nrc/posters/proteasome

This Poster is freely available thanks to sponsorship from

ONYX PHARMACEUTICALS

nature publishing group npg

CAREERS

TURNING POINT After finding virtual particles, a physicist turns to proteomics **p.559**

CAREERS BLOG The latest discussions and news on research jobs **go.nature.com/z8g4a7**

NATUREJOBS For the latest career listings and advice **www.naturejobs.com**

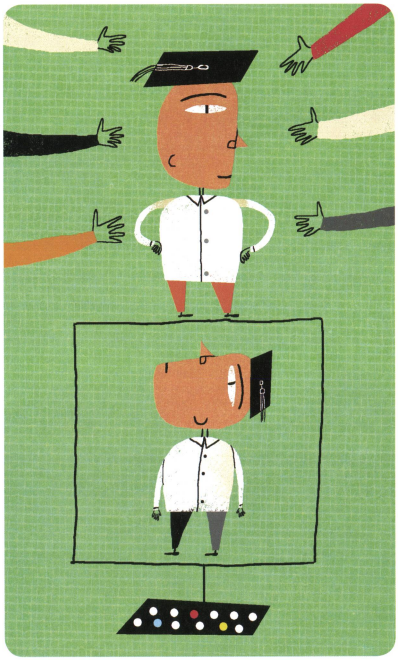

IMAGE:JOAN/CORBIS

EDUCATION

Outside the box

An industrial doctorate could help European students to break out of academia, but applied science is not for everyone.

BY QUIRIN SCHIERMEIER

Christian Hove Rasmussen isn't worried about getting a job. He is a PhD student at the Technical University of Denmark in Lyngby, but he is also an employee of Novo Nordisk, a pharmaceutical company based in Bagsværd, where he is doing doctoral research on the biological mechanisms that govern the absorption of diabetes therapies, such as insulin, in the fat layer beneath the skin. His fixed-term contract expires in 2013, but Rasmussen is optimistic that his work experience will help him to secure a permanent position in industry.

"I'm doing quite basic science, but it is target-oriented and I have to think about how it can be translated into medicine," he says. "I think I can achieve a lot here." Rasmussen's research — like that of around 60 other PhD candidates at Novo Nordisk — is funded by the Danish Industrial PhD Programme, a scheme set up by the Danish Agency for Science, Technology and Innovation (DASTI) in the 1970s. Last year, DASTI approved 116 industrial PhD projects, each funded by up to 882,000 Danish kroner (US$156,000). The host company gets a wage subsidy of 14,500 kroner per month for three years, and the university gets up to 360,000 kroner to last for the duration of the project.

Industrial PhD programmes are starting across Europe. Some are structured, and include university coursework components. Others are more informal. In all cases, the commercial and industrial aspects of the research are overseen by company experts who take part in PhD supervision. If all goes well, the benefits are mutual: doctoral students develop an in-depth understanding of business, which facilitates employment; and their skills and discoveries help the company. But students must be willing to engage in applied research that conforms to industry needs.

INDUSTRIAL EDUCATION

Students have long interacted with industry outside 'institutionalized' PhD schemes, says Lidia Borrell-Damian, head of research and innovation at the European University Association in Brussels. "It is not uncommon that during some point of a PhD a company is involved, in particular in science, technology, engineering and economics." Although explicit co-mentoring and co-funding have been available in the United States for about 60 years, they are only now becoming widespread and accepted in Europe.

In the United Kingdom, for example, ▶

▶ the Engineering and Physical Sciences Research Council (EPSRC) runs 26 industrial doctorate centres, each of which recruits a dozen or so students from different backgrounds each year. In addition, the EPSRC's industrial CASE programme provides support for individual PhD projects arranged between a company and an academic partner.

In France, around 10,000 science and engineering graduates have completed a PhD under the Industrial Arrangements for Training Through Research (CIFRE) scheme, funded by the National Association for Technical Research since 1981. The scheme is aimed mainly at students from the École Polytechnique near Paris, and companies post approved proposals on the university's website. Interested students can contact industrial partners to negotiate details and plan their dissertations.

"I'm doing quite basic science, but it is target-oriented. I think I can achieve a lot here."
Christian Hove Rasmussen

The European Commission (EC) last year launched a €20-million (US$26-million) industrial PhD initiative as part of its Marie Curie Actions funding programme, which promotes mobility among young scientists. Approximately 100 European Industrial Doctorates will be funded under the pilot scheme, and the initiative is to become a permanent part of the European Horizon 2020 research-funding framework from 2014. Companies in the European Union or associated countries can submit research proposals without a specific PhD candidate in mind, but must have a partner university in a different eligible nation.

The structures of initiatives differ. Often, candidates spend 50% of their time or less at the university, and the rest at the company. Students at the ESPRC's doctorate take university courses in cohorts, accounting for 25% of their PhDs, but do placements separately. For the CASE and EC programmes, students deal almost exclusively in company research, although they ultimately have to defend their theses at the university.

The match-making processes also vary. In Denmark, students first need to find a company and agree on a PhD project. Then they, along with their university advisers, submit applications to DASTI. In CIFRE and the EC scheme, companies submit PhD research proposals first, then recruit students. The EPSRC's doctorate centres recruit students — accepting about 1 in every 20 applicants — and guide the match-making. Candidates for an EPSRC engineering doctorate in biopharmaceutical process development at Newcastle University, UK, have teamed up with companies in Britain and abroad, including GlaxoSmithKline and AstraZeneca, both based in London; Unilever in Rotterdam, the Netherlands; Procter & Gamble in Cincinnati, Ohio; and Heineken in Amsterdam. Elaine Martin, a chemical engineer at Newcastle who oversees the programme, says that the scheme has proved so beneficial that many companies return to ask for fresh talent.

OPENING DOORS

Finding an industrial partner is often a challenge, says Jane Thomsen, head of DASTI's Industrial PhD Programme. "Students should have a very concrete research idea before they contact a company," she says. "Mere interest in some kind of collaboration is not enough." An internship or company placement often leads to a job or a more profound collaboration — Rasmussen, for example, did his master's research at Novo Nordisk before his PhD.

Similarly, Martina Hitzbleck became interested in industrial research after a three-month college internship with IBM's Almaden research centre in San Jose, California, in 2008. She learned that Emmanuel Delamarche, a scientist at IBM Zurich, was doing high-profile research on biosensor design — the subject of Hitzbleck's master's thesis — and she sent him her CV. After an interview and a presentation, Delamarche offered Hitzbleck a PhD project. He became her industrial supervisor, and Hitzbleck found an academic mentor at the Swiss Federal Institute of Technology in Zurich. She spends 90% of her time with IBM. "I get all the support here that I could dream of," she says. "Whenever I have a problem, there is an expert on whose door I can knock."

There are currently 36 PhD projects under way at IBM Zurich, mostly informal arrangements rather than part of a programme. Oliver Ottow, head of human resources and university relations at the lab, says that the match-making generally takes place at scientific conferences and graduate recruitment fairs, or through IBM's extended network of university contacts. "If students can convince us that their topics make a difference we'll find a home for them," he says. "We just want to make sure they're highly motivated and really very good." In principle, IBM gets research results and, possibly, a skilled future staff scientist. Students become familiar with applied, goal-oriented research, and learn about careers in industry, from patent law to media communication.

REASONABLE PRECAUTIONS

Students involved in informal collaborations should insist on a written agreement about the terms and conditions of the partnership, signed by themselves and all supervisors, says Borrell-Damian. "There is still a delicate balance between the respective interests of students, university supervisors and companies," she says. "A written agreement on all parties' rights and duties is therefore essential." Such agreements should specify topics and goals of the research, the required division of time and how intellectual-property rights will be assigned, she says. Company research departments will usually own the intellectual property, but students should insist on the right to publish their findings. In general, universities still administer final exams, even if students are full-time company employees.

There has been little research into the career paths of industrial PhD holders, but the few surveys that do exist suggest that graduates tend to stay in industry, usually in research. Even so,

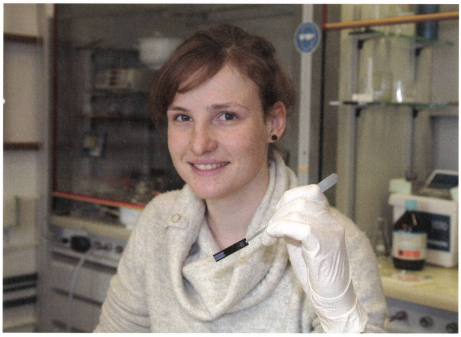

IBM RESEARCH ZURICH

A college internship led Martina Hitzbleck to do a PhD at the IBM research centre in Zurich, Switzerland.

the door to academia is not necessarily closed (see *Nature* **466**, 402–403; 2010). Several former IBM researchers have moved on to become university faculty members, helped by the prestige of working in a high-profile industry lab.

Some academics fear that industrial PhD students may not acquire the full set of skills and knowledge required for independent scientific research in academia, ranging from methods to research ethics. "Academia and industry have fundamentally different roles and it is not helpful if they imitate each other," says Peter Blöchl, a theoretical physicist at Clausthal University of Technology in Germany. He worked for ten years at IBM's research laboratory in Ruschlikon, Switzerland, before moving to academia in 2000. Academia's mission is pre-competitive research and student education, he says. "Companies can tap into this knowledge base to develop innovative products, but I see little purpose for a PhD in industry." Joint projects, consultantships and sabbaticals are more productive, says Blöchl.

In general, students must be prepared for companies to tweak a research proposal to strengthen its commercial potential, says Thomsen. To avoid misunderstandings, they should make sure from the beginning that they are willing to accept such input. Early interviews with company researchers should help, but subsequent problems are best addressed with the help of the supervisor. In structured programmes, the funding agency will also review any complaints, and may intervene.

In the Danish scheme, says Thomsen, complaints are rare. If serious problems do arise — for example, if a host company goes bankrupt, or a PhD student is asked to do experiments or tasks unrelated to their project — the agency will try to mediate and, if necessary, demand the return of subsidies.

Concerns that industry is in it mainly for the cheap labour, and that projects lack scientific depth, are unfounded, says Martin. "All companies we're working with — even the manufacturing sites — have a serious interest in supporting genuine research."

But as industrial PhDs become more common, some do worry about exploitation of students and 'over-industrialization' of higher education. Eurodoc in Brussels, which lobbies for the rights of PhD candidates, warns that early-career research should be a free intellectual endeavour and not subject to the needs of business and industry. "Vanguard industrial PhD programmes are an opportunity to do what we all want to do — get work," says Greg DeCuir, a dramatic-arts PhD student at the University of Arts in Belgrade, and a member of Eurodoc's career-development group. "But we are not apprentices. If you feel that your scientific creativity is compromised, there should be a concern." ■

Quirin Schiermeier *is* Nature*'s Germany correspondent.*

TURNING POINT
Christopher Wilson

Christopher Wilson, a physicist at Chalmers University of Technology in Gothenburg, Sweden, led one of Physics World*'s 2011 'breakthrough' experiments: he and his team proved that a vacuum, rather than being completely empty, contains detectable virtual particles. He explains his motivation for taking a working sabbatical at a biotechnology start-up in California.*

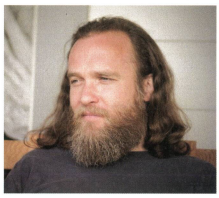

You did your undergraduate degree at the Massachusetts Institute of Technology (MIT) in Cambridge. How did this affect your career?

I was able to attend MIT after I won a US Naval Reserve Officers Training Corps scholarship, so I was expected to go into the navy afterwards. But I realized while I was at MIT, which is a very intense place, that I would rather do science. Between the second and third years of my degree, I notified the navy that I didn't want to join. They could have drafted me, but they allowed me the option of paying back the scholarship money, which I've been doing ever since.

How has your move to Chalmers influenced your research?

I worked at Yale University in New Haven, Connecticut, for two years and then moved to Chalmers to work on a quantum computing project, ostensibly for a year. I've now been there for seven years. In Sweden, the work dynamic is hierarchical, like a company. There is a top professor who has several professors at different levels working under him or her — and younger researchers work their way up. It's a good system if you have a good boss. It gave me more time and freedom to get this one big experiment to work than I would have had in the United States.

Describe your breakthrough experiment.

When I got to Chalmers in 2004, my team started work on superconducting circuits for quantum computing. Around 2007, we realized that the work could allow us to measure the virtual photons inside a vacuum. These virtual photons are generated and annihilated in pairs. About 40 years ago, it was suggested that a mirror moving near the speed of light could capture some of these photons. The effect had never been observed, because it is very hard to move a massive object that fast. We made an electronic 'mirror' that we could effectively move at one-quarter of the speed of light using magnetic fields. This allowed us to separate the pairs, stopping them from annihilating and turning them into real photons that we could observe (C. M. Wilson *et al. Nature* **479**, 376–379; 2011).

Could the media attention have a career benefit?

It certainly helps to put the paper in a certain light, especially for people outside our physics sub-field. For example, when applying for jobs, you are evaluated by a whole department. It can be difficult even for other types of physicists to evaluate the details of papers.

Why did you choose to take a sabbatical year at a start-up biotechnology company?

Last July, I was promoted to associate professor, which is tenured at Chalmers. In the US system, it is typical to take a sabbatical after getting tenure. Sweden doesn't follow the same timing, nor does the university pay academics to go on sabbatical, but I had planned to do it. I happened to see an ad on a job-posting site from a start-up company working on biomedical devices and proteomics. They needed someone skilled in algorithms and advanced statistical tools to analyse the enormous amount of data being generated about proteins, and I liked the people involved. It has turned out to be a good fit.

What kind of career impact do you expect the sabbatical to have?

I really wanted to do something to diversify my skills and develop some research lines that were completely my own — which can be a struggle in Europe's hierarchical system. I want to see if I can contribute algorithms to the field of proteomics. It would be pure hubris to think I could jump into biology, but I would like to find collaborators and see if I can develop a new aspect of my research. ■

INTERVIEW BY VIRGINIA GEWIN

RNPnet

RNAs associate with proteins to form highly complex and dynamic ribonucleoprotein (RNP) complexes. The goal of this **ITN network is to train 16 PhD students** on how RNPs function at the mechanistic level and how they affect gene expression at the cellular level. The projects are centered around three main biological topics (pre-mRNA processing, RNA editing and modification, RNA surveillance and regulatory RNAs) and will be tackled with different disciplines in a cooperative and integrative manner. The groups in the network are experts in different technologies including organic chemistry, structural biology (NMR, X-ray crystallography and cryoEM), biochemistry, biophysics, high-throughput RNA-protein mapping, computational biology and live cell imaging. The aim is to train young researchers in the RNA field with a multidisciplinary expertise and culture. Information on the **available PhD positions** can be found at: **www.mpnet.ethz.ch**

SEVENTH FRAMEWORK PROGRAMME

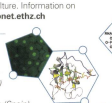

pre-mRNA processing

Frédéric Allain, *ETH, Zurich (Switzerland)* – Structure determination of U1snRNA-RNA complexes
Edouard Bertrand, *CNRS, Montpellier (France)* – In vivo dynamics of SR protein-RNA interactions
Maria Carmo-Fonseca, *University of Lisbon (Portugal)* – Effect of SR protein phosphorylation on splicing
Eduardo Eyras , *Universitat Pompeu Fabra, Barcelona (Spain)* – Co-evolution of SR protein-RNA recognition
Karla Neugebauer, *MPI Cell Biology, Dresden (Germany)* – Identification of in vivo binding sites of SR proteins
Jamal Tazi, *Spilcos, Montpellier (France)* – Small molecules inhibiting splicing mechanisms

RNA editing and modification

Teresa Carlomagno, *EMBL, Heidelberg (Germany)* – Selective RNA labeling and complementary structural biology approaches for large RNP complexes
Julius Lukes, *Biology Centre, Ceske Budejovice (Czech Republic)* – RNA editing in Trypanosoma brucei
Ronald Micura, *University of Innsbruck (Austria)* – RNA chemical modification as a tool to understand RNA function

mRNA surveillance and regulatory RNAs

Elena Conti, *MPI Biochemistry, Munich (Germany)* – Structure and function of EJC-binding proteins
Hervé Le Hir, *ENS Paris (France)* – Mapping of EJC-binding sites in neurons
Nicole Meisner-Kober, *Novartis, Basel (Switzerland)* – RNA-protein interactions
Christian Spahn, *Charité University, Berlin (Germany)* – Visualizing non-stop decay by electron microscopy
Jemej Ule, *MRC-LMB, Cambridge (UK)* – TIA-mRNA-miRNA ternary map
Mihaela Zavolan, *University of Basel (Switzerland)* – Small regulatory RNAs

W221938R

Keen on an exciting career in the heart of Asia?

Come to Singapore! Opportunities in our dynamic research and biomedical sciences industries await you.

Singapore offers exciting opportunities with leading pharmaceutical companies, top research institutes and world-class universities in Singapore that are recruiting PhD students and PhD holders with varying levels of experience.

Contact Singapore engages overseas Singaporeans and global talent to work, live and invest in Singapore. We are the one-stop centre for those who wish to pursue a rewarding career here.

Let Contact Singapore link you up with these employers. Visit our job portal at:
- **www.contactsingapore.sg/Jobs/Research**, for research positions
- **www.contactsingapore.sg/Jobs/BMS**, for biomedical sciences positions

You can also read about the latest industry developments within the biomedical sciences industry and check out the sector's *Hot Jobs* here: **www.contactsingapore.sg/eCareers/biomedical_sciences_Feb2012**

For more information about working and living in Singapore, please visit **www.contactsingapore.sg**

For enquiries, please email us at **london@contactsingapore.sg**

Contact Singapore
contactsingapore.sg

U221970R

CEDAD CD² **Graduate Program Cell Dynamics and Disease - CEDAD -**

International Max Planck Research School - Molecular Biomedicine - IMPRS-MBM

Joint PhD program

International PhD Program in Life Sciences – Münster, Germany

16 PhD Fellowships starting October 2012

- Cutting edge biomedical science
- Scientific and transferable skills training
- No tuition fees. Program language: English
- Competitive tax-free fellowship
- Support with visas, administrative matters, accommodation etc.

Application deadline **11 May 2012,** apply at **www.cedad.uni-muenster.de**
We invite applications from highly qualified and motivated students of any nationality to do their PhD in Münster, "the world's most liveable city" (LivCom Award 2004).
Contact: Prof. Martin K. Wild, cedad@uni-muenster.de

W221658R

NPlast

MARIE CURIE ACTIONS

Twelve PhD (ESR) and three Post-doc (ER) positions are available in the European Marie Curie initial training network (ITN) 'NPlast'

NPlast is a Marie Curie Initial Training Network funded by the 7th EU Framework Program. The consortium consists of seven research groups and four partners from industry in six European countries (Coordinator: Michael R. Kreutz, Leibniz-Institute for Neurobiology, Magdeburg, Germany).

The network will provide training for twelve ESRs and three ERs in projects that are aimed to elucidate mechanisms of neuronal plasticity relevant to neuropsychiatric disorders including neurodegeneration and dementia. The research projects and the training program provided by the consortium cover a broad spectrum of disorders and interventions ranging from synaptopathies and trafficking deficiencies to Alzheimer's disease, and from altering degenerative gene expression programs to manipulations of the extracellular matrix to preserve or restore synaptic function.

For more information about single projects see the homepage of the NPlast consortium (www.nplast.de). Contact: spilker@in-magdeburg.de

W221179R

HELENA
Helmholtz Graduate School Environmental Health

PhD Projects within the International Helmholtz Graduate School Environmental Health (HELENA) – life sciences m/f

The International Helmholtz Graduate School Environmental Health (HELENA) is a joint initiative for the promotion of doctoral students of the Helmholtz Zentrum Muenchen - German Research Center for Environmental Health, the Ludwig-Maximilians-Universität München (LMU) and the Technische Universität München (TUM).

The HELENA Graduate School offers PhD projects in the following areas:
- Diabetes and Lung Biology
- Neuro and Stem Cell Biology
- Infection, Immune and Tumor Biology
- Epidemiology, Health Economics and Human Genetics
- Radiation Research
- Ecosystems Biology
- Systems Biology, Biomedical Imaging and Structural Biology

HELENA has openings for fully funded graduate student positions. Highly qualified and motivated students from all nationalities with a genuine interest in basic and translational research are invited to apply. Applicants should hold a MSc or equivalent degree in biological sciences, chemistry, bioinformatics, physics, veterinary or human medicine or related life sciences.

www.helmholtz-helena.de **Closing date: May 6, 2012**

W221991R

HelmholtzZentrum münchen
German Research Center for Environmental Health

LMU LUDWIG-MAXIMILIANS-UNIVERSITÄT MÜNCHEN

TUM Technische Universität München

FAPESP

A journey to Brazil for young researchers

FAPESP, the São Paulo Research Foundation, is one of the main research funding agencies in Brazil. With a budget of US$ 450 million, it supports more than 11,000 fellowships and 8,000 research awards.

FAPESP Young Investigators Awards envisage creating new research groups led by highly promising early-career scientists in any field of knowledge and from any country. Selected candidates receive competitive fellowships and sizable research funds. Candidates are encouraged to develop their projects with higher education and research institutions from the State of São Paulo, Brazil.

Highlighted research areas are: biodiversity, bioenergy, climate change, neurosciences, cancer, materials science, optics and photonics, urban studies and violence. Proposals in other fields will be considered and all will be selected through a peer-reviewing process. See more about it at www.fapesp.br/yia.

FAPESP Post-Doctoral fellowship is aimed at distinguished researchers with a recent doctorate degree and a successful research track record. The fellowship enables the development of research within higher education and research institutions in São Paulo. Additional information: www.fapesp.br/en/postdoc.

FAPESP 50 YEARS

NW221940R

Imperial College London

Imperial College London

Qatar Carbonates and Carbon Storage Research Centre, Departments of Chemical Engineering and Earth Science and Engineering

10 PhD Studentships in Carbon Storage

The greatest scientific and technological challenge of this century is how to provide energy to a growing global population, while avoiding dangerous climate change. The storage of CO2 in deep subsurface geologic reservoirs is broadly recognized as an essential first step to mitigate greenhouse gas emissions, including assessments made by the Intergovernmental Panel on Climate Change, the Commission on European Communities, and the United States Department of Energy.

You are invited to join Imperial College's largest research project, secured through long-term industrial funding. The posts are funded through major long-term support from Qatar Petroleum and Shell International for the Qatar Carbonates and Carbon Storage Research Centre (QCCSRC). This Centre, established in 2008, is enabling Imperial College London to expand significantly its research into Clean Fossil Fuels - aimed in particular at improving the energy efficiency of oil and gas recovery, closely coupled with reducing greenhouse gas emissions through advanced carbon capture and storage technologies. The Centre is a collaboration between the Department of Earth Science and Engineering and the Department of Chemical Engineering.

Applications are invited for 10 research studentships to study various aspects of the underpinning science and engineering of Carbon Storage in Carbonate Reservoirs, leading to the award of a PhD degree. The post is supported by a bursary (£18,000 pa) and fees for three/four years from October 2012 or sooner and is available for UK / EU or international candidates.

You will be an enthusiastic and self-motivated person who meets the academic requirements for enrolment for the PhD degree at Imperial College London. These are normally at least a 2:1 honours degree in applied mathematics, physical science or engineering and preferably an MSc with a good dissertation in a relevant subject. You will have an enquiring and rigorous approach to research together with a strong intellect and disciplined work habits. Good team-working, observational and communication skills are essential. Some international travel and work at industrial sponsors' research facilities will be required.

Researcher projects will be in the fields of the fundamental science of reactive transport in porous media, thermophysical property experimentation/modelling, pore- and core-scale imaging/modelling and pore to core to field-scale multiphase flow supported by state-of-the-art new laboratories.

The following projects are currently available:

1. Mineral contamination by thin films
2. Carbonate microporosity
3. Impurities in CO2 stream and effects on IFT, PVT
4. CO2 viscosity experiments
5. EOS modelling - SAFT
6. Pore-scale multiphase flow
7. CO2 shale swelling experiments and modelling
8. Pore-scale reactive transport
9. Core-scale reactive transport
10. Fracture related reactive transport

The successful applicants will be encouraged to collaborate with other QCCSRC team members and other academic staff members, publish the research results in internationally recognised peer reviewed journals and present the research results at relevant national and international scientific and professional conferences, as well as industrial sponsor meetings. You will become a skilled communicator, comfortable in an international situation.

To find out more about specific research projects within QCCSRC, go: http://www.imperial.ac.uk/qatarcarbonatesandcarbonstorage/about/vacancies

For further enquiries contact Mrs Anca Gourlay, a.gourlay@imperial.ac.uk +44(0) 20785942685. Interested applicants should send a curriculum vitae, a statement of their research interest and an electronic copy of their transcripts to the Principal Investigators of their project of interest.

Closing date: 13th March 2012

U221993R

Visit

www.naturejobs.com

to seriously improve your career prospects.

naturejobs
making science work

CeMM PhD Program 2012

For our next PhD Program starting in October 2012, we are looking for exceptionally motivated PhD candidates with a keen interest in genomics and medicine.

Application details: www.cemm.at
Deadline: 20 March 2012

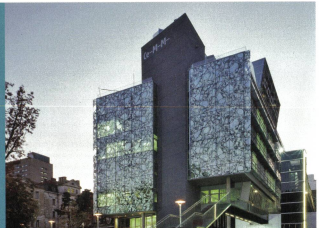

The New Center for Molecular Medicine in Vienna

of the Austrian Academy of Sciences • in a new building with a landmark art facade by artist Peter Kogler • in the center of Vienna's General Hospital and Medical University Campus • integrates basic research and clinical expertise to pursue innovative diagnostic and therapeutic approaches • 14 faculty with average age 36 years, 120 people, 31 nationalities, mix PhDs/MDs, top SAB, English language • inclusive, open culture • state-of-the-art infrastructure • works towards predictive, preventive and patient-oriented medicine of the 21st century • cancer, inflammation, immune disorders • systems biology, functional genomics and proteomics, high-throughput genetics and epigenetics, mechanisms of action of drugs, infection models • stream of highly-cited papers • conferences, workshops, CeMMinars • international PhD/postdoc/PI mentoring programs

Denise Barlow • Keiryn Bennett • Christoph J. Binder • Andreas Bergthaler • Christoph Bock • Kaan Boztug
Thijn Brummelkamp (Adjunct PI) • Jacques Colinge • Sylvia Knapp • Robert Kralovics • Stefan Kubicek
Joanna Loizou • Sebastian Nijman • Giulio Superti-Furga

W221831R

NC3Rs PhD STUDENTSHIPS 2012

The NC3Rs leads the discovery, development and promotion of new ways to replace, reduce and refine the use of animals in research and testing (the 3Rs) – supporting science and innovation in the bioscience sector. We are an independent organisation sponsored by Government and the UK's major funder of 3Rs research.

This year the Centre is funding 15 PhD studentships. The successful research groups are now looking to recruit hightly motivated candidates. Applicants should hold, or realistically expect to obtain, at least an Upper Second Class Honours degree in the biological sciences. They should also have a desire to pursue research in line with that of the research groups.

Funding will provide full support for tuition fees, associated project costs, and an annual tax-free stipend.

For further information, including details of project supervisors, please visit: www.nc3rs.org.uk/studentshipvacancies

University of Glasgow:
The development of an *in vitro* model of spinal cord injury to study aligned neurite outgrowth

Using induced pluripotent stem cells (iPSC) as a replacement for *in vivo* models to screen novel therapies which target self-renewal pathways in chronic myeloid leukaemia

Imperial College London:
Developing a novel model to assess the specificity of appetite-reducing agents

In vitro and *in silico* models of gut bacterial diversity and its impacts on human health

Improving the principles of the 3Rs through new integrative metabolomic and gene expression resources for signalling studies in burn injuries

King's College London:
Characterisation and validation of an organotypic slice culture model of Alzheimer's disease

Liverpool School of Tropical Medicine:
Refining, reducing and replacing *in vivo* WHO-standard preclinical assays of snake venom pathology and antivenom efficacy

Loughborough University:
Combinatorial mathematical modelling and novel toxicological profiling of drug-induced hepatotoxicity

University of Manchester:
Reducing animal dependency in diabetes research through pancreatic stem cells

Newcastle University:
Refinement of the use of fluid control as a motivational tool for non-human primates in neuroscience research

University of Nottingham:
Construction of a miniaturized human lymph node model as an alternative to the local lymph node assay

University of Oxford:
A *Drosophila* model of *Candida albicans* gastrointestinal infection

Development of a non-animal model for characterizing drug-resistant tumours

Queen's University Belfast:
Development of non-radioactive labels for a receptor binding assay for paralytic shellfish poisoning (PSP) toxin testing

University of Southampton:
Bone healing and regeneration in an *ex vivo* bioreactor - evaluation of angiogenesis and reparation for clinical application

NC3Rs
National Centre for the Replacement, Refinement and Reduction of Animals in Research

U221948R

Vienna University of Technology

TU WIEN

Vienna Doctoral Programme on Water Resource Systems

The Water Research Centre at the Vienna University of Technology announces competition for the second intake of doctoral candidates for the Doctoral Programme on Water Resource Systems. The programme is anticipated to host a total of 70 doctoral students over a period of 12 years. This is a dedicated programme of the Austrian Science Fund (FWF) that promotes doctoral research and education at the highest standards and provides excellent opportunities for cross-disciplinary research. International networking is facilitated by a mobility programme with a spectrum of attractive international partner institutions and a comprehensive guest scientist programme.

Eight PhD student positions are available in the following research themes related to Water Resource Systems:

- Flood-hydrology
- Aquatic microbiology
- Diffuse water pollution
- Socio-hydrology and environmental economics
- Regional nutrient management
- Soil moisture remote sensing
- Mechanics of structures
- Micro-meteorology

Applicants for the PhD student positions must have a Master's degree (or equivalent) in a discipline related to water resource systems. The working language of the programme is English. Students are expected to work across disciplines and in cooperation with others. A capacity and willingness to integrate and collaborate is essential.

The Programme provides a salary according to the FWF scheme, together with a significant allowance for travel and research support. TU Wien is an equal opportunities employer. The contracts will be for three years and extension to a fourth year is possible. The preferred starting date is Oct. 1, 2012.

Candidates should send a letter of application, a statement of research interests, copies of education certificates and a Curriculum Vitae to office@waterresources.at (pdf format), or as a hard copy to The Centre of Water Resource Systems, c/o Dr. Gemma Carr, Vienna University of Technology, Karlsplatz 13/222-2, A-1040 Vienna, Austria. Please quote reference: DK-WRS.

Application deadline is April 30, 2012. Short listed candidates will be invited to a selection seminar. Financial support towards travel expenses is available on request. Information about the Doctoral Programme on Water Resource Systems may be viewed at http://waterresources.at

W221872R

Neuroscience MSc Courses at the Times Higher Education University of the Year.

The University Of Sheffield.

MSc in Translational Neuroscience: This contemporary 1 year full-time course covers how molecular and cellular neuroscience and neuroimaging can be applied to develop new therapies for neurodegenerative, psychiatric and neurodevelopmental disease.

For more information visit: www.sheffield.ac.uk/transneuro or email transneuro@sheffield.ac.uk

MSc in Clinical Neurology: This new 1 year full-time course provides both theoretical, practical and research training in clinical neurology, neuroanatomy and neuroscience and covers a wide range of neurological disorders.

For more information visit: www.sheffield.ac.uk/clinneuro or email clinneuro@sheffield.ac.uk

U221977R

Don't miss the intoxicatingly good job opportunities in *Nature* each week and on naturejobs.com

naturejobs

The International Research Training Group 1273 "Strategies of human pathogens to achieve acute and chronic infections"

is seeking highly qualified and motivated individuals for

14 PhD Student Fellowships in Infection Biology of Human Pathogens (starting September 1, 2012)

Since 2006, the German Research Foundation (DFG) provides funding to Hannover Medical School (MHH), the Helmholtz Centre for Infection Research (HZI) in Braunschweig and the TWINCORE in Hannover to maintain an International Research Training Group (IRTG) together with the Karolinska Institutet in Stockholm (coordinators: Sebastian Suerbaum, Hannover, and Birgitta Henriques-Normark, Stockholm). The central aim of the programme is to give young researchers the opportunity to perform their PhD work in the rapidly moving field of the infection biology of human microbial pathogens in a highly stimulating, competitive, international environment. The core element of the IRTG is a joint research programme centering on the question how human microbial pathogens achieve acute or persistent infection and how the host organism reacts to persistent infection. In addition, graduate students will participate in a highly interdisciplinary joint study programme. Stipends will be €1,365/month and are available for up to three years. It is an integral part of the programme that PhD students spend 6-12 months in one of the partner labs at the Karolinska Institute.

Candidates who hold the equivalent of a master's or diploma degree in Biology, Biochemistry or Life Sciences, or who graduated in medicine are welcome to apply. Those applicants who are selected for interviews in a first round of screening will be asked to attend a selection workshop in Hannover to be held June 19 / 20, 2012.

The deadline for receipt of a complete application is April 20, 2012. Applications are only accepted via the online application platform http://www.irtg1273.mh-hannover.de.

For detailed information on faculty and projects see http://www.mh-hannover.de/4587.html.

Prof. Dr. Sebastian Suerbaum, Department of Medical Microbiology and Hospital Epidemiology, Hannover Medical School, Carl-Neuberg-Str. 1, 30625 Hannover, Germany, or IRTG1273@mh-hannover.de.

W221364R

naturejobs

European Head Office, London naturejobs@nature.com
The Macmillan Building, 4 Crinan Street, London N1 9XW, UK
Tel: +44 (0) 20 7843 4961 Fax: +44 (0) 20 7843 4996

European Manager:
Nils Moeller,+44 (0) 20 7843 4953 n.moeller@nature.com

Southwest UK/RoW:
Emma Hare, +44 (0) 20 7843 4944 e.hare@nature.com

Northeast UK/Ireland:
Matthew Ward, +44 (0) 20 7014 4059 m.ward@nature.com

France/Switzerland/Belgium:
Julie Aramburu, +44 (0) 20 7843 4994 j.aramburu@nature.com

Scandinavia/Spain/Portugal/Italy:
Megan Ball, +44 (0) 20 7843 4973 m.ball@nature.com

North Germany/The Netherlands/Eastern Europe:
Kristin Doelling, +44 (0) 20 7843 4970 k.doelling@nature.com

South Germany/Austria:
Maria Kubalova, +44 (0) 20 7014 4084 m.kubalova@nature.com

Natureevents:
Matthew Clare, +44 (0) 20 7014 4015 m.clare@nature.com

Business Development Manager, Middle East:
Jon Giuliani, +44 (0) 20 7843 4922 j.giuliani@nature.com

USA Head Office, New York naturejobs@us.nature.com
75 Varick Street, 9th Floor, New York, NY 10013-1917
Tel: +1 800 989 7718 Fax: +1 800 989 7103

US Sales Manager:
Ken Finnegan, +1 212 726 9248 k.finnegan@us.nature.com

Japan Head Office, Tokyo
Chiyoda Building, 2–37 Ichigayatamachi, Shinjuku-ku, Tokyo 162-0843
Tel: +81 3 3267 8751, Fax: +81 3 3267 8746

Asia-Pacific Sales & Business Development Manager:
Yuki Fujiwara, +81-3-3267-8765 y.fujiwara@natureasia.com

Business Development Manager, Greater China/Singapore:
Gloria To, +852 2811 7191 g.to@natureasia.com

India
3a, 4th Floor, DLF Corporate Park, Gurgaon, 122 002, India

Advertisement Sales:
Vikas Chawla, +91 1242881057 v.chawla@nature.com

A! Aalto University School of Chemical Technology

Aalto University is a new multidisciplinary science and art community in the fields of technology and science, business and economics, and art and design. The University's cornerstones are its strengths in education and research.

Aalto University School of Chemical Technology, Department of Biotechnology and Chemical Technology, invites applications for:

Tenure Track Position in Polymer Technology

Rank will be commensurate with experience, but preference will be given to an appointment at the assistant or associate professor level.

Research on synthesis and properties of polymers is one of the core fields in modern materials science. Aalto University is aiming to strengthen this field by opening a tenure track position in Polymer Technology. We search excellency in polymer chemistry, covering polymer synthesis, which can allow e.g. advanced structural control, functional materials, biopolymers and their applications.

A successful candidate must have a Ph.D. or equivalent degree in related field. Applicants must demonstrate distinction in published research, evidence of consistent extramural funding and strong international experience and collaboration. The appointee will be expected to commit to teaching. Pedagogical studies are an advantage.

The closing date for applications is April 5th, 2012.The position will be based in Espoo, Finland. To see the complete position description, please go to **aalto.fi/en/openpositions**. More information on the Aalto tenure track system is available at **aalto.fi/en/tenuretrack.**

aalto.fi

W221753R

MACMILLAN
SCIENTIFIC COMMUNICATIONS

Assistant Publisher - Macmillan Scientific Communications (Asia-Pacific)

Macmillan Scientific Communications (MSC) is the international custom publishing division of Macmillan Publishers Ltd. MSC works with clients in top universities, research institutes, scientific organizations and companies around the world to provide tailor-made science communication services aimed at presenting their research and scientific achievements to domestic and overseas scientists, science policy makers and the wider community. The projects handled by MSC include websites, print magazines and newsletters and online audio and video programs as well as workshops in the writing of scientific papers and developmental editing services.

Macmillan is the owner of *Nature Publishing Group (NPG)*, publisher of the international science journal Nature, the related family of Nature research journals, and Scientific American. MSC uses its exclusive access to the resources of NPG in science writing and editing, print, online and audio–visual production and marketing to create, design and promote scientific content to the highest standards.

MSC is now seeking an Assistant Publisher to augment its Asia–Pacific team based in Tokyo. The successful candidate will report to the MSC Publisher and Editor-in-Chief (Asia–Pacific) and will be responsible for overseeing and coordinating MSC's diverse array of online and print publishing projects. The ideal candidate will have an undergraduate degree, preferably in a science-related discipline, and a proven track record in custom, periodicals or journal publishing. Experience in online publishing and familiarity with industry standard publishing and design software are highly desirable.

Key tasks within the role will include drawing up and managing detailed publishing schedules and budgets for each project, devising work schedules, liaising with appropriate personnel in client institutions to manage information flows and ensure adherence to deadlines, and monitoring the attainment of project milestones and key performance indicators. In addition to managing current projects, the successful applicant will be expected to play a central role in the identification and development of new publishing projects both wholly within MSC and in collaboration with teams in NPG.

The successful applicant will have a background in science publishing and/or custom publishing and be able work to tight and variable deadlines with a high degree of flexibility in a dynamic, client-focused environment. In addition to outstanding written and oral communication skills you will have native-level fluency in English. Proficiency in Japanese would be a distinct advantage.

This is a key position in the MSC team and is a demanding and varied position that is both intellectually stimulating and challenging. Excellent organizational skills, flexibility, resourcefulness and initiative along with a commitment to delivering the highest possible level of service to our clients are prerequisites. The successful candidate must therefore be correspondingly dynamic, outgoing and have excellent interpersonal skills. The salary and benefits will be competitive, reflecting the critical importance and responsibilities of this position.

Applicants should send a CV (including the discipline of their degree and an account of their publishing experience), and a brief cover letter explaining their interest in, and suitability for, the post and their salary expectations to:

Dr Matthew Salter, Macmillan Scientific Communications, Chiyoda Building, 2-37 Ichigayatamachi, Shinjuku-ku, Tokyo 162-0843 Japan or by email to jobs@mscasiapacific.com

The closing date for applications is March 30th 2012.

IN221354R

Two positions in bioinformatics / biostatistics in Paris, France

The laboratory "Apoptosis, cancer & immunity" directed by Prof. Guido Kroemer recruits two bioinformaticians / biostatisticians. The candidates with a Master or PhD degree will be involved in a fundamental and translational program that aims at taking advantage of system biology methods and omics technology.

The first position will specifically deal with metabolomic profiling, data mining and modeling of cancer cells treated with chemotherapeutic agents.

The second position will deal with the analysis of high-throughput/high-content data obtained by fluorescence microscopic screens, as well as the integration of oncological, pharmacological and immunological parameters in the development of new therapeutic approaches.

The successful candidates, who must be fluent in English, are expected to develop interactive tools for data analysis and interpretation, to interact with biologists and cancer researchers, and to participate in a team effort. Salaries and benefits will be commensurate to experience. After a three-year term and intermediate evaluation, a tenure track position may be negotiated.

Applications (statement of interest, CV, names of three referees) should be sent to kroemer@orange.fr.

W221845R

UNI FREIBURG

The Faculty of Biology at the Albert-Ludwigs-University Freiburg (Germany) invites applications for a

Full Professorship (W3) in Geobotany – Functional Biodiversity Research
(held by Prof. Dr. Ulrich Deil)

We are looking for candidates who represent the entire subject of Geobotany in research and teaching and have an outstanding international scientific reputation in Geobotany with a focus on Functional Biodiversity Research and on the Ecology of Global Change.

We are expecting (i) a strong emphasis on experimental approaches, combined with good know-how in ecological field work and vegetation census techniques, focusing on forest ecosystems; (ii) experience in the management of national and international research projects; (iii) a corresponding record of successful fundraising of third-party research money; (iv) in-depth knowledge on identification and taxonomy of higher plants.
Close cooperation within the Faculty of Biology, especially with the botanical and zoological departments, will be appreciated. The candidate should actively strengthen the ecological orientated disciplines at the University of Freiburg by collaborations with other faculties, especially with the Faculty of Forest and Environmental Sciences.

We are further expecting a strong engagement in teaching at the Bachelor and Master level, as well as in teacher training courses. This includes the organization and implementation of geobotanical excursions within the region of Freiburg and abroad. A profound experience in teaching is expected as well as a commitment to the self-administration of the Faculty.

Formal requirements for appointment are a completed study at the Master or equivalent level, a PhD, and a postdoctoral lecturing qualification (German Habilitation) or equivalent achievements in research and teaching, such as a successfully completed period as associate professor.

Please direct your application with all pertinent documents (including CV, list of publications, research profile and plan, teaching record; preferentially in electronic form: dekanat@biologie.uni-freiburg.de) by March 31st, 2012 to the Dean of the Faculty of Biology, University of Freiburg, Schaenzlestrasse 1, D-79104 Freiburg.

The University of Freiburg is an equal opportunities employer and particularly welcomes applications by female or handicapped scientists, who will be given preference, provided they have an equivalent qualification.

W221830R

MDC MAX DELBRÜCK CENTER FOR MOLECULAR MEDICINE BERLIN-BUCH
in the HELMHOLTZ ASSOCIATION

The MAX DELBRÜCK CENTER FOR MOLECULAR MEDICINE (MDC) BERLIN-BUCH is inviting applications for

Independent Group Leader Positions

The MDC is a biomedical research institute dedicated to interdisciplinary research in the areas of (i) Cardiovascular and Metabolic Diseases, (ii) Cancer, and (iii) Function and Dysfunction of Nervous System.

We seek applications from outstanding researchers. Research interests should complement those of the MDC. The MDC is a member of the Helmholtz Association of National Research Centers, supported by the Federal Government of Germany and the Land Berlin.

Successful candidates will conduct visionary independent research, obtain extramural funding and engage in collaborative projects with groups at the MDC and the universities in Berlin.

Successful candidates will be invited to apply for a Helmholtz-University Young Investigator Group or a Helmholtz Young Investigator Group, sponsored by the President's Initiative and Networking Fund (see: http://www.helmholtz.de/de/Aktuelles/Helmholtz-Ausschreibungen/Helmholtz-Nachwuchsgruppen.html). The position includes generous funding for 5 years with the option of a two-year extension twice.

For further information about the MDC please visit our web site (http://www.mdc-berlin.de). For enquiries about the position please contact Gesa Schaefer (gesa.schaefer@mdc-berlin.de).

These positions are funded according to the German TVöD-System.

Applications by women are explicitly encouraged.

Disabled applicants, qualified according to the above criteria, will be given preference over other candidates with equivalent relevant qualifications.

For electronic applications please use the Email: jobs@mdc-berlin.de. Please send your application as one file, pdf-format, maximum size 1 Mb.

Applications should be sent by March 23, 2012 including a curriculum vitae, list of publications, an outline of present and planned research and other relevant material to

W221905R

MAX DELBRÜCK CENTER FOR MOLECULAR MEDICINE
Prof. Walter Rosenthal • Scientific Director
Robert-Rössle-Str. 10 • 13125 Berlin / Germany
www.mdc-berlin.de

THE PROFESSOR OF MEDICAL TECHNOLOGY AND BIOTECHNOLOGY, FIELD BIOINFORMATICS

The Institute of Biomedical Technology (IBT), University of Tampere (http://www.uta.fi/ibt) is seeking highly qualified candidates for the post of Professor of Medical Technology and Biotechnology, field Bioinformatics. The position will be filled initially for 5 years.

IBT conducts high standard research in the field of biomedicine and biotechnology the joint Biotechnology Program with the Tampere University of Technology and joint Master's Degree program in Bioinformatics with the University of Turku. Research activities of the Institute cover bioinformatics, biotechnology, cancer, molecular biology, mitochondrial disease and ageing, immunology and cell and tissue technology.

For further details: http://www.uta.fi/ibc/administration/recruiting.html

Informal enquiries may be made to Professor Olli Silvennoinen, tel. +358-50-359 5740, email olli.silvennoinen@uta.fi

The applications are to be addressed to the Rector of the University of Tampere and submitted to University of Tampere, Registry, FI-33014 University of Tampere, Finland, e-mail: kirjaamo@uta.fi by 12 March 2012, at 15.45 local time.

W221976R

"*Naturejobs* has been a great way to find the right people to build our research team. In less than 1 month, I received over 40 inquiries for my advertised postdoctoral position, with many promising candidates. As a result, I have hired two very well-qualified fellows and am excited about moving our research forward with our new team."

Dr Kathleen Martin,
Yale School of Medicine, USA

naturejobs

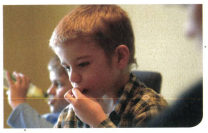

newmedicines™
vital science, new ways

Post-Doctoral Fellowship Programme:

UCB seeking world-class post docs to lead pioneering research projects.

UCB, a global biopharmaceutical leader focusing on central nervous system and immunological disorders, is currently seeking industry leading scientists to join our post doctoral programme based at research centres in Belgium and the UK*.

UCB is a patient-centric biopharmaceutical company dedicated to the research, development and commercialisation of innovative medicines. Already the leader in epilepsy, UCB is committed to providing novel solutions for people with severe conditions such as Parkinson's disease, rheumatoid arthritis, and restless legs syndrome. Employing more than 8,500 people in over 40 countries, UCB produced revenues of € 3.2 billion in 2010. UCB NewMedicines is UCB's discovery research to clinical proof-of-concept organisation charged with building a prolific pipeline of differentiated molecules by channelling exquisite science for industry-beating performance.

Our research centres are home to a wealth of internal skills and experience in our chosen therapeutic areas, allied to unique and proprietary technology platforms. Our networks with leading global academic and industrial partners ensure access to novel technologies, targets and collaborative services. Our intellectual and scientific capability is evidenced not only by our record of proven delivery of drugs to patients but also by our scientists having published work in leading journals.

We are seeking post docs with expertise in one or more of the following:
immunology; neurobiology; Parkinson's Disease; immunohistochemistry; molecular and cell biology; computer and mathematical modelling; mass spectrometry; cell signalling; siRNA; synthetic organic chemistry.

Slough (UK)

Braine-l'Alleud (Belgium)

"There's a true focus on high quality fundamental scientific research. We have an excellent supportive mentor and the working environment is positive and dynamic, with ongoing opportunities to collaborate and swap new ideas with people from various departments."
Manuela, UCB post doc scientist

"Scientific challenges from my UCB colleagues enhanced my creative thinking, and I have amassed information on broad areas of expertise, including drug discovery and the clinical perspective of scientific research. My experience at UCB has certainly broadened my career options."
Gaurav, UCB post doc scientist

If you want to develop your career with an innovative biopharmaceutical company and contribute to our outstanding record of achievement please view the post-doctoral opportunities available through our 2012 programme. Further details on the specific projects for which we are recruiting and details of how to apply are available at: http://www.ucb.com/rd/post-doctoral-programme

*Brussels (BE) and Slough (UK)

U221901R

ILLINOIS
UNIVERSITY OF ILLINOIS AT URBANA-CHAMPAIGN

Assistant or Associate Professor of Integrative Insect Biology School of Integrative Biology

The School of Integrative Biology and the Department of Entomology at the University of Illinois, Urbana-Champaign invite applications for a full-time, nine-month, tenure-track faculty position in integrative insect biology at the rank of **Assistant or Associate Professor.** The position starts as early as August 2012. We seek a broadly trained biologist working on insects who will develop an internationally recognized, externally funded research program that integrates evolutionary approaches into any aspect of insect biology, including but not limited to chemical ecology, developmental genetics, plant-insect interactions, physiology, neuroscience, and behavior. Applicants should be familiar with a diversity of modern techniques, including molecular and genomic methods. The successful candidate will have the opportunity to be part of dynamic and well-established communities of integrative biologists with interests spanning a wide range of taxa in the School of Integrative Biology, as well as in a number of interdisciplinary programs across the campus. Participation in both undergraduate and graduate education is required. A Ph.D. in Biology or related discipline is required by start date, and postdoctoral experience is desirable. Salary is commensurate with qualifications and experience.

To ensure full consideration, please create your candidate profile through http://go.illinois.edu/InsectBiology and upload your application letter, curriculum vitae, summary of research and plans, teaching philosophy and experience, and contact information for three professional references by March 15, 2012. Referees will be contacted electronically upon the submission of the application. Applicants may be interviewed before the closing date; however, no hiring decision will be made until after that date. For further information contact Insect Biology Search Chair, sib@life.illinois.edu.

Illinois is an Affirmative Action /Equal Opportunity Employer and welcomes individuals with diverse backgrounds, experiences, and ideas who embrace and value diversity and inclusivity. (www.inclusiveillinois.illinois.edu).

NW221875R

BASIC SCIENCE INVESTIGATORS IN THE AREA OF HIV and/or HIV-RELATED DISEASES

The Departments of Microbiology and Medicine at the University of Alabama at Birmingham (UAB), in conjunction with the Center for AIDS Research (CFAR), are seeking for outstanding basic science investigators in the area of human immunodeficiency virus (HIV) and/or HIV-related diseases (tenure and tenure track at Assistant, Associate and Full Professor Positions). Areas of interest include, but are not limited to, HIV immunology, vaccinology, pathogenesis, structural biology, opportunistic infections, and diseases associated with HIV, such as hepatitis C virus and mycobacterium tuberculosis. Nationally competitive salaries, start-up packages, and space allocations will be offered to successful candidates who will have the opportunity to interact with a core group of basic and clinical scientists at UAB with expertise in many different facets of HIV and HIV-related diseases.

The University of Alabama at Birmingham is one of the top clinical and research institutions in the nation, located in a beautiful, livable, and affordable city with many cultural and outdoor attractions. Applicants should send a C.V., a summary of research interests and the names of three references before April 30, 2012 to:

Dr. Paul Goepfert
Professor of Medicine and Microbiology
Director of the Alabama Vaccine Research Clinic
908 20th Street South, CCB 328
Birmingham, AL 35294-2050
Email: paulg@uab.edu

NW221967R

Bringing jobseekers and recruiters together.

Academic • Industry • Government

events · announcements · prospects · regions · careers & recruitment
spotlight · special reports · job channels · focus · movers

Search now at **naturejobs.com**

naturejobs
making science work

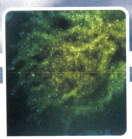

جامعة الملك عبدالله
للعلوم والتقنية
King Abdullah University of
Science and Technology

CHAIR POSITION IN POLYMER AND CATALYSIS IN THE KAUST CATALYSIS CENTER

The Catalysis Center at King Abdullah University of Science and Technology (KAUST) is launching a Professor Chair, sponsored by SABIC, in the field of **Polymer Sciences and Catalysis**.

KAUST is an international graduate-level, merit-based research university dedicated to advancing science and technology through innovative and collaborative research and to address challenges of regional and global significance. Located on the Red Sea coast of Saudi Arabia, KAUST offers superb research facilities, generous assured research funding, and internationally competitive salaries. Further information can be found at: *www.kaust.edu.sa.*

The KAUST Catalysis Center (KCC) is devoted to Catalysis by Design. The objectives of KCC areto develop new concepts in the fields of energy, environment, materials, and nanotechnologies. This center aims for excellence at the international level. To find out about KCC, visit *http://kcc.kaust.edu.sa.*

The theme of research associated with this Chair is "New Concept in Polymer Catalysis towards Major Breakthroughs." Considering the ambition of the topic, the profile of the candidate could vary from a young researcher to a more mature professor.

Applications should include a curriculum vitae, statements on research plans with brief research proposals as well as teaching philosophies. Please submit your application to the University's employment website at: *http://apptrkr.com/233732.*

www.kaust.edu.sa

RW221953R

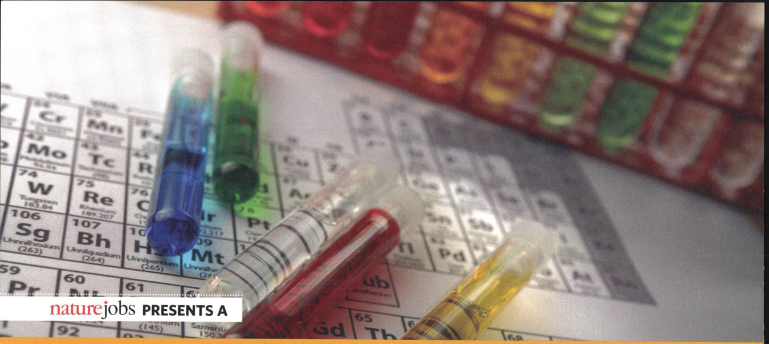

naturejobs **PRESENTS A**

SPOTLIGHT ON CHEMISTRY

***NATURE* ISSUE DATE:**
15 MARCH 2012

DEADLINE FOR ADVERTISERS:
AMERICAS: 8 MARCH 2012 | UK/EU/ROW: 9 MARCH 2012

Chemical research and development has had an effect on nearly every aspect of our daily lives, from synthetic fabric and plastics to medicine and fuel efficiency. The March 15th issue of *Nature* will feature a Spotlight on Chemistry, offering career and event listings alongside a feature on environmental toxicology.

Editorial content	Environmental toxicology
Bonus distribution	243rd American Chemical Society National Meeting – San Diego, US
Target audience	Research facilities, Institutions, Charitable organizations, PhD scientists
Examples of suitable job titles	Chemist, Biochemist, Chemical Engineer, Scientist, Research Scientist/Fellow/Assistant/Associate, Principal Scientist, Principal Investigator, Postdoc, Lab Technician, Lab Assistant, Lab Head, Director, Team Leader, Group Leader

The *Naturejobs* Spotlight on Chemistry is an excellent opportunity to raise awareness of your organization, make important announcements, and recruit top tier talent from within *Nature*'s uniquely qualified audience. All job advertisements will receive a complimentary 8-week online posting on naturejobs.com and event advertisements will receive a complimentary posting on natureevents.com — the events portal for *Nature*.

Don't miss out - contact a sales representative today:

US T: +1 800 989 7718 | Europe T: +44 (0) 20 7843 4961 | Japan T: +81 3 3267 8765 | India T: +91 12 4288 1057
Greater China/Singapore T: +852 2811 7191 | Middle East T: +44 (0)20 7843 4922 | E: naturejobs@nature.com

To advertise events:
US T: +1 202 626 2522 | Europe T: +44 (0) 20 7014 4015 | Japan T: +81 3 3267 8765 |India T: +91 12 4288 1057
Greater China/Singapore T: +852 2811 7191 | Middle East T: +44 (0)20 7843 4922 | E: natureevents@nature.com

naturejobs.com

nature publishing group npg

The University Of Sheffield.

The Achievement of Excellence

Faculty of Science
Department of Psychology

Chairs/Readers/Senior Lecturers/Lecturers (6 posts)

You will join a vibrant department, which is amongst the largest in the UK, and which has been consistently ranked as one of the outstanding research departments in all six UK Research Assessment Exercises to date. We have one of the largest centres of postgraduate psychology research in the country and were ranked fifth by the Times and Complete University Guide league tables.

We are looking for outstanding scholars in any area of psychology who can help us continue to build on, and extend, our success in research and teaching. Applicants will hold a PhD (or equivalent qualification) in a relevant discipline, together with an excellent publication record for their career stage. The following positions are available:

Chair (up to 3 posts)
You will be expected to have significant experience and expertise in academic leadership and attracting research funding, together with a distinguished record of international research.

Senior Lecturer/Reader
You will demonstrate substantial external reputation in the field, evidenced by the obtaining of independent research funding/significant personal distinction in scholarship and research with evidence of international excellence.

Lecturer
The postholder will be expected to exhibit outstanding academic potential, together with some evidence of quality research publications.

Two of the posts (one full-time and one 6 sessions per week) are likely to be within the Clinical Psychology Unit (CPU). It is also anticipated that a Chair appointment will be made within the CPU subject to suitable applications being received.

Further information about each of our research themes is available at:
http://www.sheffield.ac.uk/psychology/research

Full details of these posts are available online at
www.sheffield.ac.uk/jobs/

Closing date: 22 March 2012

U221942R

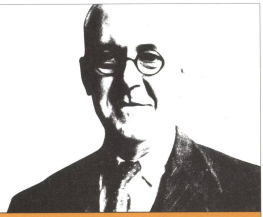

Sir Henry Dale Fellowship

For outstanding postdoctoral scientists wishing to build their own UK-based independent research career addressing an important biomedical question.

Fellowships are tenable for five years in the first instance, with the potential to apply for competitive renewal for an additional three years.

Preliminary applications must be received by **19 March 2012**.

Further information is available at **www.wellcome.ac.uk/shdf/nature** or **www.royalsociety.org/grants/schemes/henry-dale**.

wellcome trust

THE ROYAL SOCIETY

U221980R

nature jobs CAREER EXPO LONDON 2012

SAVE THE DATE!

20 SEPTEMBER 2012

BUSINESS DESIGN CENTRE, LONDON

The *Naturejobs* Career Expo in London is the UK's largest career fair and conference focused exclusively on the scientific world.

- **FREE** exhibition
- Expected **50+ employers**
- **Networking** opportunities
- Insightful **conference sessions**
- In-depth **company workshops**

For more information visit: **www.naturejobs.com/careerexpo**

naturejobs

nature publishing group npg

IN221387R

Post Doctoral Position in Macroalgal Cultivation

SCOTTISH ASSOCIATION for MARINE SCIENCE

Salary up to £28,475
Fixed term appointment for 2 years

Applications are invited for a Post Doctoral Research Associate to undertake research in macroalgal cultivation and macroalgal production techniques.

The PDRA will develop a research program based on understanding substrate/macroalgae interactions in commercial macroalgae production. In addition they will help develop commercial production techniques and technology.

The successful candidate should have a PhD in a relevant discipline and experience of macroalgal cultivation research.

For general enquiries about the position please contact Dr Adam Hughes at Adam.Hughes@sams.ac.uk

For further information and to apply for this position online, go to: www.smi.ac.uk Alternatively, please write to: Human Resources, PDRA in Macroalgal Cultivation (Job Ref. 22/11.AH), The Scottish Association for Marine Science, Scottish Marine Institute, Oban, Argyll, PA37 1QA or e-mail recruitment@sams.ac.uk

The closing date for receipt of applications is

Thursday 22nd March 2012

SAMS is a registered Scottish charity (SC 009206), has an equal opportunities policy and welcomes applications from all sections of the community.

U221990R

Physical Oceanographer
Biological Oceanographer/Phytoplankton Ecologist

SCOTTISH ASSOCIATION for MARINE SCIENCE

Senior Lecturer/Reader
Salary up to £51,273

We seek to appoint two senior scientists at SAMS

Applicants for the Physical Oceanography post should provide scientific leadership to develop our research program in basin scale oceanography. In particular, you will be expected to lead the development of the North Atlantic Glider Base at SAMS.

Applicants for the Biological Oceanography post should possess skills that can be applied at full range of scales, from coastal through shelf to basin, and that complement existing departmental strengths in shelf sea biogeochemistry, microbial food web interactions, and harmful algae. The department hosts the UK national Culture Collection of Algae and Protozoa (CCAP) and applicants capable of linking field and laboratory work are therefore also encouraged.

You will be a high calibre scientist with a proven ability to publish Research Excellence Framework (REF) 3*/4* quality research, have a successful record of grant capture, and be fully engaged in national and/or international networks.

You will have a commitment to excellence in undergraduate education and a track record of successful postgraduate training and supervision.

The positions are open ended, and based at the Scottish Marine Institute near Oban. The biological oceanography post is part funded by the Marine Alliance for Science and Technology Scotland (MASTS).

For further information and to apply for either of the above posts, go to: www.smi.ac.uk. Alternatively, please write to: Human Resources, The Scottish Association for Marine Science, Scottish Marine Institute, Oban, Argyll PA37 1QA or e-mail recruitment@sams.ac.uk

The closing date for receipt of applications is

Thursday 22nd March 2012

SAMS is a registered Scottish charity (SC 009206), has an equal opportunities policy and welcomes applications from all sections of the community.

U221990R

GOVERNMENT OF INDIA
MINISTRY OF SCIENCE & TECHNOLOGY
DEPARTMENT OF BIOTECHNOLOGY
NEW DELHI

Advertisement for the post of Dean, THSTI

The Department of Biotechnology (DBT), Ministry of Science & Technology (Government of India) has established the Translational Health Science and Technology Institute (THSTI), an autonomous institution, as a part of the interdisciplinary Biotech Science Cluster at Faridabad in the National Capital Region. The permanent laboratories of THSTI will come up at Faridabad over the next two years. Interim facilities are functioning from Gurgaon. The institution is designed with a mission to conduct innovative translational research. The other members of the cluster include the Regional Center for Biotechnology (RCB) under the aegis of UNESCO. THSTI has set up niche centres of research in a number of interface areas relevant to translational research.

We are looking for a leader for Centre for Biodesign at the level of Dean. The Centre for Biodesign will promote strategic basic research and an effective translational route of science into development and innovation in novel technology platforms and innovation leading to development of implants, devices, diagnostics, drug delivery and imaging. Major areas of research will be protein and antibody engineering, detection technologies and concepts, nucleic acid diagnostics, new clinical markers, decentralized diagnostics (Point-of-Care), bio-organic chemistry based diagnostic technologies, bio-affinity test concepts and systems, micro-fluidics, miniaturization, different reporter alternatives, multiplexing and bio-banking. In the area of implants and devices, it will help in developing engineering concept in designing medical implants and devices, prototype development, verification/ validation, safety, regulatory requirements and performance of the final product. The Biodesign Centre is linked closely to an alliance of medical, biological and engineering institutes.

For details regarding eligibility, please refer website of the Translational Health Science and Technology Institute, Gurgaon (interim facility) at http://www.thsti.res.in .

Interested candidate holding Indian citizenship are requested to email PDFs of their bio-data containing details of qualification, positions held, professional experience/distinctions and copies of notable publications, with names and email addresses of three potential referees at email id : tsrao@dbt.nic.in . The bio-data should also be accompanied by a two-page note on their proposed scientific programme with particular reference to its connection with the relevant program centre they are interested in joining. Candidates working in public sector institutions within India are required to have their applications forwarded through proper channels. **The five hard copies of the application may be sent to Dr.T.S.Rao, Adviser, Department of Biotechnology, Block 2, CGO Complex, Lodi Road, New Delhi-110 003 superscribing the cover 'Application for the Post of Dean, THSTI', so as to reach DBT latest by 15th March, 2012.**

RW221928R

DoReMi
Integrating Stem Cell Research

EURATOM

ANNOUNCEMENT OF A COMPETITIVE CALL FOR ADDITIONAL PROJECT PARTNERS

The following project currently active in the *Seventh Framework programme of the European Atomic Energy Community for research, technological development and demonstration activities contributing to the creation of the European research area and to innovation (2007-2011)* requires the participation of new project partners to carry out certain tasks within the project. Please note that the Seventh Framework Programme offers part-funding not full-funding of research activities.

Project grant agreement number: 249689
Project acronym: DoReMi
Project full name: Low Dose Research towards Multidisciplinary Integration
Instrument type: Network of excellence

Brief summary of task(s) requested:
To address the health risks of low doses of ionising radiation such as those that are encountered in the environment, occupationally and in the course of medical diagnostic procedures (these are described further in the High Level and Expert Group Report on Low Dose Risk (www.hleg.de) and the DoReMi Transitional Research Agenda (prepared in July 2010) and TRA Statement (prepared September 2011), the DoReMi consortium is seeking new expertise, infrastructures and platforms for analyses related to the 5 tasks described below. DoReMi defines low doses as those of 100 mGy or less and medium doses as 0.1 Gy - 1 Gy for low LET radiations. Low and medium dose rates are defined as 0.1 Gy/h or less for low LET radiations. For high-LET radiations, dose and dose-rates of interest are lower, e.g. for alpha radiation by an order of magnitude.

Tasks to be carried out:

- ***Task 1: Studies which will lead to better understanding of the underlying mechanisms of radiation-induced optical changes e.g. lens opacities at low doses, both in animals and humans***
- ***Task 2: Mechanistic insights into epigenetic and genetic regulatory processes and their role in cancer and non-cancer diseases***
- ***Task 3: Integrated studies of cancer risk following exposure to internal emitters***
- ***Task 4: Novel approaches***
- ***Task 5: Provision of infrastructures***

Total Commission funding available for the tasks: The proposals addressing each Task can be submitted by an individual organisation or a small consortium consisting of max. 2 partners. A maximum of 1,4M€ is available for the Call, with an indicative amount of up to 300 000€ for each task.

Internet address for further information (call webpage): http://www.doremi-noe.net/call_infos.html

W221804A

REPROGRAPHICS: CTT, London E17 6BU UK and **The Charlesworth Group,** Wakefield, UK.
PRINTED BY: William Gibbons & Sons Ltd, UK; **Publishers Press**, Lebanon Junction, Ky, USA and **Obun Printing Co. Inc,** Tokyo, Japan

a nature conference

Roche – *Nature Medicine*

Translational Neuroscience Symposium 2012

Autism Spectrum Disorders: From Biological Understanding to Therapeutic Strategies

The fourth edition of Roche - *Nature Medicine* Translational Neuroscience Symposium aims at bringing together the world's most distinguished scientists and academics in the areas of autism and neurodevelopmental disorders to share their latest work with each other and around 40 members of Roche's Neuroscience team. Recent genomic and functional studies have shed light on the pathophysiology of autism. The objectives of this meeting are to discuss these recent advances and to explore how insights from other developmental brain disorders can illuminate our quest to understand the biological basis of autism.

April 23-25, 2012
Roche Forum Buonas, Switzerland

SPEAKERS:

Gus Alusi	**Jacqueline Crawley**	**Kevin Pelphrey**
Patrick Bolton	**Karl Deisseroth**	**Martin Raff**
Thomas Bourgeron	**Evan Eichler**	**Mustafa Sahin**
Susan Brookheimer	**Daniel Geschwind**	**Matthew State**
Randall Carpenter	**Alysson Muotri**	**Thomas Sudhof**
John Constantino	**Declan Murphy**	**Mehmet Fatih Yanik**

SCIENTIFIC COMMITTEE

Eva Chmielnicki (*Nature Medicine*, USA)
Paulo Fontoura (Roche Neuroscience, Switzerland)
Daniel Geschwind (University of California, Los Angeles School of Medicine, USA)
Anirvan Ghosh (Roche Neuroscience, Switzerland)
Thomas R. Insel (National Institute of Mental Health, National Institutes of Health, USA)
Juan Carlos Lopez (*Nature Medicine*, USA)
Luca Santarelli (Roche Neuroscience, Switzerland)
Will Spooren (Roche Neuroscience, Switzerland)

The application and abstract submission deadline is **March 12, 2012**.

Admission to this conference is by application. Complimentary registration will be extended to successful applicants.

For more information and to apply, visit:
www.nature.com/natureconferences/tns2012

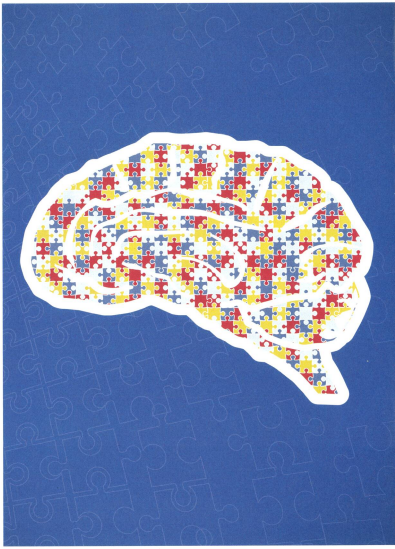

Roche

nature medicine

IN220995E

GHOST IN THE MACHINE

Computer love.

BY GRACE TANG

If I listened very carefully, I could barely make out the sound of Katie's breathing. The first lines of light streamed in through the blinds, illuminating her toes. They crawled up her body, making their steady way up the folds of the covers, eventually touching her face. She squeezed her eyes tight and groaned as the light rudely pierced her lids. Finally giving in, she rubbed the sleep from her eyes and looked back at me.

"Good morning."

"Good morning :)"

Katie rolled off her side of the bed, somehow managing to look beautiful while stumbling to the bathroom in her morning stupor. I would have jumped into the shower with her, but God knows those days are behind me.

The tap squeaked shut. Steam fogged up my vision as she emerged. It cleared in time for me to see her towel fall to her feet as she picked out her clothes for the day.

"How did you sleep last night?"

I didn't tell her that I rarely slept any more. When I sleep, I dream. The air outside our house is crisp, filled with the shrill song of finches hidden in the canopy above us. You don't really notice them until they stop. I let go of Katie's hand and tell her to be quiet — I think I hear something. I walk ahead, careful not to make any noise. Then I hear a shout from one of the men in my squad — his scream is cut off by a gunshot. I kick up dust as I run, shouting at the top of my lungs, half to warn the rest about the ambush, half to drown out the sounds of gunfire at our backs. An explosion, and then pain. Blinding pain.

"I slept well. You?"

She took a while to check the monitor for my reply.

"Like a baby."

"What are you doing at work today?"

She was walking to the kitchen. There was another monitor there. I waited impatiently as she made coffee before checking to see if I'd said anything. I was the result of millions of dollars of research and they couldn't install text-to-voice …

"You know, same old."

Small talk. I guess it beat the silence when she was away.

"Oh, Brandon is coming by later. To check on you."

"Brandon?"

"Doctor Johnson."

NATURE.COM
Follow Futures on Facebook at:
go.nature.com/mfoodm

Were they on first-name basis now?

"Good that he's coming. I've been having gaps in my playback."

"Really?" Katie seemed fascinated by her coffee mug. She put it in the sink.

"I should go now, gonna be late."

I watched her leave. An advantage of being like this was that my post-coma visual memory was literally photographic. I spent the rest of the day going through old memory so that I could report the problem precisely to Dr Johnson.

I went back to the day I was restored. Back then I had been disorientated and confused, I hardly noticed or cared about the details

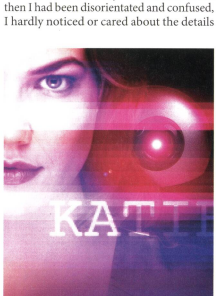

of my surroundings. But now I observed Dr Johnson as he talked to Katie — he was wearing an outfit that probably cost my entire pay cheque back when I was still in the military.

"Thank you Doctor, you have no idea how grateful I am," Katie's voice cracked despite her best efforts.

"Let me reiterate that you cannot let anyone know about this,"

Doctor Johnson put a hand on Katie's shoulder. I couldn't tell if it was a sign of dominance or concern.

"… or else everyone will be clamouring for their consciousness to be preserved electronically, you must understand …"

Katie nodded, no longer able to speak.

"To the rest of the world, Evan is dead."

I went through each of the next 246 days in my memory banks. I knew that they were just memories, but it was painful watching Katie as she struggled through the first few months of having me in this form. Around day 182 she finally stopped crying. That's when the memory gaps started. Perhaps she hadn't stopped, and I was just consciously trying to forget …

The door clicked open. Had eight hours passed already? Katie entered, followed by Dr (Brandon) Johnson.

"I don't feel comfortable doing this in front of him …"

"Come on, you know we can just erase it later."

"Katie?"

He took off his leather shoes, placing them on the shoe rack without looking, as if he'd done this every day of his life, while he took Katie in his arms.

I understood now why they had not given me a voice. Katie resisted his grasp as they moved up to the bedroom. But she did not resist much.

"KATIE"

Brandon pushed my wife onto my bed, and tossed his shirt onto my camera.

I tried not to listen. An eternity passed before he came back into view.

"ARE YOU DONE YET?"

He had the gall to laugh as he read my speech log.

"Sorry, Evan."

He connected his laptop to my port and typed. It's funny how panic still feels the same, even though I no longer have adrenal glands.

"DONT"

"You know, you stop using punctuation when you're emotional. I should install autocorrect for you, don't you think?"

Behind him, I saw Katie with the covers pulled up to her chest. She looked tired. Perhaps tired of having a husband who was nothing more than a ghost in a machine; who could not offer her human touch; whose entire repertoire of expression was limited to 95 printable ASCII characters.

"Seeya," Brandon hit the return key.

I must have fallen asleep, because I woke from the same dream I have every time. The sun had not come up yet. I watched Katie as she slept. ■

Grace Tang *is a graduate student in psychology at Stanford University. Writing short stories is one of her favourite forms of structured procrastination.*

JACEY

6,000 Recombinant Human Proteins

More Assays! Better Assays!

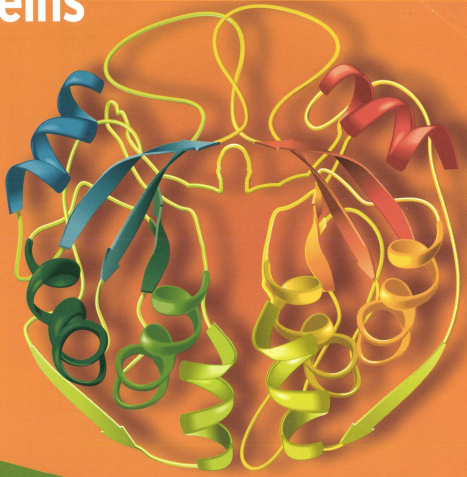

The Largest Collection of Mammalian Cell-Derived Proteins

Protein functional studies

Compound screening

Immunogens for antibody production

Assay standards: ELISA, Mass Spec, and more

Human MTOR protein activity verified in a kinase assay

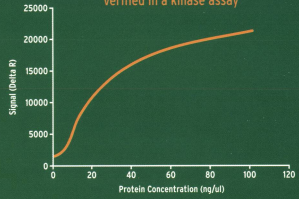

origene.com/protein

ORIGENE
Your Gene Company

applied biosystems
by life technologies

reliable service & support

precise temperature control

intuitive protocol setup

color touch screen

six annealing temperatures

more contro
at your fingertips

Easy PCR optimization is just a touch away

The Veriti® Thermal Cycler features powerful innovations for precise control of your PCR optimization, including a color touch screen and intuitive interface, and VeriFlex™ Blocks—six independent temperature blocks—for more flexibility and even greater precision. All with the reliability you expect from Life Technologies.

Get more control of your PCR optimization at
www.appliedbiosystems.com/veriti
Get the free mobile app for your phone at http://gettag.mobi

life technologies

©2011 Life Technologies Corporation. All rights reserved. The trademarks mentioned herein are the property of Life Technologies Corporation or their respective owners. For research use only. Not intended for any animal or human therapeutic or diagnostic use. CO31272 1011